AD-A039 688 ADVISORY GROUP FOR AEROSPACE RESEARCH AND DEVELOPMENT--ETC F/G 20/4
COMPUTATIONAL FLUID DYNAMICS.(U)
APR 77

UNCLASSIFIED AGARD-LS-86 NL

1 OF 2
AD
A039688

SIFIED

1 OF 2

AD

A039 688

AGARD LECTURE SERIES No. 86

on

Computational Fluid Dynamics

DISTRIBUTION STATEMENT A
Approved for public release;
Distribution Unlimited

DDC
MAY 20 1977

NORTH ATLANTIC TREATY ORGANIZATION

ADVISORY GROUP FOR AEROSPACE RESEARCH AND DEVELOPMENT

(ORGANISATION DU TRAITE DE L'ATLANTIQUE NORD)

AGARD Lecture Series No.86

COMPUTATIONAL FLUID DYNAMICS

ACCESSION for
NTIS White Section
DDC Buff Section
UNANNOUNCED
JUSTIFICATION
BY
DISTRIBUTION/AVAILABILITY CODES
Dist. AVAIL. and/or SPECIAL
A

The material in this publication has been assembled to support a Lecture Series under the joint sponsorship of the Von Kármán Institute and the Fluid Dynamics Panel, together with the Consultant and Exchange Program of AGARD. Presented at the Von Kármán Institute on 21–23 March, and at Wright-Patterson Air Force Base, Dayton, Ohio 45433, USA on 25–27 April 1977

THE MISSION OF AGARD

The mission of AGARD is to bring together the leading personalities of the NATO nations in the fields of science and technology relating to aerospace for the following purposes:

- Exchanging of scientific and technical information;
- Continuously stimulating advances in the aerospace sciences relevant to strengthening the common defence posture;
- Improving the co-operation among member nations in aerospace research and development;
- Providing scientific and technical advice and assistance to the North Atlantic Military Committee in the field of aerospace research and development;
- Rendering scientific and technical assistance, as requested, to other NATO bodies and to member nations in connection with research and development problems in the aerospace field;
- Providing assistance to member nations for the purpose of increasing their scientific and technical potential;
- Recommending effective ways for the member nations to use their research and development capabilities for the common benefit of the NATO community.

The highest authority within AGARD is the National Delegates Board consisting of officially appointed senior representatives from each member nation. The mission of AGARD is carried out through the Panels which are composed of experts appointed by the National Delegates, the Consultant and Exchange Program and the Aerospace Applications Studies Program. The results of AGARD work are reported to the member nations and the NATO Authorities through the AGARD series of publications of which this is one.

Participation in AGARD activities is by invitation only and is normally limited to citizens of the NATO nations.

The content of this publication has been reproduced
directly from material supplied by AGARD or the authors.

Published April 1977

Copyright © AGARD 1977
All Rights Reserved

ISBN 92-835-1241-3

Printed by Technical Editing and Reproduction Ltd
Harford House, 7–9 Charlotte St, London, W1P 1HD

PREFACE

This Lecture Series, sponsored by the Fluid Dynamics Panel and the Consultant and Exchange Program of AGARD, being held at the Von Kármán Institute, Rhode-Saint-Genèse, Belgium and – for the first time – also at Wright-Patterson Air Force Base, Dayton, Ohio, USA is a follow-up of the annual Lecture Series on Numerical Methods in Fluid Dynamics at VKI.

The uniform success of these Lecture Series during the past years, with more than one hundred participants each year from many European countries, the USA and Canada certainly reflects international recognition of these seminars as a forum for lively discussions, continuous advancements, and sound learning in the field of computational fluid mechanics.

The material to be presented this year comprises recent developments of the finite element method, numerical turbulence modelling, relaxation methods for time dependent equations, flow representation by discrete vortices and advances in the treatment of the full Navier-Stokes equations.

H.J.WIRZ
Lecture Series Director

LIST OF SPEAKERS

Dipl.-Ing. H.J.Wirz
Visiting Professor
Von Kármán Institute for Fluid Dynamics
Computational Fluid Dynamics Department
72 Chaussée de Waterloo
1640 Rhode-Saint-Genèse
Belgium

Dr H.Lugt
Naval Ship Research and Development Center
Bethesda
Maryland 20084
USA

Professor R.R.Clements
Department of Engineering Mathematics
University of Bristol
Bristol BS8 1TH
UK

Dr M.W.Rubesin
NASA Ames Research Center
Moffett Field
California 94035
USA

Professor R.Temam
Université de Paris
Faculté des Sciences
91400 Orsay
France

Dr S.Leventhal
Mathematics Analysis Branch
Naval Surface Weapon Center
White Oak Laboratory
Silver Spring
Maryland 20910
USA

CONTENTS

	Page
PREFACE	iii
LIST OF SPEAKERS	iv
	Reference
THE FOUNDATION AND DEVELOPMENT OF THE FINITE ELEMENT METHOD TO SOLVE PARTIAL DIFFERENTIAL EQUATIONS OF FLUID MECHANICS by A.K.Aziz and S.Leventhal	1
RECENT ADVANCES IN THE NUMERICAL TREATMENT OF THE NAVIER-STOKES EQUATIONS by H.J.Lugt	2
NUMERICAL TURBULENCE MODELLING by M.W.Rubesin	3
RELAXATION METHODS FOR TIME DEPENDENT CONSERVATION EQUATIONS *IN FLUID MECHANICS* by H.J.Wirz	4
FLOW REPRESENTATION, INCLUDING SEPARATED REGIONS, USING DISCRETE VORTICES by R.R.Clements	5
SOME FINITE ELEMENT METHODS IN FLUID FLOW by R.Temam	6

THE FOUNDATION AND DEVELOPMENT OF THE FINITE ELEMENT METHOD TO SOLVE PARTIAL DIFFERENTIAL EQUATIONS OF FLUID MECHANICS

A. K. Aziz*, S. Leventhal**

* Department of Mathematics, UMBC, and Institute of Physical Science and Technology, University of Maryland, College Park, MD 20742, USA

** Naval Surface Weapons Center, White Oak Laboratory, Silver Spring, Maryland 20910, USA

Summary

In this paper the mathematical formulation of the finite element method, and its application to fluid mechanics are considered. In Part I an introduction to the mathematical theory is given beginning with the variational formulation of a problem. The three basic steps in the finite element method are discussed: 1) the subdivision of the domain; 2) the definition of the elements to approximate the unknown functions; and, 3) the forming of the algebraic system for the unknown coefficients. In Part II the application of the finite element method to two problems in fluid mechanics is given. The first of these problems is boundary layer flow, and the other is transonic flow.

Introduction

The finite element method is an approximate method for solving the partial differential equations which arise in engineering and mathematical physics. In this method the domain of the problem is divided into many small elements of convenient shapes, e.g., triangles, rectangles. Choosing suitable points called nodes at corners, midsides, etc., on a local finite element, the variables in the differential equation are written as a linear combination of appropriately selected interpolation functions and the values of variables specified at the nodes. Using variational principles or the method of weighted residuals, the governing differential equations are transformed into a system of algebraic equations. The nodal values of the variables are obtained by solving this system.

The concept of the finite element method was introduced in a paper by R. Courant [1] in 1943. However, the development of the method was by structural engineers in the 1950's in order to analyze the large system of structural elements in aircrafts. Turner, Clough, Martin and Topp [2] presented the first paper on this subject, followed by Clough [3] and Argyris [4], among others. Applications of the method to non-structural problems such as fluid flows and electromagnetism was initiated by Zienkiewicz [5], and applications to problems of interest in nonlinear mechanics by Oden [6].

Even though engineering problems had been solved by the finite element method since the 1950's, no formal mathematical theory existed. However, due to the success of the engineering calculations mathematicians began to analyze the method in the late 1960's. Recently Babuška and Aziz [7], Strang and Fix [8], Ciarlet [9], Raviart [10], among others, have presented the finite element theory from a mathematical point of view.

In this paper we consider both the mathematical formulation of the finite element method, and its application to fluid mechanics. In Part I we give an introduction to the mathematical theory, emphasizing the different types of elements. In Part II the application of the finite element method to two problems in fluid mechanics, boundary layer flow and transonic flow.

Part I. Mathematical Formulation

The finite element method (FEM) is a method for obtaining approximate solutions to the partial differential equations which govern a given physical problem. Any approximate method for the solution of partial differential equations consists in the determination of the unknown functions at a finite number of discrete points distributed throughout the domain of the problem. The values of the functions at these points are obtained as the solution of an algebraic system of equations determined from a discrete representation of the governing equations. If the values of the unknown functions are needed at any other points in the domain, they are determined through given interpolation formulas.

In finite difference methods these basic steps are usually handled in the following manner: The discrete set of points are the corners and/or midpoints of a rectangular (usually regular) mesh. The algebraic system for the unknown values at these points are determined by replacing all the partial derivatives by finite difference approximations. The value of the functions at arbitrary points is determined by the usual interpolation formulas obtained from Taylor expansions.

The characterization of these steps for the finite element is what is to be considered in this part of these notes. The first step in this characterization is the

integral or variational formulation of the governing equations. Starting from the variational form of the equation the three basic steps are discussed, that is, the subdivision of the domain, the approximation of the unknown functions, and the determination of the solution at arbitrary points within the domain. To help illustrate the application of the above concepts a simple example of the application of the method is carried through from start to finish. Finally a brief explanation of the use of the method in time dependent problems is given.

I. Preliminary Notation

Before beginning the variational formulation, the following notation is introduced. Let Ω be a given domain with boundary Γ. Denote by $L_2(\Omega)$ the space of functions defined on Ω which are square integrable. The inner product and norm for $L_2(\Omega)$ are

$$(u,v)_{L_2(\Omega)} = \int_\Omega u \cdot v d\Omega \tag{1}$$

$$\|u\|_{L_2(\Omega)} = (u,u)^{1/2}_{L_2(\Omega)} = \left(\int_\Omega u^2 d\Omega\right)^{1/2} \tag{2}$$

The space $H^1(\Omega)$ is the space of functions defined on Ω whose first derivatives (in the sense of distributions) are in $L_2(\Omega)$. The inner product and norm for $H^1(\Omega)$ are

$$(u,v)_{H^1(\Omega)} = \int_\Omega \left(\frac{\partial u}{\partial x}\frac{\partial v}{\partial x} + \frac{\partial u}{\partial y}\frac{\partial v}{\partial y} + uv\right)d\Omega \tag{3}$$

$$\|u\|_{H^1(\Omega)} = (u,u)^{1/2}_{H^1(\Omega)} . \tag{4}$$

Finally, define $H^1_0(\Omega)$ as the subspace of $H^1(\Omega)$ which satisfies zero boundary conditions. $H^1_0(\Omega)$ has the same inner product and norm as $H^1(\Omega)$, or the equivalent inner product and norm

$$(u,v)_{H^1_0(\Omega)} = \int_\Omega \left(\frac{\partial u}{\partial x}\frac{\partial v}{\partial x} + \frac{\partial u}{\partial y}\frac{\partial v}{\partial y}\right)d\Omega \tag{5}$$

$$\|u\|_{H^1_0(\Omega)} = (u,u)^{1/2}_{H^1_0(\Omega)} \tag{6}$$

II. Variational Formulation

Given a domain Ω with boundary Γ consider the equation

$$-\Delta u = -\frac{\partial^2 u}{\partial x^2} - \frac{\partial^2 u}{\partial y^2} = f \quad \text{in } \Omega \tag{7}$$

$$u = 0 \quad \text{on } \Gamma . \tag{8}$$

This equation, known as Poisson's equation, arises in many physical situations such as potential flow.

It is well known that the solution to (7) with boundary condition (8) may also be obtained as the minimum of the quadratic functional

$$I = \int_\Omega \left[\frac{1}{2}\left(\left(\frac{\partial u}{\partial x}\right)^2 + \left(\frac{\partial u}{\partial y}\right)^2\right) - fu\right]d\Omega \tag{9}$$

taken over all $u \in H^1_0(\Omega)$.

In order to find the function that minimizes I it is necessary to take the first variation of I and set it equal to zero. The result of this operation is

$$\int_\Omega \left[\frac{\partial u}{\partial x}\frac{\partial v}{\partial x} + \frac{\partial u}{\partial y}\frac{\partial v}{\partial y}\right]d\Omega = \int_\Omega fv d\Omega \text{ , for all } v \in H^1_0(\Omega) . \tag{10}$$

The left-hand side of (10) is known as a bilinear form. The properties of this bilinear form allow one to conclude the existence and uniqueness of a minimizing function u. Equation (10) is known as a variational principle since it was derived from the first variation of a quadratic functional. Not all equations have a corresponding representation as a quadratic functional. However, all that is really necessary is to obtain an equivalent bilinear form that has the properties needed for existence and uniqueness. These properties are given by the following theorem.

Theorem I. If

1) H_1 and H_2 are two real Hilbert (inner product) spaces with inner product

$(\cdot,\cdot)_{H_1}$ and $(\cdot,\cdot)_{H_2}$ respectively.

2) $B(u,v)$ is a bilinear form on $H_1 \times H_2$, $u \in H_1$, $v \in H_2$ such that

$$|B(u,v)| \leq C_1 \|u\|_{H_1} \|v\|_{H_2} \tag{11}$$

$$\inf_{u \in H_1} \sup_{v \in H_2} |B(u,v)| \geq C_2 > 0 \tag{12}$$
$$\|u\|_{H_1}=1 \quad \|v\|_{H_2} \leq 1$$

$$\sup_{u \in H_1} |B(u,v)| > 0 \,, \quad v \neq 0 \tag{13}$$

where $C_1 < \infty$.

3) $f \in H_2'$, i.e., f is a linear functional on H_2 then

4) there exists a unique element $u_0 \in H_1$ such that

$$B(u_0,v) = f(v) \,, \text{ for all } v \in H_2 \tag{14}$$

$$\|u_0\|_{H_1} \leq \frac{\|f\|_{H_2'}}{C_2} \,. \tag{15}$$

Now we show that the conditions of Theorem 1 are satisfied for equations (7), (8). Let $H_1 = H_2 = H_0^1(\Omega)$. Take for the bilinear form

$$B(u,v) = \int_\Omega \left[\frac{\partial u}{\partial x}\frac{\partial v}{\partial x} + \frac{\partial u}{\partial y}\frac{\partial v}{\partial y}\right] d\Omega \,.$$

Using the equivalent norm in $H_0^1(\Omega)$ (eq. (6)), it follows from the Schwartz inequality that

$$|B(u,v)| \leq C_1 \|u\|_{H_0^1(\Omega)} \|v\|_{H_0^1(\Omega)} \,.$$

Thus condition (11) is satisfied. From the ellipticity it follows that

$$B(v,v) \geq C_2 \|v\|^2_{H_0^1(\Omega)} \,, \text{ for all } v \in H_0^1(\Omega) \,.$$

Thus conditions (12) and (13) are satisfied.
Let

$$f(v) = \int_\Omega fv\, d\Omega \,, \qquad f \in (H_0^1(\Omega))' \,.$$

Thus by Theorem 1, there exists a unique function u_0 such that

$$B(u_0,v) = f(v) \,,$$

and

$$\|u_0\|_{H_0^1(\Omega)} \leq \frac{\|f\|_{(H_0^1(\Omega))'}}{C_3} \,.$$

The importance of the variational formulation for approximate methods is that it is now only necessary for first derivatives of the approximate solution to exist, whereas to solve (7) directly would require second derivatives.

The most widely used method of obtaining a variational equation from a given equation is known as the method of weighted residuals. Consider the equation

$$Lu = f \tag{16}$$

with boundary conditions

$$u = 0 \,, \tag{17}$$

where L is a second order operator. A solution of (16) and (17) also must satisfy

$$\int_{\Omega}(Lu-f)d\Omega = 0 .$$

A weaker, but still necessary condition, that must be satisfied is

$$\int_{\Omega}(Lu-f)v d\Omega) = 0 \quad \text{for all} \quad v \in H_0^1(\Omega) . \tag{18}$$

A variational equation may now be derived from (18) using the Green-Gauss Theorem. The use of (18) to derive the variational principle is known as the method of weighted residuals, since for an approximate solution u_h the residual

$$R_h = Lu_h - f$$

is not zero, but it is required that its weighted integral (with weight v) be zero.

In the previous discussion Dirichlet boundary conditions have only been examined. More general boundary conditions may be easily handled by adding them to the variational principle.

III. The Finite Element Method

3.1 Definition of the Method - Consider the problem: Find $u \in V$ such that for every $v \in V$

$$B(u,v) = f(v) , \tag{19}$$

where the bilinear form $B(u,v)$ satisfies the conditions of Theorem 1. The bilinear form is obtained through the variational formulation of the given problem.

A conforming approximate method for solving eq. (19) consists in finding an approximate solution u_h in a finite dimensional subspace V_h of the space V, where u_h is the solution of the problem

$$B(u_h,v_h) = f(v_h) , \quad \text{for all} \quad v_h \in V_h \tag{20}$$

Note, that as a consequence of Theorem 1 the above problem has a unique solution and further

$$\|u-u_h\|_V \leq C \inf_{v_h \in V_h} \|u-v_h\|_V .$$

To see this, let w_h be an arbitrary element in V_h. From (19) and (20) it follows that:

$$B(u-u_h,w_h) = 0 .$$

Thus

$$\alpha\|u-u_h\|_V^2 \leq B(u-u_h,u-u_h) = B(u-u_h,u-v_h) \leq C\|u-u_h\|_V \|u-v_h\|_V$$

and the conclusion follows.

The above simple result indicates that the problem of estimating error is reduced to a problem in approximation theory, namely the distance between the solution u and the subspace v_h.

The finite element method in its simplest form may be considered as a conforming approximate method in which the subspaces V_h are of a special form. More precisely, assume that a second order problem is to be approximated. Then the problem to be faced is to construct a finite dimensional subspace V_h of the space $H^1(\Omega)$ or $H_0^1(\Omega)$. Suppose $\bar{\Omega}$ is a polygon in R^2. Consider a triangulation T_h over the set $\bar{\Omega}$, i.e., the set $\bar{\Omega}$ is expressed as a finite union $\cup_{T \in T_h} T$ of triangles T in such a way that whenever T_1 and T_2 are distinct triangles of T_h, their intersection is either empty, or a common vertex, or a common edge. An example is given in Figure 1; while Figure 2 shows a triangulation which is not permissible since the intersection of T_1 and T_2 is not a common edge.

With such a triangulation is associated a space V_h of functions defined on $\bar{\Omega}$ whose restriction to each triangle T belongs to a finite dimensional subspace P_T of function defined on the set T. So far, the subspace V_h depends on a given triangulation T_h and the subspace P_T, $T \in T_h$. Note that even if the space P_T consists of very nice functions, there is no reason why the conclusion $V_h \subset H^1(\Omega)$ should hold. For this reason a simple additional condition is needed, i.e., $V_h \subset C^0(\bar{\Omega})$ ($C^0(\Omega)$ is the set of continuous functions on $\bar{\Omega}$). It is not difficult to show using Green's formula that with the additional condition $P_T \in H^1(\Omega)$, then $V_h \subset H^1(\Omega)$. If further the functions in V_h vanish on the boundary Γ, then the inclusion $V_h \subset H_0^1(\Omega)$ holds.

The discrete problem (20) is generally solved in practice as follows: Let

$$\{\phi_j\}_{j=1}^{N}$$

be a basis for V_h, then the solution

$$u_h = \sum_{j=1}^{N} u_j \phi_j$$

of (20) is obtained by solving the linear system

$$\sum_{i=1}^{N} B(\phi_i,\phi_j)u_i = f(\phi_j) \quad 1 \le j \le N ,$$

where the matrix $A = (B(\phi_i,\phi_j))$, known as the stiffness matrix, always has an inverse. When $B(u,v)$ is symmetric then the matrix A is also symmetric and positive definite, which is not the case for finite difference methods involving non-rectangular regions.

In selecting the basis $\{\phi_j\}_{j=1}^{N}$ it is of the utmost importance, from a practical point of view, that the resulting matrix be as sparse as possible, i.e., have many zeros. Recall that the coefficients of the matrix $A = (B(\phi_i,\phi_j))$ are integrals. In the case of the previous example

$$B(\phi_i,\phi_j) = \sum_{T\in T_h} \int_T \{\frac{\partial\phi_i}{\partial x}\frac{\partial\phi_j}{\partial x} + \frac{\partial\phi_i}{\partial y}\frac{\partial\phi_j}{\partial y}\}dxdy .$$

Thus $B(\phi_i,\phi_j) = 0$, whenever the intersection of the supports of ϕ_i and ϕ_j is of measure zero. Consequently, one must try to have basis functions ϕ_j whose supports are as small as possible.

3.2. Definition of the Elements - The finite element method is distinguished from traditional Galerkin or Rayleigh-Ritz methods primarily by the special character of the system of functions used. Indeed, it is the remarkably wide variety of these systems that gives the method its flexibility and practicality. The purpose of this section is to discuss briefly a classification of the possible alternatives and to give an analysis of their basic properties. There are three essential components to the classification, namely: a) geometrical structure; b) polynomial structure; and c) nodal structure.

These terms shall be given a precise meaning in such a way that any finite element is uniquely determined by specifying each of these three components. Through this specification the order of accuracy and the smoothness, among other things, may be determined.

The starting point for any finite element is the geometric structure of the element. As indicated earlier, Ω is divided into subregions, e.g., rectangles or triangles, and the nature of the subregions constitutes a fundamental distinction between elements. To be specific, let Ω be a rectangle with sides parallel to the coordinate axes. Subdivide Ω into rectangles $R_1,\ldots,R_m$ with sides parallel to coordinate axes. The finite element space will in essence consist of functions whose restrictions to R_i, $i = 1,\ldots,n$, reduce to polynomials and precise specification of the subdivision of Ω defines the polynomial structure of the space. Begin with piecewise linear functions.

3.3. Linear Elements

3.3.1. Bilinear Elements in Rectangles - Let the space V_0 be the set of functions $v(x,y)$ which are bilinear in each rectangle R_i of the subdivision of Ω, i.e., for each $(i=1,2,\ldots,M)$

$$v(x,y) = a_i + b_i x + c_i y + d_i xy , \quad (x,y) \in R_i .$$

Note that V_0 contains discontinuous functions. Thus, as was discussed previously the space V_0 is not suitable for solving partial differential equations.

One of the more interesting aspects of finite elements is the fact that the additional smoothness can be achieved by the introduction of a nodal structure on a basic space such as V_0. To see this simple fact let

$$V = V_0 \cap H^1(\Omega)$$

and consider the set of nodes of the rectangles $\{R_i\}_{i=1}^{M}$ denoted by $\{a_j,\ldots,a_N\}$. Clearly a function $v \in V_0$ is in V if and only if v is continuous at a_j $1 \le j \le N$. To see this, let $v \in V_0$ such that it is continuous at each node a_i $(1\le i\le N)$, i.e., the different polynomial representation of v have the same function values at a fixed node a_j. One must show that v is continuous across the boundary between rectangles. Note that the line L separating any two rectangles R_i, R_j is either horizontal or

vertical. In either case the difference between the representation of v in R_i and that in R_j is linear in x or in y. Since it vanishes at the two nodes on L, it therefore must vanish everywhere on L. (This argument obviously fails if the sides of the rectangles were not parallel to the coordinate axes.)

Furthermore, note that any $v \in V$ is uniquely determined by its values, $v_1, \ldots, v_N$ at the nodes. This follows immediately from the fact that on any given rectangle $R_i (1 \le i \le M)$ v must take on specified values at four nodes. This in turn uniquely determines the constants a_i, b_i, c_i and d_i. Later in this section elements whose nodal structure is more elaborate shall be discussed. However, the point to be underlined is that all finite element spaces, even the so-called spline element, have a nodal structure and this plays a fundamental part in the theory of finite elements.

The nodal structure is also significant since it is typically the first step in the construction of a basis, which usually consists of unit vectors. The fact that each $v \in V$ is uniquely determined by its nodal values suggests that for each node consider the function $\phi_j(x,y)$ which is one at a_j and zero at other nodes $a_i (i \neq j)$. Observe that any $v \in V$ can be uniquely written

$$v(x,y) = \sum_{j=1}^{N} v(a_j)\, \phi_j(x,y) .$$

As pointed out earlier an essential feature of this nodal structure which is also present in all finite elements is its local character, i.e., the associated base

$$\{\phi_i\}_{i=1}^{N}$$

will be local in the sense that the support of each ϕ_j will approach zero as the subdivision is refined. In particular for the piecewise linear space the function ϕ_j is zero in any rectangle R_i not containing a_j as node. Finally note that the order of accuracy is 2.

3.3.2. Linear Elements in Triangles - Before leaving linear elements it is perhaps worthwhile to point out that there is an alternate element that is based on a different geometric structure and polynomial structure, but otherwise the same (i.e., the same nodal structure, smoothness, and accuracy).

In particular, assume that Ω is a polygon which has been subdivided into triangles $T_1, \ldots, T_m$. As before the basic space V_0 consists of all functions v which reduce to a linear function

$$v(x,y) = a_i + b_i x + c_i y$$

in each triangle T_i. A function $v \in V_0$ is in $V_1 = V_0 \cap H^1(\Omega)$ if and only if v is continuous at the vertices $a_1, a_2, \ldots, a_M$ of the triangles $T_1, \ldots, T_M$.

Note that the above representation of v has only three terms and does not contain the cross product term xy. This of course reflects the fact that a linear function is determined by three conditions in a triangle while a bilinear function requires four conditions in a rectangle.

3.4. Cubic Elements

In the next two sections cubic elements are considered. The reason for considering this specific class of elements is that next to linear elements it is the most widely used class.

3.4.1. Cubics in Rectangles - In this section elements having a rectangular geometric structure are considered. Thus, suppose that Ω is a rectangle with sides parallel to the coordinate axes and

$$\bar{\Omega} = \bigcup_{i=1}^{M} \bar{R}_i ,$$

where R_i are rectangles. Consider two types of nodal structures.

a) Lagrange type structure, where only function values are involved.

b) Hermite type structure, where both function values and values of derivatives are involved.

a) To begin with, consider the case $\Omega = [0,1]$. Let Ω be subdivided into smaller intervals. It is necessary to construct a space of continuous functions which are cubic on each subinterval. Four conditions determine a cubic $a + bx + cx^2 + dx^3$ on a given interval, and this suggests a nodal structure consisting of the requirement that each v in V assumes specified values at four predetermined points. To preserve continuity one chooses two of the points to be the end points of the interval and arranges the remaining two points symmetrically. More precisely, let

$$0 = a_1 < a_2 < \ldots < a_m = 1$$

be a subdivision of $\Omega = [0,1]$. Introduce the nodes

$$z_{3i-2} = a_i, \quad z_{3i-1} = a_i + \frac{\Delta a_i}{3}, \quad z_{3i} = a_i + \frac{2\Delta a_i}{3}, \tag{21}$$

where $\Delta a_i = a_{i+1} - a_i$, and $i = 1, 2, 3, \ldots, M-1$. Also, let $N = 3M - 2$ and $z_N = a_m$.

If V denotes the space of all continuous functions which reduce to a cubic polynomial on each interval (a_j, a_{j+1}), $j = 1,\ldots,M-1$, then each $v \in V$ is uniquely determined by its values at the nodes $\{z_j\}$. A basis for V is obtained in the usual manner. In particular, for each z_j, $1 \leq j \leq N$, consider the unique function ϕ_j, with

$$\phi_j(z_\ell) = \delta_{j\ell} ;$$

the set $\{\phi_i\}_{i=1}^{N}$ form a basis for V, in fact every $v \in V$ can be written

$$v(x) = \sum_{j=1}^{M} v(z_j)\, \phi_j(x) .$$

Now the space V is used to construct a two dimensional finite element space. The basic idea is to take tensor products. In particular, let $\bar{\Omega}$ be written as the cartesian product of intervals in x and y. Let $\{a_j^{(1)}\}$, $(j=1,\ldots,M_1)$ and $\{a_j^{(2)}\}$, $(j=1,\ldots,M_2)$ be grids for x and y intervals, respectively, each with corresponding nodes and piecewise cubic basis $\{z_j^{(1)}\}$, $\{\phi_j^{(1)}\}$, $(j=1,\ldots,N_1)$ and $\{z_j^{(2)}\}$, $\{\phi_j^{(2)}\}$, $(j=1,\ldots,N_2)$. The grid

$$(x_i, y_i) = (a_{i_1}^{(1)}, \; a_{i_2}^{(2)}) = a_{\underline{i}}$$

defines a rectangular subdivision of $\bar{\Omega}$, R_i, $i = 1,\ldots,M$, i.e.,

$$\bar{\Omega} = \bigcup_{i=1}^{M} R_i .$$

Now a new space V on Ω is defined as the set of all continuous functions on $\bar{\Omega}$ which reduce to polynomials

$$\sum_{i=0}^{3} \sum_{j=0}^{3} \phi_{ij}\, x^i y^j$$

in each rectangle R_i, $1 \leq i \leq M$.

As before, note that each function $v(x,y) \in V$ is uniquely determined by its values at the nodes $z_{\underline{j}} = (z_j^{(1)}, z_j^{(2)})$ and moreover it has the representation

$$v(x,y) = \sum_{i=1}^{N_1} \sum_{j=1}^{N_2} v(z_{\underline{j}}) \phi_i^{(1)}(x) \phi_j^{(2)}(y) .$$

Thus the tensor product $\{\phi_i^{(1)}(x)\phi_j^{(2)}(y)\}$ of one dimensional basis gives a basis in two dimensions.

Observe that clearly each $v \in V$ is continuous, that there are functions in V with discontinuous gradients and the order of accuracy is 4.

The first impression one may have of the Lagrange cubic element is the rather large number of unknowns, in fact 16, per rectangle. Historically this generated an interest in finding new cubic elements having fewer unknowns. The elements that resulted from this search are given the name serendipity. There exists a systematic mathematical derivation of the so-called serendipity element, we refer the interested reader to [11].

b) The Lagrange cubic elements defined above are only C^0. In order to obtain C^1 (continuous first derivatives) cubic suitable for fourth order partial differential equations the so-called Hermite elements, whose nodal structure involves not only function values but also derivatives, are constructed. As observed earlier, 16 conditions determine a bicubic of the form

$$\sum_{i=0}^{3} \sum_{j=0}^{3} \alpha_{ij} x^i y^j \tag{22}$$

in a rectangle. In what follows the redundant terms in eq. (22) are exploited so as to obtain an element with extra smoothness.

Consider the difference V between two polynomial representations P_1 and P_2 along a line L (varying only in y) joining two adjacent rectangles, say $R_j (j=1,2)$. For C^0 continuity $P_1 = P_2$ on L and for C^1 continuity

$$\frac{\partial P_1}{\partial y} = \frac{\partial P_2}{\partial y}$$

on L. To achieve C^1 continuity something about the first derivatives of v on L must be specified. Suppose v, $\frac{\partial v}{\partial x}$ (by symmetry) $\frac{\partial v}{\partial y}$ are specified at the nodes A and B, the end points of the line L. This implies that $P_1 = P_2$, $\frac{\partial P_1}{\partial x} = \frac{\partial P_2}{\partial x}$ and $\frac{\partial P_1}{\partial y} = \frac{\partial P_2}{\partial y}$ at A and B. Since $P_1 - P_2$ is cubic (in y along L) from the first and the last of the above conditions $P_1 \equiv P_2$ on L. Observe that $\frac{\partial}{\partial x}[P_1 - P_2]$ is also a cubic on L which vanishes at A and B. If

$$\frac{\partial}{\partial y}\left[\frac{\partial}{\partial x}(P_1 - P_2)\right] = 0 \text{ , at A and B}$$

then $\frac{\partial P_1}{\partial x} = \frac{\partial P_2}{\partial x}$. Thus $\frac{\partial^2 v}{\partial x \partial y}$ is also specified at all nodes, which gives four conditions per node and sixteen conditions per rectangle. Thus, a cubic of the form (22) is uniquely determined in any rectangle. Therefore any function v in the set of C^1 functions V which reduces to a cubic of the form (22) on each rectangle R_i $1 \le i \le M$ is uniquely determined by values v, $\frac{\partial v}{\partial x}$, $\frac{\partial v}{\partial y}$, and $\frac{\partial^2 v}{\partial x \partial y}$ at the vertices of the rectangles. Moreover, a basis for V is obtained by successively setting one of the nodal conditions equal to one and the others equal to zero. Thus at each node a_j there are four functions $\phi_j^{(\alpha,\beta)}$, $0 \le \alpha, \beta \le 1$ such that

$$\frac{\partial^{\alpha^i+\beta^i}}{\partial x^{\alpha^i} \partial y^{\beta^i}} \phi_j^{(\alpha,\beta)}(\underline{a}_\ell) = \begin{cases} 0 & j \neq \ell \text{ or } (\alpha^i,\beta^i) \neq (\alpha,\beta) \\ 1 & j = \ell \text{ and } (\alpha^i,\beta^i) = (\alpha,\beta) \end{cases} .$$

It is easy to see that the function $\phi^{(\alpha,\beta)}(x,y)$ is of the form

$$\phi^{(\alpha,\beta)}(x,y) = \phi^{(\alpha)}(x) \cdot \phi^{(\beta)}(y) .$$

3.4.2. Cubics in Triangles - Let

$$\bar{\Omega} = \bigcup_{i=1}^{m} T_i ,$$

where $T_1, \ldots, T_m$ are triangles.

a) The first type of elements to be considered are Lagrange cubics. As before, the space V must contain at least continuous functions. Furthermore, the cubic will have a local representation of the form

$$\sum_{i+j \le 3} a_{ij} x^i y^j \tag{23}$$

with total degree 3.

Along any line joining two adjacent triangles the difference between two representations of the form (23) will be a cubic. For this difference to vanish identically on this line it must vanish at four points. Hence, four nodes on each side of a triangle or nine nodes per triangle are needed. The representation (23) contains ten constants, thus an additional condition is needed. The choice of this extra nodal condition is somewhat arbitrary and usually the centroid of the triangle is taken for the additional node.

Let V be the set of all continuous functions in Ω which reduce to cubics of the form (23) in each T_i. Denote by $a_1, \ldots, a_N$ all the vertices, centroid and the points on the side of each triangle. Then any $v \in V$ is uniquely determined by the values of $\alpha_j(v) = v(a_j)$, and any such v can be written

$$v(x,y) = \sum_{j=1}^{N} \alpha_j(v) \phi_j(x,y) ,$$

where $\phi_j \in V$ satisfies $\phi_j(\alpha_\ell) = \delta_{j\ell}$.

b) The final cubic elements are the Hermite cubics on triangles. As in the

rectangular case, the Hermite cubic elements are a proper subspace of the Lagrange elements. However, they have continuous derivatives only at isolated points and not everywhere in $\tilde{\Omega}$, that is, they are not C^1.

In particular, the nodal configuration normally used for the Hermite cubic is to assign v, $\frac{\partial v}{\partial x}$, $\frac{\partial v}{\partial y}$ at the vertices of all triangles and the value of of v at the centroids. Observe that with this nodal assignment v and its first derivatives are continuous at the vertices of the triangles, and this in turn implies that v is continuous in Ω but not C^1. In fact, on the line L joining any two triangles T_i, T_j the difference of the respective cubic representations $P_i - P_j$ is a cubic which vanishes at the two vertices along L. In addition, having specified all first order derivatives of v at the points, the tangential derivatives of $P_i - P_j$ is zero at the vertices and hence $P_i - P_j = 0$ on the line L. Observe that the derivative of $P_i - P_j$ normal to L also vanishes at the vertices. However, the normal derivative of $P_i - P_j$ is quadratic and one other condition is needed. This condition, which comes from the centroid, is not the same for the two triangles. Hence the normal derivative is discontinuous.

To summarize: Let $\xi_1,\ldots,\xi_N$ denote the set of vertices of the triangle $T_1,\ldots,T_m$. Let V denote the set of all continuous functions which reduce to cubics of the form (23) in each triangle T_i, $1 \le i \le M$, and whose first derivatives are continuous at $\xi_1,\ldots,\xi_N$. Then each $v \in V$ is uniquely determined by the following nodal conditions.

i) The assignment of

$$\lambda_{\ell j \alpha_i \beta}(v) = \frac{\partial^{\alpha+\beta}}{\partial x^{\alpha} \partial y^{\beta}} v(\xi_\ell)$$

at each vertex ξ_ℓ with $0 \le \alpha + \beta \le 1$.

ii) The assignment of

$$\lambda_i(v) = v(n_i)$$

at each centroid $n_1, n_2, \ldots, n_m$ of the triangles $T_1, \ldots, T_m$.

There are C^1 cubics which can be defined in triangles, known as the Clough-Toucher element. However, their construction requires a great deal of ingenuity. We refer the interested reader to [12]. All the elements discussed in the previous sections may be found in Figure 3.

3.4.3. Curved Elements (Isoparametric Elements) - In many applications, the necessity arises for the introduction of elements with curved boundaries. The tool used for this is known as isoparametric elements. For the sake of brevity, the discussion is limited to finite elements corresponding to two dimensional Lagrange interpolation elements.

An isoparametric element K [11] may be described as follows. Suppose that there is

i) A set $\tilde{A} = \bigcup_{i=1}^{N} (\tilde{a}_i)$ of N distinct points of $\mathbb{R}^2$.

ii) A finite dimensional space $\tilde{V}$ of functions defined over the closed convex hull $\tilde{K}$ of $\tilde{A}$ with dimension N and such that for every real number a_i there exists a unique $\tilde{v} \in \tilde{V}$ with the property that $\tilde{v}(\tilde{a}_i) = \alpha_i$ $1 \le i \le N$.

iii) A set $A = \bigcup_{i=1}^{N} \{a_i\}$ of N distinct points in $\mathbb{R}^2$.

Then the finite element K is the image

$$K = F(\hat{K})$$

of the set $\hat{K}$ under the unique mapping $F : \hat{K} \to R^2$, which satisfies

$$F(\tilde{a}_i) = a_i, \quad 1 \le i \le N \quad (F(\tilde{x},\tilde{y}) = (F_i(\tilde{x},\tilde{y}), (F_i(\tilde{x},\tilde{y}),$$

$$\text{with } F_i(\tilde{x},\tilde{y}) \in \tilde{V}, \ i = 1,2).$$

Observe that by letting $\tilde{v}_i(\tilde{a}_j) = \delta_{ij}$, i.e. $\{\tilde{v}_i\}_{i=1}^{N}$ is a basis for $\tilde{V}$, then the mapping F is given by $F = \sum_{i=1}^{N} \tilde{v}_i a_i$.

Thus, one may associate with the finite element K the N dimensional space

$$V = \{v : K \to \mathbb{R} \ , \ v = \tilde{v} \circ F^{-1} \ , \text{ for all } \tilde{v} \in \tilde{V}\} \ .$$

Note that the restriction to the set K of the trial functions corresponding to a triangulation T_h containing the element K belongs to the space V and $\tilde{v}(\tilde{x},\tilde{y}) = v(x,y)$, for every $(\tilde{x},\tilde{y}) \in \tilde{K}$, $(x,y) \in K$, $\tilde{v} \in \tilde{V}$, and $v \in V$.

In practice there are two types of isoparametric elements which are commonly used, namely the triangular and quadrilateral finite elements. These will be illustrated by example. The first two examples deal with triangular isoparametric elements.

Example 1: Let $\tilde{A}$ be a non degenerate triangle in R^2 with the vertices $\{\tilde{a}_i\}_{i=1}^3$. where $\tilde{a}_1 = (1,0)$, $\tilde{a}_2 = (0,1)$, $\tilde{a}_3 = (0,0)$. Let $\tilde{V}(m)$ denote the space of all functions $\tilde{v}$ which reduces to a polynomial of degree $\leq m$ in the variable x,y on K . Then for every number α_i there exists a function $\tilde{v}_i \in \tilde{V}(1)$ such that $\tilde{v}_i(\tilde{a}_j) = \delta_{ij}$. Thus the isoparametric element obtained is the triangle

$$K = F(\hat{K}) \ ,$$

with vertices a_i , where $F = \sum_{i=1}^{3} \tilde{v}_i a_i$, (Figure 4).

Example 2: Let

$$\tilde{A} = \{\tilde{a}_i\}_{i=1}^3 \cup \{\tilde{a}_{ij}\},$$

where a_{ij} denotes the midpoint of the side with the endpoints a_i and a_j . As before it can easily be seen that there exist $\tilde{v}_i \subset \tilde{V}(2)$ such that $\tilde{v}_i(a_j) = \delta_{ij}$.

The boundary of the element $K = F(\hat{K})$ (Figure 5) in this case admits a parametric polynomial representation of degree ≤ 2 . In fact they are in general arcs of a parabola. In the special case when the three points a_i, a_{ij} and a_j are on the same line the corresponding arc is a straight line.

The final two examples deal with quadrilateral isoparametric elements.

Example 3: Let

$$\tilde{A} = \{\tilde{a}_i\}_{i=1}^4 = \{(0,0) \ , \ (1,0) \ , \ (1,1) \ , \ (0,1)\} \ .$$

It has been shown previously that there exists a basis in the finite element space of functions which reduce to bilinear functions (Sec. 3.31). In fact,

$$(\tilde{v}_i(\tilde{x},\tilde{y})_{i=1}^4) = \{v_1(\tilde{x},\tilde{y}) = (1-\tilde{x})(1-\tilde{y}) \ , \ v_2(\tilde{x},\tilde{y}) = \tilde{x}(1-\tilde{y}) \ ,$$

$$v_3(\tilde{x},\tilde{y}) = \tilde{x}\,\tilde{y} \ , \ v_4(\tilde{x},\tilde{y}) = (1-\tilde{x})\tilde{y}\}$$

Let $\tilde{v} = \{\tilde{v} | \tilde{v}$ is bilinear on $\tilde{K}\}, F=(F_1,F_2)$, $F_i \in \tilde{V}$ and $F(\tilde{a}_j) = a_j$, $j = 1, 2, 3, 4$. The isoparametric element K is by definition the image under F of $\tilde{K}$. The restriction of F to a side of $\tilde{K}$ depends only on one variable. Consequently the mapping F is an affine mapping and the image of $\tilde{K}$ is a straight line, (Figure 6a). Thus an arbitrary quadrilateral may be considered as an isoparametric finite element.

Example 4: Let

$$\tilde{A} = \{\tilde{a}_i\}_{i=1}^9 = \{(0,0), (1,0), (1,1), (0,1), (1/2,0), (1,1/2),$$

$$(1/2,1),(0,1/2), (1/2,1/2)\} \ .$$

It is easily seen that the function $\{\tilde{v}_i\}_{i=1}^9$ with

$$\tilde{v}_1(\tilde{x},\tilde{y}) = (1-\tilde{x})(1-2\tilde{x})(1-\tilde{y})(1-2\tilde{y})$$

$$\tilde{v}_2(\tilde{x},\tilde{y}) = (1-\tilde{y})(1-2\tilde{y})\tilde{x}(2\tilde{x}-1)$$

$$\tilde{v}_3(\tilde{x},\tilde{y}) = \tilde{x}(2\tilde{x}-1)\tilde{y}(2\tilde{y}-1)$$

$$\tilde{v}_4(\tilde{x},\tilde{y}) = \tilde{y}(2\tilde{y}-1)(1-\tilde{x})(1-2\tilde{x})$$

$$\tilde{v}_5(\tilde{x},\tilde{y}) = -\,4(1-\tilde{x})(-\tilde{x})(1-\tilde{y})(1-2\tilde{y})$$

$$\tilde{v}_6(\tilde{x},\tilde{y}) = -\,4(1-\tilde{y})(-\tilde{y})\tilde{x}(2\tilde{x}-1)$$

$$\tilde{v}_7(\tilde{x},\tilde{y}) = 4\tilde{x}(1-\tilde{x})\tilde{y}(2\tilde{y}-1)$$

$$\tilde{v}_8(\tilde{x},\tilde{y}) = 4\tilde{y}(1-\tilde{y})(1-\tilde{x})(1-2\tilde{x})$$

$$\tilde{v}_9(\tilde{x},\tilde{y}) = 16\tilde{x}\tilde{y}(1-\tilde{x})(1-\tilde{y}) ,$$

form a basis for the finite element space of funcitons which reduce to biquadratics on $\tilde{K}$. Let $A = \{a_i\}_{i=1}^9$ be arbitrary points in R^2 and define the mapping F by

$$F = \sum_{i=1}^{9} \tilde{u}_i \tilde{v}_i (\tilde{x},\tilde{y}) a_i .$$

Then the isoparametric finite element K is given by $F(\tilde{K})$ (Figure 6b). Note that the sides of K are parabolic arcs in general. They are straight lines if and only if three points are on a line, i.e. only if the mapping F is affine.

IV. Implementation

In order to clarify the concepts introduced in the previous sections an example of an application of the finite element method is now examined.

Let $\Omega = [0,1] \times [0,1]$ and Γ its boundary. Consider the problem

$$-\Delta u = f \quad \text{in} \quad \Omega \tag{24}$$

$$u = 0 \quad \text{on} \quad \Gamma . \tag{25}$$

The following steps must be carried through in order to apply the finite element method.

1) Give an equivalent variational formulation to (24), (25).

2) Define the subdivision of the domain into elements. That is, for each element give the type of element, the nodes associated with that element, the nodes relative connectivity, and the type of piecewise polynomial to be used.

3) Form the local stiffness matrix and local right hand side for each element.

4) Assemble the local stiffness matrix and local right hand sides into the global stiffness matrix and right hand side.

5) Solve the resulting linear system for the coefficients in the finite element approximation.

Steps (1)-(5) are now applied in detail for equations (24) and (25).

1) For this problem a variational principle was given in section 2. This principle was find $u \in H_0^1(\Omega)$ such that

$$a(u,v) = \int_\Omega \left(\frac{\partial u}{\partial x}\frac{\partial v}{\partial x} + \frac{\partial u}{\partial y}\frac{\partial v}{\partial y}\right)d\Omega = \int_\Omega (fv)d\Omega = f(v) , \text{ for all } v \in H_0^1(\Omega) , \tag{26}$$

As stated in the previous section the bilinear form $a(u,v)$ is used to form the stiffness matrix and the linear functional $f(v)$ forms the right hand side. However, before this can be done, step 2 of the procedure must be completed.

2) For this problem divide the domain into squares of side h and divide each square in half down its diagonal to obtain triangles (Figure 7). This process creates two types of triangles, each with its own local node numbering and local basis functions (Figure 8). For this problem piecewise linear basis functions have been chosen. The information needed for each element in Figure 7 is the type of triangle, the nodes in the element, and finally their connectivity, that is, the global node number associated with the local node numbers of the element. This information is given in Table 1.

As stated above piecewise linear polynomials have been chosen as our basis functions. The approximate solution u^h is then represented as

$$u^h(x,y) = \sum_{i=1}^{N} u_i \phi_i(x,y) , \tag{27}$$

where N is the number of nodes, $\phi_i(x,y)$ is the piecewise linear function which is one at the i^{th} node and zero at all other nodes, and u_i is the value of u at the i^{th} node.

Substituting (27) into (26) and setting $v = \phi_j$, $j = 1,\ldots,N$, the global stiffness matrix and right hand side are

$$A = (a_{ij}) = a(\phi_i,\phi_j) \tag{28}$$

$$F = (f_j) = f(\phi_j) \tag{29}$$

However, performing the integrations over the whole domain is complex and unnecessary. The integrals in (26) may be represented as the sum of integrals over each of the

elements. Thus, local stiffness matrices and local right hand sides must be computed for each element.

3) To compute the local stiffness matrix for the m^{th} element a local approximation is used. Denote this approximation by

$$u_m^h = \bar{\phi}^T \cdot \bar{u}_m \ , \tag{30}$$

where $\bar{\phi}^T = (\phi_1, \phi_2, \phi_3)$ are the local basis functions given in Figure 8 and

$$\bar{u}_m = \begin{pmatrix} u_1 \\ u_2 \\ u_3 \end{pmatrix}_m$$

are the values of the coefficients u_i in the m^{th} element. Note that the subscripts (1,2,3) represent the local node numbering. Also note that u_m^h is a scalar quantity and may be commuted with any vector quantity. Substituting (30) into (26) and setting $v = \bar{\phi}$ the local stiffness matrix is defined by

$$\int_{E_m} [\frac{\partial}{\partial x} (\bar{\phi}^T \bar{u}_m) \frac{\partial \bar{\phi}}{\partial x} + \frac{\partial}{\partial y} (\bar{\phi}^T \bar{u}_m) \frac{\partial \bar{\phi}}{\partial y}] dEm$$

$$= (\int_{E_m} [\frac{\partial \bar{\phi}}{\partial x} \frac{\partial \bar{\phi}^T}{\partial x} + \frac{\partial \bar{\phi}}{\partial y} \cdot \frac{\partial \bar{\phi}^T}{\partial y}]_{dE_m}) \cdot \bar{u}_m = LS_m \cdot \bar{u}_m \ .$$

The elements of the matrix LS_m defined by the terms within the integral are

$$LS_{ij} = \int_{E_m} (\frac{\partial \phi_i}{\partial x} \frac{\partial \phi_j}{\partial x} + \frac{\partial \phi_i}{\partial y} \frac{\partial \phi_j}{\partial y}) dE_m \qquad 1 \le i, j \le 3 \ . \tag{31}$$

The local stiffness matrix for type 1 and type 2 triangles is given in table 2.

A similar procedure is used to compute the local right hand side, that is

$$\vec{LF} = \int_{E_m} (f \cdot \bar{\phi}) dE_m \ . \tag{32}$$

Note that the integrations in (31) and (32) are actually performed by numerical quadrature [13].

4) The local stiffness matrices and local right hand sides must now be combined to form the global stiffness matrix and right hand side. This procedure is known as the assembly procedure. The information needed to carry out this procedure is contained in Table 1. In order to illustrate how this procedure is carried out the local stiffness matrices of element 4 and element 10 are assembled into the global stiffness matrix. To initialize the assembly procedure set all members of the global stiffness matrix A equal to zero. Checking element 4 in Table 1, it is a type 2 triangle so the local stiffness matrix (LS_2) for type 2 triangles is used. Now, go through each member of LS_2 and use Table 1 to find its corresponding place in A . For example, the (2,2) entry in LS_2 corresponds to the (1,1) entry in A. Hence

$$A(1,1) = A(1,1) + LS_2(2,2) = 1$$

Similarly the (2,1) entry of LS_2 corresponds to the (1,2) entry of A . Note that the (2,3) entry of LS_2 is matches with the (1,0) entry of A , that is, this entry corresponds to a boundary node and is discarded.

Checking element 10 in Table 1 finds that it is a type 1 triangle, thus LS_1 is used. In this case the (1,1) entry of LS_1 corresponds to the (1,1) entry of A . So this entry is added to what was previously placed in A when element 4 was examined, that is

$$A(1,1) = A(1,1) + LS_1(1,1) = 1 + 1/2 = 3/2 \ .$$

When this process is completed for all the elements the matrix A will be completed (Table 3). A similar procedure is performed to form the right hand side F .

5) It is now necessary to solve the linear system that has been created,

$$A\bar{u} = F \ ,$$

for the vector of coefficients $\bar{u}$. Note from the structure of A that it is a sparse banded matrix. Thus, a sparse linear equation solver may be used. However, one may also use iteration techniques for such a system. For sparse matrix methods see [14] and for

a survey on iterative methods for linear systems see [15].

V. Time Dependent Problems

The formulation of the finite element method in the preceding sections has dealt solely with stationary problems, that is, time dependence has not been considered. However, many problems in fluid dynamics do involve time, so it is necessary to see how time dependence is handled.

By using the method of weighted residuals (or other variational formulations [16]) it is possible to include time dependence in the variationsl principle, thus implying the definition of finite elements in space-time and basis functions depending on a time coordinate [17], [18]. However, this approach is seldom applied. Rather, the technique that is generally adopted for time dependent problems consists in using purely geometrical elements in the space coordinates and letting the nodal values depend on time. That is, instead of equation (27) the approximate solution $u^h(x,y,t)$ is defined by

$$u^h(x,y,t) = \sum_{i=1}^{N} u_i(t) \cdot \phi_i(x,y) \tag{33}$$

Let $\Omega \subset R^2$ and Γ its boundary. Consider the problem

$$\frac{\partial u}{\partial t} + Lu = f(x,y,t) \quad \text{in} \quad \Omega \times (0,T] \tag{34}$$

$$u(\cdot,t) = 0 \quad \text{on} \quad \Gamma \times (0,T] \tag{35}$$

$$u(x,y,0) = 0 \quad \text{in} \quad \bar{\Omega} \ , \tag{36}$$

where Lu is a second order operator for which an equivalent bilinear form $a(u,v)$ exists.

An equivalent problem to (34), (35), (36) is then find $u \in H_0^1(\Omega) \times L_2(o,T)$ such that

$$\int \frac{\partial u}{\partial t} \cdot v d\Omega + a(u,v) = \int_{\Omega} fv \quad \text{for all} \quad v \in H_0^1(\Omega) \tag{37}$$

$$u(x,y,0) = 0 \ . \tag{38}$$

If u^h is given by (33) and $v = \phi_j$ $(1 \leq j \leq N)$, is substituted in (37) and (38) then instead of the usual linear system to be solved the following ordinary differential equation (ODE) is obtained

$$M\frac{d\bar{u}}{dt} + A\bar{u} = \bar{f}(t) \tag{39}$$

$$\bar{u}(0) = 0 \ , \tag{40}$$

where A is the usual stiffness matrix, $\bar{F} = \int_{\Omega} f \cdot \phi_j d\Omega)$, and $\bar{u}(t)$ is the vector of coefficients.

The matrix M in (39) is known as the mass matrix and is defined by

$$M_{ij} = \int_{\Omega} \phi_i \cdot \phi_j d\Omega \ . \tag{41}$$

The system of ordinary differential equations (39), (40) can now be integrated with the usual finite difference methods. Before considering one such method note the following:

1) In the usual formulation of ODE's the matrix multiplying the derivative is a diagonal matrix. However, the mass matrix M in general has the same structure as the stiffness matrix A . For some sets of basis functions it is possible (without any loss of accuracy) to perturb the mass matrix so that it is diagonal. This procedure is known as lumping.

2) The advantage of lumping is that when an explicit method of integration is chosen there is no need to perform any matrix inversion. However, when an explicit method is used there is usually a restrictive stability condition of the form

$$\frac{\Delta t}{h^2} \leq c \ , \quad c \leq 0 \ ,$$

where h is an average mesh size. Thus, in general, implicit type methods are used and there is no noeed to lump.

The method of integration most widely used is the Crank-Nicolson method. This method applied to equation (39) is

$$M\,\frac{(\bar{u}^{n+1}-\bar{u}^{n})}{\Delta t} = -A\,\frac{(\bar{u}^{n+1}+\bar{u}^{n})}{2} + \frac{\bar{F}^{n+1}+\bar{F}^{n}}{2}$$

or

$$(M + \frac{\Delta t}{2} A)\bar{u}^{n+1} = (M - \frac{\Delta t}{2} A)\bar{u}^{n} + \frac{\Delta t}{2}(\bar{F}^{n+1}+\bar{F}^{n}) \tag{42}$$

Note that:

1) The solution of (42) requires the solution of a linear system of equations on each step. However, if M and A do not depend on time, then the extra work involved here is not that great.

2) The Crank-Nicolson method is second order accurate and unconditionally stable. Therefore, there is no restriction on the size of Δt .

Part II - Application to Fluid Mechanics

The purpose of this second part is to see how the finite element method is applied to two problems in fluid mechanics. The first problem to be considered is the two dimensional boundary layer equations. The reason for examining this problem is to see how in one particular instance the finite element method may be applied if the equations are nonlinear. The implementation of the method presented here was taken from Popinski and Baker [19]. No specific computational results are given, only the implementation of the method and some general comments on how well the method worked.

The second problem to be considered is one in which there is presently a great deal of activity. This problem is the solution of the equations of transonic flow by the finite element method. The major difficulties in solving the equations of transonic flow are the change of type of the equation, from supersonic (hyperbolic) to subsonic (elliptic), and the existence of a shock. Many different approaches for the solving of these problems have appeared recently [20], [21], [22], [23], [24], [25]. Three of these methods are highlighted here. Those of Chan, Brashears, and Young; Chung and Hooks; and Aziz and Leventhal.

VI. Two Dimensional Boundary Layer Equations

In this section the implementation of the finite element method for the two dimensional equations of incompressible boundary layer flow with zero pressure gradient is considered. The boundary layer equations are

$$L_1(u) = u\,\frac{\partial u}{\partial x} + v\,\frac{\partial u}{\partial y} - \frac{1}{\rho}\,\frac{\partial}{\partial y}(\mu\,\frac{\partial u}{\partial y}) = 0 \ , \quad \text{in} \quad \Omega \tag{43}$$

$$L_2(v) = \frac{\partial u}{\partial x} + \frac{\partial v}{\partial y} = 0 \ , \quad \text{in} \quad \Omega \tag{44}$$

where $\Omega = [x_0,\infty) \times [0,\delta m]$, δm is the maximum boundary layer thickness, u and v are the unknown velocities, ρ is the constant density, and $\gamma = \mu/\rho$ is the kinematic viscosity. Due to the nature of the equations the x-variable is a marching or time like variable, and the y variable is a space variable. Thus, it is necessary to specify boundary and initial conditions for u and v to complete the system. The boundary conditions are

$$\left.\begin{aligned} u(x,0) &= 0 \\ v(x,0) &= 0 \\ \frac{\partial u}{\partial y}(x,\delta_m) &= 0 \end{aligned}\right\} \ . \tag{45}$$

The initial conditions are

$$\left.\begin{aligned} u(x_0,y) &= u_0(y) \\ v(x_0,y) &= v_0(y) \end{aligned}\right\} \tag{46}$$

The method of solution of this system of equations may be outlined as follows:

1) Apply the method of weighted residuals to equation (43) using only one-dimensional piecewise linear elements (in the y variable) to obtain a system of nonlinear ordinary differential equations for u .

2) Use Crank-Nicolson time differencing to obtain a nonlinear system of equations to be solved on each time step.

3) Iterate the solution of the above system with integration of equation (44) by the trapezoidal rule.

In order to apply the method of weighted residuals to equation (43) multiply by a

function $\psi \in H^1(0,\delta_m)$ with $\psi(0) = 0$ (denote this space by $\bar{H}^1$) and integrate by parts to obtain the equations

$$\int_0^{\delta_m} u \frac{\partial u}{\partial x} \cdot \psi dy + \int_0^{\delta_m} [v \frac{\partial u}{\partial y} \psi + \gamma \frac{\partial u}{\partial y} \frac{\partial \psi}{\partial y}] dy = 0 \text{ , for all } \psi \in \bar{H}^1 . \tag{47}$$

The interval $[o,\delta_m]$ is divided into equal segments of length h and piecewise linear elements are used. Globally the approximations to u, v, ν (u^h, v^h, ν^h) are represented as

$$\left.\begin{aligned} u^h &= \sum_{i=1}^{N} u_i(x)\phi_i(y) \\ v^h &= \sum_{i=1}^{N} v_i(x)\phi_i(y) \\ \gamma^h &= \sum_{i=1}^{N} \gamma_i(x)\phi_i(y) \end{aligned}\right\} . \tag{48}$$

(Note that the $\gamma_i(x)$ are known.) However, over the m^{th} element this representation is

$$\left.\begin{aligned} u_m^h &= \bar{\phi}^T \cdot \bar{u}_m = \bar{u}_m^T \cdot \bar{\phi} \\ u_m^h &= \bar{v}_m^T \cdot \bar{\phi} \\ \gamma_m^h &= \bar{\gamma}_m^T \cdot \bar{\phi} \end{aligned}\right\} , \tag{49}$$

where $\bar{\phi} = (\phi_2^1)$ is the basis of linear functions for an element, and $\bar{u}_m = (u_2^1)_m$, $\bar{v}_m = (v_2^1)_m$ and $\bar{\nu}_m = (\gamma_2^1)_m$ are the values of u_i, v_i, ν_i respectively for the nodal points of the m^{th} element. Substituting (49) into (47) and setting $\psi = \bar{\phi}$ a local equation for the m^{th} element is obtained

$$\begin{aligned} &\bar{u}_m^T \left(\int_{E_m} \bar{\phi}\,\bar{\phi}\,\bar{\phi}^T dy\right) \frac{\partial \bar{u}_m}{\partial x} + v^T \left(\int_{E_m} \bar{\phi}\,\bar{\phi}\,\frac{\partial}{\partial y}\,\bar{\phi}^T dy\right)\bar{u}_m \\ &+ \bar{\gamma}_m^T \left(\int_{E_m} \bar{\phi}\,\frac{\partial \bar{\phi}}{\partial y}\,\frac{\partial \bar{\phi}^T}{\partial y}\, dy\right)\bar{u}_m = 0 . \end{aligned} \tag{50}$$

To help explain how nonlinear terms are handled the first term in equation (50) is derived. From equation (47) the term to be computed is

$$\begin{aligned} \int_{E^m} (\bar{\phi} u_m^h \frac{\partial u_m^h dy}{\partial x}) &= \int_{E_m} (\bar{\phi}(\bar{\phi}^T \cdot \bar{u}_m)(\bar{\phi}^T \frac{\partial \bar{u}}{\partial x}\, m) dy) \\ &= \int_{E^m} ((\bar{u}_m^T \cdot \bar{\phi})\bar{\phi}\,\bar{\phi}^T) dy \frac{\partial}{\partial x}\,\bar{u}_m = \bar{u}_m^T \left(\int_{E_m} \bar{\phi}\,\bar{\phi}\,\bar{\phi}^T dy\right) \frac{\partial \bar{u}_m}{\partial x} . \end{aligned}$$

In the linear examples studied previously when integrations were performed on a single element a local stiffness matrix was obtained. The integrals in equation (50) also represent local matrices. However, the entries in these matrices are vectors. That is, equation (50) becomes

$$\begin{aligned} &\bar{u}_m^T \frac{h}{12} \begin{bmatrix} (3_1) & (1_1) \\ (1_1) & (1_3) \end{bmatrix} \frac{\partial}{\partial x}\,\bar{u}_m + \bar{v}_m^T \cdot \frac{1}{6} \begin{bmatrix} (-2_{-1}) & (2_1) \\ (-1_{-2}) & (1_2) \end{bmatrix} \bar{u}_m \\ &+ \bar{\gamma}_m^T \frac{1}{h} \begin{bmatrix} (1_1) & (-1_{-1}) \\ (-1_{-1}) & (1_1) \end{bmatrix} \bar{u}_m = 0 \end{aligned} \tag{51}$$

Assemblying equation (51) over all the elements a nonlinear ordinary differential equation is obtained.

$$\left[(u_{n-1}+u_n)\frac{du_{n-1}}{dx} + (u_{n-1}+6u_n+u_{n+1})\frac{du_n}{dx} + (u_n+u_{n+1})\frac{du_{n+1}}{dx}\right]$$

$$= \frac{6}{h^2}\left[(\gamma_{n-1}+\gamma_n)u_{n-1} - (\gamma_{n-1}+2\gamma_n+\gamma_{n+1})u_n + (\gamma_n+\gamma_{n+1})u_{n+1}\right] \qquad (52)$$

$$- \frac{2}{h}\left[-(v_{n-1}+2v_n)u_{n-1} + (v_{n-1}-v_{n+1})u_n + (2v_n+v_{n+1})u_{n+1}\right]$$

There are several ways to lump the left hand side of (52) (and not lose accuracy) so that the form of this side becomes

$$a_n^i \frac{du_n}{dx} . \qquad (53)$$

These are

$$\begin{aligned} &\text{I.} \quad a_n^1 = 2(u_{n-1}+4u_n+u_{n+1}) \\ &\text{II.} \quad a_n^2 = (3u_{n-1}+6u_n+3_{n+1}) \\ &\text{III.} \quad a_n^3 = (u_{n-1}+10u_{n-}u_{n+1}) \\ &\text{IV.} \quad a_n^4 = 12u_n . \end{aligned} \qquad (54)$$

These formulas are the result of various consistent numerical quadrature formulas.

Applying Crank-Nicolson time integration to (52) (or any of the lumped systems) a nonlinear equation of the form

$$a_n u_{n-1}^{i+1} + b_n u_n^{i+1} + c_n u_{n-1}^{i-1} = d_n \qquad (55)$$

is obtained. Here, a_n, b_n, and c_n depend on u_n^i, u_n^{i+1}, γ_n and $v_n^{i+1/2}$. Thus, it is necessary to obtain $v_n^{i+1/2}$. Noting that

$$V_n^{i+1/2} = \frac{1}{2}(v_n^i + v_n^{i+1}) + O(\Delta x^2) .$$

$v_n^{i+1/2}$ is obtained from

$$v_n^{i+1/2} = v_{n-1}^{i+1/2} + h/2\,\Delta x(u_n^i - u_n^{i+1} + u_{n-1}^i - u_{n-1}^{i+1}) \qquad (56)$$

Equation (55) and (56) are solved sequentially in an iterative manner until u_n^{i+1} become stationary.

The method described above was programmed, and computations were made on a test problem which had the Blasius solution. Comparisons of all the finite element methods were made with the Blasius solution and a second order Crank-Nicolson finite difference method. From the studies of accuracy based on velocity and skin friction error of these schemes, it was concluded that the finite element method yields results that are comparable in terms of accuracy and efficiency with the results of the finite difference method.

VII. Transonic Flow

In this final section the solution of transonic flow over an airfoil by finite elements is surveyed. Three examples of finite element implementations are highlighted. The equation that is to be considered throughout is the nondimensionalized small disturbance equation

$$L(\phi) = [I-M_\infty^2-M_\infty^2(1+\gamma)\phi_x]\phi_{xx} + \phi_{yy} = 0 \qquad (57)$$

with boundary conditions

$$\left(1 + \frac{\partial \phi}{\partial x}\right) \frac{dg}{dx} - \frac{\partial \phi}{\partial y} = 0 \quad \text{on the airfoil} \tag{58}$$

$$\left.\begin{aligned} \frac{\partial \phi}{\partial x} &= 0 \\ \frac{\partial \phi}{\partial y} &= 0 \end{aligned}\right\} \quad \text{at infinity} \tag{59}$$

where ϕ is the perturbed velocity potential function, $M_\infty < 1$ is the freestream Mach number, γ is the ratio of specific heats, and g is a function of x defining the geometry of the airfoil.

There are two major problems in the solving of equation (57). The first of these is the change of type of the equation. That is, if the flow is subsonic ($\phi_x<1$) then the equation is elliptic, if the flow is supersonic ($\phi_x>1$) then the equation is hyperbolic, and if $\phi_x = 1$ then the equation is parabolic. The second problem occurs when the flow changes from supersonic to subsonic, a shock wave is formed. Each of the methods to be presented attempts to deal with these problems in a different form. For each of the methods the infinite domain is made finite by taking an asymptotic solution at infinity and matching the solution. Let Ω represent the finite domain and Γ its boundary

The first method is that of Chan, Brashears, and Young [21], [22]. The first step in this method is the choice of the variational formulation for the problem. The method of weighted residuals is used, that is

$$\int_\Omega L(\phi) \cdot K d\Omega\phi = 0 \ . \tag{60}$$

However, there is a small variation. The weight function K is chosen so that

$$K = L(\psi) \ .$$

The variational problem is then to find $\phi \in H^2(\Omega)$ such that

$$\int_\Omega L(\phi) \cdot L(\psi) d\Omega = 0 \ , \quad \text{for all} \quad \psi \in H^2(\Omega) \ ,$$

where $H^2(\Omega)$ is the space of functions with square integrable second derivatives.

Since L is a second order operator it is necessary to choose C^1 elements. Therefore, after dividing the domain into rectangles bicubic hermite elements are used. A nonlinear system of equations is formed which is solved by iteration.

The method as presented here does not converge. However, with a slight alteration the method is successful. Consider the rectangular element (Figure 9) with upwind station I and downwind station II. Before assembling the local stiffness matrix for this matrix into the global stiffness matrix a check is made of the sign of

$$C = 1 - M_\infty^2 - M_\infty^2 (1+\gamma)\phi_x \ . \tag{61}$$

If C is nonpositive for all nodes in the element, the first two rows in the local stiffness matrix will be ignored at assembly. In doing so, the downwind influence on the solution at the upwind station is properly blocked. On the other hand, if the sign of C is positive at any of the four nodes, no special treatment is performed in the analysis. This process is analagous to the well known upwind influence finite difference operator. Thus this method tries to treat the shock wave by a "capturing" technique.

In contrast to the approach of "capturing" the shock presented in the first method, the second method to be presented attempts to induce explicit shock discontinuities freely. This method, due to Chung and Hooks [23], acts through a combination of the variational formulation and the use of a new element.

The method begins with the standard method of weighted residuals. However, at this point the first change occurs. A quadrilateral isoparametric element is used. This element is divided into four quadrants. An independent interpolation of a quadratic basis function ϕ for each quadrant is given. This requires 24 constants to be determined. Using corner nodes, midside nodes, and center nodes 16 constants are determined. The remaining 8 constants are determined by allowing jumps in the first and second derivatives of ϕ at the center node. Thus a discontinuity of the type incurred when a shock wave exists is allowed.

The variational formulation of the problem is now altered so that whenever the coefficient of a discontinuous function is non-zero the Rankine-Hugoniot conditions are imposed at that node. This is done through the use of Lagrange multipliers [26].

The method has been implemented on some preliminary test problems. Initial results are optimistic. However, much work remains to determine the optimal way to handle all of the options present.

The last method to be considered, that of Aziz and Leventhal, is in a very preliminary stage. This method is based on the work of Aziz, Fix, and Leventhal [27] on linear mixed hyperbolic-elliptic problems. The idea of the method is as follows. The function ϕ in equation (57) is a velocity potential, that is, there is a velocity vector $\bar{u} = \begin{pmatrix} u \\ v \end{pmatrix}$ such that

$$\left.\begin{aligned} \phi_x &= u \\ \phi_y &= v \end{aligned}\right\} \quad . \tag{62}$$

Recast equation (57) in terms of u and v

$$[1-M_\infty^2-M_\infty^2(1+\gamma)u]u_x + v_y = 0 \tag{63}$$

Add to equation (63) the equation

$$u_y - v_x = 0 \tag{64}$$

and the boundary conditions

$$(1+u)\frac{dy}{dx} - v = 0 \quad \text{on the airfoil} \tag{65}$$

$$u = v = 0 \quad \text{at infinity} . \tag{66}$$

Equations (63) and (64) are denoted as the first order system $K(\bar{u})$.

The variational principle to be used is the least square variational principle. That is, find $\bar{u} \in \bar{H}$ such that

$$\int_\Omega K(\bar{u}) \cdot K(\bar{v}) = 0 \quad \text{for all } \bar{v} \in \bar{H} , \tag{67}$$

where $\bar{H}$ is the set of vector functions whose components are in $H^1(\Omega)$ and satisfy (65) and (66).

It has been shown on linear problems using linear triangular elements that the above method is able to handle the change of type from elliptic to hyperbolic very well. Whether the method is able to handle shocks has not yet been determined. It is possible that something "special", as in the previous two methods, will have to be done. This is then the direction that future research must take.

Conclusion

In this paper the foundations of the finite element method and its application to two problems in fluid dynamics has been presented. In general the finite element method has been proven to be a very effective method, especially in problems with complex geometries and boundary conditions. However, much work remains in making the method more efficient in time dependent problems, nonlinear problems, and higher space dimensions. Also, much work is needed in the handling of shock waves.

References

[1] R. Courant, "Variational Methods for the Solution of Problems of Equilibrium and Vibrations", Bull. Amer. Math. Soc., 49, 1943, pp. 1-23.

[2] M. J. Turner, R. W. Clough, H. C. Martin, L. P. Topp, "Stiffness and Deflection Analysis of Complex Structures", Journal of the Aero. Sciences, Vol. 23, No. 9, 1956, pp. 805-823.

[3] R. W. Clough, "The Finite Element Method in Plane Stress Analysis", Proceedings of the 2nd Conference on Electronic Computation, American Society of Civil Engineering, Pittsburg, Penn., 1960, pp. 345-378.

[4] J. H. Argyris, Recent Advances in Matrix Methods of Structural Analysis, Pergamon Press, Elmsford, N.Y., 1963.

[5] O. C. Zienkiewicz, Y. K. Cheung, "Finite Elements in the Solution of Field Problems", The Engineer, Sept. 1965, pp. 507-510.

[6] J. T. Oden, Finite Elements of Nonlinear Continua, McGraw-Hill, N. Y., 1972.

[7] I. Babuska, A. K. Aziz, "Lectures on the Mathematical Foundations of the Finite Element Method", Mathematical Foundations of the Finite Element Method with Applications to Partial Differential Equations, A. K. Aziz (ed.), Academic Press, 1972, pp. 1-345.

[8] G. Strang, G. J. Fix, An Analysis of the Finite Element Method, Prentice Hall, 1973.

[9] P. C. Ciarlet, "Numerical Analysis of the Finite Element Method", Séminaire de Mathématicques Supérieures Université de Montréal, 16 June-11 July 1975.

[10] P. A. Raviart, Methods des Elements Finis, Course at the University of Paris VI, 1972.

[11] O. C. Zienkiewicz, The Finite Element Method in Engineering Science (2nd edition), McGraw-Hill, London, 1971.

[12] P. G. Ciarlet, "Sur l'élement de Clough et Toucher", Revue Francaise d'Automatique Informatique Recherch Opérationêlle, R-2, 1974, pp. 19-27.
[13] R. J. Herbolt , M. H. Schultz, R. S. Varga, "Quadrature Schemes for the Numerical Solution of Boundary Value Problems by Variational Techniques", Aeq. Math, 3, 1964, pp. 96-119.
[14] D. J. Rose, R. A. Willoughby (eds.), Sparse Matrices and Their Applications, Plemun Press, 1972.
[15] R. Varga, Matrix Iterative Analysis, Prentice Hall, 1962.
[16] K. O. Friedrichs, "Symmetric Positive Linear Differential Equations", Comm. Pure Appl. Math., 11, 1958, pp. 333-418.
[17] P. LeSaint, "Finite Element Methods for Symmetric Hyperbolic Equations", Numer. Math., 21, 1973, pp. 244-255.
[18] A. K. Aziz, S. H. Leventhal, "Numerical Solution of Linear Partial Differential Equations of Elliptic-Hyperbolic Type", SYNSPADE III, B. Hubbard, ed., Academic Press, 1976, pp. 55-88.
[19] Z. Popinski and A. J. Baker, "An Implicit Finite Element Algorithm for the Boundary Layer Equations", Journal of Computational Physics, 21, 1976, pp. 55-84.
[20] S. T. K. Chan, M. R. Brashears, "Finite Element Analysis of Transonic Flow", Lockheed Technical Report AFFDL-TR-74-11, March 1974.
[21] M. R. Brashears, S. T. K. Chan, and V. Y. C. Young, "Finite Element Analysis of Transonic Flow", International Conference on Computational Methods in Nonlinear Mechanics, September 1974, paper No. L-6.
[22] S. T. K. Chan, M. R. Brashears, V. Y. C. Young, "Finite Element Analysis of Transonic Flow by the Method of Weighted Residuals", AIAA 13th Aerospace Sciences Meeting, Pasadena, Calif., January 1975, AIAA paper 75-79.
[23] T. J. Chung, C. G. Hooks, "Discontinuous Function for Calculations in Transonic Flow", AIAA 9th Fluid and Plasma Dynamics Conference, San Diego, Calif., July 1976, AIAA paper 76-329.
[24] M. M. Hafez, E. M. Murman, L. C. Wellford, "Application of the Finite Element Approach to Transonic Flow Problems", Personal Communication.
[25] M. O. Bristeau, R. Glowinski, O. Pironneau, "Numerical Solution of the Transonic Equation by the Finite Element Method via Optimal Control", to appear Proceedings of Control Theory of Systems Governed by Partial Differential Equations.
[26] I. Babuska, "The Finite Element Method with Lagrangian Multipliers, Tech. Note BN-724, IFDAM, University of Maryland, 1972.
[27] A. K. Aziz, G. Fix, S. Leventhal, "Optimal Error Estimates for Finite Element Approximation for First Order Systems", submitted to SIAM Journal on Numerical Analysis.

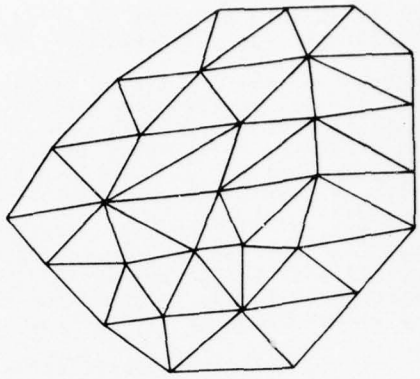

Fig.1 Correct triangulation

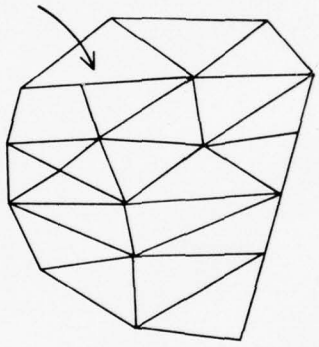

Fig.2 Incorrect triangulation

MASTER CHART

Type	Geometric Structure	Nodal + Polynomial Structure
Linear	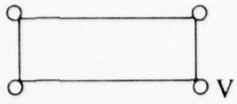	$\sum_{i=0}^{1} \sum_{j=0}^{1} a_{ij} x^i y^j$
	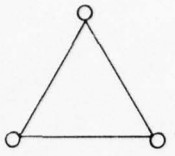	$\sum_{i+j\leq 1} a_{ij} x^i y^j$
Cubic-Lagrange	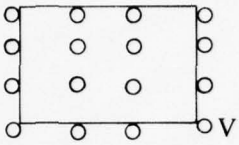	$\sum_{i,j\leq 3} a_{ij} x^i y^j$
Cubic-Serendipity	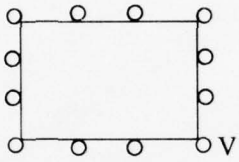	$\sum_{i+j\leq 3} a_{ij} x^i y^j + a_{31} x^3 y + a_{13} x y^3$
Cubic-Hermite	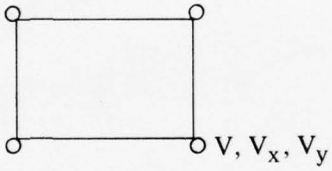	$\sum_{i,j\leq 3} a_{ij} x^i y^j$
Cubic-Lagrange	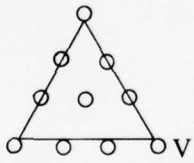	$\sum_{i+j\leq 3} a_{ij} x^i y^j$
Cubic-Hermite	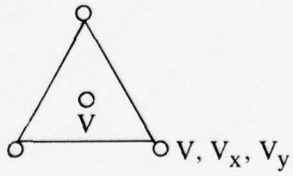	$\sum_{i+j\leq 3} a_{ij} x^i y^j$
Clough-Tucker	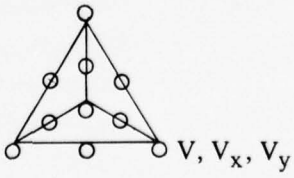	

Figure 3

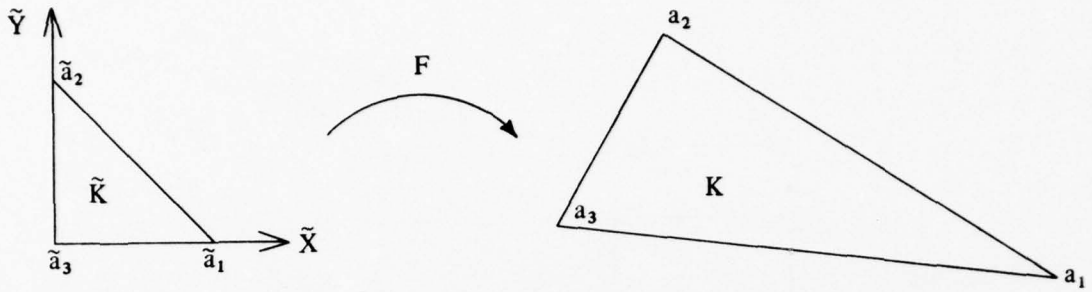

Figure 4

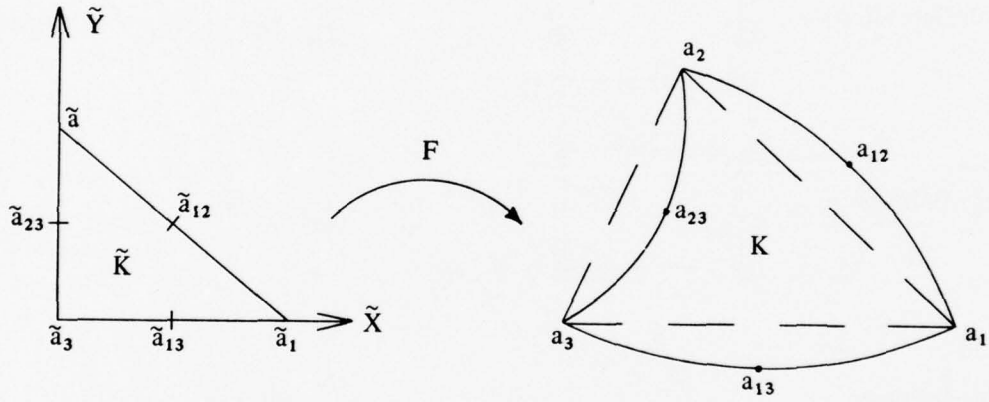

Figure 5

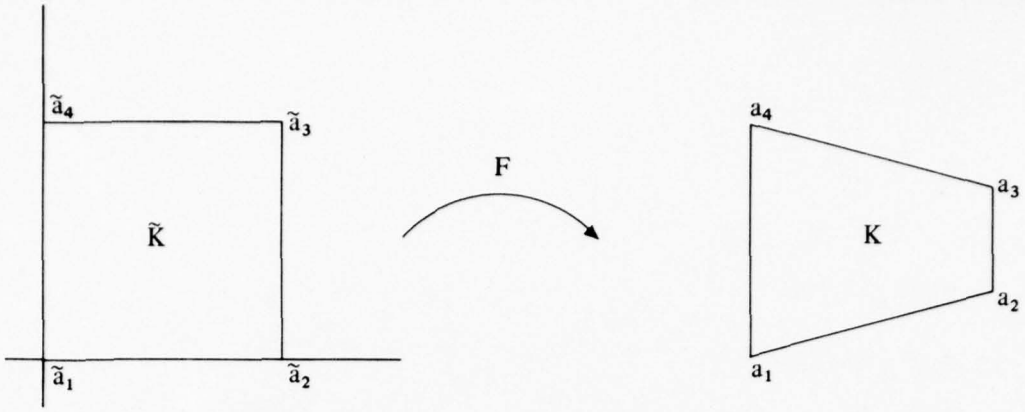

Figure 6(a)

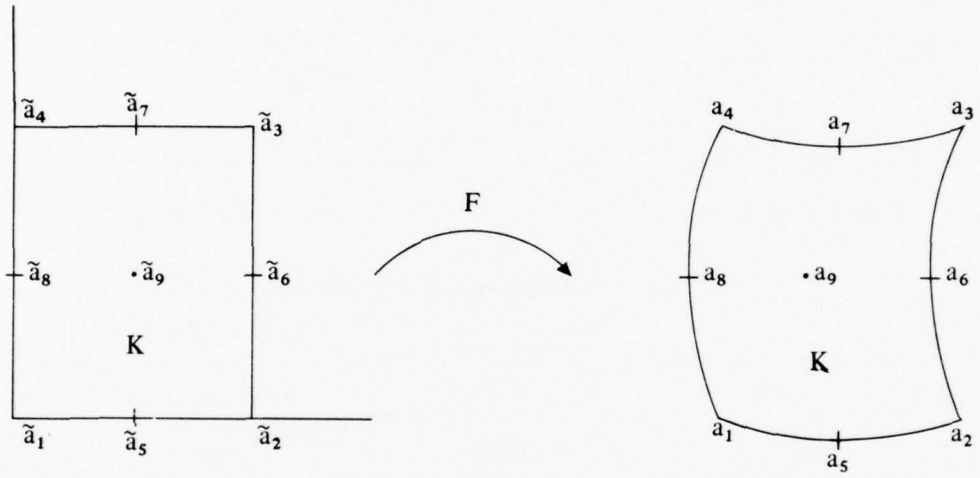

Figure 6(b)

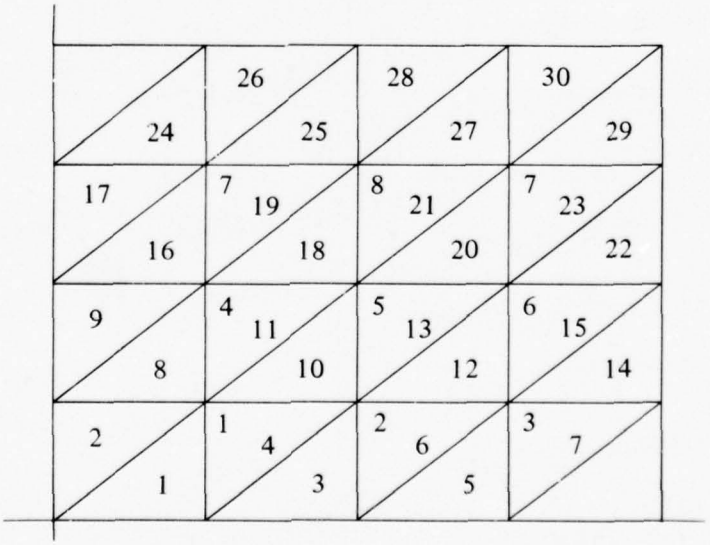

Fig. 7 The domain Ω and its division into elements

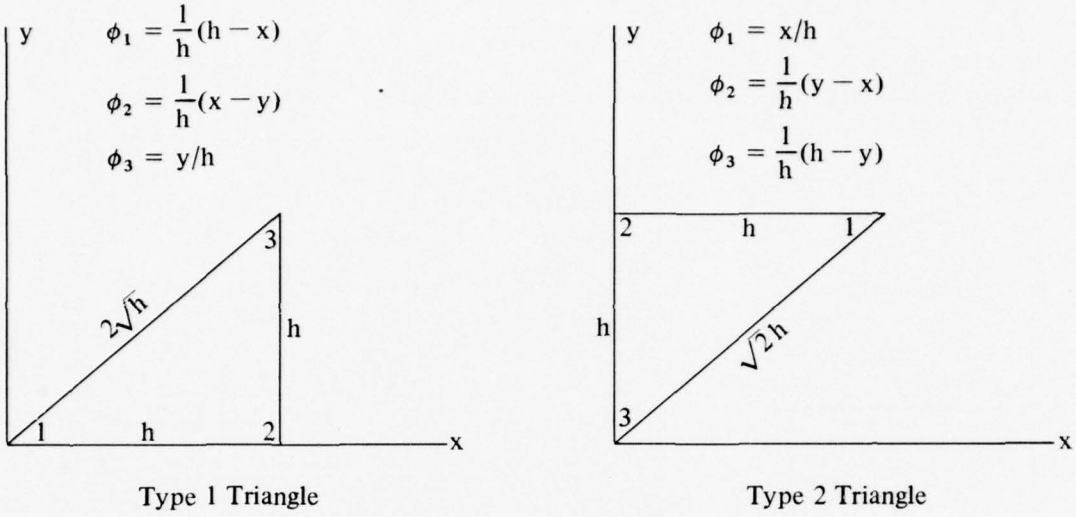

Fig.8 Types of triangles and local basis functions

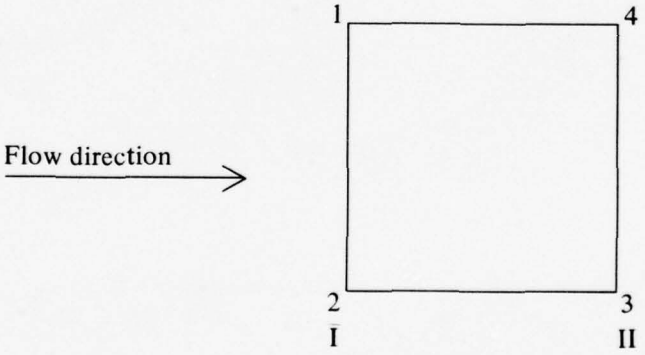

Figure 9

Triangle Information

Triangle number	Type	Node 1	Node 2	Node 3	Triangle number	Type	Node 1	Node 2	Node 3
1	1	0	0	1	16	1	0	4	7
2	2	1	0	0	17	2	7	0	0
3	1	0	0	2	18	1	4	5	8
4	2	2	1	0	19	2	8	7	4
5	1	0	0	3	20	1	5	6	9
6	2	3	2	1	21	2	9	8	5
7	2	0	3	0	22	1	6	0	0
8	1	0	1	4	23	2	0	9	6
9	2	4	0	0	24	1	0	7	0
10	1	1	2	5	25	1	0	0	7
11	2	5	4	1	26	2	7	8	0
12	1	2	3	6	27	1	8	9	0
13	2	6	5	2	28	2	0	0	8
14	1	3	0	0	29	1	9	0	0
15	2	0	6	3	30	2	0	0	9

Table 1

$$LS_1 = \begin{pmatrix} 1/2 & -1/2 & 0 \\ -1/2 & 1 & -1/2 \\ 0 & -1/2 & 1/2 \end{pmatrix} \qquad LS_2 = \begin{pmatrix} 1/2 & -1/2 & 0 \\ -1/2 & 1 & -1/2 \\ 0 & -1/2 & 1/2 \end{pmatrix}$$

Type 1 triangle Type 2 triangle

Local Stiffness Matrices

Table 2

$$\text{Stiffness Matrix} = \begin{pmatrix} A & -I & 0 \\ -I & A & -I \\ 0 & -I & A \end{pmatrix}$$

$$A = \begin{pmatrix} 4 & -1 & 0 \\ -1 & 4 & -1 \\ 0 & -1 & 4 \end{pmatrix}$$

$$I = \begin{pmatrix} 1 & 0 & 0 \\ 0 & 1 & 0 \\ 0 & 0 & 1 \end{pmatrix}$$

$$0 = \begin{pmatrix} 0 & 0 & 0 \\ 0 & 0 & 0 \\ 0 & 0 & 0 \end{pmatrix}$$

Global Stiffness Matrix

Table 3

RECENT ADVANCES IN THE NUMERICAL TREATMENT OF THE NAVIER-STOKES EQUATIONS

Hans J. Lugt
Head, Numerical Mechanics Division
David W. Taylor Naval Ship Research and Development Center
Bethesda, Maryland 20084
USA

SUMMARY

Some recent developments in finite-difference methods for the solution of the Navier-Stokes equations are discussed. Emphasis is placed on the computational difficulties encountered at and near bounding surfaces and in situations of high body acceleration. Physical and numerical aspects of initial and boundary conditions are considered along with their influence on the solutions. Slip and nonslip boundary conditions, their occurrence in reality, their significance in flow modeling, and their effect on the generation and decay of vortices and vorticity are discussed. Recent studies of higher-order approximations and the treatment of boundaries of arbitrary shape by body-fitted coordinate systems are pointed out. The interpretation of time-dependent viscous flows in various reference frames is difficult and necessitates the careful analysis of velocity and vorticity fields. This is demonstrated for flow separation, vortices, and rotating bodies.

LIST OF SYMBOLS

a	focal distance of ellipse	q	heat transfer
$a,\ldots,g$	functions in Eqs. (21) and (23)	r	distance, $r^2 = x^2 + y^2$
c_p	specific heat	Re	Reynolds number
C_D	drag coefficient	Ro	Rossby number $= 2U_c'/d\Omega'$
d	chord $= 2a \cosh \eta_1$ or diameter of a circle	t	time
		T	Temperature
E	Eckert number	u,v	velocity components in (x,y)
h_{i+1}	$= y_{i+1} - y_i$	v_n, v_s	velocity components in (n,s)
k	thermal conductivity	v_η, v_θ	velocity components in (η,θ)
M_i	$= (\partial^2\psi/\partial y^2)_i$	$U(t)$	velocity of body (or of fluid far away from the body)
n,s	intrinsic coordinates		
p	pressure	U_c	constant velocity
P,Q	source functions in Eq. (22)	U^*	velocity of reference frame
Pr	Prandtl number $= \nu/k$	x,y	cartesian coordinates
α	angle of attack	τ	shear stress
β	coefficient of velocity slip	ϕ	dissipation
γ	coefficient of temperature slip	ψ	stream function
η,θ	body-fitted coordinates	ω	vorticity
κ	curvature	Ω	angular velocity of body
μ,ν	dynamic, kinematic viscosity	Ω^*	angular velocity of reference frame
ρ	density of fluid		

Flow quantities with prime are in dimensional form, without prime in dimensionless. Subscript 1 denotes fluid condition at the surface, w the condition of the surface.

1. INTRODUCTION

In viscous Newtonian fluid flow, solutions of the Navier-Stokes equations have been shown to provide an excellent description of fluid motions within the realm of continuum physics. This has been amply demonstrated at least for laminar flows since the days of Poiseuille. Due to their nonlinearity the Navier-Stokes equations have defied solution in closed form except for a few simple cases. The advent of powerful computers, however, has opened the door for the construction of numerical approximations to solutions of those equations. Still, these solutions have required and do require the full exploitation of the latest computer technology, and the successful integration process is an intricate interplay between numerical analysis and computer capacity, that is, there is a compromise between accuracy and computer time and storage available. (This interplay is underlined by the fact that general solution recipes are not available and for reasons of economy often not even desirable.) Thus, the evolution in numerical fluid dynamics is synchronous with the rapid advancement in computer science and technology. This fact is reflected in

recent publication patterns. Lasting textbooks are almost impossible to write; the few books [1,2,3] entering the market quickly become dated, and the main source of information are articles and reviews in journals and conference proceedings. Some reviews and proceedings are cited in [4 through 9].

Today fairly complicated time-dependent flows in two space dimensions (plane or axisymmetric) can be simulated on computers, although these are restricted to moderate Reynolds numbers. Simple three-dimensional flows can now be handled with fourth-generation computers such as the CDC STAR, the TI-ASC, and the ILLIAC IV. The Reynolds-number restriction placed on current simulation is very severe. However, useful applications of numerical techniques are now possible in the areas of biofluiddynamics and lubrication with nonzero Reynolds-number flows.

This lecture is not so much concerned with discussion, comparison, or enumeration of various methods for discretizing and solving the Navier-Stokes equations. Rather emphasis will be placed on problems arising from and new techniques for the application of initial and boundary conditions which together with the flow parameters define a specific problem. In addition, some thoughts are given to the interpretation of viscous flow patterns.

For this survey certain restrictions are imposed on the physical model and the numerical approach. The motion is assumed to be two-dimensional in space since with todays available computers numerical techniques find their broadest application to such flows and since this assumption conveniently simplifies explanations. The fluid is considered incompressible, homogeneous, and Newtonian. Furthermore, the Navier-Stokes equations are written in the vorticity-stream function formulation because it appears to be a natural choice for a number of reasons [3]. After all, the diffusion and convection of vorticity defined by $\vec{\omega} = \text{curl } \vec{v}$ are the controlling processes in viscous incompressible fluid flow. As a result of the assumption of incompressibility the flow field can be computed independently from the temperature field. Then, the basic equations in cartesian coordinates and in dimensionless form are:

$$\frac{\partial \omega}{\partial t} + u \frac{\partial \omega}{\partial x} + v \frac{\partial \omega}{\partial y} = \frac{1}{Re} \nabla^2 \omega, \tag{1}$$

$$\nabla^2 \psi = \omega, \tag{2}$$

$$\frac{\partial T}{\partial t} + u \frac{\partial T}{\partial x} + v \frac{\partial T}{\partial y} = \frac{1}{PrRe} \nabla^2 T + E\phi, \tag{3}$$

with $u = -\partial\psi/\partial y$, $v = \partial\psi/\partial x$, $\nabla^2 = \partial^2/\partial x^2 + \partial^2/\partial y^2$, $\phi = 2[(\partial u/\partial x)^2 + (\partial v/\partial y)^2] + (\partial v/\partial x + \partial u/\partial y)^2$, and with proper initial and boundary conditions. For the numerical approach finite-difference and related techniques are assumed although the physical aspects and many numerical considerations are independent of the special type of discretization. Note that finite-element methods and discrete vortex techniques are covered in the other lectures.

2. BOUNDARIES OF A FLUID

2.1 Boundary conditions on solid and fluid surfaces

In order to solve the differential equations of motion, initial and boundary conditions must be prescribed. Together with the flow parameters Re, Pr, etc., they define the problem under consideration. Boundaries separate a fluid from its surrounding, being either a solid or another (inmiscible) fluid. The kinematic condition for the location of the boundary, which is considered to be at rest, is the vanishing of the velocity component normal to the surface. In addition, the tangential velocity component or some equivalent must be prescribed (dynamic condition). In general, a fluid adheres to a boundary; that is, the tangential velocity component is zero (nonslip condition). However, slip may sometimes occur. In rarefied gases, a certain flow regime can be described with the Navier-Stokes equations and slippage [10]. For Brownian motion slip provides better agreement with experiments than nonslip [11]. Also in non-Newtonian fluids, the concept of slip enters [12]. Besides these examples, slip can be useful in flow models where it may be labeled as "pseudo-slip" [13]. Examples are viscous surface waves for which the "perfect slip" condition $\tau_1 \equiv 0$ can be applied [14]. Flow over porous walls behaves as if under slip [15]. The description of an interface between two fluids in contact with a solid surface requires the slip concept [16].

Conditions on the tangential velocity component at the boundary cannot be found within the realm of continuum physics and must be obtained either from experimental data or from molecular theories [17] where the consideration of nonequilibrium thermodynamics is helpful [18]. Based on gaskinetic ideas the following conditions for the tangential velocity component v_s and the temperature T in intrinsic coordinates n,s (see [18]) with $n = n_1$ being the surface are given [17]:

$$\beta(v_s)_1 = \tau_1, \text{ velocity slip,} \tag{4}$$

$$\gamma(T_1 - T_w) = q_1, \text{ temperature slip.} \tag{5}$$

$\beta = \infty$ is nonslip, $\beta = 0$ is perfect slip. The latter condition must not be thought of as yielding potential flow which is defined by $\omega \equiv 0$. A comparison of τ and ω in intrinsic coordinates show that even for perfect slip vorticity can be produced at the surface:

$$\text{if} \quad \tau'/\mu = -\partial v_s'/\partial n' - \kappa v_s' = 0, \ \mu \neq 0 \tag{6}$$

$$\text{then} \quad \omega' = -\partial v_s'/\partial n' + \kappa v_s' \tag{7}$$

will not equal zero in general. Two examples are given in Figs. 1 and 2. For the flow past a thin elliptic cylinder the difference between nonslip and perfect slip is small since most of the vorticity is produced near the edges where κ is large. However, in the case of the fluid motion around a sphere κ is relatively small. Here, nonslip causes a recirculatory wake, perfect slip does not.

For the numerical representation of the boundary conditions it is useful to distinguish among conditions at a solid or fluid surface, at lines of symmetry, and around an infinite region. Lines of symmetry do not cause numerical difficulties. If they are part of the boundaries of a doubly-connected region one value of the stream function must be determined (see section 2.3).

Solid or fluid surfaces and their vicinity are of utmost importance to the flow behavior since in general the largest gradients of the flow quantities occur there [3]. It is important to remember that the vorticity is produced at the surface as required to satisfy the boundary conditions. Also, calculation of drag and heat transfer require the knowledge of $(\partial\omega/\partial n)_1$ and $(\partial T/\partial n)_1$. For accuracy a high field resolution is necessary and can be obtained by the use of a finer differencing grid near the surface. Similar accuracy may be obtained with a uniform grid but a higher-order scheme.

Finer grids can be accomplished by a "hybrid" network; that is, by combining grids of different cell sizes and shapes [23,24], and by coordinate transformations. The elliptic-hyperbolic system

$$x + iy = a \cosh(\eta + i\theta), \ a > 0 \tag{8}$$

used in the calculation of Fig. 1, has in the physical plane finer grids near the tips of the ellipse. In general, each coordinate can be stretched with any suitable function; for instance, it can be stretched with the e-function [25], the sin-function [26], or $Re^{-1/2}$ perpendicular to the surface [27]. Care must be taken to avoid singular behavior due to mapping. Coordinate transformations for arbitrarily shaped boundaries are discussed in section 2.3.

A multitude of various schemes for approximating the boundary conditions and their accuracy, and influence on numerical stability has been summarized and discussed in [3], and also in [28]. At the boundaries prescribed conditions must be satisfied which might not be consistent with one-sided approximations of the boundary conditions. An example shall illustrate this situation. For simplicity cartesian coordinates are used with $y = y_1$ forming a straight boundary line. The notation is displayed in Fig. 3. From the Taylor expansion (the subscript j is omitted)

$$\psi_2 = (\partial\psi/\partial y)_1 \, \Delta y + \frac{1}{2} (\partial^2\psi/\partial y^2)_1 \, (\Delta y)^2 + O(\Delta y)^3 \tag{9}$$

with $u = -\partial\psi/\partial y$ and $\psi_1 = 0$. From the corresponding expressions for ψ_3 and ψ_4 and from the fact that $\omega_1 = (\partial^2\psi/\partial y^2)_1$, one arrives at the surface vorticity

$$\omega_1 = (\psi_2 + 4\psi_3 - \psi_4)/4(\Delta y)^2 + 3u_1/2\Delta y + O(\Delta y). \tag{10}$$

By assuming the slip condition (4), $\beta u_1 \approx \omega_1$, it follows that

$$\omega_1 = (\psi_2 + 4\psi_3 - \psi_4)/2\Delta y \, (2\Delta y - \frac{3}{\beta}) + O(\Delta y)^2 \tag{11}$$

and for nonslip, $\beta = \infty$:

$$\omega_1 = (\psi_2 + 4\psi_3 - \psi_4)/4(\Delta y)^2 + O(\Delta y). \tag{12}$$

Notice the difference between Eqs. (11) and (12) in the order of accuracy. The slip condition immediately gives

$$u_1 = (\psi_2 + 4\psi_3 - \psi_4)/ 2\Delta y \, (2\beta\Delta y - 3) + O(\Delta y)^2, \quad \beta < \infty, \tag{13}$$

whereas from the one-sided scheme Eq. (9) for ψ_2 and a similar expression for ψ_3 one obtains

$$u_1 = (\psi_3 - 4\psi_2)/2\Delta y + O(\Delta y)^2. \tag{14}$$

Although both approximations are of the same order the difference in the result can be drastic [22]. Clearly, Eq. (13), which contains the exact boundary condition $\beta u_1 = \omega_1$, must be preferred over the approximation Eq. (14).

Recently, higher order approximations for discretization schemes (in the entire domain of integration) have become the focus of attention. A few are mentioned: Fourier series and other series methods [29,30] a class of techniques labeled as "compact," "Hermitian" or "Mehrstellen" differencing [31,32], and spline-interpolation techniques [33,34,35]. All these approaches can incorporate boundary conditions and evaluate field data at the boundaries more easily and more accurately than the one sided finite-difference schemes. Polynomial splines are not only advantageous in many respects (according to Rubin and Khosla their use saves considerable storage and computer time,

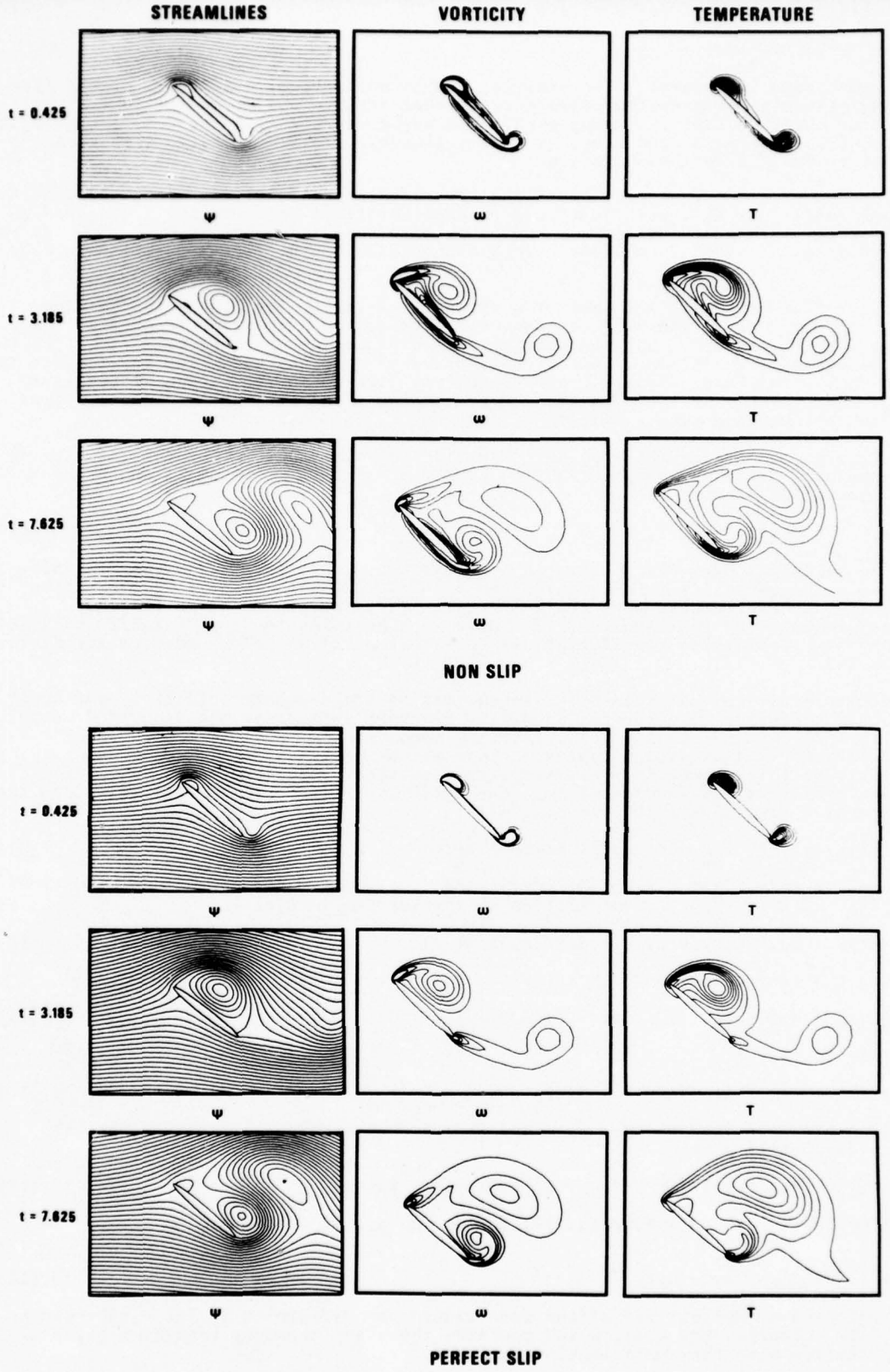

Figure 1: Streamlines, lines of constant vorticity and temperature at various times ($t = t'2U_c'/d$) after the abrupt start of an insulated-thin elliptical cylinder under (a) the nonslip and (b) the perfect slip boundary condition. $Re = U_c'd/\nu = 200$, $E = 2\nu U_c'/c_p d\Delta T'$, $\alpha = 45°$. From [20] which is based on [21].

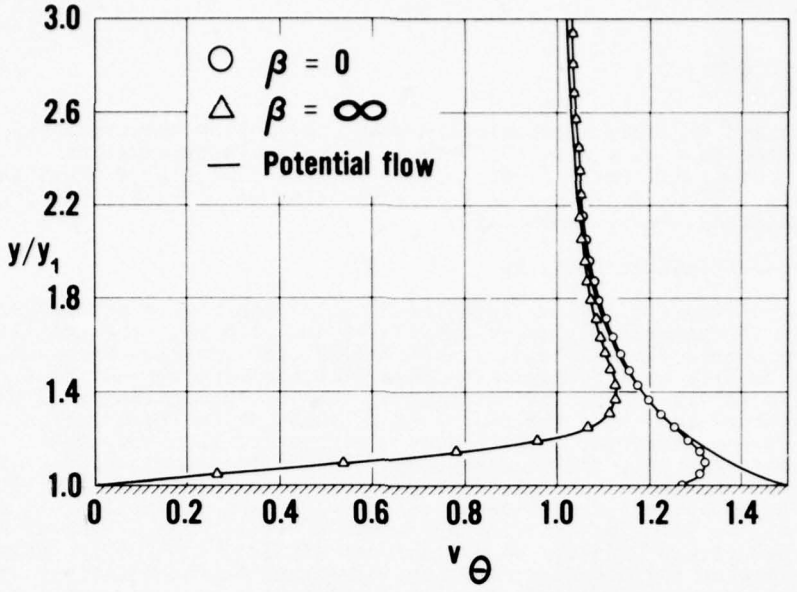

Figure 2: Velocity profiles at $\theta = 90°$ for the almost steady-state flow around a sphere under nonslip and perfect slip boundary conditions. $x + i\,y = re^{i\theta}$. $Re = U_\infty' d/\nu = 200$. For comparison the potential-flow solution is added. From [22].

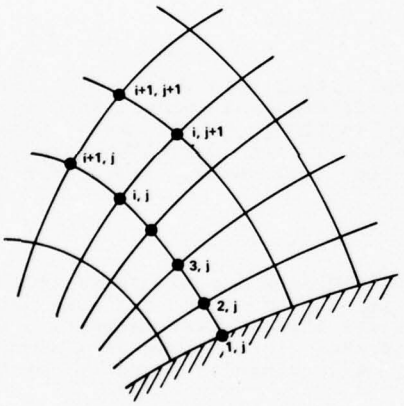

Figure 3: Notation of grid points near a surface.

and their accuracy is less sensitive to non-uniform grids), they also serve as a unifying concept for discretization. As was shown by Rubin and Khosla [35] finite-differences are identical with quadratic splines and Hermitian discretization can be derived from polynomial splines.

With spline approximations boundary conditions can be incorporated in an unambiguous way. The example Eqs. (9) through (14) is treated with cubic splines as follows. For the interval $[y_i, y_{i+1}]$ the stream function is required to be

$$\psi \approx \bar{\psi} = M_i \frac{(y_{i+1} - y)^3}{6h_{i+1}} + M_{i+1} \frac{(y - y_i)^3}{6h_{i+1}} + \left(\psi_i - M_i \frac{h_{i+1}^2}{6}\right) \frac{y_{i+1} - y}{h_{i+1}}$$

$$+ \left(\psi_{i+1} - M_{i+1} \frac{h_{i+1}^2}{6}\right) \frac{y - y_i}{h_{i+1}}, \qquad (15)$$

where $M_i = (\partial^2 \bar{\psi}/\partial y^2)_i$ is obtained as part of the solution and $h_{i+1} = y_{i+1} - y_i$. The surface vorticity is then with $\beta u_1 = \omega_1$

$$M_1 = \bar{\omega}_1 = \frac{3\beta}{3+\beta h_2} \left(\frac{\psi_2}{h_2} - \frac{h_2}{6} M_2\right) \qquad (16)$$

and, for $\beta = \infty$,

$$\bar{\omega}_1 = 3 \frac{\psi_2}{h_2^2} - \frac{1}{2} M_2 . \tag{17}$$

While Eqs. (16) and (17) are algebraically exact and follow unambiguously from Eq. (15) it should be noted that as a result of the cubic spline approximation $M_i = (\partial^2\psi/\partial y^2)_i + O(h_i^2)$ and in terms of ψ Eqs. (16) and (17) are of $O(h_2^3)$ and $O(h_2^2)$ respectively. u_1 can be expressed in a corresponding way. Details of the procedure are the (ω,ψ)-formulation are given in [33].

2.2 Boundary conditions at infinity

Boundary conditions around an infinite fluid region pose a particular problem as only a finite domain of integration can be considered numerically. The transformation of the infinite region onto a finite one does not resolve the problem. Upstream and sidewise conditions are usually easy to handle because disturbances damp out fast (except for wave-type propagation in stratified and rotating systems). The influence of those conditions at various distances away from the source of disturbance on the solution was studied in [36,37]. Downstream, however, disturbances may generate such long wakes (for instance, Kármán-vortex streets) that the boundary conditions affect the shedding of vorticity. Obviously, $\omega \equiv 0$ would be a very distorting condition. The principle difficulty of setting downstream boundary conditions across a wake lies in the fact that the boundary data are part of the solution and thus not known a priori. As a general approach to the generation of downstream boundary conditions one should use physical insight into the nature of the flow at the boundary, and sensibly simplify the equations of motion to a form which may be used as boundary conditions. A number of less restricting conditions than $\omega \equiv 0$ are listed in [3]. Thoman and Szewczyk's condition [23] $\partial\omega/\partial x = 0$, $\partial v/\partial x = 0$ (with the x-direction parallel to the flow) is mentioned. The physical interpretation causes difficulties [38]. Dawson and Marcus [24] allowed the vorticity to be convected downstream in a parallel flow. This idea was extended by Lugt and Haussling [39] to allow convection of the total flow pattern (ω and v):

$$\frac{\partial \omega}{\partial t} + U \frac{\partial \omega}{\partial x} = 0, \tag{18}$$

$$\frac{\partial v}{\partial t} + U \frac{\partial v}{\partial x} = 0. \tag{19}$$

The author considers these conditions not very restricting. An interesting idea was forwarded by Wu [40]. With the aid of an integro-differential formulation, he restricts the computation essentially to the area of nonzero vorticity (which can be much smaller than the total region of integration). He then extends this area with advancing time by following the growing wake (after the start of a body from rest). Still, for long wakes the integration area can become intractable.

2.3 Treatment of boundaries of arbitrary shape

In many practical applications of numerical fluid dynamics the shape of the boundary can only be approximated mathematically, may be time-dependent, or may even not be known a priori. Examples are ship waves, flexible surfaces through fluid-structure interactions, and parts of machinery moving relative to each other. Even on a simple flat plate edges are present which constitute mathematically singular boundary points.

In general, singular boundary points do not cause numerical difficulties since they are confined locally. Two examples are given. At the edges of an infinitesimal thin plate viscous fluids behave such that p_1 and ω_1 become unbounded according to $r^{-1/2}$ when approaching the edges [41], Fig. 4a, no matter whether the fluid separates or not. r is the distance from the edges. Integration of p_1 and ω_1 over r results in finite values (provided $r < \infty$), and thus in bounded drag and lift. The numerical calculation of the neighboring flow field can be carried out with sufficient accuracy. Whether or not a grid point is located at the singular point depends on the discretization scheme [3,36,42,43].

In the second example, a cover rotates relative to the container wall without a gap, Fig. 4b. The shear stress is proportional to r^{-1} [26]. Although this singular behavior is locally restricted and does not invalidate the overall flow field, the torque (as an auxiliary quantity) is logarithmically infinite.

Although the boundary conditions of free surface waves (for instance ship waves) are known, the location of the wave surface itself is part of the solution. The kinematic boundary condition requires that the surface moves with the local fluid velocity. If the surface is defined by $x = x(s,t)$, $y = y(s,t)$, the condition reads

$$u = \frac{\partial x}{\partial t}(s,t), \quad v = \frac{\partial y}{\partial t}(s,t). \tag{20}$$

The dynamic boundary condition postulates continuity of the normal and tangential stress across the surface [44,45]. For water waves with air above, this condition can be reduced to constant surface pressure and vanishing surface-shear stress. The latter one is the perfect-slip condition.

a b

Figure 4: Examples of singular boundary points. (a) Flow around the edge of an infinitesimal thin plate, with and without separation. (b) Relative motion between cover and container wall without a gap.

The numerical treatment of surface wave-boundary conditions is mathematically difficult, even for potential flow [46]. For viscous fluids the treatment used in the Marker-and-Cell method in its latest version, SOLA-SURF [47] is reasonably successful. In general, the problem of free-surface waves calls for more intensive investigation.

For high accuracy near the surface it is advantageous to have a body-fitted coordinate system (see section 2.1). In the last decade numerical methods have been developed which permit the transformation of an arbitrarily shaped boundary in the physical plane (x,y) onto the rectangular mathematical plane (η,θ). In addition to the desirable high resolution the application of certain integration techniques like the fast direct Poisson solvers necessitates a certain regularity of the grid. These methods, which are connected with the names of Buneman, Golub, Buzbee, Hockney et al. [48,49,50], are very powerful in solving the Navier-Stokes equations efficiently when applied to the Poisson equation for ψ. In fact, certain problems could only be solved within a reasonable amount of computer time with the aid of these methods [51]. At present, only those coordinate transformations $(x,y) \rightarrow (\eta,\theta)$ can be used which yield a separable elliptic differential equation of the form [52]

$$a(\theta)\,\frac{\partial^2\psi}{\partial\theta^2} + c(\eta)\,\frac{\partial^2\psi}{\partial\eta^2} + d(\theta)\,\frac{\partial\psi}{\partial\theta} + e(\eta)\,\frac{\partial\psi}{\partial\eta} + [f(\theta)+g(\eta)]\psi = \omega(\eta,\theta),\quad ac > 0. \tag{21}$$

This class of transformations includes any conformal mapping as a subclass. An example is Eq. (8). Work is going on to extend the range of application for fast Poisson solvers beyond the class represented by (21). In this context it may be noted that a fast fourth-order Laplace solver developed by Ohring [53] for three-dimensional potential flows may be applicable for Eq. (2) under the restrictions of $\Delta\eta = \Delta\theta$ and conformal mapping.

For simply-connected regions these body-fitting methods have been studied by Winslow, Barfield, Chu, Amsden and Hirt, and Godunov and Prokopov (see [54]). This work has been extended recently to multiply-connected regions by Thompson et al. [54,55] and Ghia et al. [56,57,58]. The latter group has improved the computer efficiency of the coordinate-transformation program by the increased speed of convergence due to the use of the ADI method, employing simultaneous solution of the coupled Poisson equations (22) below during each step of the ADI scheme. Additional improvements are in progress (according to a private communication with Prof. U. Ghia). A brief outline from [55] is given:

The coordinates (x,y) and (η,θ) are coupled with each other by the generating elliptic system

$$\begin{aligned} \theta_{xx} + \theta_{yy} &= P(\eta,\theta), \\ \eta_{xx} + \eta_{yy} &= Q(\eta,\theta). \end{aligned} \tag{22}$$

Since the computations shall be carried out in the (η,θ)-plane, the dependent and independent variables in (22) must be interchanged:

$$\begin{aligned} a\,\frac{\partial^2 x}{\partial\theta^2} - 2b\,\frac{\partial^2 x}{\partial\theta\partial\eta} + c\,\frac{\partial^2 x}{\partial\eta^2} &= -J^2\left(\frac{\partial x}{\partial\theta}P + \frac{\partial x}{\partial\eta}Q\right), \\ a\,\frac{\partial^2 y}{\partial\theta^2} - 2b\,\frac{\partial^2 y}{\partial\theta\partial\eta} + c\,\frac{\partial^2 y}{\partial\eta^2} &= -J^2\left(\frac{\partial y}{\partial\theta}P + \frac{\partial y}{\partial\eta}Q\right) \end{aligned} \tag{23}$$

with $a = \left(\frac{\partial x}{\partial\eta}\right)^2 + \left(\frac{\partial y}{\partial\eta}\right)^2$, $b = \frac{\partial x}{\partial\theta}\frac{\partial x}{\partial\eta} + \frac{\partial y}{\partial\theta}\frac{\partial y}{\partial\eta}$, $c = \left(\frac{\partial x}{\partial\theta}\right)^2 + \left(\frac{\partial y}{\partial\theta}\right)^2$, $J = \frac{\partial x}{\partial\theta}\frac{\partial y}{\partial\eta} - \frac{\partial x}{\partial\eta}\frac{\partial y}{\partial\theta}$.

Dirichlet (or Neumann) boundary conditions for x and y are prescribed and then (23) solved. The grid in the physical plane may change with time whereas the (η,θ)-grid can be kept fixed.

The simple mapping Eq. (8) transforms an ellipse in the (x,y)-plane onto a rectangle in the (η,θ)-plane. If a higher resolution of the surface is desired a doubly-connected region may be used. Fig. 5. In this figure an example from biofluiddynamics is selected. The circle (representing the ball) degenerates to a double line in the (η,θ)-plane. This arrangement provides more coordinate lines around the circle normal to the solid surface. If one wants higher resolution around the circle with regard to more parallel lines, the imbedding of an additional grid can be made. Fig. 6.

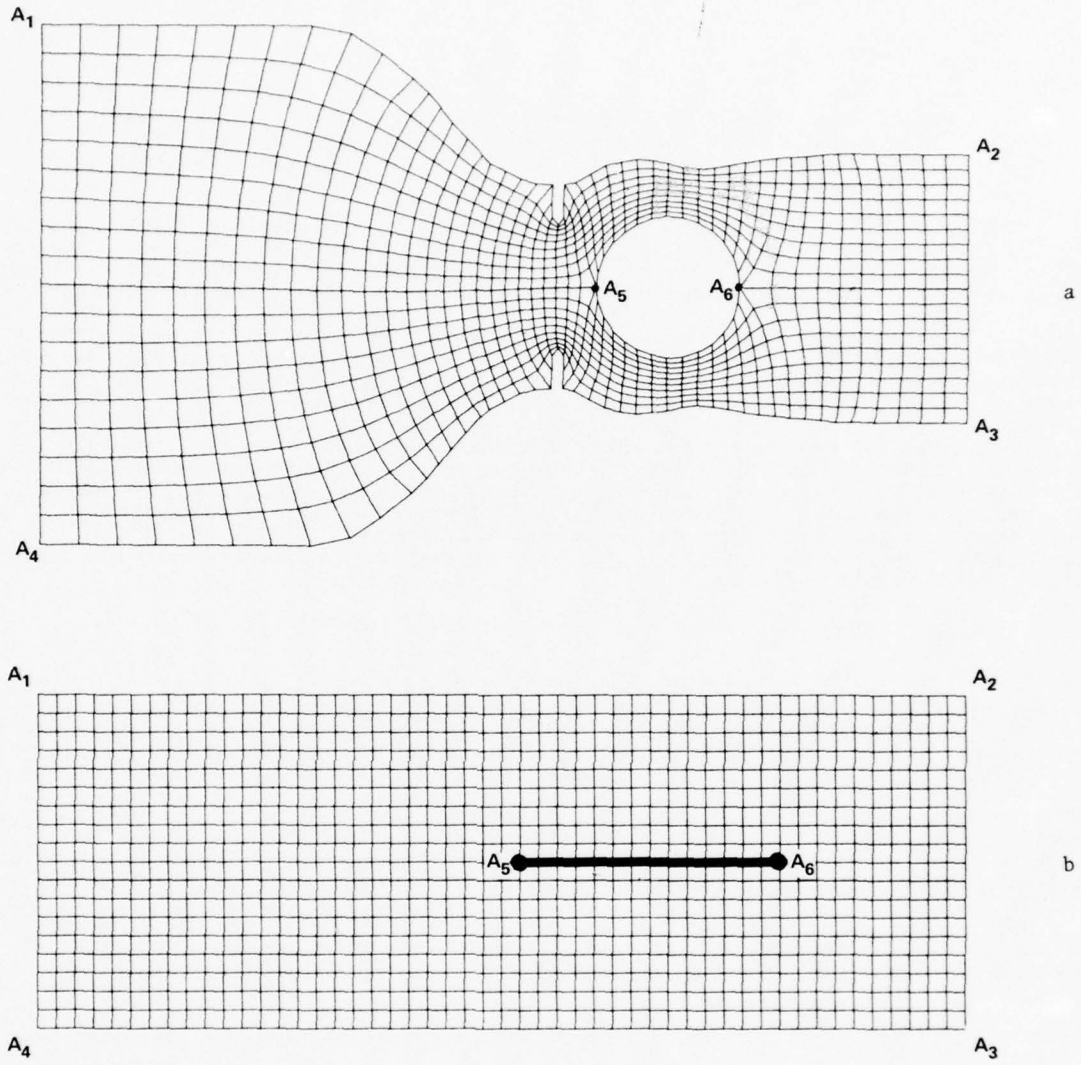

Figure 5: (a) Body-fitted coordinate system for the meridional plane of part of the aorta with caged-ball valve prosthesis. The blood flows from the left heart chamber on the left toward and around the ball which is oscillating horizontally according to the rhythm of the heart. The amplitude of the ball oscillation is given through the positions of the orifice and of the cage of the prosthesis (which is not modeled here). (b) Grid in the (η,θ)-plane. The computations were performed with the technique described in [54]. $P = Q = 0$.

For the purpose of solution, the stream-function vorticity form of the Navier-Stokes equations transforms to

$$\frac{\partial\omega}{\partial t} + \left(\frac{\partial\psi}{\partial\eta}\frac{\partial\omega}{\partial\theta} - \frac{\partial\psi}{\partial\theta}\frac{\partial\omega}{\partial\eta}\right)/J = \left(a\frac{\partial^2\omega}{\partial\theta^2} - 2b\frac{\partial^2\omega}{\partial\theta\partial\eta} + c\frac{\partial^2\omega}{\partial\eta^2} + d\frac{\partial\omega}{\partial\theta} + e\frac{\partial\omega}{\partial\eta}\right)/J^2Re \ , \tag{24}$$

$$a\frac{\partial^2\psi}{\partial\theta^2} - 2b\frac{\partial^2\psi}{\partial\theta\partial\eta} + c\frac{\partial^2\psi}{\partial\eta^2} + d\frac{\partial\psi}{\partial\theta} + e\frac{\partial\psi}{\partial\eta} = J^2\omega \ , \tag{25}$$

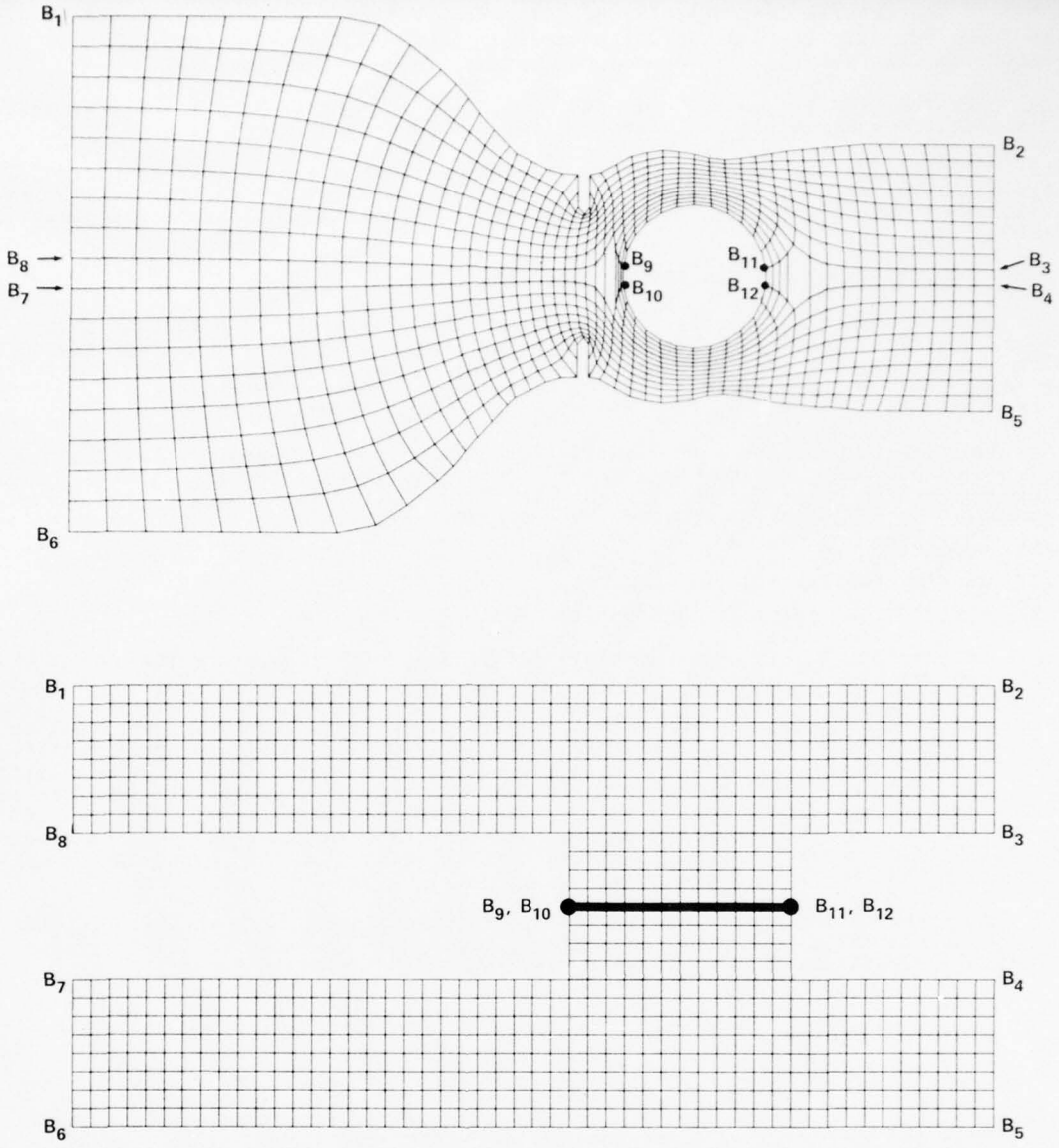

Figure 6: The same situation as in Fig. 5 except for additional spacing arrangement around the ball (suggested by Professor J. F. Thompson). P = Q = 0.

where $d = (\frac{\partial x}{\partial \eta}\, Dy - \frac{\partial y}{\partial \eta}\, Dx)/J$, $e = (\frac{\partial y}{\partial \theta}\, Dx - \frac{\partial x}{\partial \theta}\, Dy)/J$, and the functional

$D \equiv a \frac{\partial^2}{\partial \theta^2} - 2b \frac{\partial^2}{\partial \theta \partial \eta} + c \frac{\partial^2}{\partial \eta^2}$. The boundary conditions at the surface for nonslip are

$$\psi = \text{const}, \quad \sqrt{c}\,/\,J\, \partial\psi/\partial\eta = 0. \tag{26}$$

Eqs. (24) and (25) are more complicated than the original Eqs. (1) and (2). This disadvantage, however, is far outweighted by having a steady, simple grid. Eqs. (24) and (25) are only valid for plane motions, not for axisymmetric ones.

The example in Fig. 5 is of interest in three other respects: (1) the region is doubly connected, (2) the aortic wall may be considered flexible when interacting with the fluid, and (3) the surfaces touch and separate in each period of oscillation.

(1). In multiply-connected regions the constant value of ψ in (26) is different on disconnected surfaces. For instance, in Fig. 5 ψ can be set equal to zero along the aortic wall boundary and equal to B(t) on the circle. (This holds for the axisymmetric

problem. If the problem considered is planar, the ψ-values for the upper boundary A_1-A_2 and the lower boundary A_4-A_3 differ.) However, B(t) may not be known and may have to be determined with the solution. A procedure for this is described in [59].

(2). On the flexible aortic wall the same conditions apply as for the free surface of two inmiscible viscous fluids. See Eq. (20) and subsequent text.

(3). Separation and touching of two or more surfaces are described by the acceleration process involved. Discontinuous movement of the surfaces (in the velocity or the acceleration) requires special care in the numerical simulation. This is discussed in the next section.

3. INITIAL CONDITION AND MODELS FOR ACCELERATION

The initial condition specifies the state of the flow field at a certain time $t = t_0$ from which the flow field with prescribed boundary conditions develops. The instant t_0 may mark the beginning of motion or may occur later at any other time. The flow field may be continuous or discontinuous (as the beginning of motion) in time at $t = t_0$. The start of motion is chosen to be at $t = 0$ without loss of generality.

Any nonanalytic behavior of the initial condition is determined by the selection of the acceleration model. Depending on which time derivatives of the flow quantities are discontinuous, three cases are considered. They cover all possible models for numerical computations. At $t = t_0$ the discontinuity may occur in the

(1) velocity: $U(t)$

(2) acceleration: $dU/dt(t)$

(3) rate of acceleration: $d^2U/dt^2(t)$

(1) In almost all acceleration models described in the literature the abrupt start of a body from rest to a constant velocity is simulated. This is mathematically equivalent to a discontinuity in U(t). The acceleration dU/dt is therefore a δ-function, and drag and lift are infinite at that instant. Numerically, the potential-flow solution in the interior of the flow field is prescribed, as well as the dynamic boundary condition of the viscous fluid at the surface. This means that an infinitesimal sheet of vorticity exists at the surface. The subsequent spreading of vorticity (see Fig. 1) requires small time steps Δt although errors remain near $t = 0$ due to the inability of the numerical scheme to resolve very thin boundary layers. However, a comparison with series expansions for the elliptic-cylinder problem by Staniforth [60] shows that the inaccuracy is confined to a limited time span near $t = 0$.

(2) An acceleration model in which dU/dt is discontinuous has been used recently by Collins and Dennis [61]. Examples for boundary layers can be found in [62]. If the acceleration period lasts from $t = 0$ to $t = \tau$, the acceleration is

$$\frac{dU}{dt} = \begin{cases} 0 & \text{for } t < 0 , \\ 1/\tau & 0 \le t \le \tau , \\ 0 & \tau < t . \end{cases} \tag{27}$$

Discontinuities occur at $t_0 = 0$ and τ. At $t_0 = 0$ the fluid is motionless with $\omega_1 \equiv 0$ but there exists a discontinuity sheet for the vorticity flux $(\partial\omega/\partial n)_1$. As in case (1) errors in computing the flow field occur near $t_0 = 0$. Calculating the force, however, will lead to grossly inaccurate values. This can be avoided by incorporating the boundary-layer solution [63]. A similar situation must be overcome when $t_0 = \tau$. A new vorticity sheet is introduced. The resulting new boundary layer grows in a rotational rather than in an irrotational flow. As was pointed out by Taneda [64], the flow at $t_0 = \tau$ consists of the superposition of the already existing rotational flow field and the irrotational flow field resulting from the abrupt change in the acceleration. Again, the boundary-layer solution can be incorporated as in the situation at $t_0 = 0$. This was done in Fig. 7b only for the calculation of the drag coefficient but not for obtaining the flow field.

(3) For the linear acceleration described by

$$\frac{dU}{dt} = \begin{cases} 0 & \text{for } t < 0, \\ 4t/\tau^2 & 0 \le t \le \tau/2, \\ -4(t-\tau)/\tau^2 & \tau/2 < t \le \tau, \\ 0 & \tau < t, \end{cases} \tag{28}$$

the flow field at $t_0 = 0$ is motionless with $\omega_1 = (\partial\omega/\partial n)_1 \equiv 0$. This instant, as well as those at $t_0 = \tau/2$ and τ when d^2U/dt^2 is discontinuous, do not cause any numerical difficulties [63].

For comparison the drag coefficient defined by $C_D = \text{drag}/\frac{1}{4}\rho U_c^2 d$ for the three cases is plotted against t in Fig. 7, with the flow situation of Fig. 1a. Care must be taken when selecting the reference frame for computing the drag [63]. A discussion of this problem and experimental data are given by Sarpkaya [65].

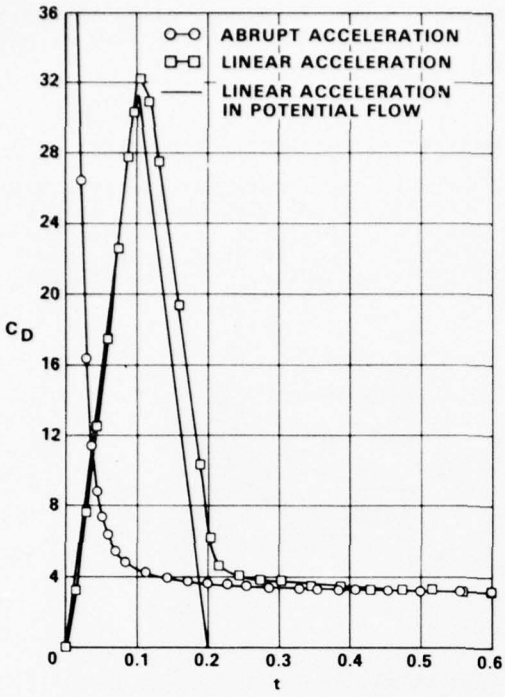

a

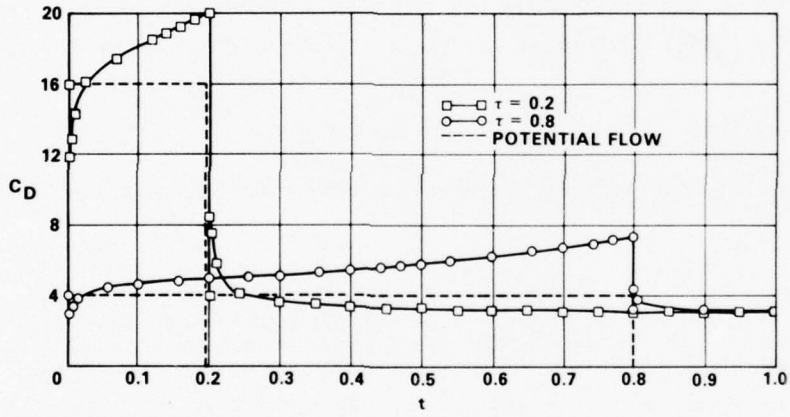

b

Figure 7: Drag coefficients for the flow situation of Fig. 1a with various acceleration models. (a) Abrupt and linear acceleration. The abrupt acceleration in potential flow is described by the δ-function at $t = 0$; (b) constant acceleration. From [63].

4. INTERPRETATION OF FLOW PATTERNS IN VISCOUS FLUIDS

With the possibility of solving complicated flow problems numerically, difficulties in interpreting time-dependent flow patterns can arise. This may even occur in two space dimensions, let alone the three-dimensional domain where the situation really becomes complicated. Steady motions imply the Eulerian form of flow description and the selection of one specific reference frame; that is, the reference frame for which the flow becomes steady. In this steady-state system streamlines, pathlines, and streaklines coincide. In truly unsteady flows no preferred reference frame exists, and the frame must be selected on the basis of other criteria. Streamlines, pathlines, and streaklines in general no longer coincide. In this text, the discussion is restricted to two-dimensional flows, and three phenomena are described: separation, vortices, and various reference frames for rotating bodies.

4.1 Flow separation

In general, flow separation may be defined for steady motions if a body streamline detaches from the surface, or more accurately, if it bifurcates. Two types exist: flow separation which is simply enforced through the conservation of mass and which can occur also in potential flow (see Fig. 10b), and flow separation due to a separating vorticity

layer from the surface. The first type of separation point is often called the point of detachment, while the second type is usually meant when one speaks about flow separation. In steady motions it is defined by (see [62,66])

$$\tau = 0, \quad v_n > 0 \quad \text{or} \quad \omega = 0, \quad \frac{\partial \omega}{\partial s} < 0 \ , \tag{29}$$

where the second definition is also valid for perfect-slip boundary conditions [21].

This definition no longer holds in unsteady flows. To understand the flow behavior, a reference frame is sought in which the motion becomes steady with respect to the separation point, at least locally. There, streamlines (and pathlines) do not change very much in time. In Fig. 8 such a change of the reference frame is shown. One immediately recognizes that in the steady frame a parallel flow exists adjacent to the surface, and that the bifurcation point is inside the fluid.

a b

Figure 8: Streamlines near a separation point. (a) The surface is fixed, and the separation point is moving with speed -U to the left. The flow is unsteady. (b) The reference frame is now fixed to the separation point by superposition of U on the flow field. The surface moves with speed U. The flow is steady, at least in the vicinity of the separation point. From [67].

Moore, Rott, and Sears [67] have suggested the following criterion for flow separation in a boundary layer:

$$\frac{\partial v_s}{\partial n} = 0 \quad \text{at } v_s = 0. \tag{30}$$

A formal definition for solutions of the Navier-Stokes equations has apparently not yet been found.

4.2 Vortices

A similar difficulty is encountered if one tries to define a vortex in unsteady flows [68]. Generally, a vortex may be described as the circulating movement of fluid elements around a common center. To transform this description of a household word into an exact mathematical definition, however, is another matter.

The textbook definitions are usually too restricted. Here are some examples: (1) The potential vortex is not applicable to viscous fluids. (2) Vorticity at a point in space does not constitute a vortex. A parallel shear flow has vorticity but is not a vortex. (3) An extremum of vorticity in viscous fluids indicates a vortex but is not necessarily one. Any nonconservative force acting on the fluid may produce local extrema, for instance in stratified fluids. Also, recirculatory regions at surfaces would be excluded from being vortices since their vorticity has its extremum on the surface (Fig. 1). (4) Closed streamlines do not necessarily represent vortices in unsteady motions. Streamlines are not invariant with regard to inertial transformations and certainly not for rotational ones. Fig. 9.

As in the case of unsteady flow separation a reference frame must be found that is at rest relative to the vortex center. This can be done iteratively by checking the pathlines or a time sequence of streamlines. When closed or spiralling pathlines are found, these patterns then constitute a vortex.

4.3 Rotating bodies

The simplest case of a rotating body in two dimensions is that of a cylinder rotating with constant angular velocity $-\Omega$ in a fluid at rest at infinity. Fig. 10a shows the instantaneous streamlines of a potential flow around a rotating cylinder with an elliptic cross-section. This flow is unsteady. By superposing the rotation Ω the flow becomes steady (Fig. 10b). The flow patterns reveal now two recirculatory regions (or vortices according to section 4.2) which are not visible in Fig. 10a. The closed streamlines within these recirculatory regions do not contradict a theorem for potential flow that in a simply-connected region closed streamlines cannot exist [44]. In Fig. 10b, a rotation Ω with constant $\omega/2$ is superposed!

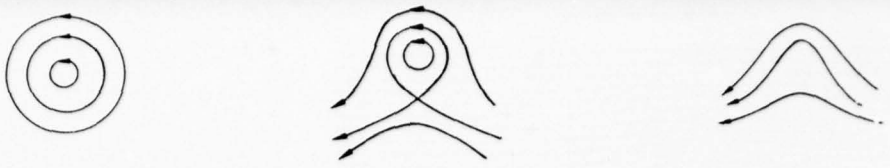

a b c

Figure 9: On a vortex (a) a constant parallel flow from right to left is superposed. This is equivalent to a reference frame moving relative to the vortex. In (b) the velocity of the parallel flow is small relative to the tangential velocity of the vortex; in (c) the velocity of the parallel flow is large.

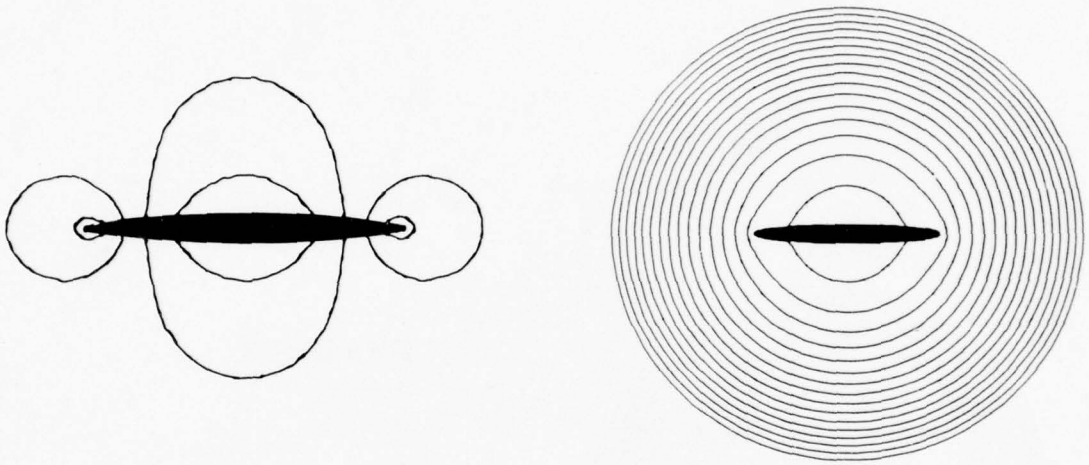

a b

Figure 10: Potential flow around a rotating thin elliptic cylinder. (a) The reference frame is fixed to the fluid at rest at infinity. The flow is unsteady. (b) The reference frame is fixed to the body. The flow is steady.

The situation becomes more complicated if a cylinder rotates with constant $-\Omega$ in a parallel stream with U_c. Then, no steady state exists. Four different frames may be distinguished. When U^* and Ω^* are the translational and angular velocities of the body relative to the reference frame, these four different frames are:

(1) $U^* = 0$, $\Omega^* \neq 0$; the frame is fixed to the body with regard to translation; but the body rotates relative to the frame.

(2) $U^* \neq 0$, $\Omega^* \neq 0$; the body is in translational and rotational motion relative to the frame. For $U^* = -U$ and $\Omega^* = -\Omega$ the frame is fixed to the fluid at rest at infinity.

(3) $U^* = 0$, $\Omega^* = 0$; the frame is fixed to the body.

(4) $U^* \neq 0$, $\Omega^* = 0$; the frame does not rotate relative to the body; but the body has a translational motion relative to the frame.

The behavior of streamlines for the four different cases is illustrated in Figures 11 and 12. For nonvanishing U^* and Ω^* these quantities are chosen to be $U^* = -U$ and $\Omega^* = -\Omega$. Since the streamlines are not invariant, all patterns differ from each other.

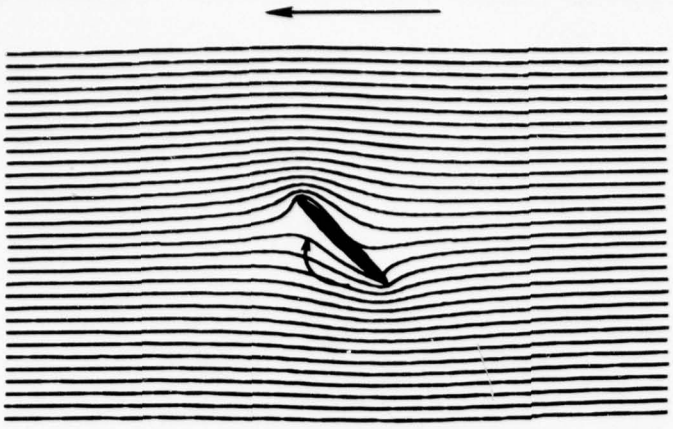

FRAME 1

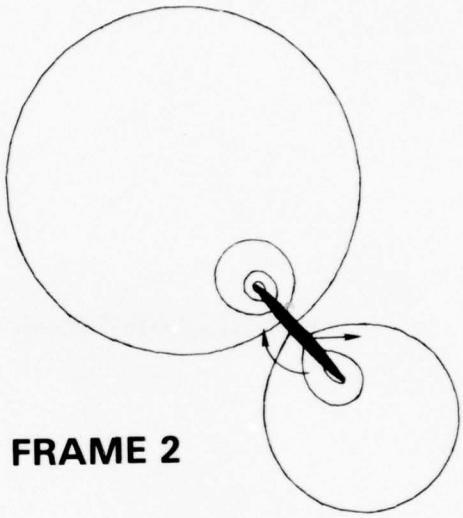

FRAME 2

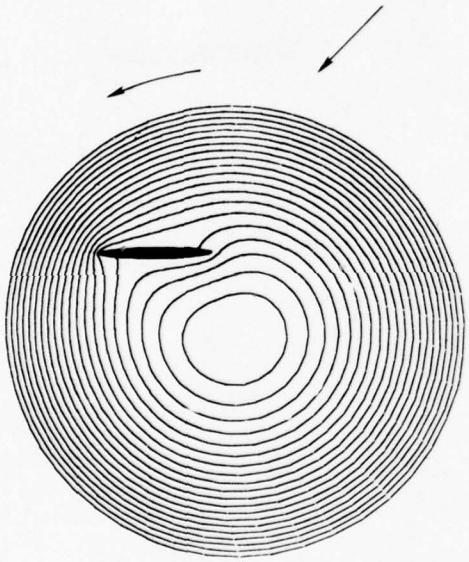

FRAME 3

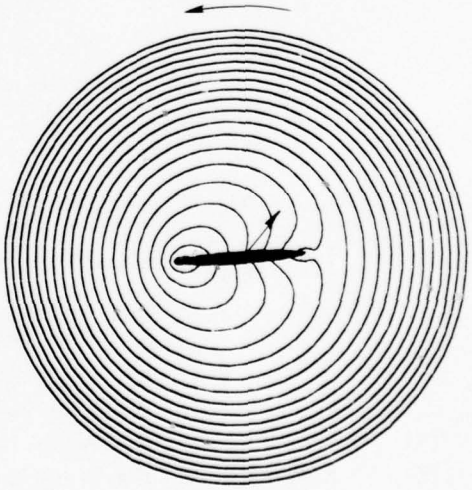

FRAME 4

Figure 11: Potential flow around a rotating thin elliptic cylinder with translational motion in four different reference frames. Ro = 0.5, α = 45°. The flow is unsteady.

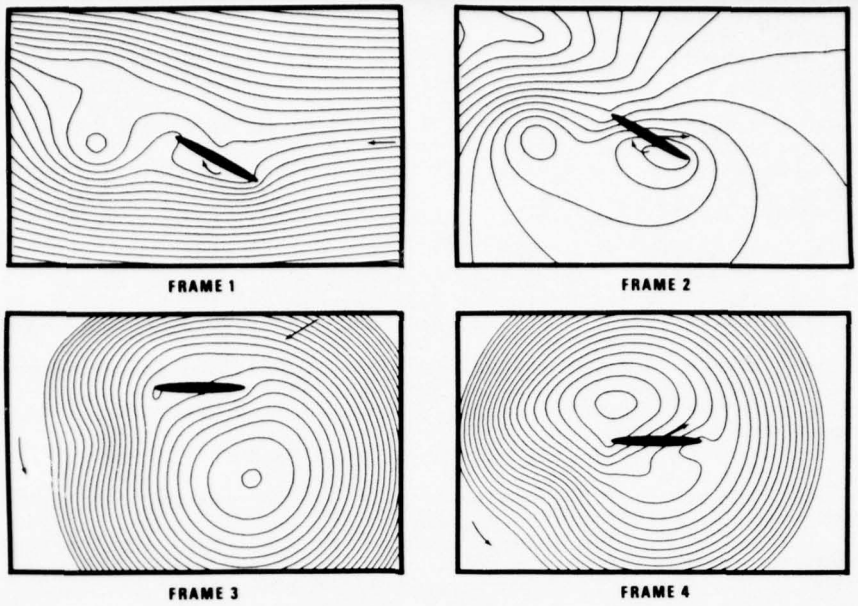

Figure 12: Streamline patterns of a viscous fluid flow in four different reference frames. Re = 200, Ro = 2, $\alpha = 30°$, t = 10.46 after the abrupt start from a vertical position. From [51].

By contrast, the vorticity field in Fig. 13 is invariant and differs under rotational transformations only by a constant. The superiority of the vorticity field over the streamline patterns for explaining flow behavior is clearly demonstrated.

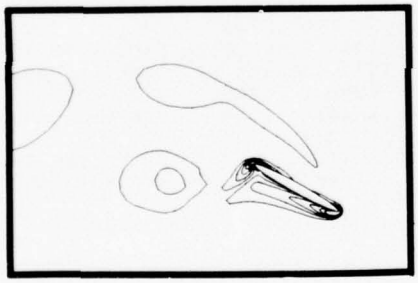

Figure 13: Equi-vorticity lines for the flow situation of Fig. 12. From [51].

For interpreting the patterns of Figs. 12 and 13 the discussions in section 4.1 and 4.2 may be consulted. For example, the separated vortex one plate length behind the body is seen in Frames 1 and 2 as closed streamlines, and in Frames 3 and 4 as wavy streamlines. Hence, the vortex is moving relative to Frames 3 and 4, but not (or only slowly) to Frames 1 and 2. The closed streamlines in Frames 3 and 4 are due to the rotation of the frames and are circular at infinity. The center of rotation coincides only with the rotation center of the body when the translational motion vanishes (Fig. 10b). Details are given in [51].

5. REFERENCES

1. Ames, W.F., Nonlinear Partial Differential Equations in Engineering. Academic Press, New York, London, 1972, Vol. 18 - II.
2. Isaacson, E. and Keller, H.B., Analysis of Numerical Methods. John Wiley & Sons, Inc., New York, London, 1966.
3. Roache, P.J., Computational Fluid Dynamics. Hermosa Publishers, Albuquerque, New Mexico, 1972.
4. Proceedings Fifth Intern. Conference on Numerical Methods in Fluid Dynamics, Enschede, Holland. Springer-Verlag, 1977.
5. Preprints Second Intern. Symposium on Finite Element Methods in Flow Problems, S. Margherita Ligure, Italy. ICCAD, Conference Series No. 2176, 1976.

6. Proceedings Intern. Conference on Numerical Methods in Fluid Dynamics, Southampton, England. Crane, Russak & Co., Inc., New York, 1974.
7. Orszag, S.A. and Israeli, M., Numerical Simulation of Viscous Incompressible Flows. Annual Review of Fluid Mechanics, Annual Reviews, Inc., Palo Alto, Calif., Vol. 6, 1974, 281.
8. Wirz, H.J. and Smolderen, J.J., Numerical Integration of Navier-Stokes Equations. AGARD Lecture Series No. 64, 1974.
9. Krause, E., Application of numerical techniques in fluid mechanics. Aeronautical Journal, Aug. 1974, 337.
10. Schaaf, S.A. and Chambré, P.L., Flow of Rarefied Gases. Princeton University Press, 1961.
11. Zwanzig, R. and Bixon, M., Phys. Rev. A2, 1970, 2005.
12. Oldroyd, J.G., in Rheology, Vol. 1, Ed. Eirich, Academic Press, New York, 1956.
13. Lugt, H.J. and Schot, J.W., A Review of Slip Flow in Continuum Physics. Proc. Second Symposium Fluid-Solid Surface Interactions, Naval Ship Research and Development Center, Bethesda, Md., 1974, 101.
14. Hirt, C.W. and Shannon, J.P., Free-Surface Stress Conditions for Incompressible-Flow Calculations. Journ. Computational Physics 2, 1968, 403.
15. Beavers, G.S. and Joseph, D.D., Boundary conditions at a naturally permeable wall. Journ. Fluid Mech. 30, 1967, 197.
16. Hocking, L.M., A moving fluid interface on a rough surface. Journ. Fluid Mech. 76, 1976, 801.
17. Lehmann,V. and Mueller, W.J.C., Boundary Conditions for the Macroscopic Slip Velocity on a Curved Wall. Z. Naturforsch. 29a, 1974, 296.
18. Bedeaux, D., Albano, A.M., and Mazur, P., Boundary conditions and non-equilibrium thermodynamics. Physica 82A, 1976, 438.
19. Milne-Thomson, L.M., Theoretical Hydrodynamics. The MacMillan Co., New York, Fifth Ed., 1968.
20. Schot, J.W. and Haussling, H.J., Heat Transfer Under Velocity Slip and Temperature Jump Boundary Conditions. Proc. Third Symposium Fluid-Solid Surface Interactions, Meersburg. Dornier System GmbH., Friedrichshafen, Germany, 1975.
21. Lugt, H.J., Generation and Propagation of Vorticity under the Perfect-Slip Condition. Naval Ship Research and Development Center Rep. 3794, Feb. 1972.
22. Lugt, H.J. and Ohring, S., Laminar flow behavior under slip-boundary conditions. Phys. of Fluids 18, 1975, 1.
23. Thoman, D.C. and Szewczyk, A.A., Numerical Solutions of Time Dependent Two Dimensional Flow of a Viscous, Incompressible Fluid over Stationary and Rotating Cylinders. University of Notre Dame, Dept. of Mech. Eng. Tech. Rep. 66-14, 1966.
24. Dawson, C. and Marcus, M., DMC - A Computer Code to Simulate Viscous Flow About Arbitrarily Shaped Bodies. Proc. 1970 Heat Transfer and Fluid Mechanics Institute. Stanford University Press, 1970, 21.
25. Rimon, Y. and Cheng, S.I., Numerical solution of a uniform flow over a sphere at intermediate Reynolds numbers. Phys. Fluids 12, 1969, 949.
26. Lugt, H.J. and Haussling, H.J., Transient Ekman and Stewartson Layers in a Rotating Tank with a Spinning Cover. IUTAM Symposium 1971, Recent Research on Unsteady Boundary Layers. Les Presses de l'Université Laval, Québec, 1972, 1366.
27. Wirz, H.J., Die laminare Umströmung einer nichtangestellten Platte bei grossen Reynoldszahlen. Dissertation (TU-Berlin) D 83, 1971.
28. Lugt, H.J. and Rimon, Y., Finite-difference Approximations of the Vorticity of Laminar Flows at Solid Surfaces. Naval Ship Research and Development Center, Rep. 3306, April 1970.
29. Dennis, S.C.R. and Chang, G.Z., Mathematics Research Center, University of Wisconsin, Tech. Summary Rep. No. 859, 1969.
30. Orszag, S.A., Numerical Simulation of Incompressible Flows Within Simple Boundaries. I. Galerkin (Spectral) Representations. Studies in Appl. Mathematics, L, 1971, 293.
31. Hirsh, R.S., Higher Order Accurate Difference Solutions of Fluid Mechanics Problems by a Compact Differencing Technique. Journ. Comp. Physics 19, 1975, 90.
32. Krause, E., Hirschel, E.H., and Kordulla, W., Fourth Order "Mehrstellen"-Integration for Three-dimensional Turbulent Boundary Layers. Computers and Fluids 4, 1976, 77.
33. Rubin, S.G. and Graves, R.A., Viscous Flow Solutions with a Cubic Spline Approximation. Computers and Fluids 3, 1975, 1.
34. Rubin, S.G. and Khosla, P.K., Higher-Order Numerical Solutions Using Cubic Splines. AIAA Journ. 14, 1976, 851.
35. Rubin, S.G. and Khosla, P.K., Higher-Order Numerical Methods Derived from Three-Point Polynomial Interpolation. NASA CR-2735, Aug. 1976.
36. Rimon, Y., Numerical Solutions of the Time-dependent Incompressible Viscous Flow over a Disk or a Sphere. Aerospace Research Laboratories, Wright-Patterson AFB, Ohio, Rep. ARL 69-0063, April 1969.
37. Boswell, W.C. and Werle, M.J., Numerical Solutions of the Navier-Stokes Equations for Incompressible Uniform Flow Past a Parabola: a Study of Finite Grid Size Effects. Virginia Polytechnic Institute, Blacksburg, Va., VPI-E-71-5, Feb. 1971.
38. Roache, P.J., Sufficiency Conditions for a Commonly Used Downstream Boundary Condition on Stream Function. Journ. Comp. Physics 6, 1970, 317.
39. Lugt, H.J. and Haussling, H.J., Laminar flow past an abruptly accelerated elliptic cylinder at 45° incidence. Journ. Fluid Mech. 65, 1974, 711.
40. Wu, J.C., Numerical Boundary Conditions for Viscous Flow Problems. AIAA Journ. 14, 1976, 1042.
41. Lugt, H.J. and Schwiderski, E.W., Flows Around Dihedral Angles. Proc. Roy. Soc. A, 285, 1965, 382.
42. Mehta, U.B. and Lavan, Z., Starting vortex, separation bubbles and stall: a numerical study of laminar unsteady flow around an airfoil. Journ. Fluid Mech. 67, 1975, 227.

43. Ghia, K.N. and Davis, R.T., Corner Layer Flow: Optimization of Numerical Methods of Solution. Intern. Journ. Computers and Fluids 2, 1974, 17.
44. Landau, L.D. and Lifshitz, E.M., Fluid Mechanics. Pergamon Press, London, 1959.
45. Hirt, C.W., Numerical Hydrodynamics - Present and Potential. Proc. Numerical Hydrodynamics. National Academy of Sciences, Washington, D.C., 1975. (See also [14]).
46. Proc. First Intern. Conference on Numerical Ship Hydrodynamics, Ed. J.W. Schot and N. Salvesen, Naval Ship Research and Development Center, Bethesda, Md., 1975.
47. Hirt, C.W., Nichols, B.D., and Romero, N.C., SOLA - A Numerical Solution Algorithm for Transient Fluid Flows. Los Alamos Scientific Laboratory Rep. LA-5852, April 1975. Addendum Jan. 1976.
48. Buneman, O., A compact non-iterative Poisson solver. Rep. 294, Stanford University Institute for Plasma Research. Stanford, 1969.
49. Buzbee, B.L., Golub, G.H., and Nielson, C.W., On Direct Methods for Solving Poisson's Equations. SIAM Journ. Num. Anal. 7, 1970, 627.
50. Hockney, R.W., The potential calculation and some applications. Methods in Comp. Phys. 9, 1970, 135.
51. Lugt, H.J. and Ohring, S., Rotating elliptic cylinders in a viscous fluid at rest or in a parallel stream. Journ. Fluid Mech. 79, 1977, 127.
52. Swarztrauber, P.N., A Direct Method for the Discrete Solution of Separable Elliptic Equations. SIAM Journ. Num. Anal. 11, 1974, 1136.
53. Ohring, S., A Fast Fourth-Order Laplace Solver for Application to Numerical Three-dimensional Water Wave Problems. In [46], p. 641.
54. Thompson, J.F., Thames, F.C., and Mastin, C.W., Automatic Numerical Generation of Body-Fitted Curvilinear Coordinate System for Field Containing Any Number of Arbitrary Two-Dimensional Bodies. Journ. Comp. Physics 15, 1974, 299.
55. Thompson, J.F., et al., Use of Numerically Generated Body-Fitted Coordinate Systems for Solution of the Navier-Stokes Equations. Proc. AIAA 2nd Comp. Fluid Dynamics Conference, Hartford, Conn., 1975, 68.
56. Ghia, U. and Ghia, K.N., Numerical Generation of a System of Curvilinear Coordinates for Turbine Cascade Flow Analysis. Dept. of Aerospace Engineering, University of Cincinnati, Rep. No. AFL 75-4-17, April 1975.
57. Ghia, K.N., Ghia, U., and Studerus, C.J., Analytical Formulation of Three-dimensional Laminar Viscous Flow Through Turbine Cascades Using Surface-Oriented Coordinates. ASME, Journ. Fluids Engineering 76-FE-22, 1976.
58. Ghia, U., Ghia, K.N., and Studerus, C.J., Use of Surface-Oriented Coordinates in the Numerical Simulation of Flow in a Turbine Cascade. In [4].
59. Sood, Des R. and Elrod, H.G., Numerical Solution of the Incompressible Navier-Stokes Equations in Doubly-Connected Regions. AIAA Journ. 12, 1974, 636.
60. Staniforth, A.N., Dissertation. Dept. Appl. Math., University of Western Ontario, 1972.
61. Collins, W.M. and Dennis, S.C.R., Symmetrical flow past a uniformly accelerated circular cylinder. Journ. Fluid Mech. 65, 1974, 461.
62. Schlichting, H., Boundary-Layer Theory, 6th Ed., McGraw-Hill, 1968.
63. Lugt, H.J. and Haussling, H.J., The Acceleration of Thin Bodies in a Viscous Fluid. To be published.
64. Taneda, S., Visualization experiments on unsteady viscous flows around cylinders and plates. In Proceedings cited in [26].
65. Sarpkaya, T., An Analytical and Experimental Study of the In-Line and Transverse Oscillations of a Circular Cylinder in Uniform Flow. Naval Postgraduate School Rep. NPS-59SL75051-B, May 1975.
66. Lighthill, M.J., in Laminar Boundary Layers, Ed. Rosenhead, Oxford University Press, 1963, 64.
67. Telionis, D.P. and Werle, M.J., Boundary-Layer Separation From Downstream Moving Boundaries. ASME, Journ. Appl. Mech. 40, 1973, 369.
68. Lugt, H.J., The Dilemma of Defining a Vortex. Naval Ship Research and Development Center, CMD-11-74, March 1974.

ACKNOWLEDGMENTS

The author enjoyed fruitful discussions with Drs. W. Grabowski, H.J. Haussling, R. Zarda and Mr. S. Ohring of the Numerical Mechanics Division. He also would like to thank Mr. R. Coleman for his assistance in preparing some of the figures.

NUMERICAL TURBULENCE MODELING

Morris W. Rubesin
Ames Research Center, NASA, Moffett Field, Calif. 94035, U.S.A.

SUMMARY

Although even the largest and fastest electronic computers are incapable of numerically evaluating the details of the smallest scales of turbulence in an entire flow field, their computational power is sufficient to permit "modeling" turbulence with detail that was impossible in the past. Descriptions are given of the underlying bases and developments in two techniques of detailed turbulence modeling where the flow is treated in the Eulerian sense, and one technique where the Lagrangian motions of vortices are followed. First, a technique is described for solving the single-point statistically averaged conservation equations. The Reynolds stresses that appear in these equations are evaluated by solving supplemental differential equations which contain terms that are "modeled." A sequence of increasingly complex, but also increasingly general, modeling equations is described and computations based on these equations are compared with experimental data. The hierarchy of models described terminates with equations for the individual components of the Reynolds stress tensor. The second Eulerian technique approach to turbulence modeling is the direct numerical simulation of turbulent fields. In this approach, all three-dimensional eddies between a predetermined range of sizes are computed in time within a specified volume of flow. Present-day computers require a tradeoff between the size of the volume that can be considered and the degree of resolution of the turbulent eddies. Techniques of "modeling" the smallest eddies are described that permit enlarging the volume, or Reynolds number, that can be considered. Computed results and experimental data are compared for turbulent flow fields at Reynolds numbers of aerodynamic interest. Finally, developments in the Lagrangian technique whereby a turbulent flow field is treated as a finite number of ring vortices whose motions and distortions are followed in time and space are described.

NOMENCLATURE

A_s	surface area of aerodynamic body
A^+	van Driest damping function
a	modeling constant (ARAP model)
B	constant in "law of the wall"
b	modeling constant (ARAP model)
C	modeling constant
C_F	average skin-friction coefficient
c_1, c_2	modeling constants
c_D, c_d	
c_m, c_p	
c_{pg2}	
c_{ps1}	
c_{pv1}	
c_{pv2}	
c_w, c_μ	
D	diameter of sphere
E	Jones-Launder dissipation function
E_{11}	one-dimensional spectral energy function
E	three-dimensional spectral energy function
f	function
G	filter function
H	Glushko turbulence Reynolds number function
h	static enthalpy
k	wave number
k_ℓ	wave number vector component
k_s	Kolmogorov wave number
$\bar{k}$	kinetic energy of turbulence per unit of mass
L	length of aerodynamic body
L	Glushko length scale
ℓ	Ng-Spalding length scale
ℓ_1, ℓ_2	length scale of turbulence
ℓ_m	mixing length
N	number of mesh points
$\underline{n}$	normal vector
NS	Navier-Stokes equation operator
P	averaged pressure
Pr_t	turbulent Prandtl number
p	static pressure
q	characteristic turbulence velocity
$\bar{q}_j$	heat transport by molecular processes
R_{ij}	Reynolds stress
Re_L	Reynolds number based on length L
Re_T	turbulence Reynolds number
r	turbulence Reynolds number, Eq. (76)
r_o	modeling constant
s	Kolmogorov microscale of length
S_R	surface roughness parameter
S_{ij}	velocity strain tensor, ref. Eq. (7)
S	skewness
t	time
t*	time
T	averaging period

u_τ	friction velocity, $\sqrt{\tau_w/\rho}$
u_i	velocity vector component in ith direction
U_i	filtered (averaged) velocity vector component in ith direction
$\underset{\sim}{u}$	velocity vector
V	velocity
V_i	filtered velocity vector component in ith direction
$\dot{V}_i$	time derivative of V_i
v_i	velocity vector component in the ith direction
w	dissipation rate in compressible Wilcox-Traci model
x_i	coordinate vector, ith direction
x_2,y	coordinate normal to a surface
α,α^*	modeling constant
β,β^*	modeling constant
γ	constant in Gaussian filter
Δ,h	computational mesh dimension
Δ_A,Δ	characteristic filtering dimension
δ	boundary-layer thickness
δ^*	boundary-layer displacement thickness
δ_{ij}	Kronecker delta
ε	eddy diffusivity
ε	kinetic energy per unit mass dissipated by turbulence
ε_{ijk}	alternating tensor
ζ	mass-weighted average modeling constant
η	coordinate
θ	boundary-layer momentum thickness
κ	von Kármán constant
λ	modeling constant or Taylor microscale
Λ	ARAP length scale
μ	viscosity of fluid
ν	kinematic viscosity of fluid
$\tilde{\pi}$	Cole's wake function parameter
ξ^*	mass-weighted average modeling constant
ξ	coordinate
ρ	density of fluid
σ	modeling constant
σ_k,σ_z	modeling constant
σ_E,σ^*	modeling constant
τ_w	surface shear
$\bar{\tau}_{ij}$	molecular stress tensor
ω	Saffman-Wilcox dissipation rate
$\underset{\sim}{\omega}$	vorticity vector
$\langle\ \rangle$	statistical or time average

Subscripts

$(\underset{\sim}{\ }),(\underline{\ })$	vector quantity
e	boundary-layer-edge condition
w	property at surface

Superscripts

+	"law-of-the-wall" coordinate
$(\bar{\ })$	averaged quantity
$(\ )'$	fluctuating quantity
$(\tilde{\ })$	mass-weighted averaged quantity
$(\ )''$	mass-weighted fluctuating quantity
$\dot{(\ )}$	time derivative

INTRODUCTION

It is generally accepted that the dynamics of a fluid at a point in space away from a discontinuity such as a shock wave is well represented physically by the Navier-Stokes equations. For compressible fluids, these equations must be supplemented by a continuity equation containing a variable density and an energy equation. These equations are second-order, nonlinear partial differential equations that can be solved analytically for only a few simple flows. Most technologically important flow fields are turbulent and are much too complex to lend themselves to these analytical methods. The solution of turbulent flow fields, then, must be accomplished through numerical analysis.

Turbulence can be thought of as the time-dependent solution of the continuum Navier-Stokes equations resulting from all the nonlinear processes that reflect the instabilities within the equations and the disturbances that existed initially within the flow field or that were impressed at its boundaries. Thus, turbulence is a property of the flow field and depends only secondarily on the property of the fluid itself. Turbulence, as observed experimentally, contains certain characteristics that impose extremely stringent requirements on a computer that is to be used for its numerical analysis. It is a phenomenon identified with high Reynolds numbers where the nonlinear inertial processes dominate the flow. Also, high Reynolds number causes the range of scales between the largest and smallest features to be extremely wide. The existence of very small length scales of the turbulent eddies coupled with the three-dimensional character of the turbulence imposes the requirement on finite-difference methods of very small mesh spacings in all three directions of space; this, in turn, requires very large storage capacities within the computer. Further, the need to solve these equations in a time-accurate fashion, together with the small length scales, imposes very short allowable time steps in the numerical solution — this imposes the requirement of extremely fast computers. Even the largest and fastest computers anticipated in the reasonably near future fall far short of the requirements for accurately resolving the smallest significant scales of the turbulence at Reynolds numbers of aerodynamic interest.

This conclusion is illustrated by an example for which the computer specifications required to numerically simulate the turbulence in the boundary layer of an aircraft are estimated from a knowledge of the smallest scales of turbulence that must be resolved by the finite-difference computations. Kolmogorov (Ref. 1) gives an expression for the length scale of the smallest significant eddy:

$$s = \left(\frac{\nu^3}{\varepsilon}\right)^{1/4} \tag{1}$$

where ν is the kinematic viscosity of the fluid and ε is the kinetic energy per unit mass being dissipated by the turbulence. The latter quantity can be estimated as

$$\varepsilon = \frac{\text{drag} \times \text{velocity}}{\text{mass in boundary layer}} \cong \frac{C_F \frac{1}{2} \rho V^2 \cdot V \cdot A_s}{0.6\, A_s \delta(L) \cdot \rho} \cong \frac{C_F V^3}{\delta(L)} \tag{2}$$

If the classic equations for the drag coefficient and boundary-layer thickness for an incompressible turbulent boundary layer on a flat plate are introduced into Eq. (2) and the resulting ε used in Eq. (1):

$$s = 1.5L/(Re_L)^{3/4} \tag{3}$$

The number of mesh points required to resolve a boundary layer of unit width is

$$N \cong \frac{\text{volume of boundary layer}}{s^3} = \frac{(L \cdot 1)[0.6\, \delta(L)]}{s^3} = \frac{0.2}{L} Re_L^{41/20} \tag{4}$$

e.g., on an aircraft surface 4 m long, 1 m wide, and $Re_L = 10^7$: $N = 10^{13}$. For even this example that treats only a portion of an aircraft surface, the number of mesh points required is about 10^8 larger than the memory unit existing in the core of a large computer such as ILLIAC IV, and about 10^6 larger than its more slowly accessed disk storage. This example illustrates the basis of the conclusion that the calculation of aerodynamic turbulence resolved to its smallest scales cannot be accomplished by current computers or those anticipated in the reasonably near future. This conclusion is reinforced when the computation times governed by the small time scales of the turbulence are considered.

To eliminate these difficulties, the point values of instantaneous velocity, pressure, and density must be replaced with new dependent variables sufficiently smooth and continuous that they can be resolved by a computer. In doing this, some of the physics contained in the basic equations is lost, especially for mechanisms such as the dissipation of turbulence into heat that is dominated by the smallest scales prevalent in the turbulence. Some of this physics must be recovered through turbulence "modeling," which relies a great deal on experimental data. Thus, numerical turbulence modeling is an interdisciplinary activity that involves both complex numerical analysis and a careful examination and interpretation of experimental data.

The dependent variables that can be resolved by the computer and utilized in the turbulence calculations are based on some sort of averaging process that filters the explicit behavior of the small scales from the problem. Linear terms transfer directly to filtered quantities. The nonlinear terms in the Navier-Stokes equations, however, form averaged moments. Thus, the averaging process introduces many new dependent variables in each equation. These moments must either be ignored or expressed in terms of the lower-order moments or individual averaged quantities to avoid the proliferation of dependent variables relative to the number of equations — known as the "closure" problem. The techniques of "closing" the equations that describe the averaged quantities is a major aspect of the turbulence modeling process.

In Eulerian finite-difference computations, the main thrust of research activity in turbulence modeling has been with two distinct though related approaches. The first can be called "statistical theory of inhomogeneous turbulence" and is a direct outgrowth of the classic papers of Rotta (Refs. 2 and 3). In his work, the basic equations result from time or ensemble averages of the Navier-Stokes equations at a single point or from velocity moment equations based on the Navier-Stokes equations at two points. The method is most applicable to steady-state, mean flow fields or to flow fields that are varying slowly relative to the turbulence time scales. The second method, called "turbulence simulation" or "sub-grid modeling," depends on averaging the primitive equations over space, which can be a line, a surface, and/or a volume. The space dimension is smaller than the largest eddies, but much larger than the tiniest eddies of the turbulence. This latter approach computes the dynamics of the eddies large enough to be resolved by a three-dimensional computation mesh. The results which are the motions of three-dimension large eddies, must be treated statistically to yield mean flow properties of engineering interest or information to aid statistical turbulence modeling. Finally, a third method of modeling turbulence utilizes Lagrangian methods. Here, vorticity fields are averaged into a sequence of discrete vortices, which are then followed in space and time.

This paper does not attempt to survey all the research taking place throughout the world on the various aspects of turbulence modeling. Emphasis is placed on the author's work, or that of his colleagues, or contracted work the author has monitored. This rather narrow view is permissible because the material to be covered represents the "state of the art" in many respects. In this paper, consideration is first given to the methods of averaging the Navier-Stokes equations for both the statistical and simulation techniques. The effects of compressibility are handled in the statistical theory of turbulence by alternative methods: where averaging is performed for the primitive variable of velocity, pressure, and density or when the velocity is mass weighted before the averaging operation. Then a sequence of turbulence models of increasing complexity is described in terms of boundary-layer flows, including the effects of compressibility. These models apply to two-dimensional compressible boundary layers. Some models employ an eddy viscosity whose magnitude is computed from one or two equations that represent the intensity and scale of the turbulence. A second turbulence model evaluates each of the Reynolds stress and turbulent heat-flux components directly. Research in simulating turbulence is described, both at very low Reynolds number where the small eddies can be resolved and at Reynolds numbers that correspond to actual flows where the

influence of eddies smaller than the finite-difference mesh spacings must be modeled. Finally, some progress in the simulation of turbulence through the use of finite ring vortices is presented.

In these presentations, the physical aspects of the turbulence modeling are emphasized. The numerical methods used in most of the work are generally accepted finite-difference techniques. When unique mathematical methods are used, they are mentioned only briefly.

AVERAGING THE NAVIER-STOKES EQUATIONS

The specific averaging process used to account for the unresolvable small-scale eddies present in turbulence depends on the general character of the flow field and the detail to which it is to be determined. This point is illustrated with three examples. The first applies to steady-state mean turbulent flows and leads to the methods called the "statistical theory of turbulence." Two subsets of this averaging process are utilized for compressible fluids: direct time averaging of the primitive dependent variables u_i, p, and ρ or time averaging where the dependent variables are mass-weighted. The second averaging process uses a time average that follows the flow in time. Such an average, then, eliminates details of the turbulence with time scales that are small compared to the averaging interval and permits computation in time and space of the larger scales of the turbulence. This approach is best suited to flows where the large eddy structure is two-dimensional. Finally, the most detailed calculation of turbulence which considers its full three-dimensional character uses averaging over space contained by a finite-difference grid system at an instant of time. These latter methods, called "large eddy simulation" methods, are the third example shown. These averaging processes are treated together in this section to illustrate features they contain in common and to delineate their differences, especially with regard to the meanings of the filtered dependent variables. The dependent variables must be defined precisely in each averaging process to interrelate the different methods and to compare the computed results with experimental data that may be filtered in their own peculiar ways.

Statistical Theory of Turbulence

The Navier-Stokes system of equations for a compressible fluid in the absence of external body forces is

$$\rho_{,t} + (\rho u_j)_{,j} = 0 \tag{5}$$

and

$$(\rho u_i)_{,t} + (\rho u_i u_j + \delta_{ij} p - 2\mu S_{ij})_{,j} = 0 \tag{6}$$

where the notation of repeated indices represents summation over all coordinate directions and the comma represents partial differentiation. Here, the instantaneous strain of the flow is

$$S_{ij} = \frac{1}{2}(u_{i,j} + u_{j,i}) - \frac{1}{3}\delta_{ij} u_{k,k} \tag{7}$$

For steady-state mean flows, the averaging process applied to Eqs. (5) and (6) is

$$\overline{f}(x_j) = \lim_{T\to\infty} \frac{1}{2T} \int_{-T}^{+T} f(x_j, t^*)\, dt^* \tag{8}$$

The averaged equations become

$$(\overline{\rho u_j})_{,j} = 0 \tag{9}$$

and

$$(\overline{\rho u_i u_j} + \delta_{ij}\overline{p} - 2\overline{\mu S_{ij}})_{,j} = 0 \tag{10}$$

when the definition represented by Eq. (8) leads to

$$\overline{(f_{,t})} = (\overline{f})_{,t} = 0 \tag{11}$$

for steady-state mean flows. Also,

$$\overline{(f_{,j})} = (\overline{f})_{,j} \tag{12}$$

In terms of the primitive variables, the local velocity and fluid properties are expressed as the sum of a mean and a fluctuating quantity:

$$f = \overline{f} + f' \tag{13}$$

In particular, then

$$u_j = \overline{u}_j + u_j' \tag{14}$$

$$\rho = \overline{\rho} + \rho' \tag{15}$$

$$p = \overline{p} + p' \tag{16}$$

$$\mu = \bar{\mu} + \mu' \tag{17}$$

Consistency of these equations with the definition in Eq. (8) requires that

$$\lim_{T\to\infty} \frac{1}{2T}\int_{-T}^{T} f'(x_j, t^*)dt^* = 0 \tag{18}$$

When Eqs. (14) and (15) are introduced into Eq. (9), and the definitions in Eqs. (8) and (18) are applied,

$$(\overline{\rho u_j} + \overline{\rho' u_j'})_{,j} = 0 \tag{19}$$

as the equation of continuity. Similarly, the momentum equation becomes

$$\left[\bar{\rho}\bar{u}_i\bar{u}_j + \overline{\rho' u_i' u_j} + \overline{\rho' u_j' u_i} + \bar{\rho}\overline{u_i' u_j'} + \overline{\rho' u_i' u_j'} + \delta_{ij}\bar{p} - \bar{\mu}\left(\bar{u}_{i,j} + \bar{u}_{j,i} - \frac{2}{3}\delta_{ij}\bar{u}_{k,k}\right)\right]_{,j} \tag{20}$$

where the small effects of the fluctuating viscosity are neglected. It is observed from Eqs. (19) and (20) that fluctuations in the fluid density introduce several additional second-order moments and one third-order moment.

These equations can be simplified by redefining the manner of expressing the instantaneous flow quantities and the properties of the fluid through the use of mass-weighted averages, originated by Favre (Ref. 4). Here

$$u_j = \tilde{u}_j + u_j'' \tag{21}$$

$$\mu = \tilde{\mu} + \mu'' \tag{22}$$

where $\tilde{}$) means a mass-weighted averaged quantity and ( )" represents the mass-weighted fluctuation. Specifically, a mass-weighted velocity is found by applying Eq. (8) to ρu_j obtained from Eq. (21). Then

$$\overline{\rho u_j} = \bar{\rho}\tilde{u}_j + \overline{\rho u_j''} \tag{23}$$

and defining $\tilde{u}_j$ as the mass-weighted mean:

$$\tilde{u}_j = \frac{\overline{\rho u_j}}{\bar{\rho}} \tag{24}$$

establishes the requirement that

$$\overline{\rho u_j''} = 0 \tag{25}$$

Equation (25) is the analog in mass-weighted averages to Eq. (18). It can also be shown (Ref. 5) that

$$\overline{u_j''} = -\frac{\overline{\rho' u_j''}}{\bar{\rho}} = -\frac{\overline{\rho' u_j'}}{\bar{\rho}} \tag{26}$$

When Eqs. (21), (22), (15), and (16) are introduced into Eqs. (5) and (6) and mass-weighted averages are taken, the mean equations of motion (Ref. 5) become

$$(\bar{\rho}\tilde{u}_j)_{,j} = 0 \tag{27}$$

and

$$\left[\bar{\rho}\tilde{u}_j\tilde{u}_i + \delta_{ij}\bar{p} - \tilde{\mu}\left(\tilde{u}_{i,j} + \tilde{u}_{j,i} - \frac{2}{3}\delta_{ij}\tilde{u}_{k,k}\right) - \overline{\rho u_i'' u_j''}\right]_{,j} = 0 \tag{28}$$

where, again, the smaller terms associated with the viscosity are neglected. A comparison of these equations with Eqs. (19) and (20) shows that mass-weighted averaging eliminates the need for considering the mass-flux correlation terms $\overline{\rho' u_j'}$. Equations (27) and (28) are identical to the equations used to compute steady laminar flows, except for the additional term $\overline{\rho u_i'' u_j''}$.

Equations (19) and (20), or Eqs. (27) and (28), represent the basic averaged or filtered transport equations used in statistical turbulence theory. The remainder of the theory applies to the evaluation of $\overline{\rho' u_j'}$, $\overline{u_i' u_j'}$, and $\overline{\rho' u_i' u_j'}$ or the equivalent $\overline{\rho u_i' u_j'}$ (see section "Statistical Turbulence Models").

Time-Dependent Mean Flow

If the "mean" flow relative to the small scales of turbulence varies with time, the averaging procedure represented by Eq. (8) can be modified to a running average (see Ref. 6):

$$\bar{f}(x_j, t) \approx \frac{1}{2T}\int_{t-T}^{t+T} f(x_j, t^*)dt^* \tag{29}$$

Here the value of T is assumed to be large compared to the periods characteristic of small scales of the turbulence and small compared to the period of the mean motion. The meaning of T will be seen more clearly after some development. From Eq. (29), it follows that

$$\overline{\frac{\partial f}{\partial t}} = \frac{\partial \overline{f}}{\partial t} \tag{30}$$

and

$$\overline{\frac{\partial f}{\partial x}} = \frac{\partial \overline{f}}{\partial x} \tag{31}$$

For clarity, the following discussion is restricted to the simpler equations of incompressible flow where the Navier-Stokes equations are

$$u_{j,j} = 0 \tag{32}$$

and

$$u_{i,t} + \left[u_i u_j + \delta_{ij}(p/\rho) - \nu u_{i,j}\right]_{,j} = 0 \tag{33}$$

The methods of Ref. 6 are applied here in terms of Eq. (29). Consider the hypothetical trace of a velocity signal (e.g., from a hot wire) in a turbulent flow (Fig. 1). The instantaneous velocity at time t^* can be represented in two ways. First, as shown in Fig. 1(a),

$$u_i(t^*;t) = U_i(t) + u_i'(t^*;t) \tag{34}$$

where t is constant in the integration of Eq. (29). If $U_i(t)$ is defined so that

$$\overline{u_j'(t)} = \frac{1}{2T}\int_{t-T}^{t+T} u_i'(t^*;t)dt^* = 0 \tag{35}$$

then

$$\overline{u_i}(t) = U_i(t) \tag{36}$$

Also,

$$\overline{u_i u_j}(t) = U_i(t)U_j(t) + \overline{u_i' u_j'}(t) \tag{37}$$

When Eqs. (32) and (33) are averaged according to Eq. (29), and the instantaneous u_i is represented by Eq. (34),

$$U_{j,j} = 0 \tag{38}$$

$$U_{i,t} + (U_i U_j + \delta_{ij}(P/\rho) - \nu U_{i,j} + \overline{u_i' u_j'})_{,j} = 0 \tag{39}$$

where both U_i and $\overline{u_i' u_j'}$ are sufficiently smooth and continuous to be resolvable.

The manner of expressing $u_i(t^*)$ in Eq. (34) is such that the small-scale turbulence can have opposite signs on either side of $t^* = t$. Intuitively, this behavior is inconsistent with the idea that turbulence is random, especially in its smallest scales. An alternative definition for the local velocity that does not suffer from this is

$$u_i(t^*) = V_i(t^*) + v_i'(t^*) \tag{40}$$

(as shown in Fig. 1(b)). The symbols V and v are used for the velocity components to distinguish the variables in this type of averaging. If T is short compared to the period of the large-scale motions, the first term on the right in Eq. (40) can be expressed with the first two terms of a time series:

$$u_i(t^*) = V_i(t) + \dot{V}_i(t)\cdot(t^* - t) + v_i'(t^*) \tag{41}$$

If $V_i(t)$ and $\dot{V}_i(t)$ are established from the requirement that

$$\overline{v_i'(t^*)} = 0 \tag{42}$$

applying Eq. (29) to (40) shows that

$$\overline{u}_i(t) = V_i(t) \tag{43}$$

A comparison of Eqs. (36) and (43) shows that the large-scale quantities in both expressions Eq. (34) or (40) are identical. The moment of velocity becomes

$$\overline{u_i u_j} = V_i(t)V_j(t) + \dot{V}_i(t)\dot{V}_j(t)\,\frac{T^2}{3} + \dot{V}_i(t)\overline{v_j'\cdot(t^* - t)} + \dot{V}_j\overline{v_i'\cdot(t^* - t)} + \overline{v_i' v_j'} \tag{44}$$

or

$$\overline{u_i u_j} = \overline{V_i(t)V_j(t)} + \dot{V}_i(t)\overline{v_j'(t^* - t)} + \dot{V}_j(t)\overline{v_i'\cdot(t^* - t)} + \overline{v_i' v_j'} \tag{45}$$

A comparison between Eq. (37) and (44) reveals that the Reynolds stresses are related as

$$\overline{u_i' u_j'} = \dot{V}_i \dot{V}_j \frac{T^2}{3} + \dot{V}_i \overline{v_j' \cdot (t^* - t)} + \dot{V}_j \overline{v_i' \cdot (t^* - t)} + \overline{v_i' v_j'} \tag{46}$$

Thus, the terms identified as small-scale Reynolds stresses in these equations depend to a large extent on the actual averaging or filtering process used. Only in the limit $T \to 0$ do the following Reynolds stresses apply:

$$\overline{u_i' u_j'} = \overline{v_i' v_j'} \tag{47}$$

However, this limit is meaningful only when the time scales of the resolved turbulence and the small-scale turbulence are widely different. Although the large-scale quantities for the two averaging processes described are identical in meaning, their computed values may differ, depending on the modeling applied to the individual subgrid terms, as in Eq. (46).

Subgrid Averaging

For the computation of time-dependent, three-dimensional fields of turbulence, the small-scale eddy filtering is customarily performed over space related to the finite-difference mesh dimensions. Deardorff (Ref. 7) utilized a running averaging over the computational grid volumes, analogous in three dimensions to the one-dimensional time averaging cited earlier leading to Eqs. (35) and (36). Schumann (Ref. 8) considered the Navier-Stokes equations in conservation form, involving volume and surface integrals, and demonstrated that space averaging should include both volume and surface averages. This sort of averaging permitted Schumann to consider noncubic mesh volumes in a most direct fashion. He was forced ultimately, however, to relate these different surface and volume averages to avoid proliferation of dependent variables to numbers exceeding the number of available equations. While the Deardorff and Schumann methods are very valuable for solving practical problems, emphasis is placed here on the filtering method suggested by Leonard (Ref. 9) and developed by Kwak et al. (Ref. 10). This latter procedure is particularly suited to illuminate the interaction of the averaging or filtering process and the spectral character of the resolved eddies.

Leonard averaging begins with representing a turbulent field variable, again with Eq. (13), but with the mean or filtered quantity defined as a volume integral

$$\overline{f}(\underline{x}) = \int_{-\infty}^{+\infty} G(\underline{x} - \underline{x}') f(\underline{x}') d\underline{x}' \tag{48}$$

Here $\underline{x}$ and $\underline{x}'$ are coordinate vectors and $d\underline{x}'$ represents an element of volume about $\underline{x}'$. The function G is the selected filter function, and its dependence on the position difference vector is most suited to homogeneous flows. If $f(\underline{x}')$ were constant, then $\overline{f}(\underline{x}) = f(\underline{x}') = C$, and the filter function G must satisfy

$$1 = \int_{-\infty}^{+\infty} G(\underline{x} - \underline{x}') dx' = \int_{-\infty}^{\infty} G(\zeta) d\zeta \tag{49}$$

For homogeneous flows, the function G extends over all space. For nonhomogeneous flows, a directional bias may be needed to define G. For the present, attention is focused on homogeneous flows.

If G is piecewise continuously differentiable and tends to zero as $(\underline{x} - \underline{x}') \to \infty$ and f is bounded in value or $f = 0$, at the surface of a finite volume of integration, then

$$\overline{\frac{\partial f}{\partial \underline{x}}} = \frac{\partial \overline{f}}{\partial \underline{x}} \tag{50}$$

and

$$\overline{\frac{\partial f}{\partial t}} = \frac{\partial \overline{f}}{\partial t} \tag{51}$$

as for a running time average, Eqs. (30) and (31). When

$$u_i = \overline{u}_i + u_i' \tag{52}$$

and the Navier-Stokes equations are averaged according to Eq. (48), there results

$$\overline{u}_{i,i} = 0 \tag{53}$$

$$\overline{u}_{,t} + (\overline{u_i u_j})_{,j} = -\left(\frac{\overline{P}}{\rho}\right)_{,i} + \nu \overline{u}_{i,j,j} \tag{54}$$

The nonlinear term expands to

$$\overline{u_i u_j} = \overline{\overline{u}_i \overline{u}_j} + \overline{u_i' \overline{u}_j} + \overline{\overline{u}_i u_j'} + \overline{u_i' u_j'} = \overline{u}_i \overline{u}_j + (\overline{\overline{u}_i \overline{u}_j} - \overline{u}_i \overline{u}_j) + \overline{u_i' \overline{u}_j} + \overline{\overline{u}_i u_j'} + \overline{u_i' u_j'} \tag{55}$$

The term $\overline{\overline{u}_i \overline{u}_j}$ represents the quadrature of filtered quantities filtered again. In a time-dependent solution of these equations, the second filtering operation can be performed at the previous time step since

the intervals between time steps are usually quite short. The other three terms in this member contain subgrid quantities that must be modeled. Some modeling processes treat them as a group:

$$R_{ij} = \overline{u_i' \bar{u}_j} + \overline{\bar{u}_i u_j'} + \overline{u_i' u_j'} \tag{56}$$

There is a striking similarity between Eqs. (55) and (56) and those resulting from time averaging in the previous section.

The contribution of the filter function can be illustrated with a few examples. First, consider a "top-hat" filter function defined as

$$\left.\begin{aligned} G(\underline{x} - \underline{x}') &= \frac{1}{\Delta_A} \quad \text{for} \quad |\underline{x} - \underline{x}'| < \frac{\Delta_A}{2} \\ &= 0 \quad \text{for} \quad |\underline{x} - \underline{x}'| \geq \frac{\Delta_A}{2} \end{aligned}\right\} \tag{57}$$

On applying Eq. (48) with (57), the mean velocity becomes

$$\bar{u}_i(\underline{x}) = \frac{1}{\Delta_A} \int_{-\Delta_A/2}^{\Delta_A/2} u_i(\underline{x} + \underline{\varsigma}) d\underline{\varsigma} \tag{58}$$

which is equivalent to a running volume average. The Fourier transform of Eq. (58) is

$$\bar{u}_i(\underline{k}) = \prod_{\ell=1}^{3} \frac{\sin(k_\ell \Delta_A/2)}{(k_\ell \Delta_A/2)} u_i(k) \tag{59}$$

To permit Fourier transformation back to physical space, one must choose Δ_A so that $k_e \Delta_A \neq m\pi$ (where m is an integer) to avoid singularities.

A filter function utilized by the Stanford group (Ref. 10) for homogeneous flows is the Gaussian filter:

$$G(\underline{x} - \underline{x}') = \left(\sqrt{\frac{\gamma}{\pi}} \frac{1}{\Delta_A} \right)^3 \exp\left[- \frac{\gamma(\underline{x} - \underline{x}')^2}{\Delta_A^2} \right] \tag{60}$$

where γ is a constant set equal to 6. With Eq. (60), the filtered velocity is

$$\bar{u}_i(\underline{x}) = \left(\sqrt{\frac{\gamma}{\pi}} \frac{1}{\Delta_A} \right)^3 \int_{-\infty}^{+\infty} u_i(x') e^{-\gamma(\underline{x}-\underline{x}')^2/\Delta_A^2} d\underline{x}' \tag{61}$$

The Fourier transforms are related as

$$\bar{u}_i(\underline{k}) \approx u_i(k) \exp\left(- \frac{\Delta_A^2}{4\gamma} k^2 \right) \tag{62}$$

A comparison of Eqs. (59) and (62) shows that the spectral intensity of the filtered velocity decreases much more rapidly for the Gaussian than for the "top-hat" filter, i.e., an exponential squared term vs. $\sin(k\Delta_A/2)/(\Delta_A/2)$. Thus for given mesh dimensions, the Gaussian filter velocity captures a smaller fraction of the total turbulence momentum and kinetic energy of the turbulence.

A third type of filter that has been used is

$$G(\underline{x} - \underline{x}') \approx \prod_{\ell=1}^{3} \frac{\sin \pi(x_\ell - x_\ell')/\Delta_A}{\pi(x_\ell - x_\ell')} \tag{63}$$

which yields a sharp cutoff in wave number or k space.

Canonical View of Filtering

The filtering methods of the Navier-Stokes equations described previously were identified with steady state-flows (statistical turbulence theory), time-dependent flows with running time averages and time-dependent, volume-averaged flows (subgrid modeling). The first category incorporates <u>all</u> turbulence into the Reynolds stresses and the filtered velocities are true mean values in a statistical sense. The finite-difference mesh spacings used for such computations are controlled by the spatial gradients of the mean flow field and are not related to the spectral character of the turbulence. When time-dependent fields are to be considered, the primary factor in establishing the filtering time period or filtering space dimension is the fraction of turbulence to be calculated explicitly and that which is to be consigned to the subgrid or subperiod Reynolds stresses. The spectral character of the turbulence plays an important role in this decision. It was shown that the form of the equations resulting from either running time averages or volume or grid averages is identical, although the dependent variables formally are based on different definitions. When consideration is given to the spatial resolution required to be consistent with the time-filtered velocity or, conversely, the corresponding time interval consistent with a volume-filtered quantity, the difference between the running time or volume-filtered quantities becomes rather indistinct. Thus, the two approaches have much in common and the modeling experiences of one can

be carried over to the other. In both approaches, the turbulence modeling becomes less important as the scales of turbulence resolved by the computations become smaller. Further, because turbulence tends toward isotropy as scales diminish the subgrid model has the greater potential of being universal in character.

MODELING STATISTICAL TURBULENCE EQUATIONS IN BOUNDARY-LAYER FLOWS

Before the equations that describe steady-state statistical turbulence (e.g., Eqs. (19) and (20) or (27) and (28)) can be solved for a specific flow field, it is necessary to provide some means of evaluating the moments of the unresolved velocity fluctuations (Reynolds stresses) which they contain. The method used has a long history and a complete description is beyond the scope of this paper. References 11 through 14 provide an excellent review of the subject. A brief description to place the current methods in the proper context follows. For illustrative purposes, it is best to start with the simpler constant property flows.

Constant Fluid Properties

The earliest models of the Reynolds stresses in a boundary-layer or channel flow were developed by Prandtl in 1925. The Reynolds shear stress was expressed with a Boussinesq eddy diffusivity:

$$-\rho\overline{u'v'} = \rho\varepsilon\,\frac{\partial\bar{u}}{\partial y} \tag{65}$$

and, as noted from the dimensions of ε, the eddy diffusivity could be expressed in terms of the properties of the turbulence, such as the velocity scale or intensity of the turbulence and measures of the scale of the eddies, their length, period, or frequency. Thus

$$\left.\begin{aligned}\varepsilon &\cong \text{velocity scale} \times \text{length scale}\\ &\cong (\text{velocity scale})^2/\text{frequency}\\ &\cong (\text{velocity scale})^2 \times \text{period}\end{aligned}\right\} \tag{66}$$

Algebraic Models

Prandtl represented the velocity scale by

$$\text{velocity scale} = \ell_1\left|\frac{\partial\bar{u}}{\partial y}\right|$$

where ℓ_1 is a characteristic length. He represented the length scale with ℓ_2, another characteristic length. The eddy diffusivity became

$$\varepsilon = \overline{\ell_1\ell_2}\left|\frac{\partial\bar{u}}{\partial y}\right| = \ell_m^2\left|\frac{\partial\bar{u}}{\partial y}\right| \tag{67}$$

where ℓ_m was called the "mixing length." At short distances away from the surface, it was found empirically that

$$\ell_m = \kappa y \tag{68}$$

where κ is the von Kármán constant ($\kappa = 0.4$). Very near the surface, the viscosity of the fluid "damps" the length scale so that $\partial\ell_m/\partial y = 0$ at the surface. There are many expressions to account for the damping, the most popular being that suggested by van Driest:

$$\ell_m = \kappa y\left\{1 - \exp\left[-\frac{y\sqrt{(\tau_w/\rho)}}{\nu A^+}\right]\right\} \tag{69}$$

The damping factor A^+ equals 26 on a flat plate, but it is sensitive to pressure gradients and surface mass transfer (Ref. 11).

About 1/4 of the boundary-layer thickness away from the wall, the mixing length begins to fall below the value represented by Eq. (68). Beyond $y/\delta \cong 0.25$, the mixing length can be represented by

$$\ell_m = 0.09 \times \delta \tag{70}$$

as suggested by Escudier (Ref. 15). An alternative direct expression for the eddy diffusivity in the outer part of a boundary layer is

$$\varepsilon = 0.0168u_e\delta^* \tag{71}$$

as suggested by Clauser (Ref. 16). Here the constant contains the relationship of the local velocity scale relative to u_e and the local length scale relative to δ^*. Sometimes Eqs. (70) and (71) are modified to account for the physical fact that the turbulence in the outer part of the boundary layer is intermittent. This group of equations, Eqs. (65) through (71), has been the basis of many successful turbulent boundary-layer or channel-flow design computations and should continue to be successful for those flow fields and boundary conditions where the turbulence can remain reasonably in equilibrium with the mean motion (see Refs. 11 and 12).

One-Equation Models

There are many flow fields where the mean flow changes so rapidly that the turbulence cannot remain in equilibrium with the mean motion; this must be accounted for by modeling the turbulence with differential equations. Early research in this modeling process accounted for the nonequilibrium by expressing the velocity scale as the square root of the turbulence kinetic energy per unit mass. The kinetic energy of turbulence was defined by a partial differential equation from moments of the Navier-Stokes equations:

$$u_j NS(u_i) + u_i NS(u_j) = 0 \tag{72}$$

where NS represents the Navier-Stokes equation operator (e.g., Eq. (6)). When Eq. (72) is averaged according to Eq. (8), contracted, and mean quantities subtracted, the following kinetic energy of turbulence results

$$(\rho\overline{k})_{,t} + (\rho\overline{u}_j\overline{k})_{,j} = -\rho\overline{u_i'u_j'}\overline{u}_{i,j} - \overline{\left[u_j'\left(p' + \frac{\rho}{2}u_i'u_i'\right)\right]}_{,j} + [\mu\overline{k}_{,j}]_{,j} - \mu\overline{u_{i,j}'u_{i,j}'} \tag{73}$$

when, for simplicity, the fluid properties are considered constant. The first term on the right is identified with the production of turbulence, the second with the diffusion of turbulence by the turbulence, the third with the diffusion of turbulence by molecular processes, and, finally, the fourth with the dissipation of the turbulence. Since the goal of the computation is to evaluate $\rho\overline{u_i'u_j'}$, the first term contains no new quantities to the problem and can stand as is. The second term contains third-order and pressure-fluctuation terms that do not appear in the conservation equations for the mean motion and are new to the problem. To avoid a proliferation of unknowns, these terms are "modeled" in terms of the mean motion and quantities such as an eddy diffusivity. The third terms, expressible in the dependent variable of interest $\overline{k}$, is treated directly. The fourth term depends on the gradients of turbulence fluctuations and therefore is produced largely by small-scale eddies. Again, this is a new unknown and must be modeled to "close" the equation at the level of the turbulence kinetic energy equation. Since k involves second-order correlations of velocity fluctuations, this is an example of "second-order closure."

An example of a one-equation closure model restricted to a boundary layer is the method of Glushko (Ref. 17). Glushko models the turbulence kinetic energy equation, Eq. (73), for a boundary layer as

$$(\rho\overline{k})_{,t} + (\rho\overline{u}_j\overline{k})_{,j} = \rho\varepsilon(r)u^2_{,2} + \left\{[\mu + \rho\varepsilon(\lambda r)]\overline{k}_{,2}\right\}_{,2} - [\mu + \rho\varepsilon(\lambda r)]c\,\frac{\overline{k}}{L^2} \tag{74}$$

where the terms on the right represent the production, diffusion, and dissipation of turbulence kinetic energy, respectively. The production term is a direct eddy diffusivity representation of the term in Eq. (73). The turbulent diffusion of kinetic energy and pressure fluctuations are grouped as an eddy diffusivity controlled gradient diffusion process. The term λ acts as a Prandtl number representing the ratio of the turbulent diffusion of mean momentum to that of turbulence kinetic energy. The dissipation term is modeled to apply both near the surface and in the fully turbulent portions of the boundary layer, i.e., the μ and $\rho\varepsilon$ terms, respectively. Although dissipation is a mechanism that occurs at the smallest scales of the turbulence, the dissipation length scale, L, has been shown from the theory of isotropic turbulence (Ref. 18) to be much greater than the Kolmogorov scale and of the same order as the mixing length, ℓ_m, when the dissipation is expressed in terms of the kinetic energy over all eddy dimensions. Specifically, the quantities in Eq. (74) were represented by Glushko as

$$\frac{\varepsilon}{\nu} = H(r)\alpha r \tag{75}$$

where the turbulence Reynolds number

$$r = \frac{\sqrt{\overline{k}L}}{\nu} \tag{76}$$

and $H(r)$ is expressed empirically as

$$H(r) = \begin{cases} r/r_o & , \quad 0 \le r/r_o < 0.75 \\ r/r_o - (r/r_o - 0.75)^2 & , \quad 0.75 \le r/r_o < 1.25 \\ 1 & , \quad 1.25 \le r/r_o < \infty \end{cases} \tag{77}$$

The length scale is given by an empirical expression based on data of the correlation length in the y direction obtained in a flat-plate boundary layer:

$$\frac{L}{\delta} = \begin{cases} x_2/\delta & , \quad 0 \le x_2/\delta < 0.23 \\ (x_2/\delta + 0.37)/2.61 & , \quad 0.23 \le x_2/\delta < 0.57 \\ (1.48 - x_2/\delta)/2.52 & , \quad 0.57 \le y/\delta < 1.48 \end{cases} \tag{78}$$

The empirical constants suggested by Glushko are

$$\left.\begin{aligned} \alpha &= 0.2 \\ r_o &= 110 \\ C &= 3.93 \\ \lambda &= 0.4 \end{aligned}\right\} \tag{79}$$

A critical examination of the Glushko model was made in Ref. 19 by comparing computed results with experimental data for an incompressible turbulent boundary layer on a flat plate and on a surface subjected initially to a large adverse pressure gradient followed by a constant pressure region. A comparison of the results obtained from the Glushko model with the Coles "law of the wall" (Ref. 20) is shown in Fig. 2. The Coles correlation is known to fit an extensive collection of constant property flat-plate boundary-layer data. In the inner part of the boundary layer, $x_2 u^*/\nu < 20$, the Glushko model yields excellent results. In the region where the Coles law is logarithmic, the Glushko model underpredicts the local velocity slightly. In the outer part of the boundary layer, the Glushko model continues to underpredict the local velocity as shown by the comparison with Clauser's velocity defect correlation (Ref. 16) shown in Fig. 3. Despite these differences in the velocity profiles, the Glushko model yielded excellent predictions of the local skin friction and shape factor, δ^*/θ, on a flat plate at Reynolds numbers corresponding to positions downstream of the end of transition. Beckwith and Bushnell (Ref. 19) investigated the consequence of modifying the function $H(r)$, Eqs. (77), the length scale, Eqs. (78), the constant C in the dissipation term, and the diffusion rate. They found that setting $H(r) = 1$ at $y/\delta > 0.5$ and increasing the diffusion by a factor of 3 slightly improved the velocity profile predictions in the outer part of the boundary layer, but had very little effect on the predicted skin friction and on δ^*/θ.

Beckwith and Bushnell next applied the Glushko model to a calculation of the boundary layer on a surface with an adverse pressure gradient followed by a constant pressure at conditions corresponding to a particular test from the data of Goldberg (Ref. 21). These data were chosen as a particularly severe test of the Glushko model because the adverse pressure gradient was sufficiently strong to drive the boundary layer toward separation. The computations were initiated at the upstream measurement station where the data for the mean velocity and turbulent kinetic energy profiles were used as initial values of the computations. Figure 4 shows the distribution of the velocity at the boundary-layer edge with distance along the test surface. The two curves represent two ways of interpreting the data, and their difference is indicative of the uncertainty in the velocity. Although the differences are quite small on the figure, it is the derivatives of the curves that enter the calculations and differences in them that affect the computations of the skin friction and form factor significantly. Figure 5 shows the skin-friction coefficient along the test surface computed by Beckwith and Bushnell with the original Glushko model and some modifications compared with Goldberg's data. The data are given in a crosshatched band that represents the scatter of different types of measurements and interpretations: a sublayer fence, a Preston tube, velocity profiles and a Clauser plot, and velocity profiles and the Ludwieg-Tillman formula. The original Glushko model with enhanced diffusion and $H(r) = 1$ at $y/\delta > 0.5$ fits the data well at the upstream and downstream ends of the test zone with either velocity distribution. The skin friction, however, does not drop as much as the data in the range $0.4 < x_1 < 0.5$ m. When the models are adjusted to follow the large drop in C_f by increasing the constant of the dissipation term or lowering the value of the maximum length scale in Eq. (78), the downstream value of C_f is missed. Since the data are most reliable there, the value of the modifications is questionable. Figure 6, showing the form factor δ^*/θ, leads to similar observations and conclusions. In either case, the Glushko model permits a reasonably accurate prediction of the general behavior of the rather severe test. Possibly, this results from the ability of the model to predict the profile of the turbulent kinetic energy quite well (as shown in Fig. 7). The modifications tried by Beckwith and Bushnell suggest a small improvement; however, the error in the data is probably larger than the differences between the various versions of the model, and even the original Glushko version yields rather good results.

Two-Equation Models

The one-equation models described previously use an algebraic length scale that implies an equilibrium between the local scale of turbulence and the mean flow. For rapidly changing mean flows, this assumption can be restrictive and is relaxed by models that express some function of the turbulence scale with a partial differential equation in addition to the one for the turbulence kinetic energy. The scale function and the turbulent kinetic energy are then combined to express the eddy diffusivity. Although there are many two-equation, second-order closure models, their general character can be described by examining four representative models, those of Jones and Launder (Ref. 22), Ng and Spalding (Ref. 23), Saffman and Wilcox (Ref. 24), and Wilcox and Traci (Ref. 25). These models are represented by the following for only the high turbulent Reynolds number portions of a boundary layer as this restriction was inherent in the form of the models presented by their originators.

Jones-Launder dissipation-function model:

$$\frac{D\bar{k}}{Dt} = \varepsilon(\bar{u}_{1,2})^2 - E + \left(\frac{\varepsilon}{\sigma_R}\bar{k}_{,2}\right)_{,2} \tag{80}$$

$$\frac{DE}{Dt} = c_1\varepsilon(\bar{u}_{1,2})^2\frac{E}{k} - c_2\frac{E^2}{k} + \left(\frac{\varepsilon}{\sigma_E}E_{,2}\right)_{,2} \tag{81}$$

where

$$\varepsilon = c_\mu \bar{k}^2/E \tag{82}$$

with the constants

$$c_1 = 1.55\,, \quad c_2 = 2\,, \quad c_\mu = 0.09\,, \quad \sigma_k = 1\,, \quad \sigma_E = 1.3 \tag{83}$$

Ng-Spalding length-scale model:

$$\frac{Dk}{Dt} = \varepsilon(\bar{u}_{1,2})^2 - c_D\frac{\bar{k}^{3/2}}{\ell} + \left(\frac{\varepsilon}{\sigma_k}\bar{k}_{,2}\right)_{,2} \tag{84}$$

$$\frac{D(\overline{k}\ell)}{Dt} = \epsilon(\overline{u}_{1,2})^2 c_p \ell - \left[c_m + C_w\left(\frac{\ell}{x_2}\right)^6\right]\overline{k}^{3/2} + \left[\frac{\epsilon}{\sigma_z}(\overline{k}\ell)_{,2}\right]_{,2} \tag{85}$$

where

$$\epsilon = \overline{k}^{1/2}\ell \tag{86}$$

with the constants

$$c_D = 0.09\ , \quad c_p = 0.98\ , \quad c_m = 0.059\ , \quad c_w = 702\ , \quad \sigma_k = \sigma_z = 1 \tag{87}$$

Saffman-Wilcox dissipation-rate model:

$$\frac{Dk}{Dt} = \alpha^*|\overline{u}_{1,2}|\overline{k} - \beta^*\omega\overline{k} + \left(\sigma^*\epsilon\overline{k}_{,2}\right)_{,2} \tag{88}$$

$$\frac{D\omega^2}{Dt} = \alpha|\overline{u}_{1,2}|\omega^2 - \beta\omega^3 + [\sigma\epsilon(\omega^2)_{,2}]_{,2} \tag{89}$$

where

$$\epsilon = \overline{k}/\omega \tag{90}$$

$$\left.\begin{aligned} \alpha^* &= \frac{3}{10}\ , \quad \beta^* = 0.09\ , \quad \sigma^* = \sigma = \frac{1}{2} \\ \alpha &= \alpha^*\left(\frac{\beta}{\beta^*} - \frac{4\sigma\kappa^2}{\alpha^*}\right), \quad \frac{5}{3} < \frac{\beta}{\beta^*} < 2 \end{aligned}\right\} \tag{91}$$

Wilcox-Traci dissipation-rate model:

$$\frac{Dk}{Dt} = \alpha^*|\overline{u}_{1,2}|\overline{k} - \beta^*\omega\overline{k} + (\sigma^*\epsilon\overline{k}_{,2})_{,2} \tag{92}$$

$$\frac{D\omega^2}{Dt} = \alpha|\overline{u}_{1,2}|\omega^2 - \left\{\beta + 2\sigma\left[\left(\frac{\overline{k}^{1/2}}{\omega}\right)_{,2}\right]^2\right\}\omega^3 + [\sigma\epsilon(\omega^2)_{,2}]_{,2} \tag{93}$$

where, again, Eq. (90) applies and

$$\alpha^* = \frac{3}{10}\ , \quad \beta^* = 0.09\ , \quad \sigma = \sigma^* = 0.5\ , \quad \beta = 0.15\ , \quad \alpha = \frac{1}{3} \tag{94}$$

Note that all of the above models use a kinetic-energy equation that contains production, dissipation, and gradient diffusion terms as does Eq. (74). Jones-Launder and Ng-Spalding do not model the production term, other than employing an eddy diffusivity in the first term of Eqs. (80) and (84). The Saffman-Wilcox and Wilcox-Traci models, however, model the production term in terms of the interaction of kinetic energy and mean strain. Chambers and Wilcox (Ref. 26) showed that these four models can be expressed in a common form; when this is done, it becomes evident that the terms in the four models representing the dissipation of kinetic energy are essentially equal. The models all use gradient diffusion, but those associated with Wilcox use half the diffusion rates of turbulence kinetic energy used by the others.

The scale equations of the four models contain dependent variables that are either expressed directly as a length (Ng-Spalding) or are quantities that involve spatial gradients in the dissipation function (Jones-Launder) or in the dissipation rate ω (Saffman-Wilcox or Wilcox-Traci). The first quantity can be expressed exactly with an extremely complex two-point correlation completely new to the system of equations. Similarly, when the second quantity is expressed exactly, many new second- and third-order single-point correlations of velocity gradients are introduced. The exact character of the equations cannot be retained, and the correlations must be modeled with approximations guided largely by dimensional arguments and analogy, term by term with the kinetic energy equation. The models identified with Saffman-Wilcox and Wilcox-Traci were modeled intuitively from the start, without reference to an exact equation. The similarity of the form of the different scale equations permits their comparison in a common form (Ref. 26). From this, it is noted that the models are essentially different in their "dissipation" terms. The Wilcox models, again, use smaller rates of gradient diffusion. The various scale variables can be interrelated as follows:

$$E = c_\mu \overline{k}\omega\ , \quad \ell = \overline{k}^{1/2}/\omega \tag{95}$$

In the above equations the absence of terms associated with molecular viscosity, e.g., those terms emphasized in Ref. 27, does not permit integration to the surface in finite-difference, boundary-layer codes. The inner boundary conditions for the turbulence variables as well as the mean flow must therefore be applied by fitting the computations to asymptotic relationships known to apply in the fully turbulent flow near a surface. These are the "law of the wall" for the mean velocity:

$$\lim_{\frac{x_2}{\delta} \to 0} \frac{\overline{u}_1}{u_\tau} = \frac{1}{\kappa}\log\frac{x_2 u_\tau}{\nu} + B$$

and, for the turbulence quantities,

$$\lim\ x_2/\delta \to 0: \quad \left.\begin{array}{ll} \left.\begin{array}{l} \overline{k} = u_\tau^2/\alpha^* \\ \omega = u_\tau/\alpha^*\kappa y \end{array}\right\} & \text{Saffman-Wilcox or Wilcox-Traci} \\ \left.\begin{array}{l} \overline{k} = u_\tau^2/\sqrt{c_\mu} \\ E = u_\tau^3/\kappa y \end{array}\right\} & \text{Jones-Launder} \\ \left.\begin{array}{l} \overline{k} = u_\tau^2/\sqrt{c_D} \\ \ell = c_D^{1/4}\kappa y \end{array}\right\} & \text{Ng-Spalding} \end{array}\right\} \tag{96}$$

Note from the modeling constant values of α^*, c_μ, and c_D that the limiting values of k for the different models are identical and, universally, the limiting eddy diffusivity is

$$\lim\ x_2/\delta \to 0: \quad \varepsilon = \kappa x_2 u_\tau \tag{97}$$

In the numerical work that led to the examples cited here, these inner boundary conditions were applied at values of $y^+ = x_2\overline{u}_1/\nu$ less than 20. The conditions at the edge of the boundary layer were set as follows:

$$\left.\begin{array}{l} \overline{u}_1 = u_e \\ \overline{k} = 0.015\ u_\tau^2/\alpha^* \\ \ell = 0.09\sqrt{\alpha^*}\delta \end{array}\right\} \tag{98}$$

The kinetic energy relationship above was found in the Wilcox models to yield velocity defects consistent with Clauser's correlation (as shown in Fig. 3). Values smaller than $k\alpha^*/u_\tau^2 = 0.015$ made little difference on the correlation, but the value given in Eq. (98) was easier to handle numerically. The expression for the length scale is equivalent to the Escudier model (Ref. 15), where the mixing length ℓ_m is given by $\ell_m/\delta = 0.09$.

The computations made with these equations, and the mean-flow equations (9) and (10), are based on a version of the now standard marching techniques utilized for the parabolic boundary-layer equations. Since the equations are applicable only to fully turbulent equations, it is necessary to initiate computations at a station where the boundary layer is fully turbulent. The initial profiles of mean velocity, $\overline{k}$, ω, E, and ℓ, are based on data when comparisons are made with experimental results. For predictions, it has been found useful to start computations on the assumption that the initial station is on a flat plate where

$$\frac{\overline{u_1}}{u_\tau} = \frac{1}{\kappa}\log\frac{u_\tau x_2}{\nu} + B + \frac{2\tilde{\pi}}{\kappa}\sin^2\left(\frac{\pi}{2}\frac{x_2}{\delta}\right) \tag{99}$$

the Coles "law of the wall" and "law of the wake" combined. The kinetic energy of turbulence can be approximated by

$$\overline{k} = \frac{u_\tau^2}{\alpha^*}\cos^2\left(\frac{\pi}{2}\frac{x_2}{\delta}\right) \tag{100}$$

and the length scale, ℓ, can be represented by the Escudier model as

$$\left.\begin{array}{ll} \ell = \kappa\sqrt{\alpha^*}x_2 \ , & x_2 < 0.09\ \delta/\kappa \\ \ell = 0.09\sqrt{\alpha^*}\delta \ , & x_2 \geq 0.09\ \delta/\kappa \end{array}\right\} \tag{101}$$

The results of computations based on the four models explained above are compared here with experimental data on flat plates (Refs. 28 and 29), on a surface experiencing an adverse pressure gradient (Ref. 30), and a favorable pressure gradient (Ref. 31).

Figure 8 compares the computations with data obtained on flat plates. The Jones-Launder (JL), Ng-Spalding (NS), and Wilcox-Traci (WT) models reproduce extremely well the Karman-Schoenherr skin-friction correlation equation downstream of the initial station. The Saffman-Wilcox model gradually rises above the other relationships, but stays within 10% of the standard formula. On a law-of-the-wall plot corresponding to the downstream station farthest from the initial station, a similar ordering of prediction occurs for the different models. The differences between the models become more evident in the velocity profiles when plotted as in Fig. 8(c). The Wilcox-Traci model does slightly better here than the other models. The difference between the models, other than SW, is very slight in terms of the shape-factor distribution (Fig. 8(d)). Finally, Figs. 8(e) and (f) show how well the models represent the dependent variables of the modeling equations at the farthest downstream station. Figure 8(e) shows the profile of the kinetic energy. Two symbols are used to represent Klebanoff's data (Ref. 29); the crosses are the kinetic energy as measured, whereas the filled circles are $9/4\overline{(u_2'^2)}$. Wilcox has argued that the quantity $\overline{k}$ in Eqs. (80), (84), (88), and (92) should be identified with $\overline{u_2'^2}$ because it is this component of the Reynolds stress tensor that primarily produces the mixing in the shear stress and should represent the velocity scale of the eddy diffusivities. This view only changes the interpretation of the data within $y/\delta < 0.2$, but does not alter the conclusions from the comparison of different models. The WT model seems to perform slightly better than the others. Figure 8(f) reveals the reasons the SW model yielded higher skin friction than the others. It overshoots the length-scale data by almost a factor of 2. The NS and JL models perform best in predicting the length scale.

Figure 9 shows the ability of the models to compute data obtained on a surface of constant pressure followed by an adverse pressure gradient. The open and closed symbols represent different interpretations of the data and suggest its possible inaccuracies. The WT and NS do best in computing skin-friction distribution and downstream velocity profiles (Figs. 9(a)-(d)). For the modeling dependent variables, there is little to choose between the models in terms of the effective kinetic energy, but again the SW model has difficulties with the length scale (as indicated in Fig. 9(f)). In Fig. 10, the computations are compared with the data obtained in a favorable pressure gradient by Ludwieg and Tillman, again interpreted in two ways (Refs. 28 and 31). When the possible error range of these data is considered, all the models do well in computing the results, based only on mean-flow measurements.

Full Reynolds Stress Modeling

Aerodynamic flow fields characterized by asymmetries, three-dimensional features, boundary-layer separation, and/or extremely rapid changes in the mean flow cannot be represented with a scalar eddy diffusivity without the introduction of additional approximations. To avoid these approximations and to utilize a system of modeling equations that, in principle, may have universal application to a variety of flow fields, much attention has been given to modeling the components of the Reynolds stress tensor directly. Rotta's pioneering effort in the area (Refs. 2 and 3) contained many of the basic elements of the current models that have been developed in research centers in various parts of the world. Emphasis is placed here on the invariant tensor modeling originated by Donaldson (Ref. 32) and further developed at the Aeronautical Research Associates at Princeton (ARAP) for atmospheric and aerodynamic flow fields (Refs. 33-35). This emphasis does not imply that this particular model is the most complete available, but it has been extended to compressible flows, a topic of particular interest to this author. It contains another feature in its boundary-layer version, i.e., terms that permit accounting for low-turbulence Reynolds numbers and thereby allowing computations to be extended to the surface. The need to fit to the law of the wall, as in the two-equation models cited earlier, is eliminated. This is particularly important near points of boundary-layer separation. The model in the form presented here, however, is restricted, even with its generality in treating the Reynolds stress tensor, to an algebraic length scale, as was the Glushko one-equation model discussed previously. It differs basically from the Glushko model, then, in that the elements of the kinetic energy are resolved and the local shear stress is computed directly without invoking an eddy diffusivity.

The basic equations of the invariant second-order closure of Donaldson and his colleagues are presented in Refs. 32 through 35. Reference 35 makes a careful comparison of computations with the Donaldson model and experimental data in a variety of incompressible aerodynamics flow fields. For brevity, only attached-boundary-layer flows are considered here. Before presenting some details of the model, it is necessary to define the term "invariant" used in connection with this model. It takes on the double meaning that (1) the modeled terms exhibit the same tensor symmetry and dimensionality as the terms they replace and (2) the goal that constants in the model need not be varied from flow to flow. Currently, the latter goal relative to the scale equation of turbulence is being pursued along lines given in Refs. 3, 36, and 37.

In Cartesian coordinates, the boundary-layer equations for the elements of the Reynolds stress tensor are:

$$\frac{D(\overline{u_1'^2})}{Dt} = 2(-\overline{u_1'u_2'})\bar{u}_{1,2} + [(\nu + c_d \cdot q \cdot \Lambda)(\overline{u_1'^2})_{,2}]_{,2} - \frac{4}{3} c_{pg1}(-\overline{u_1'u_2'})\bar{u}_{1,2} - 2c_{pg2}\frac{q}{\Lambda}\left(\overline{u_1'^2} - \frac{1}{3}q^2\right)$$

$$- \frac{q^3}{\Lambda}\left(\frac{2}{3}b + \frac{2a}{(q\Lambda/\nu)}\frac{\overline{u_1'^2}}{q^2}\right) \tag{102}$$

$$\frac{D(\overline{u_2'^2})}{Dt} = \left\{[\nu + (3c_d + 2c_{pv2}) \cdot q \cdot \Lambda](\overline{u_2'^2})_{,2}\right\}_{,2} + \frac{2}{3} c_{pg1}(-\overline{u_1'u_2'})\bar{u}_{1,2} - 2c_{pg2}\frac{q}{\Lambda}\left(\overline{u_2'^2} - \frac{1}{3}q^2\right)$$

$$- \frac{q^3}{\Lambda}\left[\frac{2}{3}b + \frac{2a}{(q\Lambda/\nu)}\frac{\overline{u_2'^2}}{q^2}\right] \tag{103}$$

$$\frac{D(\overline{u_3'^2})}{Dt} = [(\nu + c_d \cdot q \cdot \Lambda)(\overline{u_3'^2})_{,2}]_{,2} + \frac{2}{3} c_{pg1}(-\overline{u_1'u_2'})\bar{u}_{1,2} - 2c_{pg2}\frac{q}{\Lambda}\left(\overline{u_3'^2} - \frac{1}{3}q^2\right)$$

$$- \frac{q^3}{\Lambda}\left[\frac{2}{3}b + \frac{2a}{(q\Lambda/\nu)}\frac{\overline{u_3'^2}}{q^2}\right] \tag{104}$$

and

$$D(-\overline{u_1'u_2'}) = \overline{u_2'^2}\bar{u}_{1,2} + \left\{[\nu + (2c_d + c_{pv2})q \cdot \Lambda](\overline{u_1'u_2'})_{,2}\right\}_{,2} + \left[\frac{C_{pv1}}{4}\Lambda^2\bar{u}_{1,2}(\overline{u_2'^2})_{,2}\right]_{,2} - C_{pg1}\bar{u}_{1,2}\overline{u_2'^2}$$

$$- 2c_{pg2}\frac{q}{\Lambda}(-\overline{u_1'u_2'}) - \frac{q^3}{\Lambda}\left[\frac{2a}{(q\Lambda/\nu)}\frac{(-\overline{u_1'u_2'})}{q^2}\right] \tag{105}$$

where

$$q^2 = \overline{u_1'^2} + \overline{u_2'^2} + \overline{u_3'^2} \tag{106}$$

and

$$\Lambda \cong 3\ell \tag{107}$$

defined by the Escudier model, Eq. (101). The modeling constants used in the examples that follow are

C_d (diffusion of third-order correlation) = 0.1

C_{pv_1} (diffusion of pressure-velocity correlations affected by mean velocity gradient) = 0

C_{pv_2} (diffusion of pressure-velocity correlation) = 0.1

C_{pg_1} (pressure-velocity gradient correlation mean velocity gradient contribution) = 0

C_{pg_2} (pressure-velocity gradient correlations) = 0.5

a (dissipation constant near wall) = 3.25

b (dissipation constant, high turbulent Reynolds number) = 0.125

The modeling equations are given in detail above so that physical phenomena contributing to the creation and destruction of individual Reynolds stresses can be described and their interaction demonstrated. The first term on the right in each equation represents the production of the individual Reynolds stress. Note that the interaction of the shear stress and the mean strain contributes to the production of u_1', whereas the other normal stresses are not produced directly. Equation (105) shows that the shear stress is produced by interaction $\overline{u_2'^2}$ and mean velocity strain. The diffusion mechanisms for the components $\overline{u_1'^2}$, $\overline{u_2'^2}$, and $\overline{u_1'u_2'}$ are each different. If Eqs. (102) to (104) were summed to yield the kinetic energy in the left members, the different coefficients in the diffusion terms would indicate the diffusion of a quantity different from the kinetic energy since the individual normal stresses would be weighted unequally. Thus this model does not collapse to the two-equation models wherever turbulent diffusion is important. The terms resulting from pressure velocity gradient correlations, Rotta's "tendency toward isotropy," containing the modeling coefficients C_{pg_1} and C_{pg_2} in Eqs. (102) through (104), sum to zero as required in incompressible flow. Although the C_{pg_1} terms are not included in the numerical example here, the equations show that the interaction of shear with the mean velocity strain removes energy from $\overline{u_1'^2}$ and distributes it equally to $\overline{u_2'^2}$ and $\overline{u_3'^2}$. In the normal stress equations, the C_{pg_2} terms remove energy from those components greater than the average energy of the normal stresses. The pressure-velocity gradient correlations tend to deplete the Reynolds shear stress. The dissipation terms used have both high and low Reynolds number contributions, as in Glushko's Eq. (74). Finally, note that, except for the diffusion terms, the equations for u_2' and u_3' are identical.

When this model is used to evaluate the characteristics of a boundary layer, the low Reynolds number terms it contains permit initiating the computations with a laminar boundary at an upstream station. Transition to turbulence can be initiated by introducing a "spot" of turbulence within the profile at the initial station. It is not believed that this transition corresponds to the physical transition, as the modeling coefficients were established from fully turbulent flow data, but it provides a convenient way to start the calculations. On a flat plate, the ARAP model yields skin friction that starts with the Blasius laminar boundary-layer solution, passes through a form of transition, and then follows the Karman-Schoenherr correlation equation. At stations with turbulent flow, a law-of-the-wall plot agrees with mean velocity profile data, but this should be expected since this fit was used to establish the value of the modeling constant a. In particular, the results of computations corresponding to the data obtained by Klebanoff (Ref. 29) are shown in Figs. 11 through 13. The computations were adjusted so that the calculated momentum thickness agreed with the measured value at the test station. As shown in Fig. 11, the computations of the mean velocity profile agree very well with the data. The shear stress profile (Fig. 12) is also well represented by computations that use the ARAP turbulence model, the calculated values being within 4% of the measurements near the wall. Figure 13 compares calculated and measured normal stresses. Again, the model evaluates the normal stress u_2' quite well over most of the profile. The model exceeds the data somewhat near the wall, but this is the region where a u_2' measurement is least accurate. The normal stresses u_1' and u_3', however, are underpredicted significantly. In fact, the modeled value of u_3' is the same as u_2', except for $y/\delta_{exp} > 0.7$. This observation is consistent with expectations resulting from the relative sameness of Eqs. (103) and (104), even if the modeling constant C_{pg_1} is not set equal to zero. The accurate prediction of u_2' and the strong dependence of the shear stress on this quantity possibly explain why good shear stress predictions result even though the kinetic energy is being missed. The inability of the model to predict each of the Reynolds stresses with equal accuracy brings into question whether the generality of the model can be utilized to its fullest at this time. Another full Reynolds stress model (Ref. 38) shows better agreement with these data; however, this model was not integrated to the surface and the input boundary conditions based on the data may have forced the agreement elsewhere. These models, while possessing considerable potential, require further development.

Compressible Fluid Flow

When consideration is given to compressible fluid flow, it is necessary to supplement the continuity and momentum equations with an energy transport equation that contains temperature or enthalpy as its dependent variable and an equation of state. When the energy equation is filtered, as, for example, with mass-weighted averages, the steady-state equations (27) and (28) are supplemented by

$$\left[\overline{\rho}\tilde{u}_j\left(\tilde{h} + \frac{\tilde{u}_i\tilde{u}_i}{2}\right) + \overline{q}_j + \overline{\rho u_j'' h''} - \tilde{u}_i(\overline{\tau}_{ij} - \overline{\rho u_i'' u_j''})\right]_{,j} = 0 \tag{108}$$

to the leading terms. Here the transport of heat and the stresses introduced by molecular processes are represented by $\overline{q_j}$ and $\overline{\tau_{ij}}$, respectively. The new turbulence quantity introduced is $\overline{\rho u_j'' h''}$; the turbulent heat flux, which represents primarily the correlation of velocity and static enthalpy fluctuations as the density fluctuations, also present, are of higher order. Consistent with the eddy diffusivity hypothesis, the turbulent heat flux can be written:

$$\overline{\rho u_j'' h''} = \frac{\rho \varepsilon}{Pr_t} \tilde{h}_{,j} \tag{109}$$

where a new parameter, the turbulent Prandtl number Pr_t, is introduced to relate the transport of energy with momentum. For models that employ full Reynolds stress, $\overline{\rho u_j'' h''}$ are represented as the dependent variables in separate partial differential equations. The Prandtl number is replaced by the modeling constants of these equations.

Algebraic Models

The algebraic models of turbulence are extended to compressible flows by the simple hypothesis that the local eddy diffusivity is independent of the local density and is sensitive to density variations only through their overall effect of the local strain and on the overall boundary-layer thickness. The length scales, Eqs. (68) through (70), are retained unchanged except for the use of surface or local properties in the van Driest damping function. In keeping with this hypothesis, the δ^* used in Eq. (71) neglects density variations (Ref. 11). Thus, the predominant effect of the local density on the turbulent shear stresses $\overline{\rho u_i'' u_j''}$ is in their proportionality to the density, with the correlation of the velocity fluctuations being relatively insensitive to local density levels. This simple hypothesis has proven to be very accurate for boundary layers on surfaces where changes occur quite gradually.

To date, most of the aerodynamic phenomena involving compressible flows, e.g., skin friction, aerodynamic heating, transpiration cooling, and/or ablation mechanisms, have been evaluated on the basis of this simple hypothesis and the algebraic models cited earlier (Ref. 11). Also, a large body of experimental data exists to support the accuracy of these methods. The presence of shock waves or compression zones in compressible flows provides a strong mechanism for driving a turbulent boundary layer out of equilibrium, and the need arises to utilize differential equations in defining the turbulence (see Ref. 39).

One-Equation Model

The Glushko kinetic-energy-equation model of turbulence, described earlier for incompressible fluids, has been extended in Ref. 40 to account for compressibility and separated flow. The incompressible flow length scale expressions, Eqs. (78), were retained as is, in keeping with the experience with mixing length behavior cited previously. It is emphasized that retaining Eqs. (78) for separated flows as well as boundary layers imposes the restriction that the region of separation must be relatively narrow compared to the upstream boundary-layer thickness. The effects of compressibility were introduced in the local Reynolds number of turbulence, $\bar{r}$, by using local properties in Eq. (76) and evaluating the kinetic energy of turbulence, now defined as a mass-weighted average:

$$\bar{k} = \frac{\overline{\rho u_i'' u_i''}}{\bar{\rho}} \tag{110}$$

from a differential equation appropriate to compressible flow. The mass-weighted average kinetic-energy equation for compressible flow is given here only in its boundary-layer form so that a direct comparison can be made with Eq. (74):

$$\frac{D\bar{\rho}\bar{k}}{Dt} = \bar{\rho}\varepsilon(\bar{r})(\tilde{u}_{1,2})^2 + \left\{[\tilde{\mu} + \bar{\rho}\varepsilon(\lambda\bar{r})]\bar{k}_{,2}\right\}_{,2} - [\tilde{\mu} + \bar{\rho}\varepsilon(\lambda\bar{r})]c\,\frac{\bar{k}}{L^2} + \zeta\,\frac{\bar{\rho}\bar{k}}{a^2}\,\frac{\tilde{u}_1^2}{a^2}\,\tilde{u}_{1,1} + \overline{u_1''}[-\bar{p}_{,1} + (\tilde{\mu}\tilde{u}_{1,2})_{,2}] \tag{111}$$

A comparison of Eqs. (111) and (74) indicates that compressibility, other than introducing local mean fluid properties, $\tilde{\mu}$ and $\bar{\rho}$, in all the terms adds two terms on the right in Eq. (111). It is shown in Ref. 40, however, that these terms can be expected to be negligibly small, except at hypersonic speeds. Thus, mass weighting itself appears to account for much of the effect of compressibility on turbulence.

An example of the use of the one-equation model to calculate the behavior of a sharply disturbed turbulent boundary layer is given in Ref. 41, where computations were compared with the data from a carefully documented experiment (Ref. 42). Figure 14 is a sketch of the experimental configuration. A normal shock wave was generated with a blockage device inside a cylindrical test section to create an interaction with the turbulent boundary layer on the wall. The Mach number upstream of the shock, $M_{\infty,x_0} = 1.44$, was achieved by expanding air through a slightly supersonic nozzle. The shock wave could be moved along the test section by adjusting the blockage caused by the shock generator. This permitted the surface pressure, skin friction, and the local flow direction under the separation bubble to be mapped with fixed surface gages (Ref. 43). Local mean flow and turbulence were also measured within the boundary layer and separated regions. For the experimental conditions shown in the figure, the separation bubble was negligibly narrow compared to upstream boundary-layer thickness, which allowed use of the Glushko length scale expressions, Eq. (78). The results of the computation are shown in Fig. 15. The solid line labeled "0-equation baseline" corresponds to the algebraic turbulence model described earlier. The dot-dashed line is the Glushko model as defined here. The dashed line represents the Glushko model, but with the modeling constants (79) modified to $\alpha = 0.22$, $r_0 = 120$, and $C = 4.69$. The figure shows that all three models yield excellent representations of the surface-pressure distribution. In terms of the skin friction, all the models do well upstream of the interaction. The algebraic model follows the data best at the onset of the positive pressure gradient, although downstream of separation and reattachment it misses the

data badly. The variants of the Glushko model lag the data at the onset of the pressure rise, but fit the data quite well in the downstream region. The turbulence and mean flow appear to be significantly out of equilibrium for this flow condition and, yet, the one-equation model with alterations or only minor alterations of modeling constants based on flat plate, incompressible boundary-layer flow appears to capture the essentials of this flow.

Two-Equation Models

Wilcox and Traci (Ref. 25) extended their two-equation model to compressible flow by utilizing mass-weighted dependent variables. The model contains molecular viscous terms that allow it to be integrated over the entire boundary layer.

To supplement the transport equations of mass, momentum, and energy, Wilcox and Traci used the modified kinetic energy equation:

$$\frac{D\bar{\rho}\bar{k}}{Dt} = \alpha^*\bar{\rho}\tilde{u}_{1,2}\bar{k} - \beta^*\bar{w}\bar{k} + [(\tilde{\mu} + \sigma^*\bar{\rho}\varepsilon)\bar{k}_{,2}]_{,2} - \xi^*\bar{\rho}\bar{k}\tilde{u}_{1,1} \tag{112}$$

Turbulent dissipation rate for compressible flow is

$$\frac{D}{Dt}\left[\bar{\rho}\left(\frac{w}{\bar{\rho}^n}\right)^2\right] = \alpha\bar{\rho}\tilde{u}_{1,2}\left(\frac{w}{\bar{\rho}^n}\right)^2 - [\beta + 2\sigma(\ell_{,2})^2 w]\left(\frac{w}{\bar{\rho}^n}\right)^2 + \left\{(\tilde{\mu} + \sigma\bar{\rho}\varepsilon)\left[\left(\frac{w}{\bar{\rho}^n}\right)^2\right]_{,2}\right\}_{,2} \tag{113}$$

For these equations, the modeling coefficients are

$$\left.\begin{aligned} \alpha^* &= \alpha_\infty^*\left[1 - \frac{10}{11}\exp(-2Re_T)\right], \quad \alpha_\infty^* = \frac{3}{10} \\ \beta^* &= 0.09, \quad \sigma = \sigma^* = \frac{1}{2}, \quad \beta = 0.15 \\ \alpha &= \alpha_\infty\left[1 - \frac{10}{11}\exp\left(-\frac{Re_T}{2}\right)\right], \quad \alpha_\infty = \frac{1}{3} \end{aligned}\right\} \tag{114}$$

where

$$Re_T = \frac{\bar{\rho}\bar{k}^{1/2}\ell}{\tilde{\mu}} \tag{115}$$

$$\ell = \frac{\bar{\rho}\bar{k}^{1/2}}{w} \tag{116}$$

and the eddy diffusivity is

$$\varepsilon = \frac{\bar{\rho}\bar{k}}{w} \tag{117}$$

The resemblance between these equations and Eqs. (92) through (95) is striking. This is further emphasized when it is found from comparisons with experimental data on flat plates that a reasonable choice for n in Eq. (113) is $n = 0$, and from arguments similar to those used for neglecting the term that contains ξ in Eq. (111) the term in Eq. (112) that contains ξ^* can also be neglected. Thus all new terms that contain the effects of compressibility or density fluctuations are eliminated. The model is sensitive only to the value of mean density $\bar{\rho}$. Note that the effect of turbulence Reynolds number on the modeling coefficients α and α^* has been introduced as the Wilcox-Traci model evolved. The boundary conditions to the transport equations and the turbulence modeling equations are

$$\left.\begin{aligned} u_1 = 0 \qquad u_2 = v_w \qquad T = T_w \\ \text{or} \quad \left.\frac{\partial T}{\partial x_2}\right|_w = -Pr_L\frac{q_w}{C_p\mu_w} \\ \bar{k} = 0 \qquad w = \frac{\rho_w u_\tau^2}{\alpha_\infty^* v_w}S_R \end{aligned}\right\} \quad y = 0 \tag{118}$$

where $Pr_L \equiv$ molecular Prandtl number and $C_p \equiv$ specific heat at constant pressure

Here S_R is a surface roughness parameter. For smooth surfaces, $S_R > 300$ is required in the numerical calculations. The outer boundary conditions are

$$\left.\begin{aligned} u_1 = U_e \qquad T = T_e \\ \bar{k} = fU_e^2 \qquad \ell = 0.09\sqrt{\alpha_\infty^*}\,\delta \end{aligned}\right\} \text{at} \quad y = \delta \tag{119}$$

Full Reynolds Stress Modeling

The ARAP models have been extended to compressible flow (Refs. 33 and 34) through the use of averaged primitive variables (see Eqs. (13)-(20)). In this approach, the turbulence modeling considers the effects of density fluctuations in an explicit manner through additional modeling equations for the correlation of the velocity-density fluctuations. For boundary-layer flows, the turbulence modeling is expressed through four Reynolds stress equations as for incompressible flows (e.g., Eqs. (102)-(105)), but these are supplemented by a heat flux equation, an enthalpy fluctuation intensity equation, and two density-velocity

correlation equations. These equations are much to complex to present here in detail. In the computational examples that follow, the modeling constants and modeling assumptions used were as given in the appendix of Ref. 43. As with the incompressible version of the model, the modeling equations contain molecular viscous terms that permit integration of the equations directly to the surface where the inner boundary conditions, equivalent to Eq. (118), can be applied. At the surface, all turbulent correlations are equated to zero. At the outer edge of the boundary layer, just as in Eq. (119), the turbulence correlations in the model can be assigned nonzero values to account for free-stream turbulence.

Comparison of Computations with Experimental Boundary-Layer Data

The results of boundary-layer computations based on the Wilcox-Traci and ARAP models, with the specific modeling coefficients described in Ref. 43, are now presented. For comparison, boundary-layer computations based on an algebraically defined mixing length model (as described earlier) are also included. These mixing length computations were made with the boundary-layer program originally developed by Marvin and Sheaffer (Ref. 44) and later modified by them to account for turbulent flow.

To test the abilities of the various turbulence models to predict the effects of compressibility in the absence of pressure gradients, the results of the computations for a flat-plate boundary layer are compared with results based on the van Driest II transformation, a technique that has been demonstrated to conform to experimental data on flat plates to about ±10% for all but very cold surface temperatures (Ref. 45). The comparisons shown in Fig. 16 apply to an insulated flat plate, i.e., at recovery temperature and at a fixed Reynolds number based on a momentum thickness of 5000. The ordinate is the ratio of the local skin-friction coefficients, at the elevated Mach number, to that given by the classic Karman-Schoenherr formula for incompressible flow. The effect of Mach number as given by the van Driest II transformation is shown by the solid line. The algebraic mixing length model, identified as Marvin-Sheaffer in the figure, yields results that are in excellent agreement with the van Driest II line. At higher Mach numbers, the ARAP Reynolds stress program yields results a bit higher than those given by the van Driest II approach; they are near the upper limit of the range to which the van Driest method agrees with a large body of experimental data. Although the Wilcox-Traci program yields results that are low over the entire range of Mach numbers, they are still within 10% of the van Driest line and would be consistent with the lower bound of the experimental data. Generally, then, all the models do reasonably well in predicting the effects of compressibility on the skin friction at supersonic speeds in the absence of pressure gradients.

To test the accuracies of the Wilcox-Traci and ARAP models for compressible flows with strong pressure gradients, computer programs containing the turbulence models were used to evaluate the boundary layers that occur in the series of experiments indicated in Fig. 17. The experiment of Zwarts (Ref. 46) was conducted in a two-dimensional channel with a compression wedge used to create an adverse pressure gradient on the flat test wall. Peake et al. (Ref. 47) measured the boundary layer on the inner walls of an axisymmetric cylindrical duct in an adverse pressure gradient created by a compression centerbody. Sturek and Danberg (Ref. 48) created their adverse pressure gradient with a two-dimensional compression ramp over which the test boundary layer grew. In this experiment, the boundary layer not only experienced an adverse pressure gradient, but was subject to the effects of a concave streamline curvature. The experiment of Lewis et al. (Ref. 49) was also conducted on the inner walls of an axisymmetric cylindrical duct. However, the centerbody used to create an adverse pressure gradient also permitted the boundary layer to relax through a downstream favorable pressure gradient. The ranges of flow-field variables are quite limited in these four experiments. Mach number ranged between 3.5 and 4. The Reynolds number range of the experiments varied by less than a factor of 7. All experiments were conducted with the test surface at the recovery temperature. Finally, the range of maximum pressure gradients, as measured by the parameter

$$p^+ = \frac{\rho_w \mu_w (dp/dx)_w}{(\rho_w \tau_w)^{3/2}} \tag{120}$$

is quite narrow for this set of experiments.

To start all the computations, the values of the dependent variables through the boundary layer and the surface skin friction at the first measurement station were established by assuming that the region upstream of this point acted as a flat plate with uniform boundary-layer-edge conditions identical to those that existed at the first test station. The effective length of this fictitious flat plate was found by matching the calculated momentum thickness to the measured value at the first test station. The surfaces were considered smooth and the turbulence level at the boundary-layer edge was set to zero.

Figure 18 shows Zwarts' data for the local skin-friction coefficient and the shape factor, $H = \delta^*/\theta$. The latter quantity is a sensitive function of velocity and temperature profile of the boundary layer. For this mild pressure gradient flow, the algebraic model still does slightly better than either the two-equation model (WT) or the Reynolds stress model (ARAP) in calculating the skin friction upstream of $x = 30$ cm. Beyond this point, there is little to choose between the models. In terms of the shape factor, the Reynolds stress model starts at a somewhat lower value, and this persists.

Figure 19 shows the streamwise distribution of the skin-friction coefficient and shape factor for the experiment of Peake et al. (Ref. 47). The p^+ is about 50% higher than in Zwarts' experiment. The Wilcox-Traci and ARAP models predict the skin-friction data much better than the Marvin-Sheaffer mixing length model. The ARAP full Reynolds stress model performs best in predicting the shape factor distribution, although, in the region of adverse pressure gradient and downstream (the primary regions of interest), the Wilcox-Traci model does equally well.

In the experiment of Sturek and Danberg (Ref. 48), the boundary layer that developed on the surface of a concave circular ramp was measured. Thus, this boundary layer experienced the simultaneous effects of adverse pressure gradient and streamline curvature. The latter effect has been shown in Ref. 50 to be, in itself, rather significant, yet the present calculations ignore surface curvature. The skin friction and shape factors are shown in Fig. 20. Note in this figure that the Marvin-Sheaffer model shows very

little of the experimentally observed rise of the skin friction in the downstream portion of the experiment. The Wilcox-Traci model overestimates the rise in skin friction. The ARAP model overpredicts the starting value of skin friction but seems to follow the trends in the data by staying about the same amount above the data over all test stations. Caution must be used when interpreting the comparisons of calculated and measured shape factors. The Sturek-Danberg velocity profile data show an overshoot of the velocity over the free-stream value far from the surface. Such an overshoot makes it difficult to define the position of the boundary-layer edge; this is reflected in both elements of the shape factor — momentum and displacements thicknesses. Thus, Sturek and Danberg give a range of values of H at each station. Even though the ones plotted here are the larger values given, they are much lower than the results of the Marvin-Sheaffer model. The more complex models seem to capture the character of the experimental data.

The last set of data is that of Lewis et al. (Ref. 49). These data are unique in that they contain an adverse pressure gradient, as do the other experiments cited earlier, followed by a downstream region of favorable pressure gradient wherein several stations of data are obtained. The local skin-friction coefficient and the shape factor are shown in Fig. 21. On the average, the ARAP model performs best because the Wilcox-Traci model appears to underpredict skin friction in a favorable pressure gradient rather badly. The Marvin-Sheaffer model does not achieve a high enough peak value of skin friction, yet does excellently in the region of favorable pressure gradient.

From the comparisons of the computed and experimental results in Figs. 15 through 21, it can be concluded that the differential equation models of turbulence, either one, two, or more modeling equations, can represent supersonic boundary-layer data in rather severe comparison flows without adjusting the modeling constants. The algebraic models perform well only for very small and gradual compressions and for expansion regions. More complexity within the differential equation models, however, does not dramatically improve the accuracy of the models for two-dimensional boundary flows. The more complex models can be extended to more general types of flow, hopefully, without requiring changes in the modeling constants. It is not certain at this time, however, that the models of inhomogeneous turbulence will prove to have a universal character for all flow situations, at least to the accuracy required in aerodynamic applications. This concern has led to the development of methods (described in the next section) that rely on a direct computation of most of the turbulence, in terms of energy and momentum, and modeling what remains.

DIRECT SIMULATION OF LARGE EDDY STRUCTURE

A method of computing turbulent flows that potentially is universally applicable is the computer simulation of the large eddy structure of the turbulent flow fields. The basis for this belief lies in the experimentally observed spectral character of turbulent flow fields. Generally, the large eddies in these fields are created by instabilities of the mean flow. These large eddies are relatively long lived, anistropic, and are different in every type of flow. The large Reynolds numbers associated with these eddies cause them to become unstable in themselves, and they break up to produce smaller eddies. Of course, smaller eddies also interact and merge to form larger ones. This process of the production of smaller eddies through instabilities and the recombination of eddies continues until a continuous spectrum of eddies is generated. The process reaches a stationary random state when eddies are produced that are so small that the viscosity of the fluid enhances their stability and provides the means for dissipating their energy into heat. These smallest eddies have short life times and tend to be isotropic in character, having evolved from eddies that themselves were rather randomly oriented. This process is not generally uniform but is intermittent involving such events as "bursts" and "spots" of turbulence. It is the complexity of this process that makes suspect the universality of statistical turbulence theories discussed previously, especially those that contain only few statistical moments. Large eddy simulation of turbulence computes these mechanisms for the largest eddies that contain most of the energy of the turbulence and models the effects of the eddies smaller than the finite difference mesh can resolve. By modeling only a fraction of the turbulence, the overall accuracy of the method becomes less dependent on the accuracies of the closure models than statistical methods, where all of the turbulence is modeled. Also, the isotropic and, hopefully, universal character of the small-scale eddies may permit the development of closure models based on sound physical arguments. It is this potential for accurate numerical simulation of turbulence that is driving the development of methods that are, at this time, still very costly computationally. Their future use as engineering tools for the aerodynamicist will ultimately depend on the size of the smallest scales of turbulence that will have to be computed to capture the essence of particular turbulent flow fields. Because these computations provide much more detailed information than can be measured in a turbulent field they will most certainly also be useful in concert with experiments in fluid mechanics toward improving statistical turbulence models for engineering applications.

The universal character of the small scales of turbulence is shown in Fig. 22 where the data of Tieleman (Ref. 51) obtained at different positions in a boundary layer are compared with those of Compte-Bellot and Corrsin (Ref. 52) in an homogeneous essentially isotropic flow. The coordinates of the figure were chosen to collapse the data at the high wave numbers. The abscissa is the ratio of the wave number to the wave number corresponding to the Kolmogorov scale. The ordinate is the measured one-dimensional energy spectral function normalized so as to collapse the Heisenberg isotropic turbulence theory (Ref. 53) to a single line. At the higher wave numbers, the boundary-layer data at different values of turbulence Reynolds number, free-stream speeds, and positions within the boundary layer correlate quite well. The homogeneous, isotropic turbulence data measured by Compte-Bellot and Corrsin also correlate with the boundary-layer data at the higher wave numbers. This illustrates that the small scales of turbulence at different points in a particular flow or in completely different flows actually possess a universal character. Further, it appears that this character is well represented by the Heisenberg theory, which predicts the upper bound of the "inertial subrange," as $k/k_S \approx 0.5$, and the "dissipation region" for $k/k_S > 0.5$. The figure also illustrates that the larger eddies or small wave numbers contain most of the energy of the turbulence and depend in character on the local mean flow. Finally, the figure indicates that an increased local turbulence Reynolds number broadens the range of wave numbers in the flow, extends the "inertial subrange," and diminishes the fraction of the large eddies that are not universally correlated. This latter observation may prove useful in the decisions regarding coordinate mesh dimensions in aerodynamic computations.

The first large eddy simulations were applied to geophysical studies of the dynamics of the atmosphere. In the United States, the group at the National Center for Atmospheric Research and Stephen Orszag and his colleagues have been the leaders in this field (Ref. 8). Extension of this work to problems in fluid mechanics and aerodynamics introduces new conditions that require careful reexamination of the fundamental approaches utilized in the past. These conditions involve the effects of compressibility, the interaction of adjacent irrotational and turbulent fields, near surface phenomena where viscosity plays an increasingly important role, and a large variety of flow configurations. On the other hand, the aerodynamic flow fields are simpler in that gravitational forces need not be considered. In this review, emphasis will be placed on the program taking place under NASA sponsorship at Stanford University and being performed at the Ames Research Center. The objectives of this work are to enhance the understanding of the basic methods involved, to examine the interaction of the physical and numerical methods, and to test subgrid closure models as applied to the previously mentioned aerodynamic conditions. The approach of achieving these objectives is to consider a sequence of increasingly complex flow fields starting with isotropic turbulence and then considering homogeneous flows undergoing normal strains, homogeneous shear flows, the free interaction of tangent streams, and channel flows. Although channel flows have been simulated in the past, originally by Deardorff (Ref. 7) and extended by Schumann (Ref. 8), these investigations employed the "law of the wall" near the channel surface and thereby avoided integrations to the surface. In doing this they did not illuminate near surface phenomena. At present, the bulk of the work has been confined to incompressible flows.

Low Reynolds Number Simulations of Isotropic Turbulence

Many of the concepts and methods underlying large eddy simulation can be illustrated through consideration of the decay of an homogeneous, isotropic turbulent field of an incompressible fluid. In fact, it is best to start with the examination of the method by considering the case where the turbulence Reynolds number, $q\lambda/\nu$, is sufficiently small so that the wave-number range between the largest eddy and the Kolmogorov eddy can be captured by the volume of flow considered and the computational mesh into which it is divided. In this case, there is no subgrid size turbulence of significance and turbulence modeling is not required. The computation can proceed as an accurate time-dependent solution of the Navier-Stokes system of equations.

One solution to this type of problem has been reported in Ref. 54 as part of a general method to compute low Reynolds number, simply strained homogeneous turbulence. The turbulence simulation program was prepared for use on the ILLIAC IV computer and is described with the table given in Fig. 23. For this problem, the computational volume was divided into as many as 64^3 mesh cells and the magnitude of the computational effort can be seen from this figure. Even this relatively simple problem must be handled with the largest and fastest computers available. The algorithms that were used are shown at the bottom of the figure. Spatial differentiation was accomplished with Fourier transforms, similar in principle to the work of Orszag (Ref. 55) but differing in detail. Aliasing was controlled to avoid instabilities in the computations. The temporal advance in the computations was explicit and employed the fourth order Runge-Kutta scheme.

The problem is started by fitting the magnitudes of the coefficients in wave number space to an experimental spectral function (Ref. 52). Then the directions of these vector coefficients are randomized in wave number space, subject to the constraint of maintaining continuity. Because of the use of Fourier transforms, the conditions at the opposite faces of the computational volume are identical, and this periodic boundary condition together with the dimension of the computational volume being considered establishes a maximum wavelength or minimum wave number that can be computed. The ratio of the maximum to minimum wave number depends on the number of mesh points fitted into the computational volume. The results of some of these computations are shown in Fig. 24 where the evolution of the energy spectrum of turbulence, beginning from the experimentally established spectrum, is shown as a function of the computational steps in time. Figure 24(a) shows the case where the minimum wave number treated is 0.2 cm^{-1} and the ratio of the maximum to minimum wave number was constrained to 21, equivalent to 43^3 alias free computation. It is observed that the turbulence decays as a whole as a result of the viscosity of the air. Similar computations with $\nu = 0$ showed the computational schemes to be energy conserving. As the spectral energy distribution evolves, it develops a bunching of the energy at the high wave numbers, even exceeding the initial values there. Figure 24(b) shows the improvement that results from increasing the number of mesh points within the computational volume to 64^3. Finally, Fig. 24(c) shows the effect of both increasing the number of mesh points and reducing the dimensions of the computational volume, i.e., shifting the wave-number range considered to larger values. The computation now captures the smaller eddies where viscous dissipation is larger and the results are beginning to approach the expected minus 5/3 power variation with the wave-number characteristic of the inertial range. The dissipation range indicated in Fig. 22 is still not approached in these calculations.

Another example of the computation of isotropic turbulence at low Reynolds number is the work of Clark, Ferziger, and Reynolds (Ref. 56). As with the computation described previously, the computational volume was divided into 64^3 mesh points. Clark et al. used the low Reynolds number data of Ref. 52 to guide the choice of the dimensions of the computational volume being considered. Because this computation also employed periodic boundary conditions on opposite faces of the computational volume, the authors decided that minimum dimension of the computational volume had to be at least twice the distance between two points where the experiment showed the longitudinal and lateral correlation of velocity components vanished. The largest wave number computed was established by the number of mesh points employed in the computation. The problem was initialized similarly to the Ragallo calculations. The initial spectral energy data (Ref. 52) corresponded to turbulence that had decayed to such a low Reynolds number that the selected computational volume encompassed the scales of turbulence where essentially all of the dissipation occurs. The Navier-Stokes equations were solved in an explicit time-dependent manner with a third-order scheme for advancing in time developed by the authors. Fourth-order accurate differencing was used to establish gradients in physical space. Without any subgrid modeling the results of the calculations agreed very well with the experimental rates of decay of turbulence kinetic energy found experimentally in Ref. 52.

When the calculation was completed, the numerical data were used to test the accuracy of a variety of subgrid closure models. To do this, it was imagined that the computational volume had only been divided into 8^3 mesh points and that subgrid closure models were to be utilized to account for the wave numbers that could no longer be detected with the coarser grid. Each of the new mesh volumes contained 512 of the computed points of the original fine mesh. The equivalent to the "top-hat" filter represented by Eq. (58) was then applied to the fine mesh data. The filtered velocity in the coarse mesh is then

$$\bar{u}_e(i,j,k) = \frac{1}{17^3} \sum_{i'=i-8}^{i+8} \sum_{j'=j-8}^{j+8} \sum_{k'=k-8}^{k+8} u_e(i',j',k') \tag{121}$$

where i, j, k, i', j', k' are mesh point labeling indices in the x_1, x_2, x_3 directions, respectively. The averaging "volume" or Δ_A in Eq. (58) was taken as $(16/8)\Delta$. This is consistent numerically with the value of $\Delta_A = 2\Delta$ found to yield the best results in Ref. 10. The contribution to the velocity of eddies with subgrid scale dimensions is then

$$u'_e = u_e - \bar{u}_e \tag{122}$$

at each of the 512 points within the coarse mesh. To assess the modeling, each of the terms on the right of Eq. (55) was computed at the centers of the coarse mesh cells, using the values from Eqs. (121) and (122). Thus

$$\overline{\bar{u}_e \bar{u}_m} = \frac{1}{17^3} \sum\sum\sum \bar{u}_e \bar{u}_m \tag{123}$$

$$\overline{\bar{u}_e u'_m} = \frac{1}{17^3} \sum\sum\sum \bar{u}_e u'_m \tag{124}$$

and

$$\overline{u'_e u'_m} = \frac{1}{17^3} \sum\sum\sum u'_e u'_m \tag{125}$$

These quantities were then used to compare the "data" with models of the subgrid contributions, utilizing constitutive relationships expressed in terms of the filtered velocities of the coarse mesh. The quantities compared are shown in Fig. 25. The column at the left represents the actual quantities being modeled; first, the difference between the quadrature of the filtered quantities and the same quadrature itself filtered; second, the interaction of filtered and subgrid scale quantities; and third, the subgrid Reynolds stresses. The second column shows how each of these quantities contributes to the decay of the turbulent kinetic energy. These proportions, while interesting, are likely to change with Reynolds number of the turbulence and must be viewed as being characteristic of low Reynolds numbers.

The third column shows the modeled constitutive relations for these quantities. The first was derived by Leonard (Ref. 9). It is the spatial analogue of the second term on the right of Eq. (44). The second term in this column was deduced in Ref. 56. Finally, the third term is an eddy diffusivity model in terms of the instantaneous strain of the filtered field. The models for the eddy diffusivity itself are shown below. They include the early model of Smagorinsky (Ref. 57), a vorticity model, a kinetic energy model, and finally merely a constant.

The fourth column shows how well these modeling equations based on the coarse grid averages correlate with the actual quantities in the first column when evaluated from the fine grid data and Eqs. (123)-(125). Correlation means the following

$$C = \frac{\langle (\text{value of quantity}) \times (\text{modeled quantity}) \rangle}{[\langle \text{value of quantity} \rangle^2 \times \langle \text{modeled quantity} \rangle^2]^{1/2}} \tag{126}$$

The filtered quantity of the first row, albeit small in contributing to energy decay, is correlated quite well by the model. The filtered subgrid correlation terms are correlated to about 0.7, as are all the subgrid eddy diffusivity models. It is surprising that all of the models, ranging from a constant eddy viscosity to one which requires the local kinetic energy of turbulence yield essentially the same correlation with the fine mesh data. This insensitivity to the closure model may again have been forced by the low Reynolds number of the example and may not be true generally. Finally, the fifth column shows the constants in the eddy diffusivity models required to yield energy decay given by the fine mesh solution. This is an example of how the numerical simulation of turbulence can contribute to the evaluation of constants in constitutive relationships for turbulence modeling.

High Reynolds Number Simulation of Isotropic Turbulence

In the previous examples of low Reynolds number simulations of isotropic turbulence, the values of the mesh point spacing were chosen to be able to numerically resolve those eddies with large wave numbers where most of the turbulence dissipation occurs. The capacity of the computers permitted using computational volume whose sides were about 20 times as long as the transverse integral scales measured in the experiment of Compte-Bellot and Corrsin. The agreement of the results with the data indicated that this distance was sufficiently large to avoid seriously biasing the results by the assumption of periodic boundary conditions on opposite faces of the computational volume. In addition, the computer volume was sufficiently large to contain essentially all of the kinetic energy of the large eddies. When high Reynolds number flows are considered, the range of wave numbers that are present in the flow increases dramatically and all the wave numbers cannot be accommodated by the computer. The computer size limitations fix the ratio of k_{max}/k_{min}, but the appropriate values of k_{max} and k_{min} must again be established by reference to experimental data. If k_{max} were set to capture the energy dissipation, the k_{min} would be too large to encompass much of the kinetic energy of the large scales of turbulence and the results would be biased by the use of periodic boundary conditions on faces too close together relative to the correlation lengths.

STEP

The approach, then, is to move the entire wave number range to smaller values, relying on the subgrid closure models to account for the turbulence dissipation.

To determine the bounds on the wave numbers most appropriate to high Reynolds number turbulence, studies were conducted (see Ref. 58) utilizing a variety of computational schemes, sizes of computational volumes, filter functions, and closure models. The computational methods utilized in the examples shown here were fourth-order accurate in space and second-order accurate in time. The reference experimental data were the highest Reynolds number cases of Ref. 52. Figure 26 shows the development in time of the gradient skewness factor, defined as

$$S_i = \frac{\langle(\bar{u}_{i,i})^3\rangle}{\langle(\bar{u}_{i,i})^2\rangle^{3/2}} \qquad \begin{matrix} i = 1, 2, \text{ or } 3 \\ \text{(not summed)} \end{matrix} \tag{127}$$

The skewness factor was selected as the basis of comparison for these calculations because it is physically related to spectral transfer of energy in the inertial subrange and is particularly sensitive to the joint behavior of spectrally dependent scales and intensities. Figure 26(a) shows the development of the skewness when the computational volume dimension is about 10 to 14 times the experimental lateral integral scale. There are three modeling conditions shown here, and each one of these is represented by three lines for the skewness in each coordinate direction. In these examples, the computational volume is divided into 16 parts on each side and has the mesh dimensions, h, as indicated. The case labeled with Δ/h indicates the use of the Gaussian filter function with $\Delta = 2h$. The cases labeled with k_c represent uses of the sharp cut-off filter in wave space, the Fourier transform of Eq. (63). The cut-off wave number and equivalent averaging volume in physical space are related as $\Delta = \pi/k_c$. The Smagorinsky model, referenced in Fig. 25, is used for the subgrid Reynolds stress in all of these cases. In this figure, the initial skewness is small because the initially applied random field is nearly Gaussian. Over the times shown, the calculated cases develop negative skewness, as occurs in experimental data, but not with the monatonic behavior that would have been expected. It is noted that anisotropy develops in all these cases. Incidentally, quantitative comparison of these skewness factors with published experimental data cannot be made because the computed skewness factor is based on gradients of filtered velocities that could only be compared with reinterpreted raw experimental data, if it were available. Figures 26(b) and 26(c) show representative results that occur from enlarging the computational volume. Figure 26(b) is based on the use of the Gaussian filter function with two eddy diffusivity closure models, the Smagorinsky and the vorticity models, refer to Fig. 25. Figure 26(c) indicates the effect of somewhat different initial conditions used in connection with the sharp wave-number cut-off filter. Both of these figures show that the use of the larger volume, with all the different modeling combinations, yields reasonable skewness behavior and isotropy in these calculations. The asymptotic numerical values of the skewness, however, depends on the modeling details. It appears, then, that modeling volumes must have dimensions about 20 times lateral correlation length scales or about 10 times the integral scales to avoid serious biasing by the periodic boundary conditions customarily employed in these computations. The low turbulence calculations, described earlier, conformed reasonably well with these criteria.

Figure 27 shows the rate of decay of the kinetic energy of the filtered turbulence. The lines represent the Compte-Bellot and Corrsin data in their original state and as a result of being filtered by the two types of filter functions. The Smagorinsky eddy diffusivity model was used for the subgrid scale Reynolds stress in the computations with both of the filter functions. The computed results are indicated with the discrete point symbols. It is noted that the filtering process eliminates much of the actual kinetic energy of the turbulence, the ratio of retained total kinetic energy being only about 40% and 57% (at $U_\infty t/M = 100$) for the Gaussian and sharp wave-number cut-off filters, respectively. Good agreement is achieved in these comparisons when the modeling constant in the Smagorinsky model is set to $C = 0.222$ and $C = 0.215$ for the Gaussian and wave-number filter, respectively. It appears that use of different filter functions, while capturing significantly different proportions of the kinetic energy, does not have a large effect on the modeling constant in the Smagorinsky model. These constants, however, differ by about 20% from the modeling constant evaluated from the low Reynolds number data, and this may be indicative of the limitations of an algebraic eddy diffusivity closure model.

Figure 28 shows how well the numerical simulation represents the filtered experimental three-dimensional energy spectra when the sharp cut-off filter in wave-number space is utilized. The lines represent the filtered data at three times. The points are computed results at $U_\infty t/M = 98$ and 171. The computations were started by fitting the filtered experimental spectral data at $U_\infty t/M = 42$ as described previously. Both the Smagorinsky and vorticity models for the eddy diffusivity are shown. Except for the results at the highest wave numbers, the comparisons are quite good for either of the diffusivity models. Figure 29 shows the spectral character of computations based on the Gaussian filter with $\Delta = 2h$. The high wave-number results appear to be a little better than those shown in Fig. 28.

In addition to providing the results noted here for the numerical simulations of high Reynolds number homogeneous, isotropic turbulence, Ref. 58 also carefully examined the influence of different numerical schemes and alternative conservation equations. One aspect of the study was the use of the vorticity equation rather than the primitive equations given here as the primary equation in the simulation. The results showed no significant advantage of one equation over the other. The vorticity equation, perhaps, would be useful for turbulent flow fields that border irrotational flows, where $\bar{\omega} \equiv 0$. Another part of the study was devoted to examining the evaluation of $\overline{\bar{u}_i\bar{u}_j}$ and it was concluded that this could be done best numerically be directly filtering the filtered dependent variables rather than modeling as in Fig. 25. Finally, a careful examination was made of Fourier methods for spatial differencing, and despite the increased accuracy of these methods no real improvements in the simulation process resulted. In fact, the modeling constants for eddy diffusivity models, found by fitting the simulations to corresponding experimental decay rates, depended only slightly (~10%) on the different numerical methods employed.

High Reynolds Number Channel Flow

To complete this brief description of the status of large eddy simulation methods in turbulent fluid flows, it is necessary to refer to Schumann's recent calculation of channel flows (Ref. 59) that extends

the earlier work of Refs. 7 and 8. This work represents the most detailed computation extant of a flow field of engineering interest. Although presentation of all its details is beyond the scope of this paper, some of its features are given here to contrast or relate them with those in methods described earlier.

Schumann employed noncubic computational meshes and to take this into account, he utilized finite difference equations that were based on integral conservation equations rather than point partial differential equations. This complicates the averaging process in that some moments of turbulence are averaged over both surfaces and volumes. These moments were interrelated with modeling coefficients that were given values ranging from 0.6 to 0.9, where unity implies the surface and volume average are equal. In addition, the finite difference methods were geometrically adjusted to account for the different mesh dimensions in the various directions. Apparently, these effects are handled with sufficient accuracy to yield results that are insensitive to modifications in the mesh dimensions.

The overall computational volume employed in these calculations is large. It spans the channels except for the sublayer regions adjacent to the walls. The length of the computational volume along the channel axis is as long as four channel heights, and this is sufficiently large relative to integral scales that periodic boundary conditions in the direction along the channel are quite appropriate. The use of such a relatively large computational volume, with limited computer capacity, places a burden on the subgrid stress model. The lowest wave number of the subgrid motion is sufficiently small to be in the spectral region where the turbulence is inhomogeneous. To accommodate this, Schumann represents the subgrid Reynolds stress, averaged over an element of surface as the sum of an "isotropic part" and an "inhomogeneous part,"

$$\overline{u_i' u_j'} - \frac{1}{3}\delta_{ij}\overline{u_k' u_k'} = \varepsilon_{iso}(\bar{S}_{ij} - \langle \bar{S}_{ij} \rangle) - \varepsilon_{inho}\langle \bar{S}_{ij} \rangle \tag{128}$$

Here the instantaneous strain rate $\overline{S_{ij}}$ depends on the large eddies. The bracketed terms are time averages that are steady-state quantities. The first term on the right is the contribution of the locally isotropic scales of the subgrid eddies, whereas the second term is due to the larger inhomogeneous subgrid structure. Schumann uses the form indicated for the isotropic part "to get zero time-mean values of the SGS (subgrid scale) stresses for $i \neq j$." The implication of this statement is that the time correlation of fluctuations in the locally isotropic eddy diffusivity ε_{iso} and the instantaneous excess strain rate $S_{ij} - \langle \overline{S_{ij}} \rangle$ are zero. This is equivalent to the expectations that models, such as those indicated on Fig. 25, did not introduce an average shear stress in the studies of homogeneous, isotropic turbulence discussed earlier. The random character of the large eddy strains relative to their mean values may be assuring this "isotropic" behavior.

The "isotropic" eddy viscosity ε_{iso} is evaluated with a kinetic energy model. The length scale in the model is the square root of the surface area over which the Reynolds stress is acting. The subgrid kinetic energy used in the model is established with a separate modeled equation, similar to Eq. (84) but containing the time-dependent large-scale motion to feed the subgrid turbulence. When Schumann's model is reduced to a cubic mesh, it has the same form functionally as the kinetic energy model used by Clark et al. The modeling constant found by Clark et al. agrees to within 3% of the constant Schumann identified as a theoretical value (Schumann's Table I). Schumann, however, found empirically that it was necessary to reduce this constant by a factor of 1/3 in his computations. This large change in the modeling constant may indicate the shortcomings of eddy diffusivity closure models to apply over flows with largely different Reynolds numbers. The inhomogeneous eddy viscosity ε_{inho} is evaluated from the mixing length expression, Eqs. (67) and (68). Equation (70), however, is replaced by

$$\ell_m = 0.1(\Delta x_1 \cdot \Delta x_2)^{1/2} \tag{129}$$

For the finest grids used, the ℓ_m from Eq. (129) is about 1/8th that normally used in algebraic statistical modeling of channel flows, and thus, in the core of the channel it would be expected that the subgrid scale contribution to the turbulent shear stress would be only about 1/64th of the total. This expectation is consistent with Schumann's numerical results. Towards the surfaces, the contribution of the subgrid Reynolds stress rises to dominate the shear. As the surface boundary conditions are applied by matching the computations to the "law of the wall," there is a large interplay between the various modeling assumptions in the vicinity of the surfaces and the contribution of each is not clear. Schumann found rather good agreement with experimentally measured mean-channel-flow velocity profiles and shear stress. The comparisons with turbulence quantities, such as the intensity in each coordinate direction, and correlation lengths show reasonable agreement with data. Improvements in these comparisons through refinements of the computational mesh are not dramatic and may not be warranted when it is noted that the mesh changes alter the computational times on an IBM 370/165 from less than 1 hour to as high as 14 hours. Finally, Schumann used computations to test modeling constants in the statistical theories of turbulence and found that many of the so-called constants are functions of the radial position across the channel. This last result tends to establish large eddy simulation techniques as being potentially the more universal method.

LAGRANGIAN SIMULATION OF WAKES WITH DISCRETE VORTEX FILAMENTS

An alternative to the fixed mesh, three-dimensional finite difference simulation technique presented in the previous section is the modeling of turbulence by tracking vortex filaments in Lagrangian reference frame. This general approach is the topic of the paper by Professor Clements in this lecture series, therefore only a very brief description of the technique developed by Leonard at the Ames Research Center (Ref. 60) will be given here. Leonard's approach is unique in its use of three-dimensional closed vortex filaments. The technique is illustrated with the simulation of the unsteady flow over a sphere at high Reynolds number shown schematically in Fig. 30. The aggregate flow field about the sphere is composed of a boundary layer, a fluctuating vortical wake flow that translates downstream relative to the sphere, and a fluctuating potential flow that responds to the closed ring vortices to maintain the proper inviscid

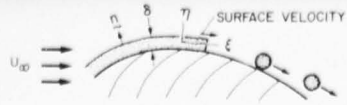

boundary conditions on the surface of the sphere and in the far flow field. The three essential mathematical elements of the problem are listed at the bottom of Fig. 30.

The boundary-layer model used by Leonard is described in Fig. 31. The boundary layer is represented by a sheet of vorticity that spills into a train of discrete vortex filaments. The amount of vorticity and the flux of circulation at each station, per unit of width of the boundary, are indicated by the equation on this figure. When the downstream front of the boundary-layer sheet, moving with a velocity $u(r_s)/2$ moves past a specified downstream latitude, a ribbon from the sheet is removed from the downstream edge and formed into the vortex filament of circulation Γ_v. The ribbon length is $u(rs)\cdot\Gamma/[2(d\Gamma/dt)]$. Besides their property of circulation, the vortex filaments are further defined with an effective core radius and are subdivided into discrete nodes along their axes. The newly formed vortex and any predecessors still in contact with the sphere constitute the remaining part of the vorticity in the attached boundary layer. The position in time of each vortex node is governed by the circulation, location, and shapes of all the vortices, including the vortex containing the node in question. The nodes of a particular vortex are identified as a set and their motion in time establishes the shape the vortex attains. The newly formed vortices follow the spherical surface for awhile and then separate from it. In the computation, they are followed in time till they either move downstream to the limit of the computational volume, $\approx 7D$, or the oldest surviving vortex is removed when their number exceeds a prescribed number. This removal process and viscous growth of the vortex cores represent the subgrid-scale modeling for this type of turbulent flow. To excite the vortex filaments into a nonsymmetric unsteady flow, the boundary-layer vortices are initially perturbed to destroy geometric symmetry about the axis through the sphere parallel to the free-stream flow.

The drag coefficient C_D computed in time is shown in Fig. 32. The points shown are averages over time spans during which the number of vortices in the outer flow is constant. The drag coefficient is somewhat higher than that characteristic of high Reynolds number flow. The corresponding side-force coefficients are shown in Fig. 33. They show some intermittency in their behavior.

CONCLUDING REMARKS

A review has been presented of techniques of turbulence modeling made possible by the capabilities of large modern computers. The two Eulerian grid methods, statistical turbulence theory and large eddy simulations, were shown to have many features in common. Advances in the statistical methods, for example the use of direct Reynolds stress modeling rather than use of eddy diffusivity, could lead to subgrid modeling sufficiently accurate to permit reducing the range of large eddy wavemembers that have to be simulated. On the other hand, detailed large eddy simulations of idealized flow fields may provide "data" to guide improved constitutive relationships in the statistical methods. Thus, the two methods complement each other, and advances in one are likely to advance the other. The Lagrangian methods that follow vortex motions, at present, are alternative and competing techniques. For certain types of problems, it may be advantageous in the future to use both discrete vortices and turbulence fields in a single computation. When the practitioner of turbulence modeling aspires to the development of a universal model, he must draw on experience with all of the computational techniques. Further, his abilities to computationally consider minute details of turbulence will force laboratory experiments that verify and guide turbulence modeling to supply data to the same or even finer levels of detail.

REFERENCES

1. Kolmogorov, A. N.: Compt. Rend. Acad. Sci., URSS, Vol. 30, 1941, p. 301, and Vol. 32, 1941, p. 16.

2. Rotta, J.: Statistische Theorie nichthomogener Turbulenz. 1. Mitteilung. Z. Phys., Bd. 129, 1951, pp. 547-572.

3. Rotta, J.: Statistische Theorie nichthomogener Turbulenz. 2. Mitteilung. Z. Phys., Bd. 131, 1951, pp. 51-77.

4. Favre, A.: Equations des Gas Turbulents Compressibles. J. Mecan., Vol. 4, No. 3, Sept. 1965, pp. 361-390.

5. Rubesin, M. W. and Rose, W. C.: The Turbulent Mean-Flow, Reynolds Stress, and Heat Flux Equations in Mass-Averaged Dependent Variables. NASA TM X-62,248, March 1973.

6. Rubesin, M. W.: Subgrid- or Reynolds-Stress-Modeling for Three-Dimensional Turbulence Computations. NASA SP-347, 1975.

7. Deardorff, J. W.: A Numerical Study of Three-Dimensional Turbulent Channel Flow at Large Reynolds Numbers. J. Fluid Mech., Vol. 41, 1970, p. 453.

8. Schumann, U.: Ein Verfahren zur direkten numerischen Simulation turbulenter Strömungen in Platten- und Ringspaltkanälen und über seine Anwendung zur Untersuchung von Turbulenzmodellen. Universität Karlsruhe. KFK 1854 (1973) NASA TT F-15,391.

9. Leonard, A.: On the Energy Cascade in Large Eddy Simulations of Turbulent Fluid Flows: Rept. TF-1, Stanford Univ., 1973.

10. Kwak, D., Reynolds, W. C., and Ferziger, J. H.: Three-Dimensional Time Dependent Computation of Turbulent Flow. Rept. TF-5, Stanford Univ., 1975.

11. Cebeci, T. and Smith, A. M. O.: Analysis of Turbulent Boundary Layers. Academic Press, New York, 1974.

12. Bushnell, D.M., Cary, A. M., Jr., and Harris, J. E.: Calculation Methods for Compressible Turbulent Boundary Layers, State-of-the-Art – 1976. Presented at the von Karman Institute for Fluid Dynamics 1976 Lecture Series, Compressible Turbulent Boundary Layers, Rhode-St.-Genese, Belgium, March 1-5, 1976.

13. Reynolds, W. C.: Computation of Turbulent Flows, AIAA Paper 74-556, 1974.

14. Wolfshtein, M., Noot, D., and Lin, A.: Models of Turbulence, Rept. ME-746(N), Ben-Gurin Univ. of the Negev, Israel, June 1974.

15. Escudier, M. P.: The Distribution of the Mixing Length in Turbulent Flows Near Walls. Rept. TWF/TN/1, Imperial College, London, 1965.

16. Clauser, F. H.: The Turbulent Boundary Layer, in Advances in Applied Mechanics, Vol. 4, Academic Press, New York, 1956.

17. Glushko, G. S.: Turbulent Boundary Layer on a Flat Plate in an Incompressible Fluid. Bull. Acad. Sci. USSR, Mech. Ser. 4, 1965, pp. 13-23.

18. Hinze, J. O.: Turbulence. McGraw-Hill Book Co., Ch. 3, 1959.

19. Beckwith, I. E. and Bushnell, D. M.: Detached Description and Results of a Method for Computing Mean and Fluctuating Quantities in Turbulent Boundary Layers. NASA TN D-4815, Oct. 1968.

20. Coles, D.: The Law of the Wall in Turbulent Shear Flow. Sonderdruck aus "50 Jahre Grenzschichtforschung," edited by H. Görtler and W. Tollmien, Vieweg & Sohn, Braunschweig, 1955, pp. 153-163.

21. Goldberg, P.: Upstream History and Apparent Stress in Turbulent Boundary Layers. Rept. 85, Gas Turbine Lab., M.I.T., May 1966.

22. Jones, W. P. and Launder, B. E.: The Prediction of Laminarization with a Two-Equation Model of Turbulence. Intern. J. Heat Mass Transf., Vol. 15, 1972, pp. 301-314.

23. Ng, K. H. and Spalding, D. B.: Turbulence Model for Boundary Layers near Walls. Phys. Fluids, Vol. 15, No. 1, 1972, pp. 20-30.

24. Saffman, P. G. and Wilcox, D. C.: Turbulence-Model Predictions for Turbulent Boundary Layers. AIAA J., Vol. 12, No. 4, 1974, pp. 541-546.

25. Wilcox, D. C. and Traci, R. M.: A Complete Model of Turbulence. AIAA Paper 76-351, 1976.

26. Chambers, T. L. and Wilcox, D. C.: A Critical Examination of Two-equation Turbulence Closure Models. AIAA Paper 76-352, 1976.

27. Hanjalić, K. and Launder, B. E.: A Reynolds Stress Model of Turbulence and Its Application to Thin Shear Flow. J. Fluid Mech., Vol. 52, Pt. 4, 1972, pp. 609-638.

28. Coles, D. E. and Hirst, E. A.: Proceedings: Computation of Turbulent Boundary Layers – 1968 AFOSR-IF P-Stanford Conference, Vol. II, Compiled Data, Stanford Univ., 1968.

29. Klebanoff, P. S.: Characteristics of Turbulence in a Boundary Layer with Zero Pressure Gradient. NACA TR-1247, 1955.

30. Bradshaw, P.: The Response of a Constant Pressure Turbulent Boundary Layer to the Sudden Application of an Adverse Pressure Gradient. ARC R & M 3575, 1969.

31. Ludwieg, H. and Tillmann, W., Ing.-Arch., Vol. 17, 1949, pp. 288-299.

32. Donaldson, C. duP.: Calculation of Turbulent-Shear Flows for Atmospheric and Vortex Motions. AIAA J., Vol. 10, No. 1, Jan. 1972, pp. 4-12.

33. Donaldson, C. duP. and Sullivan, R. D.: An Invariant Second Order Closure Model of the Compressible Turbulent Boundary Layer on a Flat Plate. ARAP Rept. 178, 1972.

34. Varma, A. K., Beddini, R. A., Sullivan, R. D., and Donaldson, C. duP.: Application of an Invariant Second-Order Closure Model to Compressible Turbulent Boundary Layers. AIAA Paper 74-592, 1974.

35. Lewellen, W. S. and Teske, M.: Turbulence Modeling and Its Application to Atmospheric Diffusion. Part II: Critical Review of the Use of Invariant Modeling. EPA-600/4-75-016b, Dec. 1975.

36. Mellor, G. L. and Herring, H. J.: A Survey of Mean Turbulent Field Closure Models. AIAA J., Vol. 11, No. 5, May 1973, pp. 590-599.

37. Nast, D., Shavit, A., and Wolfshtein, M.: Two-point Correlation Model and the Redistribution of Reynolds Stresses. Phys. Fluids, Vol. 16, No. 6, 1973, pp. 738-743.

38. Launder, B. E., Reece, G. J., and Rodi, W.: Progress in the Development of a Reynolds Stress Turbulence Closure. J. Fluid Mech., Vol. 68, Pt. 3, 1975, pp. 537-566.

39. Marvin, J. G.: Turbulence Modeling for Compressible Flows. NASA TM X-73,188, Jan. 1977.

dependent problems. The underlying initial value problem does not necessarily correspond to a natural time dependent problem (false time path methods). The convergence rate of a particular method may then be investigated considering continuous solutions of the

40. Rubesin, M. W.: A One-Equation Model of Turbulence for Use with the Compressible Navier-Stokes Equations. NASA TM X-73,128, April 1976.

41. Viegas, J. R. and Coakley, T. J.: Numerical Investigation of Turbulence Models for Shock Separated Boundary-Layer Flow. AIAA Paper 77-44, 1977.

42. Mateer, G. G., Brosh, A., and Viegas, J. R.: A Normal Shock-Wave Turbulent Boundary Layer Interaction at Transonic Speeds. AIAA Paper 76-161, 1976.

43. Rubesin, M. W., Crisalli, A. J., Horstman, C. C., Acharya, M., and Lanfranco, M. J.: A Critique of Some Recent Second Order Closure Models for Compressible Boundary Layers. AIAA Paper 77-128, 1977.

44. Marvin, J. G. and Sheaffer, Y. S.: A Method for Solving the Nonsimilar Boundary-Layer Equations Including Foreign Gas Injection. NASA TN D-5516, 1969.

45. Hopkins, E. J. and Inouye, M.: An Evaluation of Theories for Predicting Turbulent Skin Friction and Heat Transfer on Flat Plates at Supersonic and Hypersonic Mach Numbers. AIAA J., Vol. 9, No. 6, 1971, pp. 993-1003.

46. Zwarts, F. J.: The Compressible Turbulent Boundary Layer in a Pressure Gradient. Ph.D. Thesis, McGill Univ., Montreal, 1970.

47. Peake, D. J., Brakmann, G., and Romeskie, J. M.: Comparisons between Some High Reynolds Number Turbulent Boundary-Layer Experiments at Mach 4, and Various Recent Calculation Procedures. In Turbulent Shear Flows, AGARD CP-93, Sept. 1971.

48. Sturek, W. B. and Danberg, J. E.: The Supersonic Turbulent Boundary Layer in an Adverse Pressure Gradient – Experiments and Data Analysis. In Turbulent Shear Flows, AGARD CP-93, Sept. 1971.

49. Lewis, J. E., Gran, R. L., and Kubota, T.: An Experiment on the Adiabatic Compressible Turbulent Boundary Layer in Adverse and Favorable Pressure-Gradients. J. Fluid Mech., Vol. 51, Pt. 4, 1972, pp. 657-672.

50. Bradshaw, P.: Effects of Streamline Curvature on Turbulent Flow. AGARD-AG-169, Aug. 1973.

51. Tieleman, H. W.: Viscous Region of Turbulent Boundary Layer, Rept. CER67-68HWT21, Colorado State Univ., 1967.

52. Comte-Bellot, G. and Corrsin, S.: Simple Eulerian Time Correlation at Full- and Narrow-Band Velocity Signals in Grid-Generated, "Isotropic" Turbulence. J. Fluid Mech., Vol. 48, Pt. 2, 1971.

53. Heisenberg, W.: On the Statistical Theory of Turbulence. Zeitschrift für Physik, Vol. 124, 1948.

54. Rogallo, R. S.: An ILLIAC Program for the Numerical Simulation of Homogeneous Incompressible Turbulence. NASA TM X-73,203, 1977.

55. Orzsag, S. A.: Numerical Methods for the Simulation of Turbulence, Phys. Fluids, Supp. II, 1969, p. II250.

56. Clark, R. A., Ferziger, J. H., and Reynolds, W. C.: Evaluation of Subgrid Scale Turbulence Models Using a Fully Simulated Turbulent Flow. Rept. TF-9, Stanford Univ., 1977.

57. Smagorinsky, J., Manabe, S., and Halloway, J. L.: General Circulation Experiments with the Primitive Equations. Monthly Weather Review, Vol. 93, 1965, p. 727.

58. Moin, P., Mansour, N. N., Mehta, U. B., Ferziger, J. H., and Reynolds, W. C.: Improvements in Large-Eddy Simulation Technique: Special Methods and High-Order Statistics. Rept. TF-10, Stanford Univ., 1977.

59. Schumann, U.: Subgrid Scale Model for Finite Difference Simulations of Turbulent Flows in Plane Channels and Annuli. J. Comp. Phys., Vol. 18, 1975, pp. 376-404.

60. Leonard, A.: Simulation of Three-Dimensional Separated Flows with Vortex Filaments. Vth International Conf. on Numerical Methods in Fluid Dynamics, Twente University of Technology, Enschede, The Netherlands, June 28-July 2, 1976.

write

$$f_x + g_y = 0 \qquad (2)$$

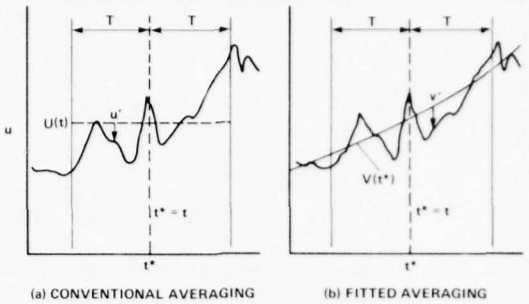

Fig. 1. Time-averaged dependent variables.

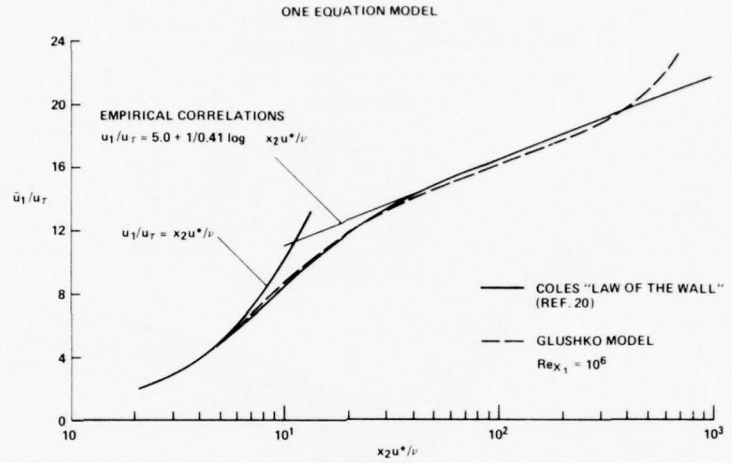

Fig. 2. Comparison of computations based on the Glushko model with the Coles "law of the wall."

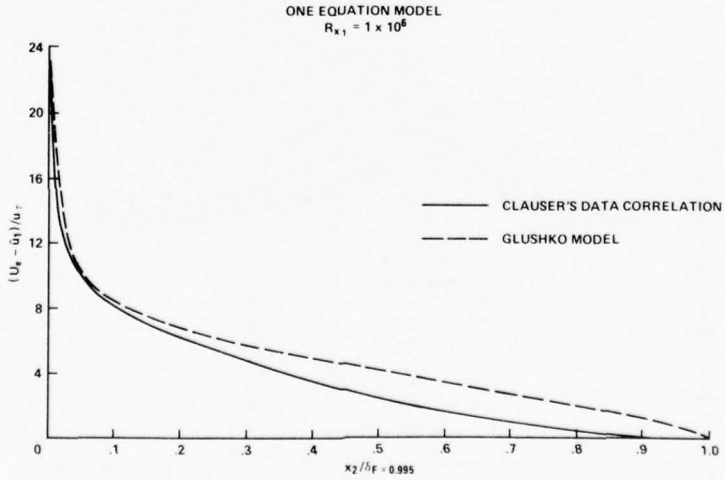

Fig. 3. Comparison of computations based on the Glushko model with the Clauser velocity defect correlation.

which may be written as

$$\phi_{m,n}^{k+1} = (1 - \omega)\phi_{m,n}^{k} + \frac{\omega}{4}(\phi_{m-1,n}^{k+1} + \phi_{m+1,n}^{k} + \phi_{m,n-1}^{k+1} + \phi_{m,n+1}^{k}) \text{ for } m,n = 1,2, \ldots M-1$$

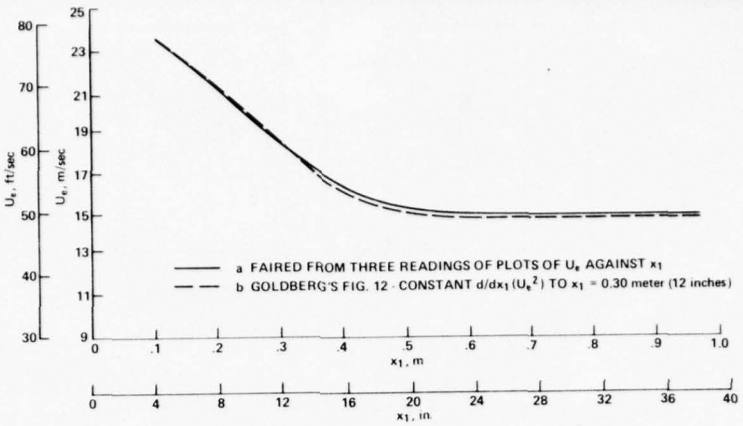

Fig. 4. Boundary-layer-edge-velocity distribution from the Goldberg experiment.

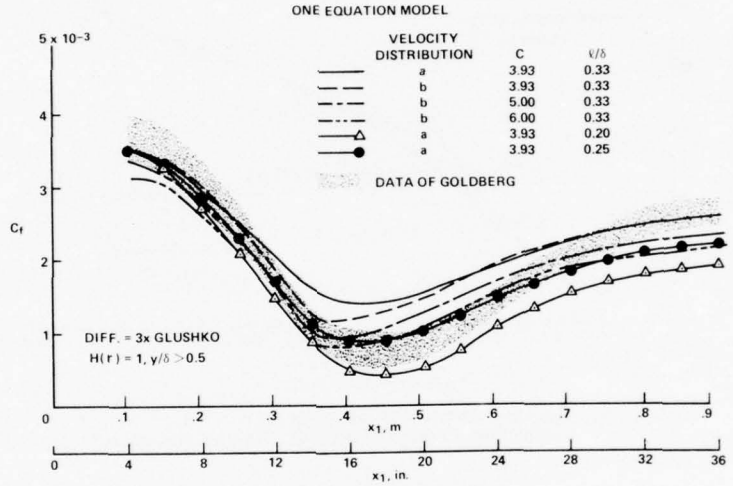

Fig. 5. Comparison of Beckwith and Bushnell calculations with the Goldberg skin-friction measurements; effect of modeling modifications.

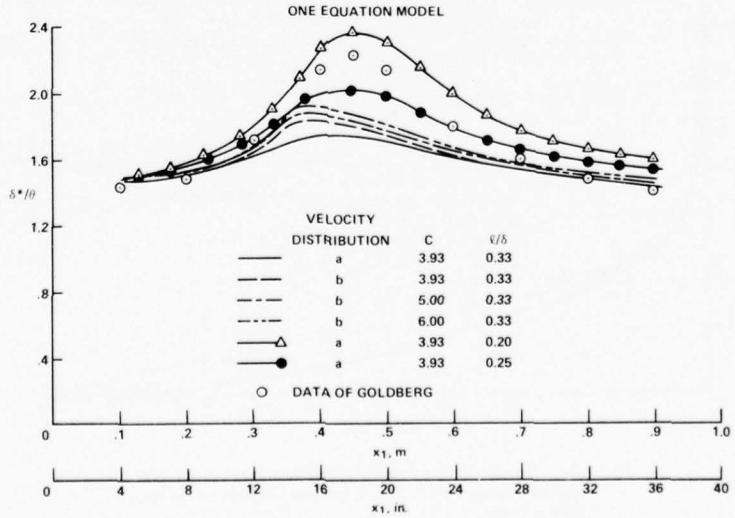

Fig. 6. Comparison of Beckwith and Bushnell calculations with Goldberg shape factor measurements.

Since the fundamental conservation laws in physics are mainly systems of low order partial differential equations, the computation times to solve these equations numerically, are excessively long and therefore extremely expensive. There are

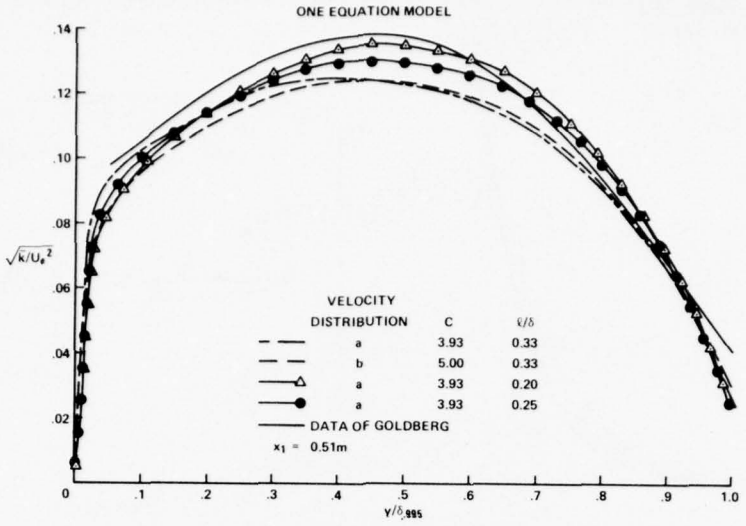

Fig. 7. Beckwith and Bushnell calculations of turbulent kinetic energy profiles compared with Goldberg's at end of run of adverse pressure gradient.

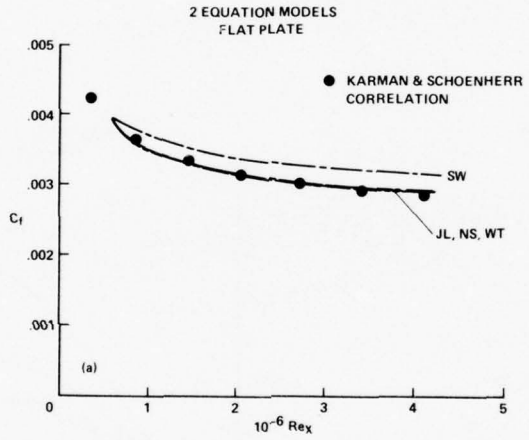

(a) Skin-friction coefficient along surface.

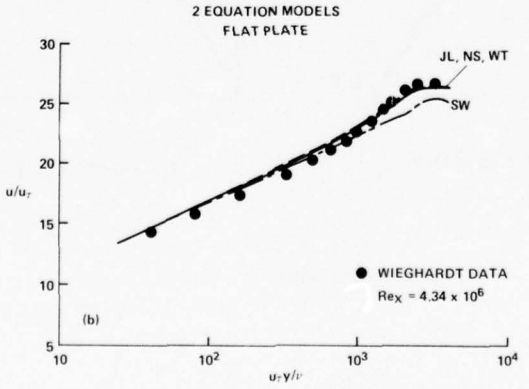

(b) Wall region velocity profiles.

Fig. 8. Comparison of computed and measured flow properties for flat-plate boundary-layer flow.

$$||C(t)|| = e^{-2t} < 1 \qquad (19)$$

for all $t > 0$. Since $||C||$ is uniformly bounded, it follows for $t \to \infty$ $||C|| \to 0$, which

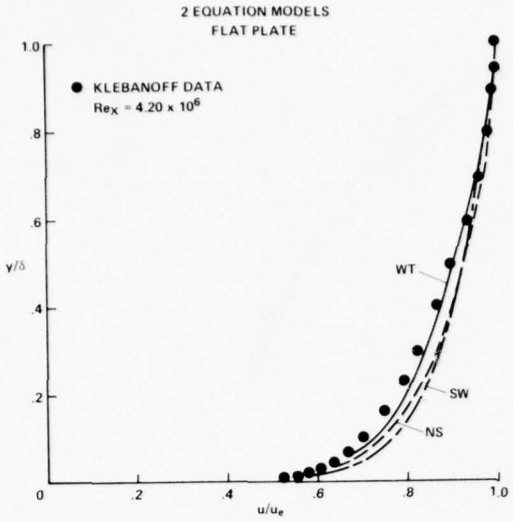

(c) Velocity profiles.

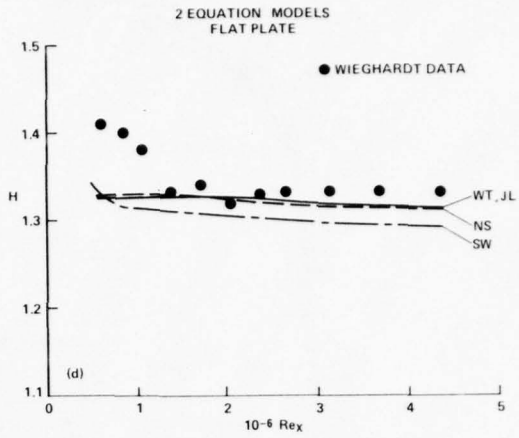

(d) Shape factor distribution.

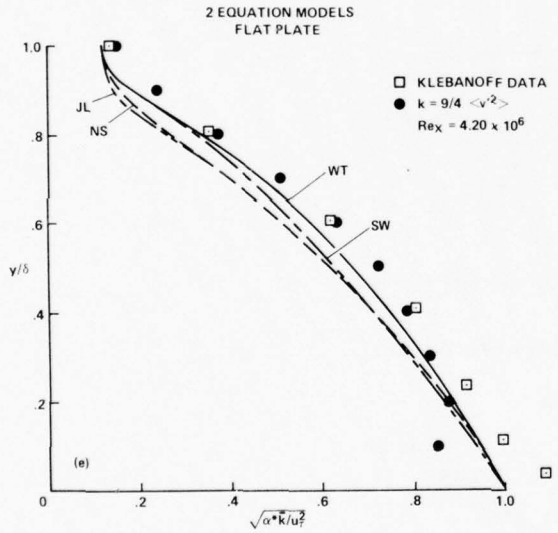

(e) Turbulent kinetic energy profiles.

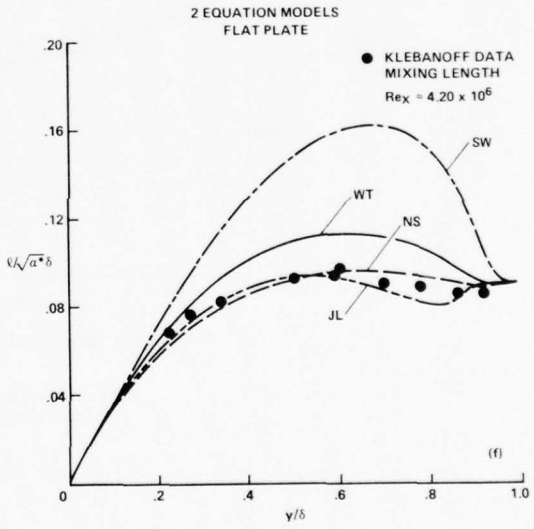

(f) Length scale profiles.

Fig. 8. Concluded.

with given boundary condition in a general bounded domain. Let the steady state solution be $u_s(\underline{x})$, where $\underline{x}$ denotes the set of independent variables.

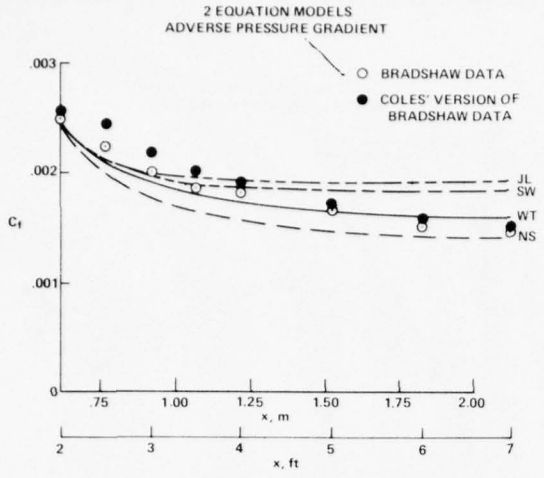

(a) Skin-friction coefficient distribution.

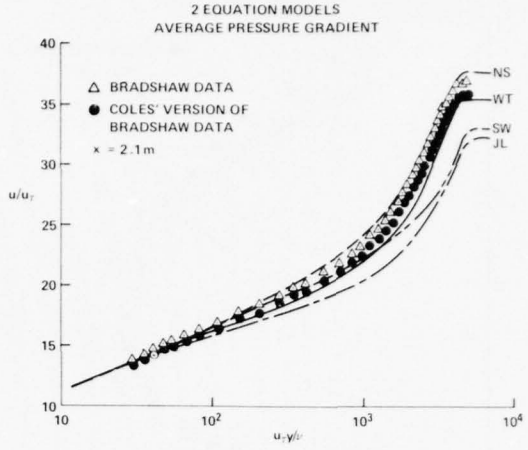

(b) Velocity profiles in "law-of-the-wall" coordinates.

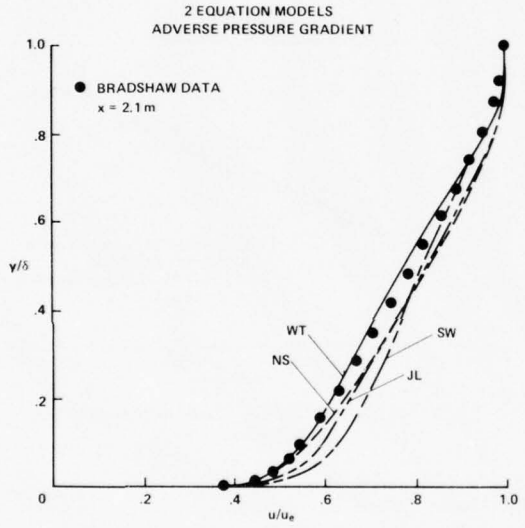

(c) Velocity profiles.

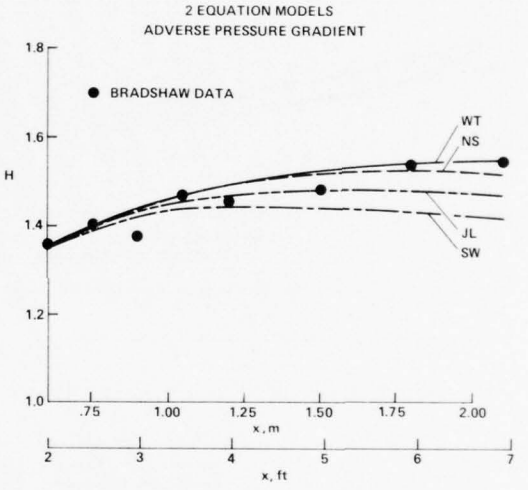

(d) Shape factor distribution.

Fig. 9. Comparison of computed and measured flow properties for the Bradshaw adverse pressure gradient flow.

the existence of a complete set of eigenfunctions for the steady state operator L(u), and the requirement that <u>all</u> roots of the characteristic polynomial $P(\sigma) = 0$ (Eq.31)

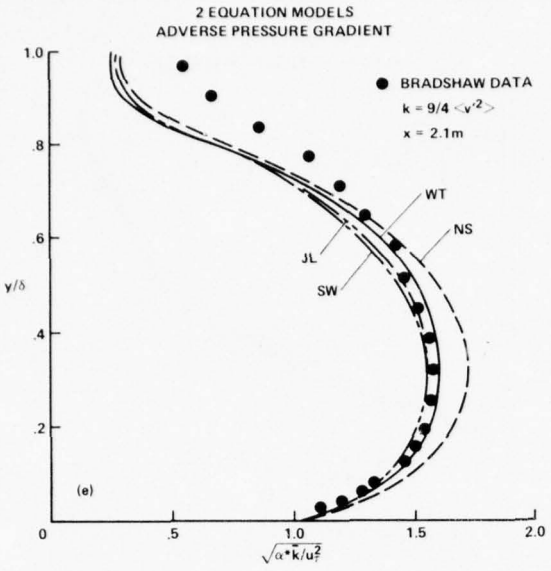

(e) Turbulent kinetic energy profile.

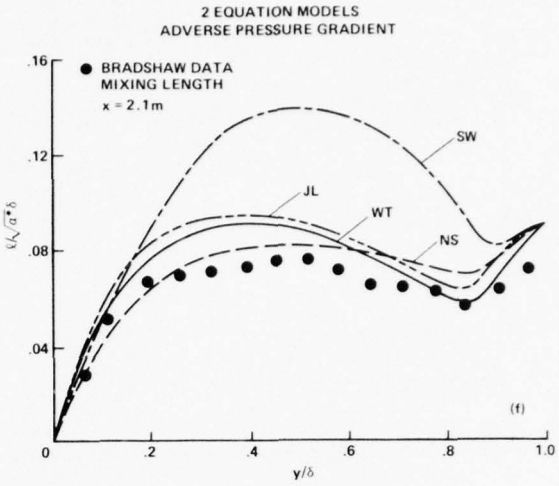

(f) Length scale profile.

Fig. 9. Concluded.

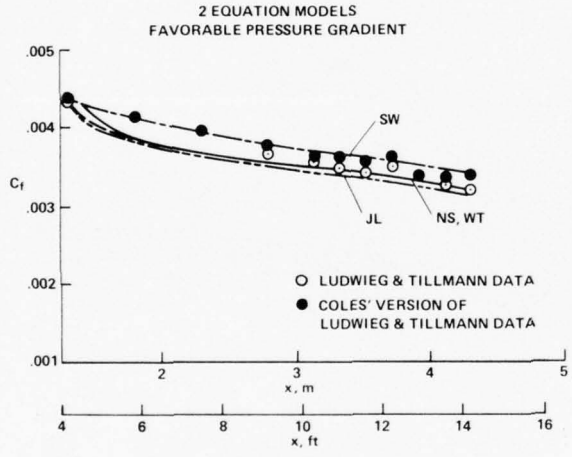

(a) Skin-friction coefficient distribution.

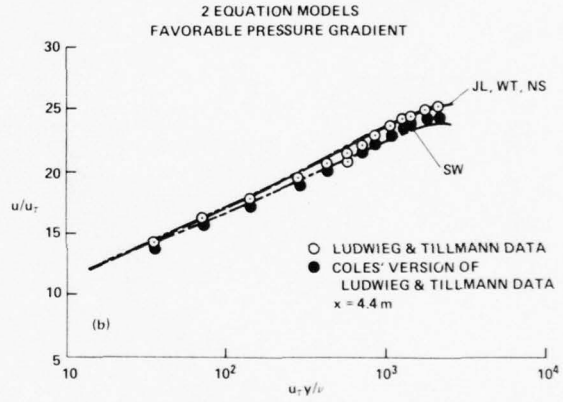

(b) Velocity profile in "law-of-the-wall" coordinates.

Fig. 10. Comparison of computed and measured flow properties for the Ludwieg-Tillmann favorable pressure gradient flow.

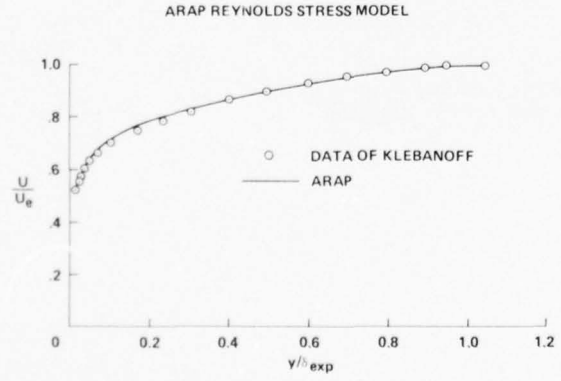

Fig. 11. Comparison of the mean velocity profile calculated with the ARAP model and Klebanoff's data.

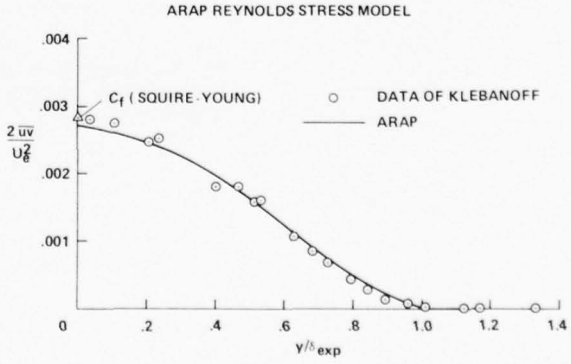

Fig. 12. Comparison of turbulent shear stress profile calculated from ARAP model with Klebanoff's data.

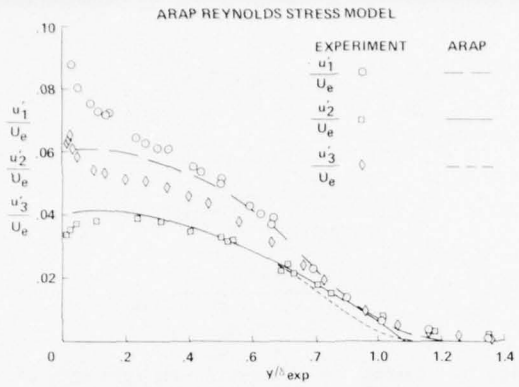

Fig. 13. Comparison of turbulent normal stress profiles calculated from ARAP model with Klebanoff's data.

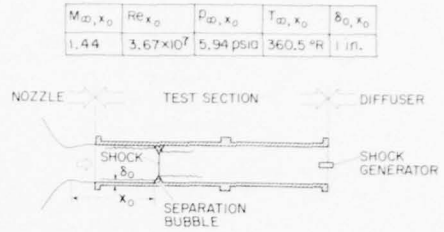

Fig. 14. Normal shock-wave-induced turbulent boundary-layer separation.

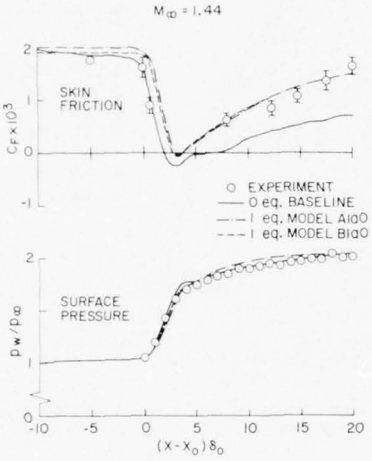

Fig. 15. Normal shock boundary-layer interaction.

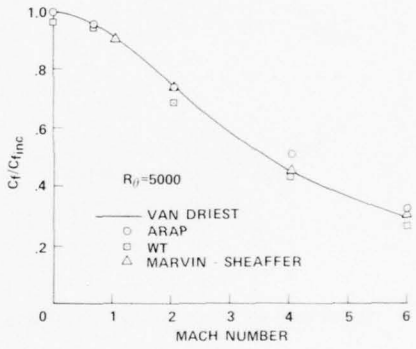

Fig. 16. Effect of compressibility on flat-plate skin friction.

REF.	EXPERIMENTAL CONFIGURATION	M_∞	$Re_{ij_\infty} \times 10^{-4}$	T_W/T_0	P^+_{max}
ZWARTS		4.02	3.5	1	0.004
PEAKE, BRAKMANN AND ROMESKIE		3.93	1.1	1	0.006
STUREK AND DANBERG		3.54	2.0–2.8	1	0.0085–0.0125
LEWIS, GRAN AND KUBOTA		3.98	0.5	1	0.011

Fig. 17. Experiments used as standards of comparison for compressible boundary-layer computations.

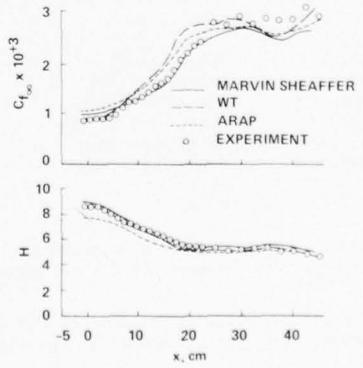

Fig. 18. Comparison of computations with Zwarts' data.

Again we find the condition that M < 1, without referring to the explicit

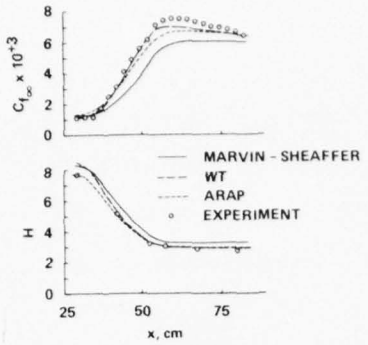

Fig. 19. Comparison of computations with data of Peake et al.

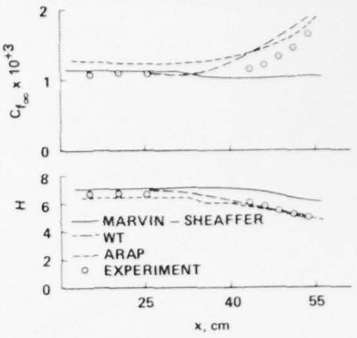

Fig. 20. Comparison of computations with data of Sturek and Danberg.

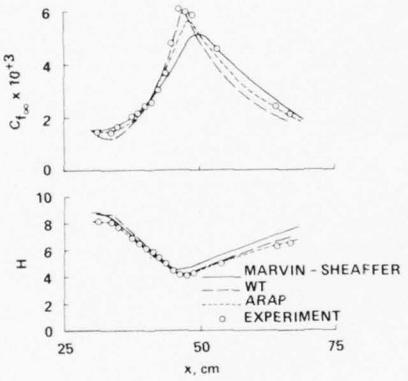

Fig. 21. Comparison of computations with data of Lewis et al.

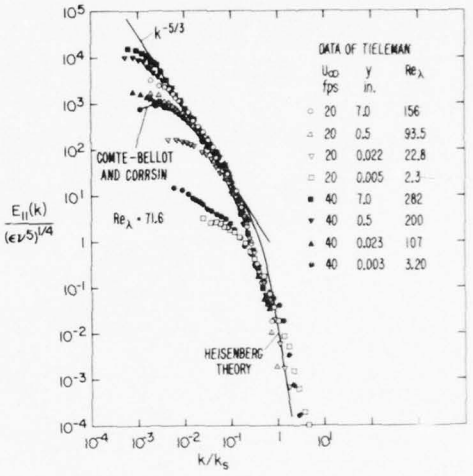

Fig. 22. Comparison of energy spectra of boundary layer and homogeneous turbulent flows.

(ILLIAC)

NUMBER OF MESH CELLS	262144 $(= 64^3)$
DEPENDENT VARIABLES	786432 $(= 3 \cdot 64^3)$
MEMORY REQUIRED	3.14×10^6 $(= 12 \cdot 64^3)$
FFT'S PER STEP	442368 $(= 4 \cdot 27 \cdot 64^2)$
COMPUTER TIME PER STEP	100 sec (REAL TIME)
COMPUTER TIME PER RUN	2 TO 6 hr (REAL TIME)

ALGORITHM

SPATIAL RESOLUTION	SPECTRAL (ALIAS-DAMPED)
TEMPORAL RESOLUTION	RUNGE-KUTTA (FOURTH-ORDER)

Fig. 23. Computational simulation program for low Reynolds number turbulence, method of Rogallo with ILLIAC IV.

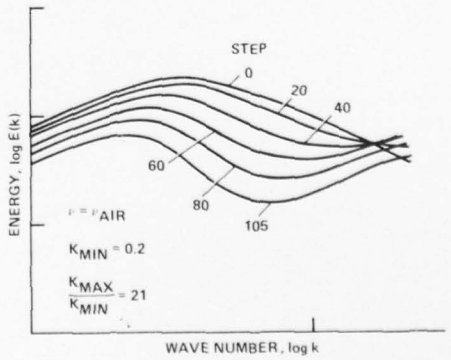

(a) Base computation.

Fig. 24. Evolution of the turbulence energy spectrum.

k_{max}/k_{min}, but the appropriate values of k_{max} and k_{min} must again be established by reference to experimental data. If k_{max} were set to capture the energy dissipation, the k_{min} would be too large to encompass much of the kinetic energy of the large scales of turbulence and the results would be biased by the use of periodic boundary conditions on faces too close together relative to the correlation lengths.

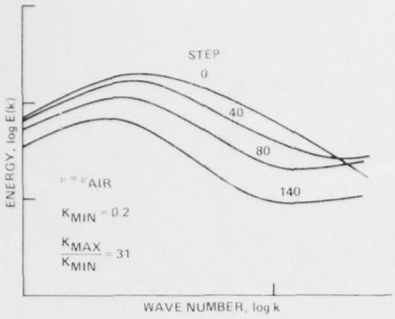

(b) Increased wave-number range.

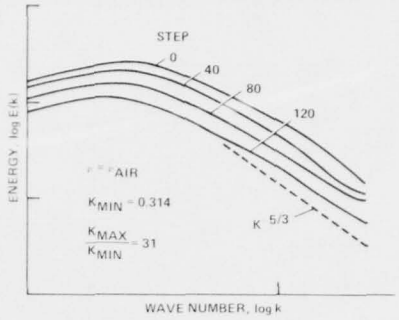

(c) Increased wave-number range with shift to larger wave numbers.

Fig. 24. Concluded.

	MODELED QUANTITY	CONTRIBUTION	MODELING RELATIONSHIP	CORRELATION	CONSTANT
(1)	$\overline{\bar{u}_i \bar{u}_j} - \bar{u}_i \bar{u}_j$	-3%	$\frac{\Delta_A^2}{24} \nabla^2 \bar{u}_i \bar{u}_j$	0.935	—
(2)	$\overline{u_i' \bar{u}_j} + \overline{\bar{u}_i u_j'}$	48%	$\frac{\Delta_A^2}{24} (\bar{u}_i \nabla^2 \bar{u}_j + \bar{u}_j \nabla^2 \bar{u}_i)$	0.685	—
(3)	$\overline{u_i' u_j'} - \frac{1}{3}\delta_{ij} \overline{u_k' u_k'}$	55%	$\epsilon \bar{S}_{ij}$, $\bar{S}_{ij} = \frac{1}{2}(\bar{u}_{i,j} + \bar{u}_{j,i})$	—	—
			ϵ MODELS		
			SMAGORINSKY $\epsilon = (C\Delta_A)^2 \sqrt{2\bar{S}_{ij}\bar{S}_{ij}}$	0.710	0.186
			VORTICITY $\epsilon = (C\Delta_A)^2 \sqrt{\bar{\omega}_i \bar{\omega}_i}$, $\bar{\omega}_i = \epsilon_{ijk} \bar{u}_{k,j}$	0.700	0.202
			KINETIC ENERGY $\epsilon = (C\Delta_A) \sqrt{\frac{1}{3} \overline{u_k' u_k'}}$	0.723	0.085
			CONSTANT $\epsilon = 1$	0.716	—

NOTE THAT IN EQ (55) $\overline{\bar{u}_i \bar{u}_j} = \bar{u}_i \bar{u}_j + (\overline{\bar{u}_i \bar{u}_j} - \bar{u}_i \bar{u}_j)$

Fig. 25. Evaluation of subgrid models for energy decay.

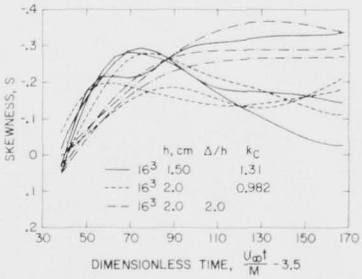

(a) Small computation volume, comparison of Gaussian and Sharp wave-number cut-off filter functions.

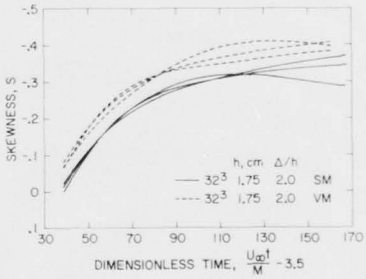

(b) Enlarged computation volume, comparison of Smagorinsky and vorticity models with Gaussian filter function.

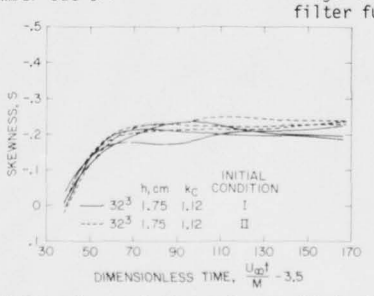

(c) Enlarged computation volume, effect of initial conditions with sharp wave-number cut-off filter function and Smagorinsky model.

Fig. 26. Development of skewness during "isotropic" flow computation.

To complete this brief description of the status of large eddy simulation methods in turbulent fluid flows, it is necessary to refer to Schumann's recent calculation of channel flows (Ref. 59) that extends

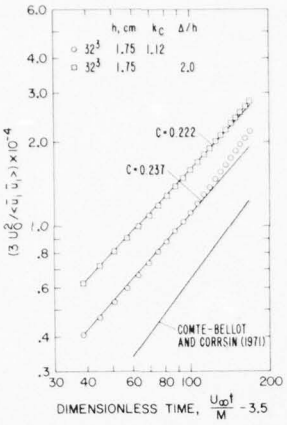

Fig. 27. Prediction of decay rate of isotropic turbulence, Smagorinsky model.

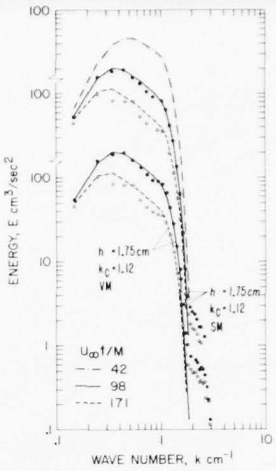

Fig. 28. Simulation of energy spectrum in decaying isotropic turbulence, sharp wave-number cut-off filter.

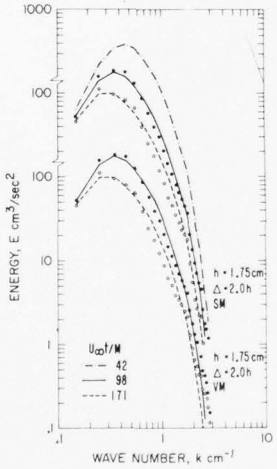

Fig. 29. Simulation of energy spectrum in decaying isotropic turbulence, Gaussian filter.

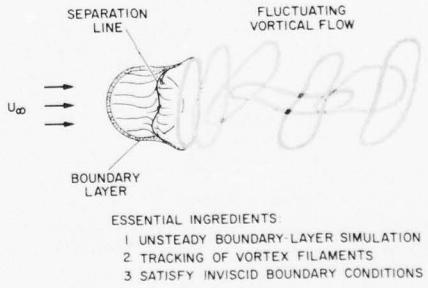

Fig. 30. Simulation of 3-D unsteady separated flow.

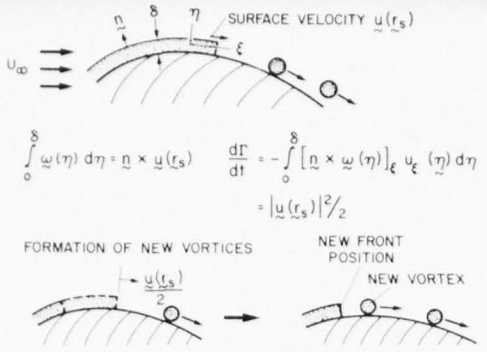

Fig. 31. Boundary-layer model.

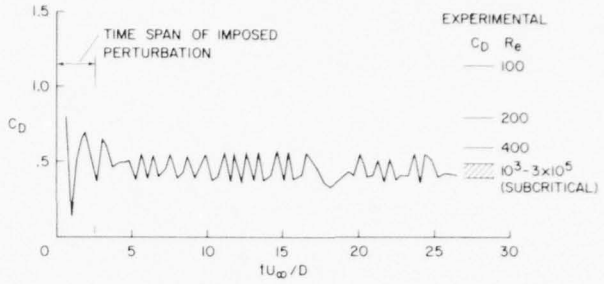

Fig. 32. Sphere drag coefficient.

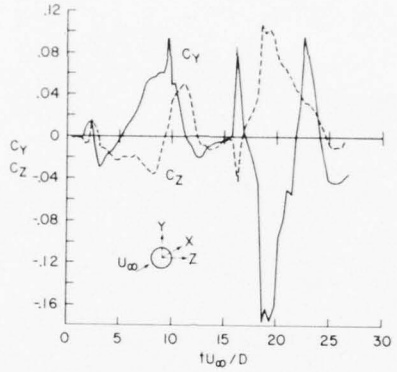

Fig. 33. Side force coefficients.

RELAXATION METHODS FOR TIME DEPENDENT CONSERVATION EQUATIONS IN FLUID MECHANICS

H.J. WIRZ
von Karman Institute for Fluid Dynamics
Rhode-St-Genèse, Belgium

Dedicated to the 70th anniversary of Prof.Dr.-Ing. A. Walz

1. INTRODUCTION

The approximate discrete solution of the fundamental steady state conservation equations of classical physics and in particular fluid mechanics leads in general to large non linear systems of algebraic equations, which must be solved iteratively. Of predominant interest is, of course, the reliability of the discrete analogue of the basic conservation laws (numerical model) for finite mesh size.

Due to the inherent limitations of available computers (speed, capacity) a second issue plays an equally important role namely the problem of efficiency of iterative methods. The acceleration of the convergence of these methods to solve stationary partial differential equations is the subject of relaxation.

Iterative methods in general are characterised by three important elements : the successive application of a method should lead to a state, which is invariant with respect to further iterations (convergence), this invariant state (which will be identified with the steady state for our purpose) should be independent of the choice of the initial guess (unicity). Since only a limited amount of iteration steps is carried out, the question of accuracy of the solution (error estimation) must be considered. This problem is, of course, independent of the reliability of the discrete model being used to represent the continuous conservation equation.

It is desirable and crucial for the success of the application of an iterative method, that the process converges as fast as possible to the invariant state (rate of convergence) using a minimum amount of operations per iteration step.

The suitable definition of a norm for the associated iteration matrix and its contraction property in a Benach space represent the most fundamental aspect of any iteration method. The essence of relaxation therefore is to improve significantly the contraction property, thus improving the rate of convergence. If the eucledian norm is used, an eigenvalue spectrum must be controlled, which is, unfortunately not an easy matter for coupled systems of partial differential equations.

The above-mentioned elements of a descriptive definition of iteration methods do not exclude the application of discrete methods which resolve transient solutions between a physically given initial state and an asymptotic final state (steady state) of a natural time dependent problem, assuming that such a steady state exists (time accurate methods). This idea has the appealing property that nature is closely imitated; see for example Crocco (1965), however, one cannot hope that a time accurate discrete representation of a natural time dependent problem automatically leads to an efficient iteration method. Time dependent hyperbolic problems are typical examples for which an asymptotic steady state, in principle, does not even exist.

On the other hand it is interesting and often possible to interprete iterative methods for the discrete solution of steady state problems as "artificial" time

dependent problems. The underlying initial value problem does not necessarily correspond to a natural time dependent problem (false time path methods). The convergence rate of a particular method may then be investigated considering continuous solutions of the given initial boundary value problem.

Apparently there are two possibilities to develop effective iteration methods to solve discrete steady state problems.

The discretized stationary conservation equations (all time dependent terms of the original unsteady problem have been dropped) are used directly to construct some kind of iteration method for the resulting (non-linear) system of algebraic equations. The success of this approach, in general, remains a matter of luck, since only an a-posteriori analysis of the resulting iteration matrix will decide, whether the method is acceptable. Nevertheless the well-known SOR (successive overrelaxation) process (Frankel, 1950, Young, 1954) is an excellent example for this approach for the Laplace equation.

From a methodological point of view, it appears therefore more promising to investigate first the natural time dependent conservation equations and, if necessary, to modify them (false time path) such that their discrete analogue leads to effective iteration methods. The well-known ADI (alternating direction implicit) method, Peaceman and Rachford (1955) is an example for this approach, where the heat conduction equations furnishes the time dependent problem for the solution of the Laplace equation.

The other important advantage is, that this approach is beforehand independent of the actual numerical method being employed (finite element, finite difference) to discretise these artificial time dependent equations.

The first known relaxation methods (pencil computations, of course) to solve elliptic difference equations have been developed by Gauss (1823) and Seidel (1874) although the term "relaxation" was later introduced by Southwell (1946) and Fox (1948). A recent survey about relaxation methods in fluid mechanics, is provided by Lomax and Steger (1975), where further literature may be found. The conclusion from this article is that relaxation methods for coupled systems of equations have not yet been sufficiently considered.

2. LINEAR RELAXATION METHODS

2.1 A model problem

Before starting with mathematical details, we establish a simple steady state problem of fluid mechanics, which will serve throughout this chapter as our model problem.

The two-dimensional, incompressible potential flows, are governed by the continuity equation (conservation of mass) and the condition of vanishing vorticity. These are the well-known elliptic Cauchy-Riemann equations :

$$u_x + v_y = 0 \tag{1a}$$

$$-v_x + u_y = 0 \tag{1b}$$

where u, v may denote the velocity components and x, y the space co-ordinates. We want to solve this problem in a bounded domain, say $B = \{x,y \mid 0 \leq x,y \leq \pi\}$, with some prescribed boundary conditions. Introducing vector valued functions f(w), g(w) we may

write

$$f_x + g_y = 0 \qquad (2)$$

where the vectors w, f and g are given by

$$w = \begin{pmatrix} u \\ v \end{pmatrix}; \qquad f = \begin{pmatrix} u \\ -v \end{pmatrix}; \qquad g = \begin{pmatrix} v \\ u \end{pmatrix}. \qquad (2a)$$

The system (2) has the typical form of a conservation equation and may equally be expressed as

$$Aw_x + Bw_y = 0 \qquad (3)$$

where the matrices $A = \frac{\partial f}{\partial w}$, $B = \frac{\partial f}{\partial w}$ are symmetric and read

$$A = \begin{pmatrix} 1 & 0 \\ 0 & -1 \end{pmatrix} \qquad B = \begin{pmatrix} 0 & 1 \\ 1 & 0 \end{pmatrix} . \qquad (3a)$$

Although our primary interest is focussed on the development of relaxation methods to solve first order coupled systems of equations, like Eq.(2), we will adopt for a moment also another formulation for Eq.(2) and come back later to our original problem.

Introducing a velocity potential ϕ, such that

$$u = \phi_x; \qquad v = \phi_y, \qquad (4)$$

the system (1) is reduced to the well-known Laplace equation

$$\Delta\phi = \phi_{xx} + \phi_{yy} = 0, \qquad (5)$$

which, of course, has the advantage that only one dependent variable is occuring. The boundary conditions are also by far more easy to establish.

In order to apply finite difference methods, we consider a typical grid function $\phi^k_{m,n} = \phi(x_m, y_n)$, where the superscript denotes the iteration level, $\phi_{m,n}$ being defined on an equally spaced grid with mesh size h, such that (M natural number)

$$x_m = mh; \qquad y_n = nh; \qquad m,n = 0,1,2, \ldots M \; ; \; h = \frac{\pi}{M} \qquad (6)$$

Furthermore the familiar difference operators

$$\delta_x \phi_{m,n} = \phi_{m+1,n} - \phi_{m-1,n}$$

$$\delta_x^2 \phi_{m,n} = \phi_{m+1,n} - 2\phi_{m,n} + \phi_{m-1,n}; \qquad S_x\phi_{m,n} = \phi_{m+1,n} + \phi_{m-1,n} \qquad (7)$$

are used together with similar expressions for the y co-ordinate. The discretisation of the Laplace equation then leads to

$$\{\delta_x^2 + \delta_y^2\}\phi_{m,n} = 0 \quad \text{for } m,n = 1,2, \ldots M-1 \qquad (8)$$

which is a consistant, second order correct approximation. One of the most popular explicit methods to solve (8) iteratively is the SOR method, which was independently developed by Frankel (1950) and Young (1954). Although many derivates of this method, for example : SLOR (successive line overrelaxation) or improvements (example : SSOR; symmetric successive overrelaxation) are existing by now, we use here the basic form

which may be written as

$$\phi^{k+1}_{m,n} = (1-\omega)\phi^{k}_{m,n} + \frac{\omega}{4}(\phi^{k+1}_{m-1,n} + \phi^{k}_{m+1,n} + \phi^{k+1}_{m,n-1} + \phi^{k}_{m,n+1}) \quad \text{for } m,n = 1,2, \ldots M-1 \tag{9}$$

It can be shown that this method not only converges for values of the relaxation parameter ω between $0 < \omega < 2$ but may be optimised to accelerate the rate of convergence significantly, if ω_{opt} is of the form $\omega_{opt} \sim 2 - C_1 h$, $C_1 > 0$, a constant.

In an actual computed case for a given mesh size h, the number of iterations to achieve a certain convergence level may be N_1 (optimised). If the mesh size is now reduced, say, by a factor of ten for better accuracy, then the number of iterations N_2 (optimised) to reach the same convergence level will be of the order $N_2 \sim 10\ N_1$. Thus we see that this reduction of the mesh size leads only to a rather modest increase of the number of necessary iterations.

Next we want to solve the system of equations given by (3), the discretised version of (3) reads

$$A\delta_x w_{m,n} + B\delta_y w_{m,n} = 0 \qquad \text{for } m,n = 1,2, \ldots M-1 \tag{10}$$

which is again a consistent, second order correct approximation.

Converting (3) into a hyperbolic (artificial) time dependent problem[x]

$$w_t + Aw_x + Bw_y = 0 \tag{11}$$

leads to the possibility of employing one of the well-known explicit methods to integrate numerically (11). We consider here the optimised two-step Lax-Wendroff method (Lax and Wendroff 1960, 1964), in which the first step is a predictor (the subscripts m,n are not written)

$$\bar{w}^{k+1} = \frac{1}{4}(S_x + S_y)w^k - \frac{r}{2} A\delta_x w^k - \frac{r}{2} B\delta_y w^k \tag{12a}$$

and the second, final step reads

$$w^{k+1} = w^k - r A\delta_x \bar{w}^{k+1} - r B\delta_y \bar{w}^{k+1}$$

for m,n = 1,2, ... M-1. This method converges in some sens for values of the "relaxation" parameter $0 < r \leq \frac{1}{\sqrt{2}}$, if the boundary conditions are sufficiently smooth and carefully implemented.

Again we compute an actual case for a given mesh size h and denote the number of iterations by N_1 ($r = 1/2$). Reducing h by a factor of ten leads to a number of iteration of about $N_2 \sim 10^4\ N_1$ (assuming the same convergence level).

It is evident that the Lax-Wendroff method is about three orders of magnitude slower than the simple optimised SOR process.

---

[x] this is not at all a trivial matter for more complicated problems. One might also wonder whether this system is a natural one, since the vorticity is physically not a conservation quantity.

Fig. 6. Comparison of Beckwith and Bushnell calculations with Goldberg shape factor measurements.

Since the fundamental conservation laws in physics are mainly systems of low order partial differential equations, the computation times to solve these equations numerically, are excessively long and therefore extremely expensive. There are problems, for example transonic flows, where first order coupled systems of partial differential equations should be employed, if discontinuities are to be properly represented also numerically (Lax and Wendroff (1960)).

We are therefore led to think about possibilities to accelerate the convergence of iterative methods for coupled first order systems, namely conservation laws.

2.2 Time dependent equations and relaxation operators

We consider first again the problem to find solutions of the simple Laplace equation

$$\Delta\phi = 0$$

with given boundary conditions (Dirichlet) on the boundary of $B = \{x,y \mid 0 \leq x,y \leq \pi\}$. Replacing the Laplace equation by the simplest possible time dependent problem, we have the (parabolic) heat conduction equation for $u(x,yt)$.

$$u_t = \Delta u \tag{13}$$

with initial conditions $u(x,y,0) = u_o(x,y)$ and the same boundary conditions as for ϕ. Then

$$v(x,y,t) = u(x,y,t) - \phi(x,y) \tag{14}$$

satisfies equally (13) with homogeneous boundary conditions and initial values $v(x,y,0) = v_o = u_o - \phi$.

It is clear that the solution of $v_t - \Delta v = 0$, can be written as

$$v(x,y,t) = \sum_{k_1=1}^{\infty} \sum_{k_2=1}^{\infty} A_{k_1,k_2}(t) \sin k_1 x \sin k_2 y, \tag{15}$$

where

$$A_{k_1,k_2} = a_{k_1,k_2} e^{-(k_1^2+k_2^2)t} \quad \text{and} \tag{16}$$

where the a_{k_1,k_2} are the Fourier coefficients of $v_o(x,y)$. It is important to note that the harmonics $\sin k_1 x \sin k_2 y$ form a complete set of orthogonal eigenfunctions of our Laplace operator, thus allowing the representation (15).

Eq.(15) may be written as

$$v = C(t)v_o \tag{17}$$

where $C(t)$ represents an operator. If now the L_2 norm is introduced

$$||v|| = \left(\int_B |v|^2 \, dxdy\right)^{1/2} \tag{18}$$

then the norm of the operator $C(t)$ in L_2 will be

Fig. 8. Comparison of computed and measured flow properties for flat-plate boundary-layer flow.

$$||C(t)|| = e^{-2t} < 1 \tag{19}$$

for all $t > 0$. Since $||C||$ is uniformly bounded, it follows for $t \to \infty$ $||C|| \to 0$, which implies

$$||u(x,y,t) - \phi(x,y)|| \to 0 \; ; \tag{20}$$

the solution of the unsteady problem $v(x,y,t)$ converges uniformly to the steady state solution $\phi(x,y)$ with the same boundary conditions, independent of the choice of the initial data.

The existence of a norm and the completness of the eigenfunctions which we have used to construct the solution, define a Banach space. The fact that the operator $C(t)$ is bounded and, that

$$||C|| < 1 \tag{21}$$

implies, of course, automatically that the time dependent problem is well posed. The conditions of well posedness are usually by far weaker than $||C|| < 1$.

In order to solve $\Delta\phi = 0$ with a different approach, we next consider the (hyperbolic) time dependent problem

$$u_{tt} = \Delta u \tag{22}$$

together with two initial conditions and the same boundary conditions as before. Suppose that a steady state solution $\phi(x,y)$ is existing, inserting (14) into (22) yields

$$v_{tt} = \Delta v \tag{23}$$

with homogeneous boundary conditions. This time the Fourier coefficients are

$$A_{k_1,k_2} = a_{k_1,k_2} \, e^{\pm i\sqrt{k_1^2+k_2^2}\,t} \tag{24}$$

and the norm of the step operator $C(t)$ will be

$$||C(t)|| = 1 \; . \tag{25}$$

The solution $v(x,y,t)$, represented by Fourier modes, will therefore not converge in $L_2(B)$ to the desired, and nevertheless existing, steady state solution. The problem, of course, is well posed in L_2 since the norm of the operator $C(t)$ remains bounded.

We conclude from this discussion that the condition of well posedness for time dependent problems does not necessarily imply the convergence of the unsteady solution to the steady state. It is, of course, hopeless to expect that transient solutions of a time dependent problem will ever converge to a steady state, if the problem is not at least well-posed.

Consider now a general linear elliptic boundary value problem of the form

$$L(u) = 0 \tag{26}$$

with given boundary condition in a general bounded domain. Let the steady state solution be $u_s(\underline{x})$, where $\underline{x}$ denotes the set of independent variables.

A general class of artificial time dependent equations may be written as

$$R(\frac{\partial u}{\partial t}) = L(u) \tag{27}$$

where the time dependent operator $R(\frac{\partial u}{\partial t})$ is defined by

$$R(\frac{\partial u}{\partial t}) = a_n \frac{\partial^n u}{\partial t^n} + a_{n-1} \frac{\partial^{n-1} u}{\partial t^{n-1}} + \ldots a_1 \frac{\partial u}{\partial t} \tag{28}$$

with (for the moment) constant real coefficients a_ν, $\nu = 1,2, \ldots n$. Adding on both sides of (27) the term λu, leads to solutions of the form, of which we write only a typical term,

$$u - u_s(\underline{x}) \sim b_j e^{\sigma_j t} v_j(\underline{x}) \tag{29}$$

and where the $v_j(\underline{x})$ represents the eigensolutions of the elliptic operator $L(u)$

$$L(v_j) + \lambda_j v_j = 0 \tag{30}$$

with positive[×] eigenvalues λ_j. In order to find the values σ_j (they are assumed to be distinct for a moment), we obtain from the left hand side of (27) the characteristic polynomial

$$P(\sigma) = a_n \sigma^n + a_{n-1} \sigma^{n-1} + \ldots + a_1 \sigma + \lambda = 0, \tag{31}$$

for the n roots σ_j for each eigenvalue λ_j.
The solution of Eq.(27), using the n (given) initial conditions, may again be represented as

$$u(\underline{x},t) - u_s(\underline{x}) = C(t)(u(\underline{x},o) - u_s(\underline{x})) \tag{32}$$

Taking the norm, we obtain (this requires again the completeness of the eigensolution v_j)

$$||u(\underline{x},t) - u_s(\underline{x})|| \leq ||C(t)||\ ||u(\underline{x},o) - u_s(x)||\ . \tag{33}$$

Suppose now that the norm of the operator, $||C||$, is uniformly bounded, by less than one for $t \to \infty$, then $||u(\underline{x},t) - u_s(\underline{x})||$ converges uniformly to zero for $t \to \infty$, which again establishes the convergence for any set of initial conditions. We now introduce the following definition.
Definition : the artificial time dependent equation (27) is called a relaxation equation of order n if and only if the norm of the operator, $||C(t)||$, is uniformly bounded by

$||C(t)|| = K_o(t)\, e^{-\varepsilon t}$, $\varepsilon > 0$, real and $K_o(t)$ a polynomial of degree $m < n$ with positive coefficients. The time dependent operator $R(\frac{\partial u}{\partial t})$ will be called a relaxation operator of order n.

We then may summarize the preceding discussion. The time dependent solution of a linear relaxation equation of order n with n independent initial conditions and the same boundary conditions as for the steady state problem converges uniformly to the steady state, independent of the initial conditions. The proof comprises two essential points, namely

[×] An eigenvalue $\lambda = 0$ corresponds to a pure Neumann problem for the Laplace equation, where an arbitrary constant can be added to the solution.

the existence of a complete set of eigenfunctions for the steady state operator L(u), and the requirement that all roots of the characteristic polynomial $P(\sigma) = 0$ (Eq.31) have negative real parts. This, in particular, requires the existence of positive eigenvalues.

It is interesting to note that initially the error norm can grow with increasing time, a phenomenon often observed for optimised relaxation procedures. This, of course, is a consequence of multiple roots of the characteristic polynomial.

From a practical point of view, it is important to know the conditions for which all roots of the characteristic polynomial have negative real parts. These algebraic conditions are known for quite long time as Routh-Hurwitz (1877, 1895) criteria[×].

A necessary condition is that all coefficients of the polynomial $P(\sigma) = 0$ (35a) must exist and must be positive.

Sufficient conditions are given by $D_r > 0$, where the D_r are the sub-determinants of the following determinant

$$D = \begin{vmatrix} a_{n-1} & a_{n-3} & a_{n-5} & \cdots \\ a_n & a_{n-2} & a_{n-4} & \cdots \\ 0 & a_{n-1} & a_{n-2} & \cdots \\ 0 & a_n & \cdot & \\ \cdot & \cdot & \cdot & \\ \cdot & 0 & \cdot & \cdots \end{vmatrix} \qquad (35b)$$

D_0 D_1 D_2

For a second order polynomial the necessary condition is also sufficient. The sufficient conditions for some higher order polynomials are given below :

$$\begin{aligned} &\text{3nd order} && a_2a_1 - a_3a_0 > 0 \\ &\text{4th order} && a_1a_2a_3 - a_4a_1^2 - a_0a_3^2 > 0 \\ &\text{5th order} && a_3a_4 - a_2a_5 > 0 \quad \text{and} \\ & && (a_3a_4 - a_2a_5)(a_1a_2 - a_0a_3) - (a_1a_4 - a_0a_5)^2 > 0. \end{aligned} \qquad (36)$$

There are a number of practical situations, where the time dependent equation (Eq.27) has a form, which would not allow immediately the application of the results, we have obtained so far.

As an example, we consider the well-known time dependent equation of acoustics, which we want to transform into a relaxation equation. This equation reads, where $\phi(x,y,z,t)$ is the perturbation potential, and M the (constant) Mach number

$$M^2\phi_{tt} + 2M^2\phi_{tx} - (1 - M^2)\phi_{xx} - \phi_{yy} - \phi_{zz} = 0 \qquad (37)$$

[×] there are, of course, also other possibilities to determine, whether $Re(\sigma) < 0$.

A simple relaxation equation would be ($M^2 \neq 1$).

$$M^2\phi_{tt} + \omega M^2\phi_t + 2M^2\phi_{tx} - (1 - M^2)\phi_{xx} - \phi_{yy} - \phi_{zz} = 0 \tag{38}$$

where ω represents the (positiv) inverse relaxation time. Applying a transformation

$$\tau = t + \frac{M^2}{1 - M^2}\, x; \qquad \xi = x; \qquad \eta = y; \qquad \zeta = z. \tag{39}$$

yields the canonical form of (38)

$$\frac{M^2}{1 - M^2}\,\phi_{\tau\tau} + \omega M^2\phi_\tau - (1 - M^2)\phi_{\xi\xi} - \phi_{\eta\eta} - \phi_{\zeta\zeta} = 0 \tag{40}$$

hence this artificial hyperbolic time dependent equation is indeed a relaxation equation for values of $M < 1$.

We may also contruct the set of eigensolutions for the steady state operator

$$L(\phi) = (1 - M^2)\phi_{\xi\xi} + \phi_{\eta\eta} + \phi_{\zeta\zeta}$$

leading to the eigenvalue problem :

$$L(\psi_j) + \lambda_j\psi_j = 0 \tag{41}$$

which has a complete set of eigensolutions for values of $M < 1$. Finally we obtain the characteristic polynomial :

$$\frac{M^2}{1 - M^2}\,\sigma^2 + \omega M^2\sigma + \lambda_j = 0 \tag{41a}$$

of which the roots have all negative real parts, provided that $\lambda_j > 0$, $M < 1$, $\omega > 0$.

If now Fourier series are considered, we may either use the original time dependent equations (38), or the canonical form (40) to obtain the temporal amplification factor for the errors between the transient solution $\phi(x,y,z,t)$ and the steady state one.

Since we have a linear problem, only a single component needs to be considered.

$$\phi(x,y,z,t) - \phi_s \sim \hat{\phi}(k_1,k_2,k_3)\, e^{\sigma t}\, e^{i(k_1x + k_2y + k_3z)} \tag{42}$$

where the k_1,k_2,k_3 are the wavenumbers, leading to the following characteristic polynomial for Eq.38 :

$$P(\sigma) = M^2\sigma^2 + M^2(\omega + ik_1)\sigma + (1 - M^2)k_1^2 + k_2^2 + k_3^2 = 0$$

with a complex coefficients. In order to guarantee that for all admissible wavenumbers k_1,k_2,k_3, the errors are tending to zero for $t \to \infty$, the roots of $P(\sigma) = 0$, must have negative real parts. The Routh-Hurwitz conditions (Eq.35), however, cannot be applied immediately, since a complex coefficient is occuring.

The new polynomial $H(\sigma) \equiv P(\sigma)\,\bar{P}(\sigma) = 0$ where $\bar{P}(\sigma)$ is $P(\sigma)$ with the complex conjugate coefficients, has only real coefficients. The real parts of the roots of $P(\sigma)$ are not altered considering $H(\sigma) = 0$, the proof for this being obvious. The resulting forth-order polynomial in σ may then be investigated applying the Routh-Hurwitz conditions.

Again we find the condition that $M < 1$, without referring to the explicit knowledge of the eigensolutions and eigenvalues of the steady state operator of the relaxation equation. We expect that this concept can be generalised.

So far we have treated certain classes of continuous relaxation equations for general (steady state) elliptic operators. Consider now the steady state linear operator with constant coefficients in two space dimensions, expressed as a system

$$\ell(w) = Aw_x + Bw_y, \tag{43}$$

where the matrices A,B are of dimension m, with real coefficients, the vector w representing the set of unknowns. Furthermore we introduce a matrix $P(k_1,k_2)$

$$P = k_1A + k_2B \qquad \text{with } -\infty < k_1,k_2 < +\infty \qquad k_1,k_2 \neq 0,\text{real} \quad . \tag{44}$$

The operator $\ell(W)$ is called elliptic, if for all k_i with the possible exception $k_1 = k_2 = 0$, $\det(P(k_1,k_2)) \neq 0$. It is called hyperbolic, if the characteristic condition $\det P(k_1,k_2) = 0$ is identically satisfied for certain values of k_1, $k_2 \neq 0$. These definitions are still useful, if the matrices contain variable coefficients, depending even on the unknowns w. For our model problem (Eq.3) it is easily verified that the operator is elliptic.

We want to solve the homogeneous problem $\ell(W) = 0$ in a bounded space domain with appropriate conditions on the given boundary. The proper formulation of these conditions, is not at all a trivial matter, since the operator may be elliptic or hyperbolic and may even change its type, if a variable coefficient problem is considered (transonic flows).

Consider now a set of artificial time dependent equations which may be written as

$$R(w_t, w_{tt}, \ldots; w_{xt}, w_{yt}, \ldots) = \ell(w) \tag{45}$$

where the time dependent operator is a vector valued function, containing a certain amount of time and space-time differentials for w and coefficients, which are, in general, matrices with variable coefficients. The formidable problem, whether this artificial time dependent equation is a relaxation equation, in the sense that our operator $||C(t)||$ is uniformly bounded by less than one for $t \to \infty$, certainly cannot be solved immediately.

In order to attack this problem, we shall use the following assumptions :

(i) We consider only linear problems with constant coefficients. The error between the time dependent solution $w(x,y,t)$ and the steady state solution $w_s(x,y)$ therefore satisfies also Eq.(45) with homogeneous conditions on the boundary

(ii) Since the eigensolutions of the operator $\ell(w)$ are not known, (they may not even exist), we shall use Fourier-series, or more general, Fourier transforms, to represent the solutions.
As a consequence, the influence of the conditions on the boundaries is not taken into account properly, except if periodicity conditions are assumed.

The error between the time dependent solution and the steady state solution $\ell(w) = 0$ then typically may be represented by

$$v(x,y,t) \sim \hat{v}(k_1,k_2) \exp[\sigma t + i\,(k_1x + k_2y)] \tag{46}$$

where k_1, k_2 denote the wavenumbers and the term $\exp(\sigma t)$ the familiar amplification factor. Inserting this into the artificial time dependent equation (45) leads to the following eigenvalue problem for σ

$$\det \{\hat{R}(\sigma,k_1,k_2) - i\, P(k_1,k_2)\} = 0 \qquad (47)$$

where the matrix $\hat{R}$ represents the Fourier transform of the time dependent operator R of Eq. 45. The set of artificial time dependent equations are called relaxation equations, if all eigenvalues σ of the complex eigenvalue problem (Eq.47) have negative real parts for all wavenumbers $0 < |k_j| < \infty$.

This condition, which of course can be applied also for a single time dependent problem is probably not sufficient[x], practical evidence, however, clearly indicates it necessary character for that $||C(t)||$ is uniformly bounded by less than one for $t \to \infty$.

There are two interesting situations, where one or even more σ may be zero. Suppose that one σ is zero independently of the wavenumbers. This leads to the "catastrophy" that the steady state will depend on the initial data. Nevertheless there are examples, where this phenomenon has a very significant physical meaning as we will see later. It may also occur (supersonic flows) that only for certain wavenumbers $Re(\sigma) = 0$. This arises for the artificial time dependent problem (Eq.45) if the characteristic condition, $\det P(k_1,k_2) = 0$ is identically satisfied for certain $k_j \neq 0$. In consequence, the relaxation operator must be modified if "damping" is required in regions where $\ell(w)$ is hyperbolic.

Finally, we note that the problem of optimisation will be treated in connection with discrete relaxation methods.

As an example, let us consider again the artificial time dependent equation (i.e. Eq. 11) for our model problem.

$$w_t + Aw_x + Bw_y = 0 \qquad (11)$$

the matrix P has the form :

$$P = \begin{pmatrix} k_1 & k_2 \\ k_2 & -k_1 \end{pmatrix}$$

so that $\det P = -(k_1^2 + k_2^2) \neq 0$ for $k_1, k_2 \neq 0$. The eigenvalue problem (Eq.47) leads to

$$\sigma + i\, \mu_p(k_1,k_2) = 0; \qquad p = 1,2$$

where the $\mu_p = \pm \sqrt{k_1^2 + k_2^2}$ are the eigenvalues of the matrix P. Since $Re(\sigma) = 0$ for all wavenumbers $k_j \neq 0$, our artificial time dependent problem is not a relaxation equation. As a consequence, we expect that schemes with high order stable approximations of Eq.11 will converge extremely slow to the steady state.

---

[x] Sufficient conditions may be obtained with the so-called "energy method" taking into account the boundary conditions.

AD-A039 688 ADVISORY GROUP FOR AEROSPACE RESEARCH AND DEVELOPMENT--ETC F/G 20/4
COMPUTATIONAL FLUID DYNAMICS.(U)
APR 77

UNCLASSIFIED AGARD-LS-86 NL

2 OF 2
AD
A039688

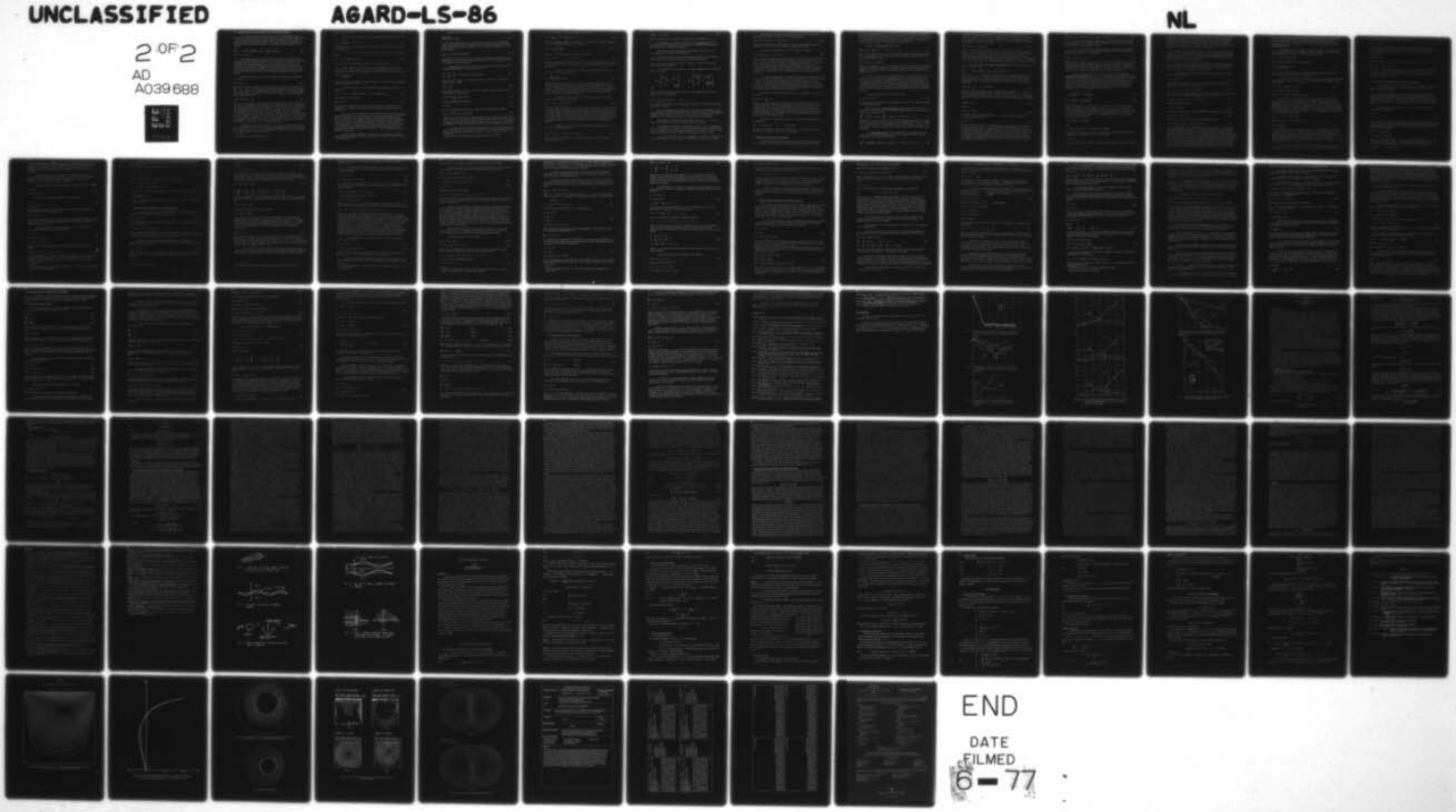

END
DATE
FILMED
6-77

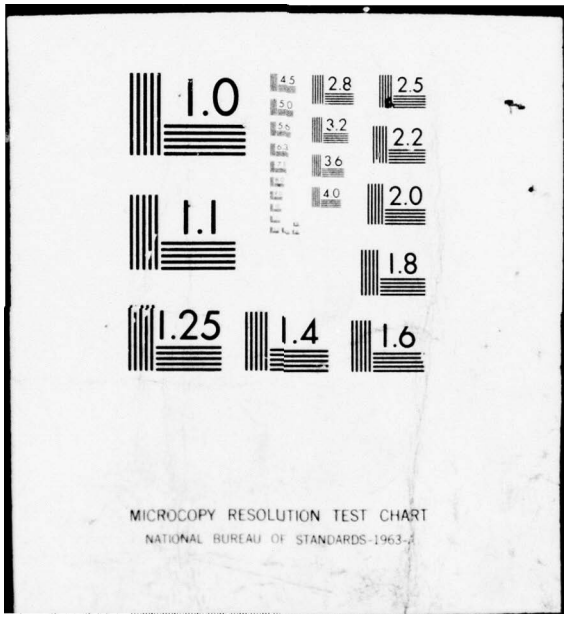
1.0
1.1
1.25
1.4
1.6
1.8
2.0
2.2
2.5
2.8
3.2
3.6
4.0
4.5
5.0
5.6
MICROCOPY RESOLUTION TEST CHART
NATIONAL BUREAU OF STANDARDS-1963-A

2.3 Convergence and rate of convergence of discrete iterative methods

It is evident that the ideas developed in the last chapter may be used immediately to construct discrete relaxation methods, which are consistent approximations of the time dependent relaxation equations. Before proceeding along these lines, we consider discrete iterative methods without referring to the explicit knowledge of the underlying continuous relaxation equations. As an example we may take again the SOR process

$$\phi_{m,n}^{k+1} = (1 - \omega)\phi_{m,n}^{k} + \frac{\omega}{4}(\phi_{m-1,n}^{k+1} + \phi_{m+1,n}^{k} + \phi_{m,n-1}^{k+1} + \phi_{m,n+1}^{k}) \tag{48}$$

for $m,n = 1,2, .. M-1$.

This equation belongs to a class of two level schemes for one grid function $\phi_{m,n}$, which have been analysed sufficiently in the literature and therefore this needs not be repeated here. The problems involved are the convergence of the iteration, the uniqueness of the discrete steady state solution and the formulation of an error estimation for the iteration. Assuming that these questions have been answered, then the important practical problem remains, how rapid the iteration converges. This aspect, which is of direct economic interest, therefore usually determines the popularity of a method.

Suppose that the class of two level schemes have been written in matrix form, such that

$$\phi^{k+1} = T\,\phi^{k} + r \tag{49}$$

where ϕ^{k} is a vector (of dimension $2(M-1)$ in our case), collecting all values $\phi_{m,n}^{k}$ for $m,n = 1,2, .. M-1$; T is a matrix (called iteration matrix) and r another vector, independent of the iteration level. Suppose further that the operator T is uniformly bounded and has the property of contraction, such that for two elements x,y of the Banach space, the following relation holds

$$||Tx - Ty|| \leq L\,||y - x|| \tag{50}$$

with $0 < L < 1$. As norm $||\,.\,||$, we may use the discrete euclidian, or any other suitable one. Then the well-known fix-point theorem (see for example Collatz (1964)), guarantees not only the convergence but also the uniqueness of the final solution of the iteration for arbitrary initial conditions. The assumption of a Banach space is a statement about the completeness of this linear space, or - in other words - that a Cauchy sequence $\{\phi^{k}\}$ has a fix-element, which is again an element of the Banach space. The usual problem is to find bounds for the operator T, such that the contracting property is established. For linear operators, we may use $L = ||T||$ with the requirement $||T|| < 1$. Since for the same operator T the norm $||T||$ may be greater or less than one depending on the vector norm employed, the condition $||T|| < 1$ is only sufficient.

A necessary and sufficient condition is that the spectral radius of the operator $\rho(T)$ is less than one, where the spectral radius is the maximum absolute eigenvalue of T. We therefore may put $L = \rho(T)$. It should be mentioned that $\rho(T)$ is not a norm, in general. The following equations holds for any matrix[x]

---

[x] The equal sign holds for normal matrices.

$$\rho^n(T) \leq ||T^n|| \leq ||T||^n. \tag{51}$$

For the euclidean vector norm, the corresponding matrix norms (spectral norm) is

$$||T|| = \sqrt{\lambda_{max}(T^x T)} \quad \text{with} \quad T^x = \bar{T}', \tag{52}$$

the square root of the largest eigenvalue of the matrix T multiplied with its complex conjugate transpose.

It is easy to show that the following simple error estimation of the iteration holds

$$||\phi^x - \phi^k|| \leq \frac{L}{1 - L} ||\phi^k - \phi^{k-1}|| \tag{53}$$

where ϕ^x denotes the fix-element (solution) of the iteration process.

Finally, a measure for the rapidity of the convergence may be introduced, observing that - roughly speaking - the error is reduced by a factor of $\rho(T)$ by each iteration. The reciprocal rate of convergence of the method is defined by (Young (1954)).

$$RR(T) = \frac{1}{-\log_{10}\rho(T)} \quad . \tag{54}$$

One shows also that the asymptotic number of iterations to achieve a certain convergence level is proportional to RR(T).

For small mesh size h, the spectral radius may be developed in powers of h, leading to

$$\rho(T) = 1 - \delta h^n \qquad \text{with real constants} \quad \delta, n > 0, \text{ independent of h.} \tag{55}$$

Inserting this into Eq.54 yields

$$RR(T) \sim \frac{1}{\delta} h^{-n} \quad . \tag{56}$$

It is therefore desirable for an effective iteration process to minimize n and to maximize δ. It is usually by far more important, to make n as small as possible than to maximize δ.

The trouble with this beautiful fix-point theorem is that there are many methods, where the application of this theorem leads to extremely difficult problems. We have seen that the heart of the fix-point theorem is the contraction property, leading (in our formulation) to the problem of determining the spectral radius of the iteration matrix. This turns out to be extremely difficult, if, instead of a single equation, like the SOR process, a coupled system of iteration equations must be considered and/or of the implementation of boundary conditions destroys the uniform structure of the iteration matrix. Problems with variable coefficients or even non-linear ones lead to additional complications.

In order to develop alternative conditions for the convergence of iterative methods, especially systems of equations, we consider first again the iterative solution of the Laplace equation.

Suppose that the following discrete iterative method for a single grid function

$$B \frac{\phi^{k+1}_{m,n} - \phi^{k}_{m,n}}{\Delta t} = A \phi^{k}_{m,n} \tag{57}$$

is a consistent approximation of a well-posed artificial or natural time dependent equation, where B,A are linear, uniformly bounded difference operators with constant coefficients, Δt being the time increment. Let A be a discrete approximation[x] of the Laplace equation

$$A\phi_{m,n} = L_h(\phi) = \frac{1}{h^2} (\delta_x^2 + \delta_y^2) \phi_{m,n} \, . \tag{58}$$

Since Eq.(57) is linear, the error $v^{k}_{m,n}$ between the transient solution $\phi^{k}_{m,n}$ and the steady state solution of $L_h(\phi) = 0$ with given boundary conditions satisfies also Eq.57 with homogeneous boundary conditions.

Suppose that the operators A,B have as eigensolutions Fourier modes, then the following representation of the error may be used

$$v^{k}_{m,n} = \sum_{k_1=1}^{M-1} \sum_{k_2=1}^{M-1} a^{k}(h,k_1,k_2,\Delta t) \sin k_1 hm \sin k_2 hn \tag{59}$$

where $a^{k} = g\, a^{k-1} = g^{k} a^{o}$ and $g(h,k_1,k_2,\Delta t)$ is the contraction factor of the general iteration scheme

$$v^{k+1}_{m,n} = C\, v^{k}_{m,n} \tag{60}$$

with the "step operator" $C = E + \Delta t\, B^{-1}A$ (B^{-1} is assumed to exist); the norm of the step operator in L_2 then yields

$$g_o = ||C|| = \max_{k_1,k_2} |g(\Delta t,h,k_1,k_2)| \tag{61}$$

The k-th iteration may be written as

$$v^{k} = C^{k} v^{o} \tag{62}$$

where v^{o} represents the initial error. Taking the norm (L_2) of Eq.62 we obtain

$$||v^{k}|| \leq ||C^{k}||\, ||v^{o}|| \leq ||C||^{k} ||v^{o}|| \tag{63}$$

leading to the conclusion that the method converges to the steady state, if and only if $||C^{k}|| \to 0$ for $k \to \infty$ for arbitrary initial elements. Since the norm of the step operator C is bounded by less than one, the condition, that the absolute value of the contraction factor must be less than one for all wave numbers $k_j \neq 0$, is necessary and sufficient.

In order to achieve the most rapid convergence, we select the time increment Δt such that the norm $||C||$ is minimized. Since Eq.(57) is a consistent approximation of a time dependent problem, there exists a relation $\Delta t = f(h)$, in our case $\Delta t = sh^2$, $s > 0$

---

[x] There are possible schemes, where A approximates L_h only in some sens.

such that the norm $||C||$ can be minimised with respect to s

$$g_{op} = \min_{0<s\leq s_{max}} ||C|| = \min_{0<s\leq s_{max}} g_o(s,h) \tag{64}$$

where the relaxation parameter s is bounded only by a stability requirement. Furthermore the rate of convergence can be defined similarly.

$$RR(C) = \frac{1}{-\log_{10} g_o(s,h)} \tag{65}$$

with $g_o < 1$, we expand $g_o(s,h)$ in powers of h, such that

$$g_o = 1 - \delta(s)h^n \qquad \delta(s) > 0,\ n > 0 \tag{66}$$

leading to the representation of $RR(C) = \frac{1}{\delta} h^{-n}$. Comparing this approach with the previous one, there is much similarity. As a matter of fact, all we have done is changing the Banach space.

Let us now consider general iterative schemes (in two-dimensions, for simplicity), which may be written as

$$R(\Delta t) \frac{w^{k+1}_{m,n} - w^{k}_{m,n}}{\Delta t} = H\, w^{k}_{m,n} \tag{67}$$

where the matrix operators R and H are containing linear difference operators with constant coefficients and where the $w^{k}_{m,n}$ represent a vector of dimension m, Δt being the time increment. Suppose that $R(\Delta t)$ and H are uniformly bounded and that the inverse of $R(\Delta t)$ is existing. Let us further assume that Eq.(67) is a consistent approximation of an artificial or natural time dependent problem, not necessarily a relaxation equation as defined in the previous chapter.

Introducing the errors between the transient solution and the steady state, denoted by $w^{\times}_{m,n}$, we obtain again

$$v^{k+1}_{m,n} = C\, v^{k}_{m,n}; \qquad C = E + \Delta t R^{-1} H \tag{68}$$

with the assumption that $H\, w^{\times}_{m,n} = 0$ and that a steady state exists. It is also important to note here that the steady state solution vector may well contain more components than the original steady state differential problem would require to be completely specified. The practical essence of relaxation methods is indeed to add artificial equations to the original problem. Since the steady state solution vector $w^{\times}_{m,n}$ contains more unknowns than we actually need, the consistency conditions ensures that for vanishing mesh size no additional steady state differential operators other than the required one are appearing.

Suppose now that the errors can be represented by Fourier series. Then we may write for a typical component

$$v^{k}_{m,n} \sim g^{k}\, \hat{v}(k_1,k_2, ..) \exp\left[i(k_1 hm + k_2 hn)\right] \tag{69}$$

where g represents the contraction . Inserting into Eq.(68) yields the following eigenvalue problem for g

$$\det\left[\hat{R}(g - 1) - \Delta t\, \hat{H}\right] = 0, \qquad (70)$$

where the operators $\hat{R}, \hat{H}$ are the Fourier transformations of the operators R, G.

Then we define : the system of Eq.(67) are called relaxation equations, if the maximum absolute eigenvalue of the step operator is bounded by less than one for all wavenumbers $k_j \neq 0$ satisfying $\max_j |k_j h| \leq \pi$.

Again there exists for some applications the possibility that $g = 1$ for all wavenumbers, which requires special attention.

Finally, we can state that the iteration scheme converges to the consistent steady state solution, if the system (Eq.67) are relaxation equations.

All we have to show is that $||\hat{C}^k|| \to 0$ for $k \to \infty$, where $\hat{C}$ is the Fourier transform of the step-operator.

Transforming $\hat{C}$ by a unitary matrix U into upper triangular form, we obtain with $U\hat{C}U^{\times} = D + V$, where

$$D = \begin{pmatrix} g_1 & & & 0 \\ & g_2 & & \\ & & \ddots & \\ 0 & & & g_m \end{pmatrix} \qquad V = \begin{pmatrix} 0 & V_{12} & \cdots & V_{1m} \\ & 0 & \ddots & \vdots \\ & & \ddots & V_{m-1\,m} \\ 0 & & & 0 \end{pmatrix}$$

hence

$||\hat{C}^k|| = ||(UCU^{\times})^k|| = ||(D + V)^k||$ and, after a little algebra, using that V is certainly also uniformly bounded

$$||\hat{C}^k|| \leq \sum_{j=0}^{m-1} \binom{k}{j} ||D||^{k-j} ||V||^j \qquad \text{for } k > m - 1$$

Now, if all the eigenvalues of the step operator are bounded by less than one in modulus, then $||\hat{C}^k|| \to 0$ for $k \to \infty$.

One is therefore tempted to believe that the boundness of the spectral radius is a necessary and sufficient condition. This is, however, not true, since the fundamental assumption namely that Fourier series can be used, is-with the exception that C is a normal matrix - not justified as they are not eigensolutions of the operator C .

Nevertheless, the condition that $|g_\nu(k_1, k_2)| < 1$ for $\nu = 1, .. m$, $k_j \neq 0$ is certainly a necessary one, as also our practical experience indicates.

Since relaxation schemes have the property that $|g_\nu| < 1$ for all wavenumbers $k_j \neq 0$ with $\max_j |k_j h| \leq \pi$ the concept of "dissipative" schemes, first introduced by Kreiss (1964) may be generalised. Indeed, relaxation methods are necessarily dissipative, since, physically speaking, the entropy increase is positive for a relaxation process.

From a practical point of view, it is important to know algebraic conditions for which the eigenvalues of the step operator $\hat{C}$ are bounded by less than one in modulus.

Suppose that the eigenvalue problem for g Eq.(70) leads to the following characteristic polynomial of order m with complex coefficients,

$$P(g) = a_m g^m + a_{m-1} g^{m-1} + \ldots + a_1 g + a_o = 0 \tag{72}$$

Applying a transformation $g = \frac{1 + z}{1 - z}$, where z is again a complex variable, maps the interior of the unit circle on to the left half plane of the z plane.

Inserting the transformation into P(g) = 0, yields a polynomial

$$Q(z) = A_m z^m + A_{m-1} z + \ldots A_1 z + A_o = 0 \tag{72a}$$

with coefficients A_r. Suppose that the coefficients A_r are real; then the Routh-Hurwitz conditions (Eq.35) provide necessary and sufficient conditions for that Re(z) < 0, or $|g| < 1$. If the coefficients are complex, we construct a polynomial $H(z) \equiv Q(z)\bar{Q}(z) = 0$ with real coefficients only. For a second order polynomial, the condition $a_r > 0$, r = 0,1,2 are necessary and sufficient. Finally the problem of determining the rate of convergence must be considered, since, alfter all, this is besides the contraction property of the step operator, the most interesting quantity to compare methods with each other.

It is evident that the rate of convergence is determined by the spectral radius of the step operator (iteration matrix) C. From the representation of the errors (Eq.69) it follows that the $|g_\nu|$ are the eigenvalues of the Fourier transform of the step operator, and therefore are determining how these errors will tend to zero for each wavenumber. Since conditions on the boundaries, except periodicity ones, are not taken into account, we are in general unable to find the correct wavenumbers, which minimise the spectral radius of the transformed step operator.

Nevertheless, using the consistency condition, to replace Δt by a function of h, we define

$$g_o(h, k_j, s_\alpha) = \max_{1 \le \nu \le m} |g_\nu|$$

where h, k_j, s_α are the meshsize, the wavenumbers for each spatial coordinate, the relaxation parameters, respectively. Suppose that the steady state operator of the original problem is elliptic, the characteristic condition det $P(k_j)$ with $k_j \neq 0$ being positive for all wavenumbers, one observes that the rapidity of convergence of a method is governed by the fundamental modes, which are the lowest possible wavenumbers corresponding with the boundary conditions while stability requires that the highest possible modes remain bounded.

This allows us, to expand g_o in powers of h for fixed wavenumbers leading to an expression

$$g_o = 1 - \delta(s_\alpha, |k_j|)\, h^n, \qquad \delta > 0, \qquad k_j \neq 0, \text{ fixed.}$$

The method is optimised if, for a fixed wavenumber, g_o is minimised with respect to the relaxation parameters. Details will be given later.

2.4 Examples and simple relaxation operators

The following brief review of a few well-known convergent iterative methods is not intended to discuss in detail their application and the derivation of their

respective convergence rates, but to identify and discuss the underlying time dependent relaxation equations and operators. Again, for simplicity, we consider first the solution of the Laplace equation with Dirichlet conditions in a bounded domain $B = \{x,y | 0 \leq x,y \leq 1\}$ and treat later systems of first order equations in the same domain, corresponding with our model problem. We refer to the notations introduced earlier.

Consider the Jacobi method (Jacobi (1845)

$$\phi^{k+1}_{m,n} - \frac{1}{4}(S_x + S_y)\phi^{k}_{m,n} = 0 \qquad \text{for } m = 1,2, \ldots M-1 \tag{75}$$

which is the simplest, explicit, two-level iteration scheme requiring only an averaging of the neighbourghing values of $\phi^{k}_{m,n}$. Rewriting this method as an approximation for a time dependent problem, gives

$$\phi^{k+1}_{m,n} - \phi^{k}_{m,n} - s(\delta_x^2 + \delta_y^2)\phi^{k}_{m,n} = 0 \tag{75a}$$

where the step parameter s ($s \leq \frac{1}{4}$ for convergence) may now be interpreted as a relaxation parameter. The asymptotic number of iterations to achieve a certain convergence level is proportional to the reciprocal rate of convergence (Eq.54). For the Jacobi method, one obtains $RR = 2/\pi^2\ h^{-2}$.

In order to establish the correspondence between the iteration process and an (continuous) initial value problem, let $\phi^{k}_{m,n}$ represent the value at a time $t = k\ \Delta t$, $k = 1,2,..$, of a continuous time dependent function $\phi(x,y,t)$. Expanding formally the iteration method in a Taylor series about x,y,t and truncating the series, leads to a time dependent equation which is a continuous representation of the iteration for small time (Δt) and small space (h) increments. This idea has been used first by Garabedian (1956) to derive the correct asymptotic artificial time dependent equation for the SOR process.

For the Jacobi method, we obtain with $s = \Delta t/h^2$

$$\phi_t - \Delta\phi = 0 + O(\Delta t, h^2)\ . \tag{76}$$

It is evident that this equation is the simplest possible form of a relaxation equation to integrate the Laplacian.

Next we mention the Gauss-Seidel method (Gauss, Seidel, 1874) which is an improvement to the Jacobi process. If new values $\phi^{k+1}_{m,n}$ are immediately inserted into the right term of Eq.(75), we obtain

$$\phi^{k+1}_{m,n} - \frac{1}{4}(\phi^{k+1}_{m-1,n} + \phi^{k}_{m+1,n} + \phi^{k+1}_{m,n-1} + \phi^{k}_{m,n+1}) = 0 \text{ for } m,n = 1,2, \ldots M-1 \tag{77}$$

Again we have a two level method, which is implicit although the computation is carried out entirely explicit, however. The superiority of this method ($RR = 1/\pi^2\ h^{-2}$) compared with the Jacobi method is a consequence of the theoretical implicit structure of the step operator. The time like aspect of this method will be discussed together with the SOR process.

The Dufort-Frankel method (Dufort, Frankel 1953) is an example for a three level explicit method and was meant originally to integrate numerically the time dependent heat conduction equation (Eq.76)

$$\phi^{k+1}_{m,n} - \frac{1-4s}{1+4s}\phi^{k-1}_{m,n} - \frac{2s}{1+4s}(S_x + S_y)\phi^{k}_{m,n} = 0 \qquad \text{for } m,n = 1,2, .. M-1. \tag{78}$$

The method is unconditionally stable for any value of the step parameter $s = \Delta t/h^2$. In order to integrate correctly the time dependent heat conduction equation, a condition $\Delta t \sim h^2$ must be imposed. If the method is employed as an iterative process for the Laplace equation, s may have any value to achieve the most rapid convergence. Expanding this scheme into a Taylor series yields

$$\kappa^2 \phi_{tt} + \phi_t - \Delta\phi = 0 + O(\Delta t^2, h^2) \tag{79}$$

where $\kappa = sh = \Delta t/h$. This time dependent equation is asymptotically parabolic, if for $\Delta t, h \to 0$, s remains bounded; it is hyperbolic if κ remains fixed for the same limiting process. Eq.(79) is certainly also a relaxation equation (the coefficients of the relaxation operator are positiv), where κ may be used to achieve the most rapid convergence to the steady state. The Dufort-Frankel method may be optimised, using $s_{op} \sim h^{-1}$ leading to $RR = 1/\pi\ h^{-1}$, which is an order of magnitude better than the Jacobi or Gauss-Seidel process.

Let us now consider the Successive Overrelaxation method (Frankel 1950, Young, 1954) in the form of Eq.(9)

$$\phi^{k+1}_{m,n} - (1 - \omega)\phi^{k}_{m,n} - \frac{\omega}{4}(\phi^{k+1}_{m-1,n} + \phi^{k}_{m+1,n} + \phi^{k+1}_{m,n-1} + \phi^{k}_{m,n+1}) = 0 \tag{9}$$

for m,n = 1,2, .. M-1. It is applied in the same way as the Gauss-Seidel method to which it reduces for $\omega = 1$, the relaxation parameter being ω. The method converges for any value of ω between $0 < \omega < 2$ and may be optimised. As Garabedian (1956) showed, the asymptotic artificial time dependent equation for h, $\Delta t \to 0$ such that $r = \Delta t/h$ remains fixed, reads

$$r(\phi_{xt} + \phi_{yt}) + r\mu\phi_t - \Delta\phi = 0 + O(\Delta t^2, h^2) \tag{80}$$

where $\mu = 2\,\frac{2 - \omega}{\omega\ h}$. In order that also μ remains bounded, we require $\omega \sim 2 - \alpha h$, $\alpha > 0$. This artificial time dependent equation is again hyperbolic and for $0 < \omega < 2$, it is also a relaxation equation, as may be verified with the Routh-Hurwitz conditions, for example. Even simpler, we may put Eq.(80) into its canonical form, transforming the time coordinate by

$$\tau = \frac{h}{\Delta t}\, t + \frac{1}{2}\,(x + y) \tag{81}$$

leading to :

$$\phi_{\tau\tau} + 2\mu\phi_\tau - 2\Delta\phi = 0\,. \tag{81a}$$

With respect to the Gauss-Seidel method ($\omega = 1$), we find a relaxation operator, if $\Delta t = sh^2$, s fixed, for $\Delta t, h \to 0$

$$2s\phi_t - \Delta\phi = 0 \tag{81b}$$

Since $s \leqslant \frac{1}{4}$ the method cannot be optimised any more. The reciprocal rate of convergence of the SOR process for $\omega_{opt} \sim 2 - \alpha_{opt} h$ yields for our model problem $RR = 1/2\pi\ h^{-1}$. The method therefore is faster than the Dufort-Frankel scheme, however not significantly. The analysis of Garabedian, of course, was meant to be valid only for the limiting case of vanishing Δt and h and one might wonder up to which finite h Eq.(80) is a valid representation. This question may be answered, considering the next higher order terms of the Taylor series expansion thereby finding also the relaxation equation for finite h. We obtain the canonical form

$$h\frac{\partial}{\partial\tau}\left[\lambda\phi_{\tau\tau}+\mu\phi_{\tau}-\Delta\phi\right]+\phi_{\tau\tau}+2\mu\phi_{\tau}-2\Delta\phi=0+O(\Delta t^4,h\Delta t^3) \tag{82}$$

with $\lambda = (8-\omega)/6\omega$. This equation is indeed again a relaxation equation, if in addition to the condition $0 < \omega < 2$, the mesh size is limited by $0 < h < \frac{3}{2}$. The proof follows immediately from the Routh-Hurwitz conditions.

Eq.(82) has a very interesting general structure, which may be seen as follows. Suppose that μ is zero and $\lambda > 0$ may be a free parameter, then a relaxation equation of the form is obtained ($\lambda < \frac{1}{2}$, h arbitrary)

$$\frac{h}{\lambda}\frac{\partial}{\partial\tau}\left(\phi_{\tau\tau}-\frac{1}{\lambda}\Delta\phi\right)+\phi_{\tau\tau}-2\Delta\phi=0 \tag{83}$$

where the ratio of h/λ may be interpreted as a relaxation time and the factor λ^{-1} and 2 are representing *different speeds of sound*, since the basic operator is representing travelling acoustic waves. These are damped, if the speed of sound of the relaxation process ($\frac{1}{\lambda}$ in our notation) is greater than the usual one, leading to a damping mechanism for these waves in hyperbolic problems which is not based on viscosity.

Finally we consider a class of methods, which are known as <u>ADI methods (Alternating direction implicit)</u> to solve the time dependent heat conduction equation or iteratively the Laplace one. These methods, first introduced by Peaceman and Rachford (1955), have been generalised considerably, in particular by mathematicians of the Soviet Union, see for example Yanenko (1969). They are also known as fractional step methods, since the operators are split spatially and in time. As an example we may consider the original method of Peaceman and Rachford, which cannot immediately be generalised to 3-D problems, however. These equations are

$$\{1-\frac{s}{2}\delta_x^2\}\phi_{m,n}^{k+1/2}-\{1+\frac{s}{2}\delta_y^2\}\phi_{m,n}^{k}=0 \tag{84a}$$

$$\{1-\frac{s}{2}\delta_y^2\}\phi_{m,n}^{k+1}-\{1+\frac{s}{2}\delta_x^2\}\phi_{m,n}^{k+1/2}=0 \tag{84b}$$

for m,n = 1,2, .. M-1.
This totally implicit, two level method is applied as follows. Intermediate values $\phi_{m,n}^{k+1/2}$ are computed (Eq.84a) inverting for each row n = 1,2, .. M-1 a tridiagonal system of equations. Final values $\phi_{m,n}^{k+1}$ are obtained solving Eq.84b for each m = 1,2, .. M-1. The method converges for any value of the step parameter $s > 0$ and therefore s may be used to accelerate the convergence. The intermediate values may be eliminated, leading to the representation

$$\{1-sD_1\}\phi_{m,n}^{k+1}-\{1+sD_2\}\phi_{m,n}^{k}=0$$

where

$$D_1=\frac{1}{2}(\delta_x^2+\delta_y^2)-\frac{s}{4}\delta_x^2\delta_y^2;\qquad D_2=\frac{1}{2}(\delta_x^2+\delta_y^2)+\frac{s}{4}\delta_x^2\delta_y^2\ .$$

The underlying relaxation operator is, of course, the time dependent heat conduction equation. If s is chosen as $s = \gamma h^{-1}, \gamma > 0$ we obtain

$$\phi_t-\gamma\Delta\phi=0$$

where γ is now used for optimisation. We find with $s_{opt}\sim\frac{1}{2\pi}h^{-1}$; $RR\sim\frac{1}{2\pi}h^{-1}$, equal with

the SOR process. A word of warning may be added for the application of these methods for problems with variable coefficients. Since none of the fractional step equations are consistent approximations of the correct steady state operator, the transient solutions do not converge to the correct steady state. The essential requirement is that the split operators must be commutative, which usually prohibits the application of these methods for problems with variable coefficients.

As a result of the preceding discussion, we have found several relaxation operators, of which the one for the SOR process is most interesting for the extension to hyperbolic problems. As far as the numerical methods are concerned, we note that only implicit methods usually allow an optimisation with the result of improving the rate of convergence by an order of magnitude.

In order to conclude this chapter, we consider essentially only two methods to solve first order system of equations namely the Lax (Lax, 1954) and the Lax-Wendroff method (Eq.12). Since the underlying time dependent equations are known, we focuss our interest on the convergence of these methods.

The artificial time dependent hyperbolic equations (they are not relaxation ones) for our model problem

$$w_t + Aw_x + Bw_y = 0 \tag{11}$$

are discretised employing the consistent first order Lax-method, leading to the representation (subscripts m,n are suppressed).

$$w^{k+1} = \frac{1}{4}(S_x + S_y)w^k - \frac{1}{2} r A\delta_x w^k - \frac{1}{2} r B\delta_y w^k \tag{85}$$

where $r = \Delta t/h$ is the iteration parameter and k denotes, as usual, the iteration level. It is easy to show that the Fourier transform of our step operator is

$$\hat{C} = \frac{1}{2}(\cos\xi_1 + \cos\xi_2)I - irD, \quad \xi_1 = k_1 h;\ \xi_2 = k_2 h \tag{86}$$

where the matrix D is given by

$$D = A \sin\xi_1 + B \sin\xi_2 . \tag{87}$$

If μ_D are the eigenvalues of D, we obtain immediately the eigenvalues of $\hat{C}$, namely

$$g_L = \frac{1}{2}(\cos\xi_1 + \cos\xi_2) - ir\mu_D \tag{88}$$

thus with $\mu_D^2 = \sin^2\xi_1 + \sin^2\xi_2$ for our model problem, we obtain

$$|g_L|^2 = \frac{1}{4}(\cos\xi_1 + \cos\xi_2)^2 + r^2(\sin^2\xi_1 + \sin^2\xi_2). \tag{89}$$

The method satisfies the necessary condition for stability of $|g| \leq 1$ which imposes on the step parameter the limits $0 < r \leq 1/\sqrt{2}$. Let us now ask whether the Lax method is a discrete relaxation method, which requires the contraction property for all wavenumbers $k_j \neq 0$ with $\max_j|\xi_j| \leq \pi$. It is easy to see that this is not completely the case, since for $\xi_j = \pi$, $j = 1,2$ $|g| = 1$. On the other hand, assuming sufficiently smooth initial and boundary data the method is reasonably converging $0 < r \leq 1/\sqrt{2}$ for many iteration steps, until no further convergence is observed. The reason for this behaviour lies, of course, in the existence of so called 2-h waves, which are not damped, but also not amplified. Since for smooth functions the amplitudes of these 2-h waves are small, the number of possible iterations are usually sufficient in order to obtain a

reasonable steady state solution, within the limits of the Lax method with its rather poor accuracy (order of consistency). The situation, however, is drastically changed, if a coupling between the 2-h waves and other modes are possible *in non linear cases*. Since for all modes $|g| < 1$ except $\xi_j = \pi$, $j = 1,2$, we may call methods of this type <u>weak relaxation</u> schemes.

The convergence rate for a number of iterations, say $N_1 >> 1$, until the errors of two successive iterations are not reduced any more, is governed by the fundamental modes. Expanding $|g|$ in powers of the mesh size therefore, gives

$$|g| \sim 1 - \frac{1}{2}(\frac{1}{2} - r^2)(k_1^2 + k_2^2)h^2 \tag{90}$$

leading to the reciprocal rate of convergence $RR(\hat{C})$

$$RR = \frac{2}{(\frac{1}{2} - r^2)(k_1^2 + k_2^2)}\ h^{-2} \tag{91}$$

hence the method converges with the same order as the Jacobi method, provided that $\frac{1}{2} - r^2 \neq O(h)$, which, we have seen, is unacceptably slow.

Similarly, we consider the Lax-Wendroff method, already earlier mentioned (Eq.12), which belongs to a class of second order (in space and time) two step methods. The step operator reads

$$\hat{C} = I - 2r^2D^2 - ir(\cos\xi_1 + \cos\xi_2)D \tag{92}$$

with the absolute eigenvalues of $\hat{C}$.

$$|g_{LW}|^2 = (1 - 2r^2\mu_D^2)^2 + r^2\mu_D^2(\cos\xi_1 + \cos\xi_2)^2\ . \tag{93}$$

Again we find that this method is only a weak relaxation scheme since for $\mu_D = 0$ for $\xi_j = \pi$, $j = 1,2$, hence $|g_{LW}| = 1$ for our model problem. In contrast to the Lax method, however, any $\mu_D = 0$ may cause $|g| = 1$, which usually makes this scheme unacceptable as an iteration method for problems where $\mu_D = 0$ in a portion of the field. The remedy, of course, is known by adding "artificial viscosity". For our model problem with sufficiently smooth initial and boundary data the Lax-Wendroff method is converging in the sense described for the Lax method, if $0 < r < 1/\sqrt{2}$. Expanding $|g|$ in powers of h for the fundamental modes yields

$$|g_{LW}| \sim 1 - r^2(1 - 2r^2)(k_1^2 + k_2^2)^2\ h^4 \tag{94}$$

and hence, with the "optimal" choice of $r = \frac{1}{2}$

$$RR_{LW} = \frac{8}{(k_1^2 + k_2^2)^2}\ h^{-4}\ . \tag{95}$$

The Lax-Wendroff method with the desirable property of second order accuracy therefore converges extremely slow. It is clear, that such a rate of convergence prohibits the application of this method as an iteration scheme, although this has been done (for example, Magnus and Yoshihara, 1970; Burstein and Mirin, 1972) where, artificial viscosity had been introduced, however, in order to prevent "non linear instabilities". This additional damping, in a linear case, may improve the rate of convergence such that formally $RR \sim O(h^{-2})$.

In conclusion, we see that the time dependent approach, as we presented it so far, appears not to be very promising for systems of equations. This has led earlier to

develop methods, converting the steady state operator

$$\ell(w) = Aw_x + Bw_y = 0 \tag{96}$$

into a higher order system. The idea is briefly outlined here for a linear case, although it has been applied successfully for the steady state non-linear Euler equations of fluid mechanics (Johnson and Wirz, 1976) as well. Eq.(96) is differentiated by a matrix operator D

$$D = M_1 \frac{\partial}{\partial x} + M_2 \frac{\partial}{\partial y}$$

leading to a coupled system of second order equations (for simplicity $M_1 = A$, $M_2 = B$)

$$A^2 w_{xx} + (AB + BA) w_{xy} + B^2 w_{yy} = 0 \tag{97}$$

this system is solved numerically with the method of successive line over-relaxation (SLOR), marching in the x-direction (downstream). Details may be found in the above reference. We remark only, that the choice of $M_1 = A$, $M_2 = B$ maintains the basic eigenvalue structure of Eq.(96).

2.5 Time dependent-relaxation methods for the Laplace equation

We present here a number of time dependent methods of different relaxation order to solve iteratively the Laplace equation. Of course, more general elliptic operators may equally be treated.

First order relaxation methods are based on the heat conduction equation, examples being the Jacobi (explicit) and the ADI methods (implicit). Second order methods for a single equation are the Gauss-Seidel (explicit) SOR (implicit), Dufort-Frankel (three level, explicit) . We add now a few methods, which employ additional partial differential equations, leading to systems of first order (in time) relaxation methods.

The simple Jacobi method can be improved, considering the following time dependent relaxation equations.

$$\psi_t - \Delta\phi = 0 \tag{98a}$$

$$\phi_t + \frac{1}{\tau}(\phi - \psi) = 0 \tag{98b}$$

where ϕ and ψ are the dependent variables and τ the (positive) relaxation time. It is easy to see that this system is a relaxation equation. There are two initial conditions required together with $\psi = \phi$ on the boundaries. A discreet version of Eq.(98) reads (subscripts m,n are suppressed)

$$\begin{aligned} \psi^{k+1} &= \psi^k + s(\delta_x^2 + \delta_y^2)\phi^k \\ \phi^{k+1} &= \frac{1}{1+\omega}\phi^k + \frac{\omega}{1+\omega}\psi^{k+1} \end{aligned} \tag{99}$$

where s is a step parameter ($\Delta t/h^2$) and ω the relaxation coefficient ($\Delta t/\tau$). In order to optimise the numerical method, it is important that Eq.(98b) is discretised implicitly. The transient solutions converge uniformly to the steady state, if

$$s \leq \frac{1}{4}\frac{2+\omega}{\omega} \qquad \omega > 0, \text{ arbitrary.}$$

It is optimised with $s_{max} = \frac{1}{4}\frac{2+\omega}{\omega}$ and $\omega_{opt} \sim \frac{1}{2\pi} h^{-1}$ for our model problem, leading to $RR = 1/\pi\ h^{-1}$. Thus we see that the convergence rate of this relaxation method is comparable to the SOR method, being an order of magnitude faster than the original Jacobi one. It can be further accelerated, if a sequence of relaxation coefficients is considered.

The second equation (99) is an algebraic relation between the transient solutions ϕ and ψ. Such relations are often used to accelerate a particular iterative method to solve elliptic equations. Here it arises naturally from a consistent approximation of a time dependent relaxation equation.

There are easily other second order relaxation methods to derive, for example

$$\psi_t - \Delta\phi = 0$$
$$\phi_t - \lambda\Delta\phi + \frac{1}{\tau}(\phi - \psi) = 0 \qquad (100)$$

$\lambda, \tau > 0$. However, a system of equations of the following form

$$\psi_t - \Delta\phi = 0$$
$$\phi_t + \lambda^2\Delta\psi + \frac{1}{\tau}(\phi - \psi) = 0;\ \lambda^2, \tau > 0, \qquad (101)$$

requires special attention, since at the steady state ϕ not necessarily equals ψ. The function ψ satisfies at the steady state

$$\lambda^2\Delta\Delta\psi - \frac{1}{\tau}\Delta\psi = 0$$

which is an equation of fourth order, requiring therefore additional boundary conditions for ψ.($\Delta\psi = 0$). In order to keep the relaxation equations *as simple as possible*, we generally avoid such solutions.

Next we consider a few third order methods, of which the first example (which can be further generalised) may be written as

$$\psi_t - \mu\Delta\phi = 0$$
$$\phi_t + \alpha_{11}(\phi - \psi) + \alpha_{12}\chi = 0 \qquad (102)$$
$$\chi_t + \alpha_{21}(\phi - \psi) + \alpha_{22}\chi = 0$$

where $\mu > 0$ and the following conditions for the relaxation coefficients must be imposed

$$\det(\alpha_{ij}) > 0;\ \alpha_{11} + \alpha_{22} > 0;\ \alpha_{11}^2 + \alpha_{12}\alpha_{21} > 0 \qquad (103)$$

in order that Eq.(102) is a relaxation equation. The relations (103) are expressing the positiv definiteness[x] of the matrix (α_{ij}). As boundary conditions, we require $\chi = \psi = \phi$, as usual. A discretised version of Eq.(102), if optimised, is at least as rapid as the SOR process.

---

[x] For a reader familiar with irreversible thermodynamics, these conditions are expressing the second law of thermodynamics.

Another third order method, based on one hyperbolic time dependent operator, for the first relaxation equation, may be used to accelerate the convergence of the leap-frog method.
The time dependent relaxation equations are ($\lambda^2 > 1$, $\tau > 0$)

$$\psi_{tt} - \Delta\phi = 0$$
$$\phi_t - \lambda^2\psi_t + \frac{1}{\tau}(\phi - \psi) = 0 \qquad (104)$$

A discrete analogue may be written as (subscripts are suppressed)

$$\psi^{k+1} - 2\psi^k + \psi^{k-1} - r^2(\delta_x^2 + \delta_y^2)\phi^k = 0$$
$$\phi^{k+1} - \frac{\lambda^2 + s}{1 + s}\psi^{k+1} - \frac{1}{1 + s}(\phi^k - \lambda^2\psi^k) = 0; \qquad (105)$$

where $r = \Delta t/h$; $s = \Delta t/\tau$. The method converges, if the following conditions are met

$$r \leq \frac{s}{2}\frac{1}{\sqrt{4\lambda^2 + s}}; \quad \lambda^2 \geq \frac{4}{3}$$

and may be optimised, taking r_{max} and s_{opt}, λ_{opt}. There are, of course, also other ways to discretise Eq. 104.

2.6 Relaxation methods for systems of first order equations

As already formulated earlier, we are looking for solutions of the general steady state problem (only the 2-D case is treated here)

$$\ell(w) = Aw_x + Bw_y = 0, \qquad (106)$$

where A,B are real matrices of dimension m. Furthermore we introduce again the matrix P, which we defined as

$$P(k_1,k_2) = Ak_1 + Bk_2 \text{ with } k_1,k_2 \text{ real}, -\infty < k_1,k_2 < \infty$$

and the characteristic condition $C_c = \det P(k_1,k_2)$. We recall, that $\ell(W)$ is elliptic, if for $k_j \neq 0$, $\det P \neq 0$ and hyperbolic , if for $k_j \neq 0$ $\det P = 0$ for certain k_1,k_2. Finally we generally assume that the eigenvalues of P are real for all k_j.

In order to develop second order relaxation methods, we start with our familiar problem to solve the Laplace equation, taking the simplest hyperbolic relaxation equation. This equation reads

$$\phi_{tt} + \frac{1}{\tau}\phi_t - \Delta\phi = 0 \qquad (107)$$

where the parameter $\tau > 0$ is the relaxation time. Instead to discretise Eq. 107 immediately, we convert this relaxation equation into a system of first order p.d.e.'s. Defining

$$q = -\phi_t; \quad u = \phi_x; \quad v = \phi_y \qquad (108)$$

we obtain the first order system

$$u_t + q_x = 0$$

$$v_t + q_y = 0 \qquad (109)$$

$$q_t + (u_x + v_y) + \frac{1}{\tau} q = 0$$

for the unknown u,v,q, in which the last equation introduces the relaxation process. We note that Eq.(109) is essentially of third order, while Eq.(107) is only a second order relaxation equation. Thus we expect that one eigenvalue of the system is identically zero, which is indeed the case. Rewriting Eq.(109) in vector form, yields

$$\bar{w}_t + A_1 \bar{w}_x + A_2 \bar{w}_y + B_o \bar{w} = 0 \qquad (110)$$

$$\bar{w} = \begin{pmatrix} u \\ v \\ q \end{pmatrix} \quad A_1 = \begin{pmatrix} 0 & 0 & 1 \\ 0 & 0 & 0 \\ 1 & 0 & 0 \end{pmatrix} \quad A_2 = \begin{pmatrix} 0 & 0 & 0 \\ 0 & 0 & 1 \\ 0 & 1 & 0 \end{pmatrix} \quad B_o = \begin{pmatrix} 0 & 0 & 0 \\ 0 & 0 & 0 \\ 0 & 0 & \frac{1}{\tau} \end{pmatrix}$$

which may be regarded as a general relaxation equation, provided that A_1, A_2, B_o satisfy certain conditions. It is easy to see that Eq.(110) is hyperbolic, since the eigenvalues of

$$\bar{P}\ (k_1,k_2) = A_1 k_1 + A_2 k_2$$

are real for all values $-\infty < k_1,k_2 < \infty$. These are

$$\mu_1 = 0,\ \mu^2_{2,3} = k_1^2 + k_2^2,$$

which confirms that one eigenvalue is indeed zero, leading to the interesting and fundamental fact, that the above relaxation system is singular hyperbolic. The steady state of Eq.(109), if it exists, is apparently given by $q = 0$ and $u_x + v_y = 0$, which is obviously not the steady state operator, we wish to have, namely $u_x + v_y = 0$ and $-v_x + u_y = 0$. Taking the curl of the first two equations of (109) yields the representation

$$\frac{\partial}{\partial t}\ (-v_x + u_y) = 0 \qquad (112)$$

with the general solution $-v_x + u_y = C(x,y)$, where $C(x,y)$ is an arbitrary function not depending on t. In order to meet the required condition $-v_x + u_y = 0$[x], we therefore have to impose an initial condition on u and v, such that $-v_x + u_y = 0$. Eq.(112) expresses the well-known fact, found by Lagrange, that a potential flow, which is vorticity free at any time remains irrotational for all times.

It is evident that a numerical analogue of the relaxation equations (Eq.109) therefore must also meet the Lagrange condition. If this is done properly, the occurrence of an eigenvalue identical zero does not affect the convergence of a numerical method.

---

[x] It is nevertheless possible, to include certain discreet distributed vortices.

We shall see later, how this method may be generalised to treat also compressible potential flows.

In order not to be restricted, however, we next consider our general problem (Eq.106), which may be solved by the following time dependent relaxation process (two-step procedure)

$$\bar{w}_t + Aw_x + Bw_y = 0 \tag{113a}$$

$$w_t + \lambda(Aw_x + Bw_y) + \frac{1}{\tau}(w - \bar{w}) = 0 \tag{113b}$$

with the additional boundary conditions $\bar{w} = w$ and where λ and τ are parameters, τ being the relaxation time. Eliminating the intermediate step, we obtain the second order relaxation equation

$$\tau\frac{\partial}{\partial t}\{w_t + \lambda(Aw_x + Bw_y)\} + w_t + Aw_x + Bw_y = 0 \tag{114}$$

with the characteristic polynomial (Cf Eq. 47)

$$\tau\sigma^2 + (1 + i\tau\lambda\mu_p)\sigma + i\mu_p = 0 \tag{115}$$

where the μ_p ($p = 1,2, .. m$) are the real eigenvalues of the matrix P (Eq.106a). It is easy to show that the time dependent system (Eq.113) is indeed a relaxation equation, if

$$0 < \tau < \infty;\ \lambda > 1;\ \mu_p \neq 0 \text{ for } k_j \neq 0,\ j = 1,2;\ p = 1,2, .. m.$$

There are several remarks to be made about these equations. First we note that the complete system is again singular hyperbolic. This is a consequence of a fundamental requirement, that the speeds of propagation of disturbances of the time dependent system 113 are only a multiple of each eigenvalue of the matrix P. If the steady state equations 106 are hyperbolic, the characteristic condition $\det P(k_1, k_2)$ being zero for certain wavenumbers $k_j \neq 0$ ($j = 1,2$), then there exists at least always one eigenvalue $\mu_p = 0$. This implies that the time dependent system (Eq.113) is no longer representing a relaxation process, as can be seen immediately from the characteristic polynomial. The differential equations, however, remain strictly well posed, since the time dependent operator remains strictly bounded. It is therefore necessary to add some additional "damping", usually in the form of artificial viscosity, to the system of Eqs 113.

From a numerical point of view (optimisation), it would be desirable to have a system of the form

$$\bar{w}_t + Aw_x + Bw_y = 0 \tag{116a}$$

$$w_t + \lambda^2(A\bar{w}_x + B\bar{w}_y) + \frac{1}{\tau}(w - \bar{w}) = 0^{\times} \tag{116b}$$

which would allow an implicit discretisation of Eq. 116b, which are again relaxation equations, if $\lambda^2 > 1$ with the same conditions as for the system 113.

However, at the steady state we have in general $w \neq \bar{w}$, a situation which appeared already earlier (Cf. Eq.101) for a simpler problem, where additional boundary

---

$^{\times}$ It is equally acceptable, to drop the last term in the relaxation function $(w - \bar{w})/\tau$, leading simply to w/τ.

conditions had to be imposed. We therefore do not consider this scheme further.

In order to conclude with second order relaxation methods, we consider a scheme, which requires a pre-differentiation of the steady state equations 106. Using

$$\ell^2(w) = \{A \frac{\partial}{\partial x} + B \frac{\partial}{\partial y}\}(Aw_x + Bw_y)$$

the following relaxation process is obtained.

$$\bar{w}_t - \lambda\{A^2 w_{xx} + (AB + BA)w_{xy} + B^2 w_{yy}\} = 0 \qquad (117a)$$

$$w_t + \frac{1}{\tau}(w - \bar{w}) = 0 \qquad (117b)$$

provided that the conditions are met

$$0 < \tau < \infty;\ \lambda > 0;\ \mu_p \neq 0 \text{ for } k_j \neq 0;\ j = 1,2;\ p = 1,2, \ldots m.$$

The solution of the above system requires additional boundary conditions, which are given by $\ell(w) = 0$ on the boundaries. Again we find that additional dissipation is necessary, if $\ell(w)$ is hyperbolic.

Since for a steady hyperbolic problem one of the space co-ordinates can always be interpreted as a time like variable, it appears physically and mathematically not to be justified to introduce a superfluous independent time variable. In consequence, we would employ a time dependent relaxation process only in regions where $\ell(w)$ is elliptic and use another space marching method in regions where $\ell(w)$ is hyperbolic. This is perfectly acceptable, if the boundaries between the different domains are known a priori. However, in transonic flows, for example, these boundaries are a part of the solution and the switch from one method to the other one leads usually to extremely complicated logical structures of the computer program. It is this (technical) reason which motivates the search for a universal method.

As already pointed out, additional dissipation is required, if the operator $\ell(w)$ is hyperbolic. This is accomplished introducing some artificial viscosity[×], of which we consider here only a simple linear model to demonstrate the effect.

The relaxation equations 113 then become

$$\bar{w}_t + Aw_x + Bw_y - \varepsilon\Delta w = 0 \qquad (118a)$$

$$w_t + \lambda(Aw_x + Bw_y) + \frac{1}{\tau}(w - \bar{w}) = 0 \qquad (118b)$$

where $\varepsilon > 0$ is a (usually) small scalar and where Δ represents the Laplace operator. The characteristic polynomial for the above time dependent equations

$$\tau\sigma^2 + (1 + i\tau\lambda\mu_p)\sigma + i\mu_p + \varepsilon(k_1^2 + k_2^2) = 0 \qquad (p = 1,2, \ldots m) \qquad (119)$$

now has only roots with negative real parts if

$$0 < \tau < \infty,\ \lambda > 1,\ \varepsilon > 0, \qquad (120)$$

× Originally, von Neumann and Richtmyer (1950) added artificial viscosity to certain hyperbolic schemes in order to capture shocks properly.

independent of the eigenvalues μ_p. Although ε may be a small quantity, inevitably we have introduced a small error[x] since the steady state solution of the system 118 is not the solution of the problem $\ell(w) = 0$. All boundary conditions remain unchanged, in order to avoid a singular perturbation problem for vanishing ε.

The second order relaxation methods, so far discussed, are not completely convincing since the optimisation problem for the finite difference analogue of the system 118 cannot be solved satisfactorily.

We now consider two third order methods, of which the first one is based on a third order relaxation operator to solve the Laplace equation. In connection with the interpretation of the SOR process (Eq.83), we considered a relaxation equation of the form

$$\tau\frac{\partial}{\partial t}\{\phi_{tt} - \lambda^2\Delta\phi\} + \phi_{tt} - \Delta\phi = 0 \tag{121}$$

where τ ($\tau > 0$, finite) is the relaxation time and $\lambda(\lambda > 1)$ a ratio of two different speeds of sound, if ϕ is interpreted as the perturbation potential for acoustic waves.

Defining

$$q = -\phi_t;\ \rho_t = -\Delta\phi;\ u = \phi_x;\ v = \phi_y \tag{122}$$

Eq.121 can be written as a system of first order equations

$$\begin{aligned} &\rho_t + u_x + v_y = 0 \\ &u_t + q_x = 0 \\ &v_t + q_y = 0 \\ &q_t + \lambda^2(u_x + v_y) + \frac{1}{\tau}(q - \rho) = 0 \end{aligned} \tag{123}$$

This is now a fourth order equation, where one eigenvalue is identical zero, similar to the system 109, expressing the fact

$$\frac{\partial}{\partial t}(-v_x + u_y) = 0$$

or, physically, that the density (ρ) and pressure (q) fluctuations are independent of the vorticity field. Again we have a singular hyperbolic system. Considering now a one-dimensional version of Eq.123, we may write

$$\begin{aligned} &\rho_t + u_x = f(x) \\ &u_t + q_x = 0 \\ &q_t + \lambda^2 u_x + \frac{1}{\tau}(q - \rho) = \lambda^2 f(x) \end{aligned} \tag{124}$$

where $f(x)$ represents a "forcing function" being introduced in order to avoid a constant steady state solution for u. The main part of the last set of equations may be written in vector form

---

[x] A physical relaxation process, described by non-equilibrium thermodynamics has a similar effect.

where $w_t + Aw_x + \ldots = 0$ (125)

$$w = \begin{pmatrix} \rho \\ u \\ q \end{pmatrix} \; ; \quad A = \begin{pmatrix} 0 & 1 & 0 \\ 0 & 0 & 1 \\ 0 & \lambda^2 & 0 \end{pmatrix}$$

leading to the conclusion that one eigenvalue of A is zero, hence we have again a singular hyperbolic problem. These examples clearly demonstrate that singular time dependent hyperbolic equations are necessarily occurring if higher order relaxation operators are converted into systems of first order (The eigenvalue structure remains essentially unchanged).

The generalisation of this idea for a system of first order equations does not pose any problems, leading to the general time dependent relaxation process (three step procedure)

$$\bar{w}_t + Aw_x + Bw_y = 0$$

$$\hat{w}_t + A\bar{w}_x + B\bar{w}_y = 0 \qquad (126)$$

$$w_t + \lambda^2 A\bar{w}_x + \lambda^2 B\bar{w}_y + \frac{1}{\tau}(w - \hat{w}) = 0$$

with the additional boundary conditions $\bar{w} = \hat{w} = w$, independent of the time. The characteristic polynomial for the above system reads

$$\tau\sigma^3 + \sigma^2 + \tau\lambda^2\mu_p^2\sigma + \mu_p^2 = 0 \qquad p = 1,2, \ldots m \qquad (127)$$

so that the system Eq.126 represents a relaxation process, if

$0 < \tau < \infty \quad \lambda^2 > 1$; $\mu_p \neq 0$ for $k_j \neq 0$; $j = 1,2$; $p = 1,2, \ldots m$.

Again we find that artificial viscosity is needed, if one or some of the eigenvalues μ_p are zero for non vanishing wavenumbers (hyperbolic steady state operator).
Using the simplest possible model to introduce artificial viscosity, the system Eq.126 becomes

$$\bar{w}_t + Aw_x + Bw_y - \varepsilon_1\Delta\bar{w} = 0$$

$$\hat{w}_t + A\bar{w}_x + B\bar{w}_y - \varepsilon_2\Delta\hat{w} = 0 \qquad (128)$$

$$w_t + \lambda^2 A\bar{w}_x + \lambda^2 B\bar{w}_y + \frac{1}{\tau}(w - \hat{w}) = 0$$

where ε_1, ε_2 are small positive scalar quantities (constants here), Δ being again the Laplace operator.

The following characteristic polynomial is now obtained

$$A_3\sigma^3 + A_2\sigma^2 + A_1\sigma^2 + A_0 = 0 \qquad (129)$$

with coefficients ($k^2 \equiv k_1^2 + k_2^2$)

$$A_3 = \tau \; ; \; A_2 = 1 + (\varepsilon_1 + \varepsilon_2)k^2$$

$$A_1 = \tau\lambda^2\mu_p^2 + (\varepsilon_1 + \varepsilon_2)k^2 + \tau\varepsilon_1\varepsilon_2 k^4$$

$$A_0 = \mu_p^2(1 + \tau\lambda^2\varepsilon_2 k^2) + \varepsilon_1\varepsilon_2 k^4$$

so that a relaxation equation for the system (128) is obtained independent of the eigenvalues μ_p, if the following conditions are met.

$0 < \tau < \infty$; $\lambda^2 > 1$; $\varepsilon_1, \varepsilon_2 > 0$.

The basic system Eq. 126 has the important advantage , compared with the second order relaxation method, that the last equation of Eq.126 can be integrated numerically implicit, thus allowing to select arbitrary values of the relaxation time for the purpose of optimisation. The storage requirements are heavier, however.

One might ask whether continuous time dependent relaxation equations can be developed which employ only one scalar additional relaxation equation. This is indeed possible, of which an example will be given later treating the compressible Euler equations.

2.7 Difference methods for systems of relaxation equations

The relaxation methods presented in the last chapter (disregarding the influence of the artificial viscosity) are essentially hyperbolic time dependent first order systems, for which numerous numerical methods exist; of which we mentioned the Lax (Eq.85) and the Lax-Wendroff (Eq.12) methods. Further methods may be found in the text book of Richtmyer and Morton (1967). One may be led to think therefore that these methods are equally useful to integrate the relaxation equations. This is, however, not the case, as will be seen in what follows.

For simplicity, we consider the model problem which was derived from the third order relaxation operator to integrate the Laplace equation. These time dependent relaxation equations (Eq.124) are written again for convenience

$$\begin{aligned} \rho_t + u_x &= f(x) \\ u_t + q_x &= 0 \\ q_t + \lambda^2 u_x + \frac{1}{\tau}(q - \rho) &= \lambda^2 f(x), \end{aligned} \qquad (124)$$

where $f(x)$ represents the forcing function. We want to solve this problem in a strip $B = \{x,t \mid 0 \leq x \leq 1;\ t \geq 0\}$ with initial and periodic boundary conditions. As forcing function we may use for simplicity $f(x) = \sin 2\pi x$.
Employing the finite difference notations, already earlier introduced, we want to solve the above problem with the simple Lax method (the Lax-Wendroff method gives similar results) which is written as

$$\begin{aligned} \rho_m^{k+1} &= \frac{1}{2} S_x \rho_m^k - \frac{1}{2} r\delta_x u_m^k + \Delta t f(x_m) \\ u_m^{k+1} &= \frac{1}{2} S_x u_m^k - \frac{1}{2} r\delta_x q_m^k \\ q_m^{k+1} &= \frac{1}{2} S_x q_m^k - \frac{1}{2}\lambda^2 r\delta_x u_m^k - s(q_m^k - \rho_m^k) + \Delta t\lambda^2 f(x_m) \end{aligned} \qquad (130)$$

for $m = 1,2, \ldots M-1$ and where $r = \Delta t/h$ is the step parameter and $s = \Delta t/\tau$ the relaxation coefficient. Since the errors between the transient and the corresponding steady state solutions satisfy the homogeneous problem, a typical Fourier mode may be considered for each solution.

$$\{\rho_m^k,\ u_m^k,\ q_m^k\} \sim \{\rho_0(k_1),\ u_0(k_1),\ q_0(k_1)\}\ g^k \exp(ik_1hm) \tag{131}$$

leading to the characteristic polynomial ($|k_1h| \leq \pi$)

$$\eta^3 + s\eta^2 + \lambda^2 r^2 \sin^2 k_1h\ \eta + sr^2 \sin^2 k_1h = 0 \tag{132}$$

where η is defined as $\eta \equiv g - \cos k_1h$. Without further analysis it is easily seen that the following particular mode $k_1h = \pi$ (2-h wave) yields the following solutions of Eq.127.

$$\eta_1 = 0; \quad \eta_{2,3} = -s$$

and hence the eigenvalues of the transformed step operator of the iteration

$$|g_1| = 1 \quad |g_{2,3}| = 1 + s = 1 + 0(\Delta t) \quad \text{for fixed } \tau.$$

These are perfectly acceptable results from the point of numerical stability in the Lax-Richtmyer sense, since the step operator remains bounded for a fixed number of iterations (time steps). However, according to our definition of a discrete relaxation scheme, such an error growth cannot be permitted. Indeed, the contraction property of the step operator is not established, at least not for the 2-h waves. In an actually computed case, the following occurred. The iteration converges correct for a certain (rather small) number of iterations, then levels off and finally, if the calculation proceeds, the solution is swamped completely. A similar situation arises, if the Lax-Wendroff method would have been employed.

If the corresponding 2-D case (Eq.123) would have been treated with the Lax method, the results are useless immediately since the discrete analogue of the Lagrange condition (Eq.112) is violated.

We therefore have to use different methods, which turn out to be even simpler than the preceding ones.

Since time accuracy is of less ocncern to us, we have used, throughout the following, two level explicit methods for time dependent relaxation equations, that is

$$\begin{aligned}
\rho_m^{k+1} &= \rho_m^k - \frac{r}{2}\,\delta_x u_m^k + \Delta t\ f(x_m) \\
u_m^{k+1} &= u_m^k - \frac{r}{2}\,\delta_x q_m^k \qquad m = 1,2,\ \ldots\ M-1 \\
q_m^{k+1} &= q_m^k - \frac{1}{2}\lambda^2 r\ \delta_x u_m^{k+1} - s(q_m^{k+1} - \rho_m^{k+1}) + \Delta t\ \lambda^2\ f(x_m)
\end{aligned} \tag{134}$$

which is a consistent second order space and first order time accurate approximation, r being again the step parameter, s the relaxation coefficient.

There are two interesting points about this scheme. First we note that the above method applied to the simplest single first order wave equation is unconditionally unstable, whereas Eq. 134 is perfectly stable. The second remark pertains to the last equation of Eq. 134, which is written as an implicit approximation although the calculation nevertheless is carried out explicitely. This turns out to be important for the optimisation.

The characteristic polynomial for this scheme, employing the same notations as before (Cf Eq. 131), reads

$$(1 + s)\eta^3 - (s + \lambda^2 r^2 \sin^2 k_1 h)\eta^2 + (s + \lambda^2) r^2 \sin^2 k_1 h\, \eta - s\, r^2 \sin^2 k_1 h = 0 \qquad (135)$$

for wavenumbers $|k_1 h| \leq \pi$ and where the contraction factor g is simply related to η by $g = 1 - \eta$. It is easily seen that for the 2-h waves ($k_1 h = \pi$), the following solutions for g are obtained :

$$g_{1,2} = 1;\ g_3 = 1 - \frac{s}{1 + s}$$

which indicate that the contraction property is not established for these waves. In contrast, however, to the Lax method for example, the amplitudes of these waves will not be amplified, how many iterations are carried out (linear case).

In order to find the bounds for the various parameters of the characteristic polynomial, such that $|g_\nu| < 1$, $\nu = 1,2,3$ for all $0 < k_1 h \leq \pi$, we map the interior of the unite circle onto the left half z-plane with the transformation $\eta = -2z/(1 - z)$, leading to the new third order polynomial

$$A_3 z^3 + A_2 z^2 + A_1 z + A_0 = 0 \qquad (135a)$$

where the coefficients A_ν, $\nu = 0, .., 3$ are given below :

$$\begin{aligned} A_3 &= 8 + 4s - (2\lambda^2 - s)\, r^2 \sin^2 k_1 h \\ A_2 &= s(4 - r^2 \sin^2 k_1 h) \\ A_1 &= (2\lambda^2 - s) r^2 \sin^2 k_1 h \\ A_0 &= s\, r^2 \sin^2 k_1 h \ . \end{aligned} \qquad (136)$$

The Routh-Hurwitz conditions (Eq.35), applied for the polynomial 135a, therefore yield the conditions

$$(i)\ \lambda > 1;\ (ii)\ 0 < s \leq \lambda^2 - 1;\ (iii)\ \lambda r \leq 2 \qquad (137)$$

for that all contraction factors $|g_\nu|$ ($\nu = 1,2,3$), the eigenvalues of the step operator, remain bounded by less than one for all wavenumbers with the already mentioned exception of $|g| = 1$ for $k_1 h = \pi$, only.

Condition (i) is essentially the same as for the original time dependent problem, while the second one imposes a limit on the relaxation factor, if small values of λ are to be used. In practice, λ^2 is of the order of ten, thus s can be varied sufficiently. The last condition (iii) imposes a limit on $\Delta t \leq 2h/\lambda$, as one would expect from an explicit scheme (CFL condition).

Although the time dependent equations (Eqs 124) are certainly relaxation equations, the numerical analogue, unfortunately, is only a weak relaxation process (the conditions 137 are assumed to be fulfilled), since the contraction property is not established for the 2-h waves. It appears to be an interesting question, whether numerical methods can be found, without introducing artificial viscosity, to improve this situation.

From a practical point of view, linear elliptic problems with constant coefficients and with sufficiently smooth initial and boundary data can be solved without adding artificial viscosity, as may be seen from the first figure.

In Fig.1, we have plotted the computed convergence "history" versus the number of iterations of a non-optimised case using the maximal allowable time step for a mesh size of h = 0.05. The error $|\varepsilon_{max}|$ is defined as the error of two successive iterations ($1 \leq m \leq M-1$)

$$|\varepsilon_{max}|^{\times} = \max_m|\rho_m^{k+1} - \rho_m^k| + \max_m|u_m^{k+1} - u_m^k| + \max_m|q_m^{k+1} - q_m^k| \ .$$

From this figure, it is seen that the errors are reduced by several orders of magnitude until the amplitudes of the 2-h waves becomes dominant. Further iterations are therefore useless, although no amplification occurs.

These experimental results are in perfect agreement with our theoretical conclusions from the characteristic polynomial.

Before passing on to the problem of optimisation, we consider the general third order time dependent relaxation process as given by the Eqs (126). In order to have a concrete model in mind, we consider the following generalised linear steady state equations

$$\begin{aligned} \gamma u_x + v_y &= 0 \\ - v_x + u_y &= 0 \end{aligned} \qquad (138)$$

where γ is a constant, which may be positive or negative. For $\gamma = 1$, we recover the elliptic Cauchy-Riemann equations, whereas for $\gamma < 0$, we have a hyperbolic system. The time dependent hyperbolic equations[xx] for the above system may be written as

$$w_t + Aw_x + Bw_y = 0$$

where

$$w = \begin{pmatrix} u \\ v \end{pmatrix}, \qquad A = \begin{pmatrix} \gamma & 0 \\ 0 & -1 \end{pmatrix} ; \qquad B = \begin{pmatrix} 0 & 1 \\ 1 & 0 \end{pmatrix} . \qquad (138a)$$

The discretised version of the general time dependent relaxation (Eq.126) then reads, employing the same method as for the 1-D case, (the subscripts m, n, indicating the spatial co-ordinates, have been dropped).

$$\begin{aligned} \bar{w}^{k+1} &= \bar{w}^k - \frac{1}{2} r \ (A\delta_x w^k + B\delta_y w^k) \\ \hat{w}^{k+1} &= \hat{w}^k - \frac{1}{2} r \ (A\delta_x \bar{w}^k + B\delta_y \bar{w}^k) \\ w^{k+1} &= \frac{1}{1+s} w^k + \frac{s}{1+s} \hat{w}^{k+1} - \frac{1}{2} \frac{r\lambda^2}{1+s} (A\delta_x \bar{w}^{k+1} + B\delta_y \bar{w}^{k+1}) \ . \end{aligned} \qquad (139)$$

The characteristic polynomial for this set of equations is obtained as a third order polynomial for each eigenvalue μ_q

$$(1+s)\eta^3 + (s + \lambda^2\mu_q^2)\eta^2 + (s + \lambda^2)\mu_q^2 \eta + s\mu_q^2 = 0,$$

where the contraction factor g is related to η by $g = 1 + \eta$, and where the μ_q are the eigenvalues of the matrix

---

[x] It would have been more consistent to employ the L_2 norm.

[xx] They remain hyperbolic, for arbitrary γ.

$$Q(k_1,k_2) = r \sin k_1 h\, A + r \sin k_2 h\, B \qquad (141)$$

in which k_1, k_2 are the wavenumbers foe each spatial co-ordinate. In order that the eigenvalues of the step operator, the solutions of the characteristic polynomial for the contraction factors g, are bounded by less than one for all wavenumbers $k_j \neq 0$ with $\max_j |k_j h| \leq \pi$, the following conditions must be met.

$\lambda^2 > 1$; $0 < s \leq \lambda^2 - 1$; $\max_{q,k_j} |\mu_q| \leq 2/\lambda$ together with $\mu_q \neq 0$ for $k_j \neq 0$. The first three conditions, of which the last one is the CFL condition, are easy to satisfy by a suitable choice of λ, s and r. The last condition, however, causes a problem, if for certain k_j the eigenvalues of the matrix Q are zero, since some of the contraction factors have the value one ($\eta = 0$). The remedy then is to add artificial viscosity, as indicated in the equations (128).

For the example (Eq.138a), the eigenvalues μ_q are given by

$$(\mu_q + r \sin k_1 h)(\mu_q - \gamma r \sin k_1 h) - r^2 \sin^2 k_2 h = 0. \qquad (q = 1,2)$$

For the elliptic steady state problem (subsonic flows), $\gamma = 1$, we obtain therefore

$\mu_q^2 = r^2 (\sin^2 k_1 h + \sin^2 k_2 h)$ demonstrating that only the 2-h waves lead to $\mu_q = 0$, while for the steady state hyperbolic problem (for example with $\gamma = -1$), $\mu_q = -r \sin k_1 h \pm r \sin k_2 h$. The locus of $\sin k_1 h \pm \sin k_2 h = 0$ therefore always leads to $\mu_q = 0$. This situation confirms that time dependent relaxation methods, if they are being employed also for steady state hyperbolic problems (supersonic flows) necessarily demand for artificial viscosity as it should be for a true physical relaxation process. Furthermore, we note that the necessity to add artificial viscosity is not a consequence of handling properly possible existing discontinuities.

Coming back to the problem of optimisation, we see that the general 2-D problem leads essentially (subsonic flows) to the same characteristic polynomial, as for our simple 1-D problem (Eq.129). We therefore treat this case further.

The contraction factors g with $g = 1 - \eta$ are solutions of the characteristic polynomial (Eq.135). The optimisation problem essentially consists of minimising the maximal absolute vlaue of the contraction factors for those wavenumbers, for which the amplitudes of these errors are greatest. In addition , we select the largest possible time increment Δt.

The solutions of the characteristic polynomial can be obtained analytically, leading to rather complicated algebraic expressions, which we therefore do not want to present here.

In Fig.2, however, we have plotted these results for a special case where the forcing function f(x) was given by $f(x) = \sin 2\pi x$ for the problem Eq.124 to be solved in a strip $B = \{x,t | 0 \leq x \leq 1,\ t \geq 0\}$. From the CFL condition, Δt_{max} was selected as $2h/\lambda$ (condition (iii) of Eq. 137), h being the meshsize ($h = 0.05$). The fundamental wavenumber for this problem is, of course, simply $k_1 = 2\pi$.

For each $\lambda > 1$, there exists an optimal value of the relaxation coefficient s, s_{opt}, such that $|g|_{max}$ is minimised. Selecting λ therefore also optimal, an absolute optimum for $|g|_{max}$ is obtained.

It is interesting to see that the optimum relaxation factor can vary between zero and two, depending on the choice of λ. For sufficient large values of λ, $|g|_{max}$ as

a function of s behaves essentially the same way as the simple SOR process.

Fig.3 summarises these results where λ and the corresponding minimum of $|g|_{max}$ are plotted versus the (optimal) relaxation factor.

From a general point of view, it is more important to know, how $|g|$ depends on the mesh size h for $h \to 0$, keeping $r = \Delta t/h$ fixed with Δt_{max}.

Putting therefore $\eta = \sigma\varepsilon$ and $s = \omega\varepsilon$, where ε is given by $\varepsilon = \kappa|\sin k_1 h|$, together with $r = \kappa/\lambda$, $0 < \kappa \leq 2$, the characteristic polynomial (Eq.135) may be written as

$$(1 + \omega\varepsilon)\sigma^3\varepsilon^3 - (\omega\varepsilon + \varepsilon^2)\sigma^2\varepsilon^2 + (\omega\varepsilon + \lambda^2)\frac{\varepsilon^2}{\lambda^2}\sigma\varepsilon - \frac{\omega}{\lambda^2}\varepsilon^3 = 0.$$

Since $\varepsilon \sim O(h)$, retaining only the leading terms $O(\varepsilon^3)$, we obtain the polynomial for σ as a function of ω, independent of h.

$$F(\sigma) \equiv \sigma^3 - \omega\sigma^2 + \sigma - \omega/\lambda^2 = 0 \tag{143}$$

The contraction factors therefore can be expressed as

$g = 1 - \sigma\kappa|\sin k_1 h|$ together with $s = \omega\kappa|\sin k_1 h|$ or simply, taking $\kappa = 2$ (the limiting value), $k_1 = 2\pi$ (for our case)

$$g \sim 1 - 4\pi\sigma h; \quad s \sim 4\pi\omega h \tag{144}$$

for sufficiently small h.

Suppose that for certain finite values of ω and λ the roots of the polynomial are real, then the important conclusion follows that the reciprocal rate of convergence of this relaxation method is given by

$$RR = \frac{1}{4\pi\sigma_{min}} h^{-1} \tag{145}$$

This result indicates that the third order relaxation methods for systems of (elliptic) first order equations converge three orders of magnitude faster than the Lax-Wendroff methods previously used (periodicity boundary conditions).

It is of interest to study the properties of the polynomial for σ (Eq.143) for a moment. Again we avoid to write down the rather complicated analytical expressions for the solutions for σ, of which one is always real, whereas the other two are conjugate complex, in general.

In Fig. 4, 5 and 6, these results are plotted for three different values of $\lambda^2(5,9,12)$, where real and imaginary parts are separately shown. It is evident that the best values (mini-max) for σ are obtained for $\lambda = 3$ (Fig.5) where the imaginary part becomes zero for the first time with increasing λ and ω. This condition is met if the discriminant d of the polynomial $F(\sigma) = 0$ (Eq.143) vanishes. Since $d \equiv q^2 + p^3$ with $3p \equiv 1 - \frac{1}{3}\omega^2$ and $2q \equiv -\frac{2}{27}\omega^3 + \frac{1}{3}\omega - \frac{\omega}{\lambda^2}$, we obtain the numbers $\omega = \sqrt{3}$; $\sigma_{1,2,3} = \frac{1}{3}\sqrt{3}$; $\lambda = 3$

and finally

$$RR = \frac{3}{4\pi\sqrt{3}} h^{-1}; \quad s_{opt} \sim 4\pi\sqrt{3}\, h \tag{146}$$

The convergence history for three different values of λ with optimised relaxation coefficients are depicted in Fig.7 for a fixed meshsize h (h = 0.05). The number of iterations is significantly reduced for the same convergence level taking $\lambda = 3$ and $s_{opt} = 1.08$. Furthermore, near the absolute optimum one observed that the errors $|\varepsilon|_{max}$ (defined as previously) have the tendency to increase cyclic before they decrease again. This phenomenon, is related to the occurrence of multiple equal solutions of the characteristic polynomial.

Similar results have been obtained for 2-D problems, employing the general third order relaxation process Eq.139.

We emphasise again that the ideas we have used to optimise the preceding relaxation methods are applicable only for systems of which the stationary problem is essentially elliptic. It is not yet clarified, how this problem can be solved (assuming that the contraction property of the step operator is established), if the stationary problem (time independent) is hyperbolic. Physical intuition suggests that the question is probably irrelevant.

Finally, we consider the second order relaxation process (Cf. Eq. 113) which may be discretized as (the subscripts m, n are not written)

$$\begin{aligned} \bar{w}^{k+1} &= \bar{w}^{k} - \frac{1}{2} r A\delta_x w^{k} - \frac{1}{2} r B\delta_y w^{k} \\ w^{k+1} &= \frac{1}{1+s}(w^{k} - \lambda \bar{w}^{k}) + \frac{\lambda + s}{1+s} \bar{w}^{k+1} \end{aligned} \tag{147}$$

the characteristic polynomial for these equations is given by ($\lambda > 0$).

$$(1+s)\eta^2 + (s + i(\lambda + s)\mu_q)\eta + is\mu_q = 0, \tag{148}$$

where η is related to the contraction factor g by $g = 1 + \eta$, and the μ_q are the eigenvalues of the matrix Q given by equation (141).

One shows that the eigenvalues g of the step operator are satisfying the contraction property, if the following conditions are met.

$$0 < s < 1;\ \lambda^2 > \frac{1}{2}\frac{s^2}{1-s}\ ;\ \max_{k_j q} |\mu_q|^2 \leq 2\frac{s}{\lambda}\frac{2+s}{2\lambda + s} \tag{149}$$

and $\mu_q \neq 0$ for $k_j \neq 0$.

We do not consider the problem of optimisation.

All the methods for systems of first order partial differential equations, we have presented so far, may be easily generalised to treat conservation equations of the general (non-linear form)

$$\partial_j F_j(w) = 0 \qquad j = 1,2,3, \tag{150}$$

where $\partial_j = \frac{\partial}{\partial x_j}$ and the F_j are vector valued functions, expressing the conservation of mass, momentum and energy. Since theoretical conclusions for these (in general non-linear) problems are extremely difficult to obtain, if time dependent relaxation methods are considered, numerical experiments are required. Our practical experience indicates, that if the continuous or numerical relaxation method is not established for the linearised problem, there is little hope that the method will work in a non-linear case.

3. TIME DEPENDENT RELAXATION METHODS FOR FLOW PROBLEMS

In this chapter we mainly consider two classes of problems, namely the compressible Euler equations and the incompressible Navier-Stokes equations with the primary interest to develop systems of first order continuous time dependent relaxation equations.

3.1 The compressible Euler equations

The general and natural hyperbolic time dependent equations, expressing the conservation of mass, momentum and energy, are given as

$$\frac{d\rho}{dt} + \rho \partial_j c_j = 0 \tag{151}$$

$$\rho \frac{dc_i}{dt} + \partial_i p = 0 \tag{152}$$

$$\rho \frac{d\varepsilon}{dt} - \frac{p}{\rho} \frac{d\rho}{dt} = 0 \tag{153}$$

where ρ is the density, p the pressure, ε the internal energy and c_i the vector of velocities with its components $c_i = (u,v,w)$. The material derivative $\frac{d}{dt}$ is defined as

$$\frac{d}{dt} = \frac{\partial}{\partial t} + c_j \frac{\partial}{\partial x_j}$$

where the summation of j is extended from j = 1 to j = 3. The above system is completed by two equations of state, the caloric and thermal one, which for a perfect gas read

$$\varepsilon = c_v T; \qquad p = (\gamma - 1)\rho\varepsilon \tag{154}$$

where T is the absolute temperature, c_v the specific heat (constant volume), and γ the ratio of the specific heats. The energy equation (153) can be replaced by an equation for the entropy $\frac{ds}{dt} = 0$. Since the entropy s is not a conservation variable, Eq.(153) is retained.

The basic system can be casted into a form which expresses the conservation of the different fluxes directly

$$\partial_t \rho + \partial_j (\rho c_j) = 0 \tag{151a}$$

$$\partial_t (\rho c_i) + \partial_j (p\delta_{ij} + \rho c_i c_j) = 0 \tag{152a}$$

$$\partial_t e + \partial_j \left[c_j (e + p)\right] = 0 \tag{153a}$$

where e denotes the "total" energy defined as $e = \rho\varepsilon + k$, where k is the kinetic energy $k = \frac{1}{2}\rho c_i^2$ of the flow. The quantity δ_{ij} denotes the usual δ tensor. The pressure becomes $p = (\gamma - 1)(e + k)$.

Finally, an equation for the kinetic energy can be derived,

$$\partial_t k + c_j \partial_j k + c_j \partial_j p = 0 \tag{154}$$

which indicates that this quantity is not a conservation variable.

As already mentioned, the time dependent Euler equations are hyperbolic for all speed ranges. If shocks or other discontinuities are excluded, the entropy remains

a constant for each streamline, hence the system has no dissipation. In consequence, a method which solves the initial value problem, would never converge to a steady state.

Of course, the Euler equations are representing not the "reality", since the influence of viscosity and heat conduction is not taken into account, which are representing typically dissipative effects.

Our problem to find an initial value problem which introduces dissipation, such that the steady state is obtained asymptotically for large times, therefore cannot be solved re-introducing viscosity or heat conduction terms, since the steady state equations are necessarily altered. However, as the preceding chapter showed, the concept of relaxation provides a mechanism which introduces during the transient phase dissipation without altering the asymptotic steady state.

We consider first compressible potential flows, which are governed by the following equations

$$\frac{d\rho}{dt} + \rho \partial_j c_j = 0 \tag{151}$$

$$\rho \frac{dc_i}{dt} + \partial_i p = 0 \tag{152}$$

together with $p = A\rho^{\gamma}$ ($A > 0$ const.)(isentropic flows) and where the following relation for the (local) speed of sound a may be used

$$d\left(\frac{a^2}{\gamma - 1}\right) = a^2 \frac{d\rho}{\rho} \quad . \tag{156}$$

Assuming that a scalar potential ϕ exists, and that $c_j = \partial_j \phi$ for $j = 1,2,3$, the momentum equation yields the generalised Bernoulli equation ($\tilde{k}$ being defined as $\frac{1}{2} c_i^2$!)

$$\partial_t \phi + \tilde{k} + \frac{a^2}{\gamma - 1} = f(t) \tag{157}$$

where the right hand side of this equation is only a function of time. We assume, however, this function to be a constant.

Combining the Bernoulli with the continuity equation,finally yields the basic equation of (classical) gas dynamics, expressed as

$$\phi_{tt} + 2c_j \partial_j \phi_t + c_j \partial_j \tilde{k} - a^2 \partial_j \partial_j \phi = 0 \quad . \tag{158}$$

The time dependent operator of this equation is now changed into a relaxation operator, such that a relaxation equation results. This relaxation equation reads

$$\phi_{tt} + \frac{1}{\tau} \phi_t + 2 c_j \partial_j \phi_t + c_j \partial_j \tilde{k} - a^2 \partial_j \partial_j \phi = 0 \tag{159}$$

where τ denotes the relaxation time. We showed already earlier that this artificial time dependent equation is indeed a relaxation equation for Mach numbers less than one ($0 < \tau < \infty$)(linearised case). It is evident that this relaxation equation can be used directly for numerical purposes (relaxation schemes).

Since we are interested to deal with first order systems, we express Eq.159 as follows.

Defining $q = -\frac{d\phi}{dt} = -(\partial_t\phi + c_j\partial_j\phi)$ (160)

we obtain after some manipulations the first order system.

$$\begin{aligned} &\partial_t c_i + \partial_i(2\tilde{k} + q) = 0 \\ &\partial_t q + a^2\partial_j c_j - c_j\partial_j\tilde{k} + \frac{1}{\tau}(2\tilde{k} + q) = 0 \end{aligned} \tag{161}$$

where the local speed of sound is expressed as

$$a^2 = a_\infty^2\left(1 + \frac{\gamma - 1}{2}M_\infty^2\right) + (\gamma - 1)(q + \tilde{k}) \tag{161a}$$

in which a_∞ and M_∞ are the velocity of sound and the Mach number at infinity (reference state), respectively. The first three equations of Eq.161 are expressing the fact that the flow is irrotational, while the second (scalar) one of Eq.161 contains essentially the residuals of the steady state problem we want to solve.

We write down the system for a two-dimensional case

$$\begin{aligned} &u_t + 2uu_x + 2vv_x + q_x = 0 \\ &v_t + 2uu_y + 2vv_y + q_y = 0 \\ &q_t + (a^2 - u^2)u_x - uv(v_x + u_y) + (a^2 - v^2)v_y + \frac{1}{\tau}(u^2 + v^2 + q) = 0 \end{aligned} \tag{162}$$

or expressed in vector form, with $w^T = \{u,v,q\}$

$$w_t + Aw_x + Bw_y + b = 0 \tag{163}$$

where the matrices are

$$A = \begin{pmatrix} 2u & 2v & 1 \\ 0 & 0 & 0 \\ a^2 - u^2 & -uv & 0 \end{pmatrix}; \qquad B = \begin{pmatrix} 0 & 0 & 0 \\ 2u & 2v & 1 \\ -vu & a^2 - v^2 & 0 \end{pmatrix}$$

and $b^T = (0,0,\frac{1}{\tau}(u^2 + v^2 + q))$. It is clear that the problem (163) therefore is again singular hyperbolic, the eigenvalues of the matrix $P = k_1A + k_2B$ with $-\infty < k_1,k_2 < \infty$ being

$$\mu_1 = 0; \quad \mu_{2,3} = uk_1 + vk_2 \pm a.$$

The system 161 is not completely in conservation form since the relaxation equation is not expressed as a divergence free equation. Apparently the system (Eq.161) is valid only for Mach numbers less than one. If the calculation is extended into supersonic domains ($2\tilde{k} > a^2$), then the relaxation function must vanish (which is accomplished by $\tau \to \infty$) and artificial viscosity is required, in order to obtain convergence. Since the flow is assumed to be irrotational, the viscosity terms require a specific form, of which we give a simple example. The complete system therefore becomes

$$\begin{aligned} &\partial_t c_i + \partial_i(2\tilde{k} + q) - \alpha\partial_i\partial_j c_j = 0 \\ &\partial_t q + a^2\partial_j c_j - c_j\partial_j\tilde{k} + \frac{1}{\tau}(2\tilde{k} + q) = 0 \quad \text{where } \alpha > 0 \text{ is a (usually small) scalar.} \end{aligned} \tag{164}$$

It is, of course, desirable not to be restricted to potential flows only. We therefore consider now the general Euler equations, for which relaxation methods (linearised forms) have been presented in the preceding chapter (Cf Eqs 116, 126 and the discussion pertaining to them).

For the second order relaxation process, the non-linear system may be written as

$$\begin{aligned} &\bar{w}_t + \partial_j F_j(w) - \alpha \partial_j \partial_j w = 0 \\ &\\ &w_t + \lambda \partial_j F_j(w) + \frac{1}{\tau}(w - \bar{w}) = 0 \end{aligned} \tag{165}$$

whereas for the third order relaxation process, one obtains

$$\begin{aligned} &\bar{w}_t + \partial_j F_j(w) - \alpha \partial_j \partial_j \bar{w} = 0 \\ &\\ &\hat{w}_t + \partial_j F_j(\bar{w}) - \alpha \partial_j \partial_j \hat{w} = 0 \\ &\\ &w_t + \lambda^2 \partial_j F_j(\bar{w}) + \frac{1}{\tau}(w - \hat{w}) = 0 \ . \end{aligned} \tag{166}$$

In either system, the vector w is represented as $w^T = \{\rho, \rho c_i, e\}$ and the vector valued functions $F_j(w)$ essentially are given by

$$F_j = \begin{pmatrix} \rho c_j \\ p\delta_{ij} + \rho c_i c_j \\ c_j(e + p) \end{pmatrix} \qquad (j = 1,2,3) \tag{167}$$

For completeness we have indicated the principle, how artificial viscosity may be included in these systems, if necessary ($\alpha > 0$).

The storage requirements for these methods are not negligible small and one therefore may ask whether relaxation methods can be developed which employ less equations. This is indeed possible, if a restriction on the Mach number is accepted.

We consider again the general system (Eqs 151a - 153a) in which the pressure is now replaced by a variable q, called the relaxation pressure, which should become the usual equilibrium pressure p (in the thermodynamic sense), if the steady state is reached. Since a new variable has been introduced, we need, of course, an additional time dependent equation which may be called the master equation for the relaxation process.

The time dependent relaxation equations for the Euler equations then may be written as (other forms are possible to derive).

$$\begin{aligned} &\partial_t \rho + \partial_j(\rho c_j) = 0 \\ &\\ &\partial_t(\rho c_i) + \partial_j(q\delta_{ij} + \rho c_i c_j) = 0 \\ &\\ &\partial_t e + \partial_j\left[e_j(e + q)\right] = 0 \\ &\\ &\partial_t q - \lambda^2 \partial_t p - 2(\lambda^2 - 1)\partial_t k + \frac{1}{\tau}(q - p) = 0 \end{aligned} \tag{168}$$

where τ is the positive relaxation time and λ^2 a positive parameter. There are several remarks to be made about this system. The relaxation pressure q at the steady state (assuming that it exists) equals the equilibrium one. The steady state therefore is not altered. As a consequence the above system necessarily is singular hyperbolic, which implies that no additional characteristic directions (eigenvalues) have been introduced. For $\lambda^2 = 1$ the system is obviously decoupled and the relaxation pressure becomes a time dependent function of p. The time derivatives for the pressure p and the kinetic energy k of the master equation may be replaced by spatial derivatives, if the thermal equation of state is used (for a perfect gas, we have $p = (\gamma - 1)(e + k)$ and if the equation for the kinetic energy.

$$\partial_t k + c_j \partial_j k + c_j \partial_j q = 0 \tag{169}$$

is inserted. Finally we remark that the energy equation (total energy) may be dropped, if the equilibrium pressure is a function of the density alone (adiabatic flows).
In order to get a better understanding for the above relaxation equations, we consider a one-dimensional version, which may be written as ($k = \frac{\rho}{2} u^2$, $\frac{d}{dt} = \frac{\partial}{\partial t} + u \frac{\partial}{\partial x}$)

$$\frac{d\rho}{dt} + \rho u_x = 0 \qquad \text{mass} \tag{170a}$$

$$\rho \frac{du}{dt} + q_x = 0 \qquad \text{momentum} \tag{170b}$$

$$\rho \frac{d\varepsilon}{dt} - \frac{q}{\rho} \frac{d\rho}{dt} = 0 \qquad \text{energy} \tag{170c}$$

$$q_t - \lambda^2 p_t - 2(\lambda^2 - 1)k_t + \frac{1}{\tau}(q - p) = 0 \qquad \text{relaxation} \tag{170d}$$

together with an equation of state $p = (\gamma - 1)\rho\varepsilon$ (A forcing function has not been added, for convenience). The energy equation is rewritten, using the equation of state, hence

$$\frac{dp}{dt} - \frac{1}{\rho}\left[p + (\gamma - 1)q\right] \frac{d\rho}{dt} = 0 \ . \tag{171}$$

The above system is linearised around the steady state using the following representations (acoustic theory)

$$u = u_o + u'; \quad q = p_o + q'; \quad p = p_o + p'; \quad \rho = \rho_o + \rho' \tag{172}$$

where u_o, p_o, ρ_o are constant reference values at the steady state and $a_o^2 = \gamma p_o/\rho_o$ is the (adiabatic) speed of sound. Inserting these expressions into the system and dropping higher order terms of the perturbations, we finally obtain the linear system with constant coefficients where the primes have been omitted.

$$\begin{aligned}
&\frac{d\rho}{dt} + \rho_o u_x = 0 \\
&\rho_o \frac{du}{dt} + q_x = 0 \\
&\frac{dp}{dt} - a_o^2 \frac{d\rho}{dt} = 0 \\
&q_t - \lambda^2 p_t - 2(\lambda^2 - 1)(\rho_o u_o u_t + \tfrac{1}{2} u_o^2 \rho_t) + \frac{1}{\tau}(q - p) = 0
\end{aligned} \tag{173}$$

where the material derivative is given by $\frac{d}{dt} = \frac{\partial}{\partial t} + u_o \frac{\partial}{\partial x}$. Eliminating ρ, p, q successively from the system, a single partial differential equation is obtained for the velocity perturbations.

$$\tau \frac{\partial}{\partial t} \left[u_{tt} + 2\lambda^2 u_o u_{xt} - \lambda^2 (a_o^2 - u_o^2) u_{xx} \right] + u_{tt} + 2u_o u_{xt} - (a_o^2 - u_o^2) u_{xx} = 0 \qquad (174)$$

This is a third order hyperbolic relaxation equation (and therefore also the singular system 173) if we require

$$0 < \tau < \infty; \quad \lambda^2 > 1; \quad u_o^2 < a_o^2 \ . \qquad (175)$$

The 2-dimensional case, which is not presented here, introduces again an additional eigenvalue identical zero, but otherwise no further conditions. The occurrence of an additional zero eigenvalue expresses the fact

$$\frac{d}{dt} (- v_x + u_y) = 0$$

which implies that the flow particles maintain their vorticity. The relaxation equation 174 is representing travelling damped acoustic waves which propagate with the "relaxation speed of sound" $\lambda a_o > a_o$. The application of the relaxation equations (Eq.168) is restricted essentially to subsonic flows ($M < 1$). We remark that the discrete version of Eq.168, may well need some artificial viscosity. This aspect is not discussed here since only the continuous time dependent equations are of interest.

3.2 The incompressible Navier-Stokes equations

In order to conclude this chapter, we finally consider incompressible flows, in particular those which are governed by the full Navier-Stokes equations. Most of the previously published methods (see for example Wirz and Smolderen, 1973) are based on a formulation which involves essentially the vorticity and the stream function as dependent variables, thus eliminating the pressure in the original equations. There is, however, an increasing interest to solve these equations employing the original dependent variables.

The incompressible non-dimensional and natural time dependent Navier-Stokes equations may be written, following the notations earlier introduced for the Euler equations

$$\begin{aligned} &\partial_j c_j = 0 && \text{continuity} \\ &\frac{dc_i}{dt} + \partial_i p - \frac{1}{Re} \partial_j \partial_j c_i = 0 && \text{momentum} \end{aligned} \qquad (176)$$

where Re represents the Reynolds number. For $Re \to \infty$, the incompressible Euler equations are obtained. These time dependent equations are degenerated since the continuity equation contains no time derivative, which obviously complicates time dependent methods intended to integrate the above equations.

Chorin (1967) presented an idea for an artificial time dependent system, re-introducing a weakly compressible gas, (the method of artificial compressibility)

$$\begin{aligned} &\partial_t p + \delta \partial_j c_j = 0 \\ &\partial_t c_i + c_j \partial_j c_i + \partial_i p - \frac{1}{Re} \partial_j \partial_j c_i = 0 \end{aligned} \qquad (177)$$

where $\delta > 0$ is a constant parameter. One shows that this system is hyperbolic, if $Re \to \infty$ and equally that it is not a relaxation one. Thus we expect that a stable finite difference approximation for Eq. 177 for high Reynolds numbers converges extremely slow, if it converges at all. This fact is confirmed by the computations carried out by Chorin.

In order to accelerate the convergence of the artificial time dependent methods based on the system 177, we introduce a relaxation process, leading to the system

$$\frac{dc_i}{dt} + \partial_i q - \frac{1}{Re}\Delta c_i = 0$$

$$p_t + \delta \partial_j e_j = 0 \qquad (174)$$

$$q_t - \lambda^2 p_t - (\lambda^2 - 1)\tilde{k}_t + \frac{1}{\tau}(q - p) = 0$$

where $\tilde{k} = \frac{1}{2} c_i^2$ and q is the relaxation pressure, τ the relaxation time, λ^2 a positive constant parameter. For a linearised version of these equations (travelling acoustic waves) it is possible to show that indeed a relaxation equation follows, if $\delta > 0$, $\lambda^2 > 1$; $\tau \neq 0$, finite, for arbitrary Reynolds numbers. It is extremely difficult, if not impossible, to establish the contraction property of the time operator for general multi-dimensional flows. For modest Reynolds numbers, numerical computations may give some evidence.

Proceeding along these lines, a finite difference method has been developed to solve the above relaxation equations numerically. It appeared to be more convenient to employ a somewhat different continuous relaxation system, which may be written as

$$\frac{dc_i}{dt} + \partial_i(p + \tilde{g} - g) - \frac{1}{Re}\Delta c_i = 0$$

$$p_t + \delta \partial_j c_j = 0 \qquad (175)$$

$$g_t + \frac{1}{\tau}(g - \tilde{g}) = 0$$

where $\tilde{g}$ is defined as $\tilde{g} = (\lambda^2 - 1)(p + \tilde{k})$. The following 2-D test problem was selected (Couette flow with pressure gradient), of which the steady state is known analytically. Consider a parallel flow between two planes, of which the upper wall is moving in the streamwise direction (the x co-ordinate) with the constant velocity u = 1, the other being at rest. Then the streamwise velocity $\tilde{u}$ is essentially a polynom in the y co-ordinate, the pressure a linear function of the x co-ordinate, and, of course, $v \equiv 0$. The above time dependent relaxation equations then were solved in the domain

$$B = \{x,y,t \mid 0 \leq x,y \leq 1,\ t \geq 0\}$$

by an explicit, two level finite difference method employing only central difference operators and where the last two time dependent equations of the system 175 have been discretised implicitely.

It is evident that the numerical method is creating immediately a velocity component $v \neq 0$, which is therefore a measure for the error committed during the transient part of the solution.

In Fig.8, we have depicted a typical result of the convergence history for a Reynolds number of 100 (non-optimised, $\delta = 1$), versus the number of iterations, N. The top right corner shows the steady state of the flow configuration considered. The parameters are h, the meshsize (equal for both spatial co-ordinates), Δt the time increment, s the relaxation coefficient $\Delta t/\tau$. The errors, depicted in Fig.8, are defined as the maximum value over the entire domain B.

These results confirm that the above relaxation method converges to the correct steady state also for a non-linear case, which could be shown theoretically only for a linear system with constant coefficients, however. No attempts have been made to solve the problem of optimisation, however.

In conclusion we see that efficient time dependent relaxation methods may equally be developed for the incompressible Navier-Stokes equations employing the original dependent variables.

LITERATURE CITED

BURSTEIN S.Z. and MIRIN A. (1972) : "Time dependent calculations for transonic flow", Third International Conference on Numerical Methods in Fluid Dynamics, Springer, Paris.

CHORIN J.A. (1967) : "A numerical method for solving incompressible viscous flow problems", J. of Computational Physics 2, pp. 12-26.

COLLATZ L. (1964) : Funktionanalysis und Numerische Mathematik, Springer Verlag, Berlin, pp. 164-177.

CROCCO L. (1965) : "A suggestion for the numerical solution of the Navier-Stokes equations", AIAA J., Vol.3, No.10, pp. 1824-1832.

DUFORT E.C. and FRANKEL S.P. (1953) : "Stability conditions in the numerical treatment of parabolic differential equations", Math. Tables and other Aids to Computation, Vol.7, pp. 135-152.

FRANKEL S.P. (1950) : "Convergence rates of iterative treatments of partial differential equations", MTCA, Vol.4, p.65-75.

FOX L. (1948) : "A short account of relaxation methods", Quart. J. Mech. Appl. Math., Vol.1, pp. 253-280.

GARABEDIAN (1956) : "Estimation of the relaxation factor for small mesh size", Math. Tables Aids Comp., Vol.10, pp. 183-185.

GAUSS C.F. (1823) : Brief an Gerling, 26. Dez. 1823, Werke, Vol.9, pp. 278-281 (also available as translation : "Gauss to Gerling on relaxation", Math. Aids Comp., Vol.5 (1951), pp. 255-258).

GAUSS C.F. and SEIDEL L. (1874) : "Uber ein Verfahren, die Gleichungen, auf welche die Methode der kleinsten Quadrate führt, sowie lineare Gleichungen überhaupt, durch successive Annäherung aufzulösen", Abh. Math.-Phys. Kl., Bayr. Akad. Wiss. München, Vol. 11 (III), pp. 81-108.

HURWITZ A. (1895) : "Über die Bedingungen, unter welchen eine Gleichung nur Wurzeln mit negativen reellen Teilen besitzt", Mathem. Ann. Bd. 46, p. 273-284.

JACOBI C.G.J. (1845) : "Über eine neue Auflösungsart der bei der Methode der kleinsten Quadrate vorkommenden linearen Gleichungen", Astr. Nachr., Vol. 22, No. 523, pp. 297-306.

JOHNSON G.M. and Wirz H.J. (1976) : "The computation of non potential transonic flows by relaxation methods", von Karman Institute for Fluid Dynamics, Brussels.

KREISS H.O. (1964) : "On difference approximations of the dissipative type for hyperbolic differential equations", Com. Pure Appl. Mathem., Vol. 17, p. 335.

LAX P.D. (1954) : "Weak solutions of non linear hyperbolic equations and their numerical computation", Comm. Pure Appl. Mathem., Vol. 7, pp. 159-193.

LAX P.D. and WENDROFF B. (1960) : "Systems of conservation laws", Comm. Pure Appl. Mathem., Vol. 13, pp. 217-237.

LAX P.D. and WENDROFF B. (1964) : "Difference schemes with high order of accuracy for solving hyperbolic equations", Comm. Pure Appl. Mathem., Vol. 17, pp. 381.

LOMAX H. and STEGER J.L. : "Relaxation methods in fluid mechanics", Annual Review of Fluid Mechanics, Vol.7, (1975), p. 63-88.

MAGNUS R. and YOSHIHARA H. (1970) : "Inviscid transonic flow over airfoils", AIAA 8th Aero. Space Sc. Meeting, N.Y.

von NEUMANN J. and RICHTMYER R.D. (1950) : "A method for the numerical calculations of hydrodynamical shocks", J. Appl. Phys., Vol. 21, p.232.

PEACEMAN D.W. and RACHFORD H.H. (1955) : "The numerical solution of parabolic and elliptic differential equations", J. Soc. Industr. Appl. Math. 3, p. 28-41.

ROUTH E.J. (1877) : "A treatis on the stability of a given state of motion", p. 74-81.

RICHTMYER R.D. and MORTON K.W. (1967) : "Difference methods for initial value problems", John Wiley and Sons, 2nd ed., New York.

SOUTHWELL R.V. (1946) : "Relaxation methods in theoretical physics", Clarendon Press, Oxford, Vol.1, pp. 248, Vol.2, pp. 250-522.

WIRZ H.J. and SMOLDEREN J.J. (1973) : "Numerical integration of Navier-Stokes equations", AGARD-LS N°64 on Advances in Numerical Fluid Dynamics, pp.3.1 - 3.13, Paris.

YANENKO N.N. (1969) : Die Zwischenschrittmethode zur Lösung mehrdimensionaler Probleme der mathematischen Physik, Lecture notes in Math. N° 91, Springer.

YOUNG D. (1954) : "Iterative methods for solving partial difference equations of elliptic type", Amer. Math. Soc. Trans., Vol. 75, p.92-111.

ACKNOWLEDGEMENTS

The numerical computations have been carried out by Mr. Mike Hill, M.S. and Mr. Nguyen Hung, Ing.Civ.Ph.

This article was prepared while the author was a Visiting Professor and Head of the Computational Fluid Dynamics Department at the von Karman Institute. He is greatful to the members of the VKI for their hospitality, in particular to Professor J.J. Smolderen. He is further indebted to the D.F.V.L.R., who made this extended stay possible thanks to the exceptional interest for international collaboration of Dr. phil. Theodor Benecke.

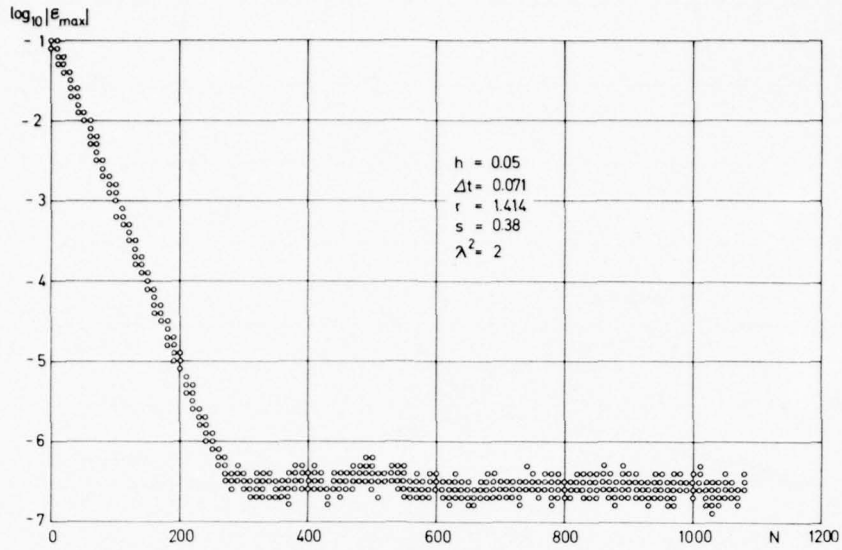

FIG. 1 : Maximum absolute error versus the number of iterations N for the third order discrete time dependent relaxation method.

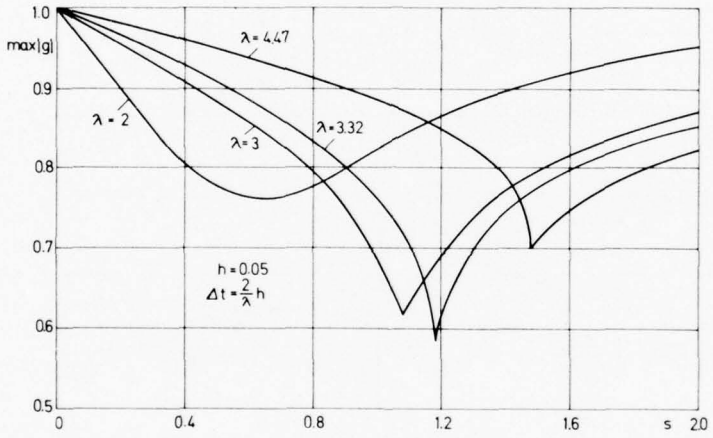

FIG. 2 : Maximum absolute contraction factor g as a function of the relaxation coefficient for different values of the parameter λ.

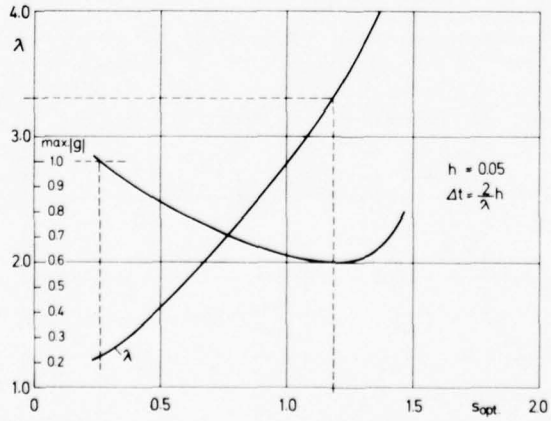

FIG. 3 : Optimum values for λ and minimised maximum absolute contraction factor as a function of the relaxation coefficient.

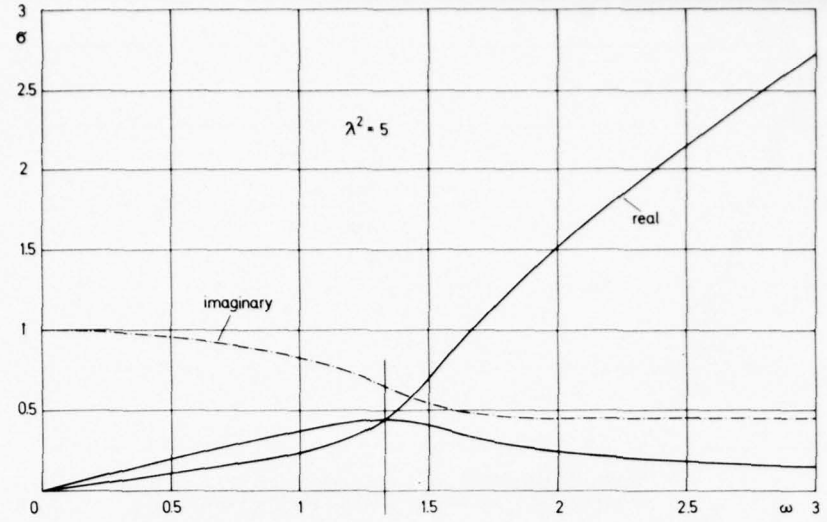

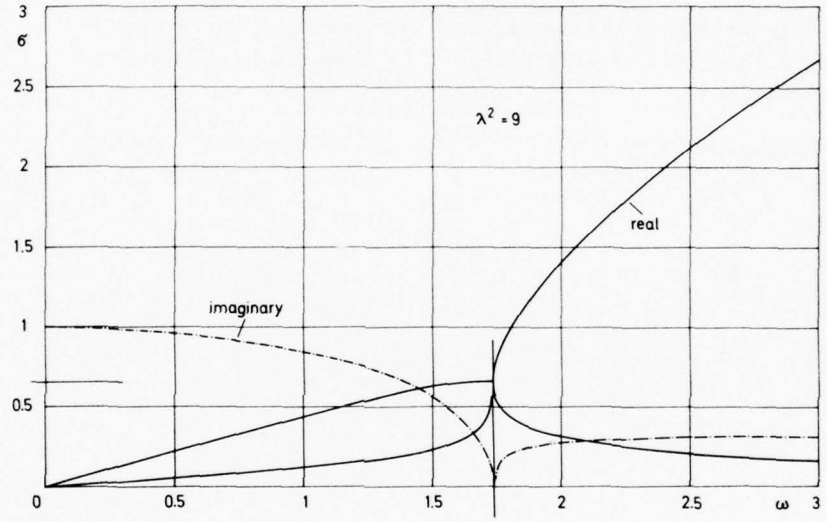

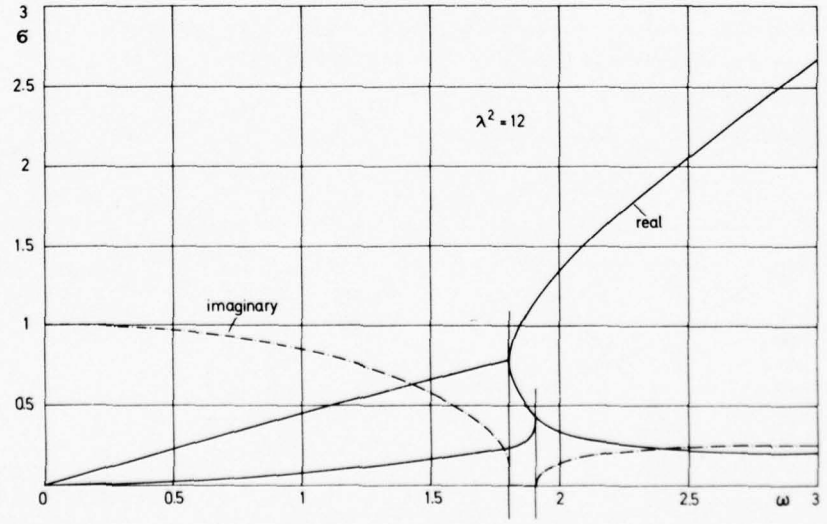

FIGS. 4,5,6 : Roots of the characteristic polynomial σ as a function of the relaxation coefficient ω for three different values of the parameter λ.

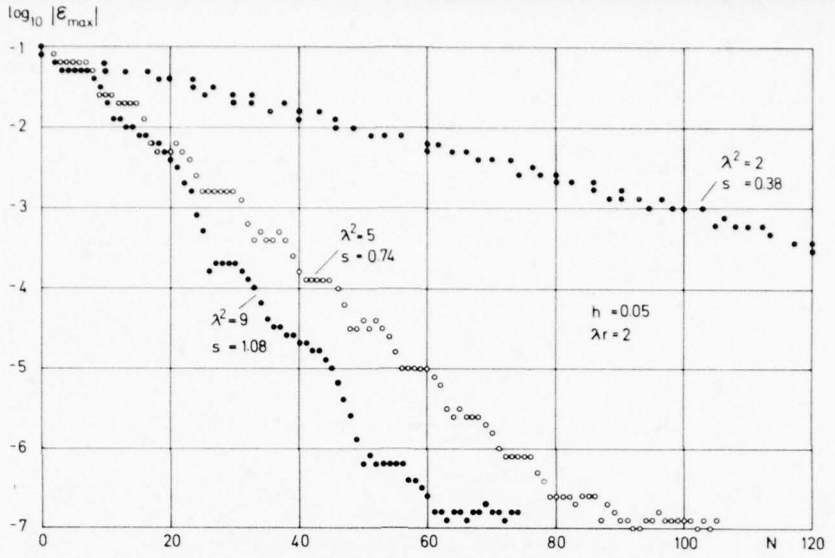

FIG. 7 : Maximum absolute errors versus the number of iterations for different values of λ and s (third order relaxation method, optimised).

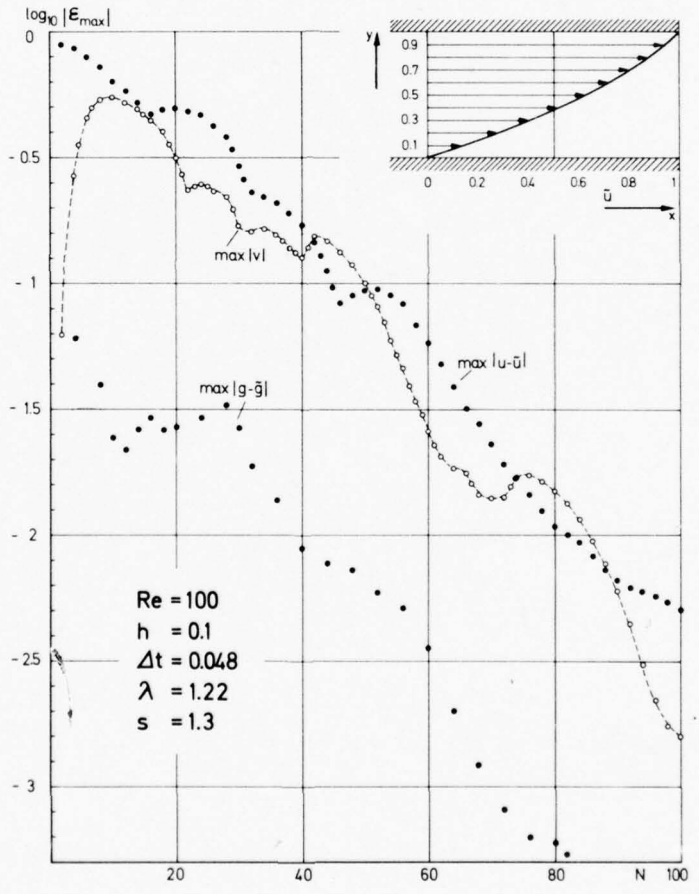

FIG. 8 : Maximum absolute errors versus the number of iterations N (Navier-Stokes equations, Reynolds number 100).

FLOW REPRESENTATION, INCLUDING SEPARATED REGIONS, USING DISCRETE VORTICES

R.R. Clements
Department of Engineering Mathematics
University of Bristol
BRISTOL BS8 1TR
England

0. INTRODUCTION

Fluid flows containing vorticity which is confined to restricted sub-regions of the fluid are amenable to treatment by the discrete vortex method. This method involves the continuous vorticity distribution being represented by a number of discrete line vortices. The kinematic properties of fluid motion are utilised to determine the motion of the line vortices and the evolution of the flow field is inferred from this motion. Two-dimensional, axisymmetric and fully three-dimensional flows have been treated by such methods, the complexity and duration of the computations increasing greatly as one progresses through these categories. One of the interesting aspects of the method is the various means which its users have developed for the incorporation of solid boundaries into the flow field. Two-dimensional complex potential flow theory and the surface source/sink method have both been used in a variety of contexts. Many computations have involved imbedded solid objects of a nature such that the vorticity creating boundary layers separate from the object to create separated shear layers in the flow, and it is to the treatment of these separated layers that the method is applied. The various models of the connection between the shear layers and the discrete vortices form another most interesting aspect of the subject.

The first recognisable use of the method was by Rosenhead (1931), but the main impetus to its development came with the advent of the high-speed digital computer. The first few generations of computers have seen the development of the method for mainly two-dimensional and axisymmetric flow situations, but the development of the current new generation of computers (ICL's Distributed Array Processor, CDC's Star, the Cray and similar machines) will bring three-dimensional discrete vortex flow computations within the bounds of reasonable cpu time. Some use of the method for three-dimensional flows has, in fact, already appeared in the literature.

The method is not, in the author's opinion, one which lends itself to the creation of computerised general flow simulation packages into which the user need only enter minimal data concerning boundary and other flow conditions and then allow the package to create the model, but one which depends for its success on an intelligent and often ingenious use of the anticipated features of the flow to create the most useful model of any given situation. This presentation will therefore be dominated by an historical description of much of the work that has used the method, highlighting the difficulties that have been overcome and the methods that have been used. Firstly, however, some basic theoretical background is built up to provide an overall understanding of the context within which the method can be used

1. SOME THEORETICAL FOUNDATIONS

1.1 Fluid Motion as the Result of Vorticity and Divergence Fields

In analysing the motion of a fluid near a point $\underline{x}$ it is found that, to first order in linear dimensions, the velocity field consists of the superposition of

(i) a uniform motion with velocity $\underline{u}(\underline{x})$;

(ii) an isotropic expansion whose rate of increase of volume/unit volume is $\nabla.\underline{u}$;

(iii) a straining motion without change of volume;

(iv) a rigid body rotation of the fluid with angular velocity $\frac{1}{2}(\nabla \times \underline{u}) = \frac{1}{2}\underline{\omega}$, say.

Batchelor (1967) gives an elegant derivation of these results. The quantities $\nabla.\underline{u}$ and $\nabla \times \underline{u}$, the divergence and curl of a vector function of position, are independent of the choice of axes in fact. We give the name *vorticity* to $\nabla \times \underline{u}$ and write $\underline{\omega} = \nabla \times \underline{u}$. If we seek the velocity field that is consistent with a given divergence, Δ, and vorticity, $\underline{\omega}$, distribution in some region of space, we can write

$$\underline{u} = \underline{u}_1 + \underline{u}_2 + \underline{u}_3 \qquad \ldots (1.1)$$

where

$$\nabla.\underline{u}_1 = \Delta \qquad \nabla \times \underline{u}_1 = 0 \qquad \ldots (1.2)$$

$$\nabla.\underline{u}_2 = 0 \qquad \nabla \times \underline{u}_2 = \underline{\omega} \qquad \ldots (1.3)$$

$$\nabla.\underline{u}_3 = 0 \qquad \nabla \times \underline{u}_3 = \underline{0} \qquad \ldots (1.4)$$

It is known that a solution for $\underline{u}_1$ is

$$\underline{u}_1(\underline{x}) = \frac{1}{4\pi} \iiint_V \frac{(\underline{x} - \underline{x}')}{|\underline{x} - \underline{x}'|^3} \Delta(\underline{x}')\, dV(\underline{x}') \qquad \ldots (1.5)$$

and for $\underline{u}_2$ is

$$\underline{u}_2(\underline{x}) = -\frac{1}{4\pi}\iiint_V \frac{(\underline{x}-\underline{x}')\times\underline{\omega}(\underline{x}')}{|\underline{x}-\underline{x}'|^3}\,dV(\underline{x}'). \qquad \ldots (1.6)$$

$\underline{u}_3$ is a velocity field with zero divergence and vorticity and is normally determined by the conditions to be satisfied on the boundaries of the region occupied by the fluid.

The form of (1.5) and (1.6) suggests that we may regard the velocity at $\underline{x}$ as partly composed of the sum of contributions from the divergence, $\Delta(\underline{x}')$, and vorticity, $\underline{\omega}(\underline{x}')$, at all points $\underline{x}'$ of the fluid. This concept of the velocity field as being driven by vorticity and divergence fields is fundamental to the discrete vortex method. It often happens that the vorticity and divergence fields are only non-zero on restricted sub-regions of the region occupied by the fluid. In this case, we can restrict the integrals of (1.5) and (1.6) to these sub-regions. Suppose in (1.5) the region in which $\Delta(\underline{x}') \neq 0$ is V_1. Now let the volume V_1 contract to contain only the point $\underline{x}_1$ and $\Delta(\underline{x}_1) \to \infty$ in such a way that

$$\iiint_{V_1} \frac{(\underline{x}-\underline{x}')}{|\underline{x}-\underline{x}'|^3}\,\Delta(\underline{x}')dV \to \frac{m(\underline{x}-\underline{x}_1)}{|\underline{x}-\underline{x}_1|^3}$$

then we say that there is a point source of strength m at $\underline{x}_1$. If there are many such points then, of course,

$$\underline{u}_1(\underline{x}) = \frac{1}{4\pi}\sum_i \frac{m_i(\underline{x}-\underline{x}_i)}{|\underline{x}-\underline{x}_i|^3}\,. \qquad \ldots (1.7)$$

Similarly, we may define a line source and sheet source in which the region of non-zero divergence $\Delta(\underline{x}')$ is restricted to a line or surface in space. Vorticity is amenable to nearly the same treatment. Let us first define a vortex line as a curve everywhere parallel to $\underline{\omega}(\underline{x})$ and a vortex tube as the volume enclosed by a number of vortex lines (see Figure 1.1). Since $\underline{\omega} = \nabla \times \underline{u}$, $\nabla.\underline{\omega} = 0$, so by Gauss theorem applied to the volume occupied by the vortex tube between S_1 and S_2

$$\iint_{S+S_1+S_2} \underline{\omega}.d\underline{S} = 0.$$

Now

$$\iint_S \underline{\omega}.d\underline{S} = 0$$

since S is a surface composed of vortex lines so

$$\iint_{S_1} \underline{\omega}.d\underline{S} = \iint_{S_2} \underline{\omega}.d\underline{S}$$

(changing the direction of the positive normal on one of S_1 or S_2 so that both point in the same direction). Hence

$$\iint_{S'} \underline{\omega}.d\underline{S} = \text{constant}$$

for any surface S' spanning the tube and is called the strength of the tube. A result of this is that vortex lines cannot begin or end in the body of the fluid. Either they are closed or end on a boundary of the region occupied by the fluid (possibly at infinity). It is obviously nonsensical to talk about a point vortex, but line and surface vortices may exist. If the vorticity in a fluid is confined to a vortex tube surrounding a curve C, then by letting the cross-sectional area of the tube tend to zero and the vorticity at its centre tend to ∞ in such a way that

$$\left|\iint_{S'} \underline{\omega}.d\underline{S}\right| \to k$$

we find that

$$\underline{u}_2(\underline{x}) = -\frac{1}{4\pi}\iiint_V \frac{(\underline{x}-\underline{x}')\times\underline{\omega}(\underline{x}')}{|\underline{x}-\underline{x}'|^3}\,dV(\underline{x}') \to -\frac{k}{4\pi}\int_C \frac{(\underline{x}-\underline{x}')\times d\underline{\ell}}{|\underline{x}-\underline{x}'|^3}\,. \qquad \ldots (1.8)$$

This entity is known as a line vortex of strength k per unit length lying along the curve C. The curve may, of course, be closed or extend to the boundaries of the fluid. If there are a number of line vortices present in a fluid flow region we will have

$$\underline{u}_2(\underline{x}) = -\sum \frac{k_i}{4\pi}\int_{C_i} \frac{(\underline{x}-\underline{x}')\times d\underline{\ell}(\underline{x}')}{|\underline{x}-\underline{x}'|^3}\,.$$

The concept of a line vortex is fundamental to the discrete vortex method of flow analysis. Of course, we can also define a sheet vortex when the induced velocity field will be a surface integral over the whole vortex sheet.

1.2 The Vorticity Equation

Taking the curl of the Navier-Stokes equation

$$\frac{\partial \underline{u}}{\partial t} + \underline{u}.\nabla\underline{u} + \frac{1}{\rho}\nabla p = \nu\nabla^2\underline{u} \qquad \ldots (1.9)$$

we obtain

$$\frac{\partial \underline{\omega}}{\partial t} + \underline{u}.\nabla\underline{\omega} = \frac{D\underline{\omega}}{Dt} = \underline{\omega}.\nabla\underline{u} + \nu\nabla^2\underline{\omega} \; . \qquad \ldots)1.10)$$

The change in the vorticity $\underline{\omega}(\underline{x},t)$ is caused by two effects; firstly, an intensification due to stretching of the vortex lines by the fluid motion, and secondly, a diffusion of vorticity due to viscosity of the fluid. If the viscosity is negligible, at least in the body of the fluid, then the motion there is purely kinematic and vortex lines follow fluid material lines. Their strength, of course, changes as the material lines are stretched or compressed by the motion. For a vortex tube the stretching will reduce its cross-section and the two effects, intensification of vortex lines and reduction of cross-section, are balanced so that the strength of the tube is unchanged.

Two properties of line vortices in an inviscid fluid region thus emerge. Firstly, a line vortex is, and remains, associated with a fluid material line and so convects with the fluid, and secondly the strength of the line vortex is constant. For three-dimensional discrete vortex computations the effects of vortex stretching does become important in that, for a curved ideal line vortex, the self-induced velocity at any point is infinite. This problem is overcome by modifying the velocity induced at any point by the immediately adjacent segments of the line vortex to an expression appropriate to a vortex tube of small but finite cross-section. This cross-section is then modified as the line vortex is stretched or compressed. We shall return to this point later.

1.3 Two-Dimensional Fluid Motion

In two-dimensional flow we have

$$\underline{u}(\underline{x}) = (u(x,y),v(x,y),0) \qquad \ldots (1.11)$$

and

$$\underline{\omega}(\underline{x}) = \nabla \times \underline{u} = (0,0,\frac{\partial v}{\partial x} - \frac{\partial u}{\partial y}) \qquad \ldots (1.12)$$

so $\underline{\omega}$ is a vector in the z-direction. Then the vorticity equations gives

$$\frac{D\underline{\omega}}{Dt} = \nu\nabla^2\underline{\omega}.$$

Thus the vorticity remains confined to the z-direction and, in the absence of viscosity, the vorticity associated with any fluid element remains constant. It is this constancy of vorticity and motion of vorticity with fluid lines which gives the discrete vortex method its appealing simplicity in two-dimensional flow analysis.

In irrotational flow, when $\underline{\omega}(\underline{x}) = \underline{0}$, $v_x = u_y$, which is the condition that udx + vdy is a perfect differential, that is that there exists $\phi(x,y)$ such that $u = \phi_x$ and $v = \phi_y$. Similarly in incompressible flow, $\nabla.\underline{u} = 0 \Rightarrow u_x = -v_y$, that is -vdx + udy is a perfect differential so that there exists $\psi(x,y)$ such that $u = \psi_y$, $v = -\psi_x$. ϕ is called the complex potential of the flow and ψ the stream function. Now obviously

$$u = \phi_x = \psi_y \qquad v = \phi_y = -\psi_x \qquad \ldots (1.13)$$

and these are the Cauchy-Riemann relations between ϕ and ψ. Thus we are assured that

$$\phi + j\psi = f(z) \qquad \text{where } z = x + jy$$

and the function f of the complex variable z is called the complex potential of the flow. f(z) is an analytic function of z except at singularities of the flow, that is line sources, line vortices and some more complicated entities such as line dipole sources which will not concern us. Some relatively simple analysis (see Batchelor for details) reveals that the complex potentials for a line source of strength m and a line vortex of strength k at $z = z_0$ are

$$f(z) = \frac{m}{2\pi}\ln(z - z_0) \qquad \text{and} \qquad f(z) = -\frac{jk}{2\pi}\ln(z - z_0) \qquad \ldots (1.14)$$

respectively.

For a complex potential to exist the flow must be irrotational and inviscid. Under these conditions the governing equations are linear, so complex potentials are additive. For example, the potential of the flow due to n line vortices of strengths k_i at positions z_i is

$$f(z) = -j \sum_{i=1}^{n} \frac{k_i}{2\pi} \ell n(z - z_i). \qquad \ldots (1.15)$$

Since

$$\frac{df}{dz} = \frac{\partial \phi}{\partial x} + j \frac{\partial \psi}{\partial x}$$

we have

$$\frac{df}{dz} = u(x,y) - jv(x,y) \qquad \ldots (1.16)$$

so the velocity at any position z is easily found by differentiating the complex potential.

A property of complex potential which has important repercussions in discrete vortex work is that it is a transformal invariant. If we have a mapping $z = \zeta(\lambda)$ from z to λ planes then, writing

$$\left.\begin{aligned} f(z) &= f(\zeta(\lambda) = f_1(\lambda) \\ f(z) &= \phi + j\psi \\ f_1(\lambda) &= \phi_1 + j\psi_1 \\ \lambda &= \xi + j\eta \end{aligned}\right\} \qquad \ldots (1.17)$$

we have $\psi(x,y) = \psi_1(\xi,\eta)$ so lines ψ = constant in the z-plane become lines ψ_1 = constant in the λ-plane, which can thus be interpreted as a new flow field in the λ-plane. So given a conformal mapping $z = \zeta(\lambda)$ and a flow field in either plane a corresponding flow field in the other plane is defined. In particular, solid boundaries are of course streamlines, so a known flow past a solid boundary will define a flow past the transform of that solid boundary. It can further be shown that the flow fields due to sources and vortices transform to corresponding flow fields due to sources and vortices of the same strength.

1.4 Conclusion

This review of the theoretical foundations of the discrete vortex calculation method is necessarily somewhat abbreviated and the reader who requires a more detailed exposition of the material is particularly referred to Batchelor (1967) and Milne-Thomson (1938) amongst the many texts which contain this material.

2. AN ILLUSTRATIVE HISTORY OF THE METHOD FOR TWO-DIMENSIONAL FLOW CALCULATIONS

The first work to use discrete vortices to represent a vortex sheet was that of Rosenhead (1931). He presented a linear stability analysis of small perturbations of the two-dimensional infinite vortex sheet separating two semi-infinite spaces in which fluid of equal density was flowing uniformly in opposite directions with equal velocity (U) parallel to the sheet. The stability analysis revealed that a sinusoidal disturbance of wavelength λ and amplitude ε would grow exponentially like $(2\pi Ut/\lambda)$. However, on taking second order terms, he found that there would be an accompanying perturbation of wavelength $\frac{1}{2}\lambda$ and amplitude proportional to ε^2 which would grow exponentially like $\exp(4\pi Ut/\lambda)$ and so would ultimately swamp the first-order term. Subsequently, the third, fourth and higher order terms would successively become dominant. In order to study this non-linear development of the perturbed vortex sheet, Rosenhead replaced it by an array of two-dimensional line vortices arranged along the initially slightly perturbed vortex sheet (see Figure 2.1). The strength of the vortex sheet is -2U/unit length, thus if n vortices per wavelength are used, the strength of each will be $-2U\lambda/n$. An array of equally-spaced vortices along the original position of the sheet is, of course, a stable configuration so the vortices were initially placed on a sine wave of amplitude 0.1λ, the predicted form of small disturbances using the linear stability theory. Thus $y_r = 0.1\lambda \sin(2\pi x_r/\lambda)$. In this configuration the rth vortex, the (r + n)th, (r + 2n)th, (r - n)th etc., form an infinite row of vortices with spacing λ. The complex potential of such a row is

$$f(z) = \sum_{m=-\infty}^{\infty} \frac{j}{2\pi} \frac{2U\lambda}{n} \ell n(z - z_r - m\lambda) \qquad \ldots (2.1)$$

where z_r is the position of the rth vortex in the basic wavelength illustrated. This infinite sum can be shown to yield

$$f(z) = \frac{jU\lambda}{n\pi} \ell n \left\{ \sin \frac{\pi(z - z_r)}{\lambda} \right\} . \qquad \ldots (2.2)$$

Thus the complex potential of the n rows of vortices which make up the sheet is

$$f(z) = \sum_{r=1}^{n} \frac{jU\lambda}{n\pi} \ell n \left\{ \sin \frac{\pi(z - z_r)}{\lambda} \right\} \qquad \ldots (2.3)$$

which gives

$$u(x,y) = \frac{U}{n} \sum_{r=1}^{n} \frac{\sinh k(y - y_r)}{\cosh k(y - y_r) - \cos k(x - x_r)} \qquad \ldots (.24)$$

$$v(x,y) = -\frac{U}{n} \sum_{r=1}^{n} \frac{\sin k(x - x_r)}{\cosh k(y - y_r) - \cos k(x - x_r)} \qquad \ldots (2.5)$$

where $k = 2\pi/\lambda$. The velocity of the flow at any point can be computed from a knowledge of the positions of the n vortices making up the basic wavelength. Now we know that, in inviscid flow, the vortices remain unchanged in strength and convect with the fluid lines so the velocities of the vortices can be deduced from the velocity of the fluid at the vortex positions. Of course, the row of vortices of which a particular vortex is a member does not induce any velocity on that vortex, so the summation in Equations 2.4 and 2.5 excludes the term representing this contribution. The time development of the configuration was computed by Rosenhead by using the Euler integration scheme. At each time step the velocities of each vortex were computed, the positions of each advanced by $\underline{u}\,\delta t$ and then the velocities of the vortices in this new configuration computed and so the process repeated itself. Using 2, 4, 8 and 12 vortices per wavelength, Rosenhead was able to observe a smooth rolling up of the vortex sheet into concentrated clusters of vortices with a spacing equal to the wavelength of the original perturbation. Of course, the numerical computation was performed on a desktop hand calculator - a very laborious procedure. As a result, Rosenhead used large time steps. The implications of this were to become apparent at a later date when the power of digital computers was brought to bear on the problem.

Birkhoff and Fisher (1959) repeated Rosenhead's computation with the same initial perturbation to the vortex sheet, but using one of the early UNIVAC computers to perform the integration over time by the Runge-Kutta algorithm. They were able to use a larger number (22) of vortices per wavelength and smaller time steps, of the order of one-tenth to one-fiftieth of Rosenhead's, because of the availability of computer power. They found that the paths of individual vortices of the sheet were irregular and contorted and often crossed over one another - an event which is physically impossible for a vortex sheet and so unrealistic in a simulation of it. They argued, from invariance theorems, that in the long term an organised array of vortices might be expected to become increasingly random and, as suggested by the title of the paper, questioned whether the discrete vortex representation of shear layers has any validity. The observation of contorted vortex paths is one that has subsequently been made by other workers studying aircraft wing trailing vortex sheets, and we shall return to this point below.

Hama and Burke (1960) also performed a follow-up study to Rosenhead's work. Using twelve vortices per wavelength, as Rosenhead had, but time steps one quarter as long, they found essentially the same behaviour as Birkhoff and Fisher - roll up into periodic clusters of vortices, but individual vortex paths being somewhat contorted. Hama and Burke, however, pointed out that, in Rosenhead's linear stability analysis, two modes of perturbation of the vortex sheet are found. Both are sinusoidal in form and one grows exponentially with time whilst the other decays exponentially. Both forms involve a sinusoidal variation in the *strength* of the sheet, and Rosenhead's assumed perturbation form was in fact the sum of equal parts of the two separate modes of perturbation. Hama and Burke then repeated the Rosenhead work using an initial perturbation appropriate to a pure growing mode perturbation in which the line vortices were spaced unequally along the curve $y = 0.1 \sin(2\pi x/\lambda)$ in such a way that the vorticity per unit length distribution $2U(1 - 0.2\pi \cos(2\pi x/\lambda))$ was approximated. Using this initial condition the rolling up of the line vortices into vortex clusters was found to be much smoother. The fundamental question of the stability of the discrete vortex representation was not completely resolved, however.

The studies described so far have all assumed the shear layer between the two counterflowing fluid streams to be of zero thickness. Since viscosity is also neglected, there is no length scale available and the shear layer is equally unstable to all wavelengths of perturbation and the amplification factor is constant. A linear stability analysis of a finite thickness shear layer was given by Michalke (1963). He considered a shear layer with a linear velocity change across its thickness (i.e. constant vorticity) and derived the wavenumber of the most unstable perturbation and that of the neutrally stable perturbation. He then applied the discrete vortex method to compute the subsequent non-linear growth of the shear layers. To account for their finite thickness he used three and four parallel rows of line vortices distributed across the thick layer to represent the vorticity distribution. Computations for different wavenumbers revealed that the rolling up of the configuration into areas of concentrated vorticity was indeed tightest for the most unstable perturbation. It is apparent from the figures in Michalke's paper that, not only did the thick shear layer as a whole roll up into vortex concentrations, but also each of the separate rows of vortices rolled up individually within those concentrations. This behaviour is obviously unrepresentative of the fine structure of the rolled-up vortex concentrations.

Concentration has recently been focussed on another aspect of the rolling up of a single shear layer by the urgent interest in aerodynamic noise generation in the mixing layer at the edge of a jet, and means of attenuating this. It has been observed that the mixing layer at the jet boundary contains organised vortex

structures (see Brown and Roshko (1974)). These structures are convected with a constant mean velocity and have a spacing proportional to the distance downstream of the jet source. It is apparent then that some vortices must disappear or amalgamate as they move downstream for the two observations to be consistent. Two mechanisms have been proposed; in one a weaker vortex structure is 'torn apart' and its vorticity absorbed by stronger neighbours on either side, and in the other, neighbouring vortex structures begin to rotate about one another and subsequently coalesce into a single larger structure. The latter process has been observed in the experiments of Winant and Browand (1974) and a study of the mechanism using discrete vortices has been made by Acton (1976). This study was essentially similar to that of Michalke. A thick shear layer consisting of several parallel rows (in most cases four) of vortices was sinusoidally perturbed and the subsequent development computed as before. Acton used vortices with finite 'cores' to alleviate the problems described by Birkhoff and Fisher. These vortices have a stream function ψ such that

$$\psi = \begin{cases} \frac{\kappa}{2\pi} \ell n(x^2 + y^2)^{\frac{1}{2}} & x^2 + y^2 > \sigma^2 \\ \frac{\kappa}{2\sigma\pi}(x^2 + y^2)^{\frac{1}{2}} & x^2 + y^2 < \sigma^2 \end{cases} \qquad \ldots (2.6)$$

in other words, from a distance greater than σ their effect is identical to that of a line vortex and closer than σ the velocity induced by such a vortex is that of a rigidly rotating fluid core. This device was first suggested by Chorin and Bernard (1973) of whom we shall make mention below. The effect of using such vortices, combined with the different relative cross shear layer and along shear layer separations of the vortices used by Acton, was to suppress the rolling up of the individual vortex rows within the shear layer found by Michalke and give a more realistic picture of the process. Nonetheless, Acton does state that the discrete model used does not accurately model the fine-scale shear-layer structure. As the purpose of this study was to obtain information about the process subsequent to rolling up into primary vortex concentrations, irregularities in the primary perturbation had to be introduced, for otherwise the form of the rolling up would necessarily remain periodic with wavelength λ. A very small irregularity of wavelength 2λ was found to trigger a subsequent rotation of the vortex concentrations around one another, and a final coalescence into a larger vortex concentration in the manner observed by Winant and Browand.

The first mechanism was also studied, using discrete vortices, by Moore and Saffmann (1975). In their study they derived a condition on the ratio of the separation of the vortex concentrations in the mixing layer to their diameter for each vortex concentration to be stable in the shearing flow induced by all the other vortices. They predicted that if this ratio exceeded approximately 2.8 the concentrations would remain distinct although oscillating in shape, and that otherwise a vortex would be torn apart by the shearing action of its neighbours and eventually absorbed by them. They considered an infinite array of circular vortex concentrations of different separation diameter ratios. Each vortex concentration was represented by a number of discrete vortices appropriately distributed. The results of their computations were seen to be consistent with their original hypothesis.

An earlier study of the formation of vortex concentrations in the mixing layers of jets had been made by Beavers and Wilson (1970). In their study they considered the two mixing layers on either edge of a two-dimensional plane jet. They set out to investigate the rate at which disturbances of two initially parallel infinite shear layers of opposite sign, representing the shear layers on either edge of a jet, would propagate upstream. To achieve this they considered local perturbations only, rather than periodically repeated perturbations. Since the flow was not periodic, considerations of computing time imposed a limitation on the length of shear layer that could be considered and the effect of the portions of shear layer beyond a finite section had to be neglected. The vortices at the ends of the finite section were therefore constrained not to move so that the effect of the remainder of the layers was closely approximated. Beavers and Wilson experimented with small symmetric and non-symmetric disturbances. They found that both types of disturbance propagated at such a rate that the disturbance would move upstream despite the mean downstream motion of the shear layers as a whole. The non-symmetric perturbations were observed to become more symmetric as they propagated. Typically, the evolution of the system involved a rolled up vortex cluster forming around the initial perturbation and a kink in the sheet was then propagated from this cluster about which a new cluster would roll up and so the process was repeated.

One of Beavers' and Wilson's inspirations must have been the work of Abernathy and Kronauer (1962). Their work was designed to elucidate the mechanism whereby the two free shear layers which spring from the separated boundary layers of a two-dimensional bluff body roll up into the typically antisymmetric staggered array of vortex concentrations known as the Von Karman vortex street or wake. They, like Rosenhead,

started with a linear stability analysis, but of two infinite, plane, parallel vortex sheets of zero thickness separating a central region in which the fluid flowed uniformly with velocity U in one direction from two exterior regions in which fluid flowed with uniform velocity U in the opposite direction. The stability analysis indicated four modes of perturbation, all of periodic sinusoidal form. Two of the modes grew exponentially with time, whilst two decayed. Of the two of each type, one was symmetric in the two sheets, whilst the other was antisymmetric. To model the vortex street formation they considered an initial disturbance consisting of a mixture of the two antisymmetric modes and replaced the continuous vorticity distribution by discrete vortices (see Figure 2.3). The complex potential of the flow was found in the same way as described for Rosenhead's work, but now the summation in Equations 2.3, 2.4 and 2.5 was over the vortices in the basic wavelengths in both shear layers. The non-linear evolution of the perturbations was computed for a number of configurations with different ratios of perturbation wavelength to initial vortex sheet separation. The purpose of these studies was to try to throw some light on the status of the so-called Von Karman spacing ratio of h/a = 0.281, which is derived from a stability analysis of a staggered array of opposite-signed vortices representing such a street. Calculations were performed for configurations with sheet separation/perturbation wavelength in the range 0.12 to 0.34. In each case, the vortex arrays were seen to roll up into concentrations of vortices in an antisymmetric pattern which could be identified as a vortex street. Further, the smallest ratio for which only two vortex concentrations were formed to each wavelength of the perturbation was 0.28 and below this four concentrations were formed - thus providing some further evidence that the Von Karman ratio is indeed the naturally preferred ratio. Another feature of vortex wakes that was well modelled is the cancellation of vorticity in the formation process. Experimental work, for instance Fage and Johansen (1927), has indicated that only about 60% of the vorticity generated in the boundary layers is eventually found in the wake vortices. The computations of Abernathy and Kronauer showed vortices from one shear layer being drawn across the central void and caught up in concentrations formed predominantly of vortices from the other shear layer. It was postulated that such vortices would cancel with some of the vortices of the opposite layer, resulting in a reduction in total vorticity in that concentration.

The application of the method to the study of the formation of vortex wakes was taken a stage further by Gerrard (1967). The work of Abernathy and Kronauer suffered from two major limitations. Firstly, the effect of the generating body was not represented, and secondly, the initial strength of the vortex sheets was constant - whereas in reality the sheets are being fed with vorticity from the separating boundary layers on the bluff body, which varies with time. Gerrard considered the wake of a circular cylinder. The complex potential of n line vortices of strengths κ_i at positions z_i in the presence of a cylinder of radius a, centre the origin and a flow whose velocity far from the cylinder tends to $(U_0,0)$ is known to be

$$f(z) = U_0\left(z + \frac{a^2}{z}\right) - \sum_{i=1}^{n} \frac{j\kappa_i}{2\pi} \ln(z - z_i) + \sum_{i=1}^{n} \frac{j\kappa_i}{2\pi} \ln\left(z - \frac{a^2}{z_i^*}\right) - \sum_{i=1}^{n} \frac{j\kappa_i}{2\pi} \ln(z) \qquad \ldots (2.7)$$

where z^* represents the complex conjugate of z. A physical interpretation of this is that the first term represents the underlying irrotational flow which satisfies the conditions at the boundaries of the flow region; the second is the effect of the vortices in the flow and the third of image vortices of opposite signs at the inverse points within the cylinder of all the real vortex positions. These images cause the boundary condition of no flow across the cylinder to be satisfied. The last term represents further images of all the vortices at the cylinder centre and is necessary if the total circulation around the cylinder is to be zero. In his work, Gerrard removed this term, since the vorticity shed from the cylinder leaves an equal and opposite vorticity behind it on the cylinder. The major problem then, the availability of a complex potential from which to compute the vortex velocities, is solved. The other problems are to determine the strength of the separating boundary layers and the position of their separation. The rate at which vorticity is shed into the separated shear layers is theoretically $\frac{1}{2}U_s^2$, where U_s is the velocity at the outer edge of the boundary layer at separation. The separation points on a cylinder, however, oscillate during vortex shedding and the incorporation of this behaviour into a discrete vortex model of vortex shedding has proved problematical. In fact, the whole area of the relationship of the shed vorticity in free shear layers to the flow around the shedding body is one that gives rise to major problems in this field, and we shall comment further on this below. Gerrard chose, instead, to ignore the portion of separated shear layer between the separation points and a 'control plane' which he located perpendicular to the flow direction and touching the rear face of the cylinder. The distance of the points of introduction of the vortices into the flow from the centre line of the wake was determined and taken to be representative of the Reynolds number. The strengths of the vortices were determined from the velocity of the fluid

at the points of introduction. The flow computation was started by placing three vortices in assigned positions, computing their velocities, advancing their positions by one time step and introducing two new vortices - one to each shear layer - at appropriate positions and strengths and then repeating the process. Gerrard obtained curves of the variation of lift and drag with time, but it is difficult to obtain any accurate estimate of the frequency of the oscillations from these.

A similar calculation was undertaken by Sarpkaya (1968). He modelled the physical process of separation more closely. He first argued that separation would take place halfway along the cylinder surface between the point z_f where the first maximum of velocity occurred when traversing the cylinder from the forward stagnation point and the point z_r where the first maximum of reverse flow velocity when traversing from the rear stagnation point occurred. New vortices were introduced at each time step at the separation points and a small distance from the cylinder surface. The strength of the new vortices was made equal to $\frac{1}{2}(v_f^2 - v_r^2)$ to account for the negative vorticity contributed to the shear layer by the reverse flow on the rear face of the cylinder. The points z_f and z_r will, of couse, vary as the whole configuration changes and both have to be recalculated at each time step. Thus, the separation point and strength of each new vortex is allowed to respond to changes in the flow field downstream of the cylinder. Sarpkaya started his flow impulsively from rest and constrained it to remain symmetric about the whole centre line, so only modelling the initial flow round a bluff body before asymmetry sets in. His results show the free shear layers rolling up into concentrated vortices and, interestingly, a smaller-scale secondary rolling up of the individual layers into sub-scale vortex concentrations which is very reminiscent of the flow visualisation pictures obtained by Pierce (1961). The drag coefficient computed from his model was also in good agreement with some experimental measurements, particularly Sarpkaya (1966). Sarpkaya's work was extended by Davis (1970), working with Sarpkaya, to include the subsequent non-symmetric flow. The model developed to show periodic vortex shedding behaviour and the computed drag showed realistic behaviour in reaching a maximum soon after the impulsive start, then decreasing somewhat and oscillating about a mean level. The computation was not continued far enough to give any good estimate of the Strouhal number of the vortex shedding.

Subsequently, similar models have been described by Laird (1971) and Chaplin (1973). In both of these the separation points and the strength of the line vortices introduced into the shear layers were fixed. A significant new feature was introduced by Deffenbaugh and Marshall (1976). In their model an inner flow sub-model was introduced in which a boundary layer calculation on the upstream part of the cylinder was carried out at each time step. This calculation determined the position of forward separation. The back flow velocity on the rear face and rear separation was also considered. At each time step four new vortices were introduced into the flow, two at the forward and two at the rear separation points. The strengths of the vortices were determined from the velocities at the outer edge of the boundary layers by the relation quoted previously that $\dot{\Gamma} = \frac{1}{2}U_s^2$, where $\dot{\Gamma}$ is the rate of shedding of vorticity. The distance from the cylinder surface of the newly introduced vortices was determined from the condition that there should be no slip at the surface at the separation points. The sign of the vortices from the rear separation points was, of course, opposite to that of the vortices from the corresponding front separation points. This computation again started impulsively from rest, and shows the typical development of a pair of symmetrical attached vortices eventually succumbing to an asymmetry and periodic vorted shedding behaviour subsequently developing. By the time the first vortex has been shed and the second, opposite, vortex is well formed the forward separation points have moved forward to around 67^0, and remain close to that value for the remainder of the computation. Deffenbaugh and Marshall comment that this is about 20% lower than the accepted angle of quasi-steady separation for a cylinder of around 82^0 (in the laminar case). They comment that " ... the difficulty lies in the influence the newly-created vortices have on the separation points. It was found that the separation point velocity is strongly influenced by vortices in its immediate vicinity, and that the effect was to promote separation". This comment serves to highlight once again the difficulty of satisfactorily modelling the separation process and the relationship of free shear layer to boundary layer. Nonetheless, it is the author's opinion that the inclusion of a boundary layer sub-model is one of the measures that must be taken before an entirely satisfactory model is obtained.

Another line of development of discrete vortex modelling has involved the vortex shedding process behind non-circular holes. The cylinder had the advantage that the boundary condition on the cylinder surface could easily be satisfied by image vortices inside the cylinder. The drawback was, of course, the complication of the separation points and process. Clements (1973a) described a model of the flow in the wake of a square-based elliptical-nosed two-dimensional body. The separation points on such a body are

fixed at the downstream corners. One reason for choosing such a body was the large volume of experimental data gathered on the characteristics of flow round such bodies by Bearman (1965, 1967). The body was idealised to extend to infinity in the upstream direction as, once the length exceeds about four base widths, the nose effects on the wake are negligible. It was then possible to derive the Shwartz-Christoffel transformation mapping the exterior of this body into an upper half plane (see Figure 2.4). As pointed out in Section 1.3, line vortices in one plane transform to line vortices in the other. Thus the complex flow potential for the flow due to any arrangement of vortices in the physical plane can be found by computing the corresponding arrangement in the transformed plane. The transformed body boundary is now the real axis, and the boundary condition here can be satisfied by the provision of image vortices of opposite sign at the conjugate points of the vortex positions. Thus the complex potential in the transformed plane is known and, since this is an invariant of the transformation, the complex potential in the physical plane can be found. Thus, if the transformation is $z = \zeta(\lambda)$, and there are vortices of strengths $\{\kappa_i\}$ at positions $\{z_i\}$, and $\{\lambda_i\}$ are defined by $z_i = \zeta(\lambda_i)$ the complex potential in the λ plane is

$$f(\lambda) = f_1(\lambda) - \sum \frac{j\kappa_i}{2\pi} \ell n(\lambda - \lambda_i) + \sum \frac{j\kappa_i}{2\pi} \ell n(\lambda - \lambda_i^*) \qquad \ldots (2.8)$$

where $f_1(\lambda)$ is the potential of the irrotational underlying flow which represents the steady flow far from the body. Then we have

$$\frac{df}{dz} = \frac{df}{d\lambda}\frac{d\lambda}{dz} = \left\{ f_1'(\lambda) - \frac{j}{2\pi} \sum \kappa_i \left(\frac{1}{\lambda - \lambda_i} - \frac{1}{\lambda - \lambda_i^*} \right) \right\} \Big/ \zeta'(\lambda). \qquad \ldots (2.9)$$

Thus the velocity of the fluid at nearly any point z can be found by finding the transform of z and the $\{z_i\}$ and substituting in the above expression. The differentiation fails when the point whose velocity we require is the position of a line vortex, as it will usually be in the computational procedure. In this case we have to incorporate a modification of Equation 2.9 known as Routh's correction. If $f_{z_1}(z)$ and $f_{\lambda_1}(\lambda)$ denote the potentials due to all causes except a vortex of strength κ at z_1, then

$$f_{z_1}(z) - \frac{j\kappa}{2\pi} \ell n(z - z_1) = f_{\lambda_1}(\lambda) - \frac{j\kappa}{2\pi} \ell n(\lambda - \lambda_1). \qquad \ldots (2.10)$$

Hence

$$f_{z_1}(z) = f_{\lambda_1}(\lambda) - \frac{j\kappa}{2\pi} \ell n \frac{\lambda - \lambda_1}{z - z_1} \quad . \qquad \ldots (2.11)$$

Now if

$$\lambda = \zeta^{-1}(z) = \Lambda(z), \text{ say,}$$

$$\lambda = \Lambda(z_1) + (z - z_1)\Lambda'(z_1) + \tfrac{1}{2}(z - z_1)^2 \Lambda''(z_1) + O(z - z_1)^3 \qquad \ldots (2.12)$$

i.e.
$$\lambda - \lambda_1 = \lambda - \Lambda(z_1) = (z - z_1)\Lambda'(z_1) + \tfrac{1}{2}(z - z_1)^2\Lambda''(z_1) + O(z - z_1)^3 \qquad \ldots (2.13)$$

so
$$f_{z_1}(z) = f_{\lambda_1}(\lambda) - \frac{j\kappa}{2\pi} \ell n\left[\Lambda'(z_1) + \tfrac{1}{2}(z - z_1)\Lambda''(z_1) + O(z - z_1)^2\right] \qquad \ldots (2.14)$$

$$\frac{df_{z_1}}{dz} = \frac{df_{\lambda_1}}{d\lambda}\frac{d\lambda}{dz} - \frac{j\kappa}{2\pi} \frac{\tfrac{1}{2}\Lambda''(z_1) + O(z - z_1)}{\Lambda'(z_1) + O(z - z_1)} \quad . \qquad \ldots (2.15)$$

Then as $z \to z_1$ and $\lambda \to \lambda_1$

$$\left.\frac{df_{z_1}}{dz}\right|_{z_1} = \left.\frac{df_{\lambda_1}}{d\lambda}\right|_{\lambda_1} \left.\frac{d\lambda}{dz}\right|_{z_1} - \frac{j\kappa}{2\pi} \frac{\Lambda''(z_1)}{2\Lambda'(z_1)} \qquad \ldots (2.16)$$

the final term in Equation 2.16 being Routh's correction. Thus df/dz for any point in the z-plane is known and so the velocities. The remaining details of the computation are similar to the previously described cylinder models. The separation points are fixed so new vortices were introduced at appropriate time steps at a fixed point near to the corner with a strength fixed by the condition $\dot{\Gamma} = \frac{1}{2}U_s^2$ where U_s was taken as the velocity at a point near the corner. The actual corner could not be used as the velocity will tend to infinity there in inviscid flow. The effect of choosing different points near the corner was studied.

Clements' model was started impulsively from rest, and after an initial period in which a symmetric arrangement of vorticity formed behind the body asymmetry developed and vortex shedding behaviour followed. Clements was able to allow the simulation to continue to run over as many as 20 periods of the vortex shedding. The Strouhal number of the shedding, the observed form of the rolling up and other measured parameters showed excellent agreement with experimental data. Subsequently, the model was modified to allow the rate of shedding of vorticity into the shear layers to be determined by the imposition of a Kutta condition at the corners. This work is described in Clements (1973b) and Clements and Maull (1975). Gratifyingly, the conclusion was that the model simulated vortex shedding flow equally well with either means of determining shed vorticity and the major flow parameters were unaltered between the two models. A notable failure of Clements' work was its inability to predict a usable base pressure coefficient. This was found

to be unduly sensitive to the value of some numerical parameters in the model, in particular the exact position chosen as the point whose velocity would represent U_s.

Sarpkaya (1975) used the well-known transformation of a circle to a flat plate to construct a model of the flow past an inclined flat plate where the incident flow made an angle with the plate in the range 40^0 to 80^0. He used a Kutta condition to determine the strength of the newly introduced line vortices at each time step. The exact procedure is somewhat complex, but the effect of it was to allow both strength and position of introduction of the new vortices to respond to changes in the flow in the wake of the plate. This is obviously more satisfactory than Clements' Kutta procedure, in which vortex strength only was varied to satisfy the Kutta condition with the new vortices being introduced at a fixed point in the vicinity of the separation points. As might, by now, be expected, the results of Sarpkaya's computations showed vortex shedding behaviour that was in good agreement with the expected pattern at all angles of attack studied. He also computed the normal force coefficient from the vortex position data at each time step and found that the asymptotic mean level of this quantity was about 20-25% higher than that obtained in the experimental studies of Fage and Johansen (1927). Both Sarpkaya's and Clements' models predicted that the vortex concentrations of the wake would contain about 80% of the shed vorticity in contrast to the experimentally-measured value of around 60% mentioned before. Sarpkaya associated the overestimate of the mean normal force with this underestimate of vorticity attenuation in the vortex formation process. Obviously this is a feature that may be common to other discrete vortex models of vortex street formation, and is a feature to which research effort must be devoted in the future.

For completeness we should also note that Belotserkovskii and Nisht (1975) have described a model, similar to Sarpkaya's, of the flow past a flat plate at a range of angles of attack.

3. THE USE OF THE METHOD IN AXISYMMETRIC AND THREE-DIMENSIONAL FLOW

Professor P.O.A.L. Davies has been using the discrete vortex method to study the development of the mixing layer surrounding a circular jet for a number of years. In Davies and Hardin (1973) and Davies, Hardin, Edwards and Mason (1975) a model of the jet using toroidal vortices is described. As noted in Section 1, a circular *line* vortex would have infinite *self*-induced velocity. A toroidal vortex of radius R and small circular cross-section with radius r whose circulation is Γ and whose vorticity is, to leading order, uniformly distributed across its cross-section, has a self-induced velocity U, normal to the plane of the torus, given by

$$U = \frac{\Gamma}{4\pi R}\left[\ell n\,\frac{8R}{r} - \frac{1}{4}\right] + O\left(\frac{r}{R}\right) \qquad \ldots (3.1)$$

(see Lamb (1932)). Of course, as the vortex ages, its cross-section radius increases due to viscous diffusion at a rate $(4\nu t)^{\frac{1}{2}}$, where ν is kinematic viscosity and t age from a notional birth when the vorticity was concentrated in a circular line vortex. Further, although the self-induced velocity of a toroidal vortex induces no change of shape, other co-axial tori will induce a velocity field that causes the torus to increase or decrease in diameter. As we noted in Section 1, the vorticity lines in the torus will be intensified or attenuated in such a way that the total circulation will remain constant but, of course, the cross-section will be reduced or increased. The volume $2\pi^2 r^2 R$ will remain constant, so it is seen that

$$r = \left[\frac{4\nu t\, R_0}{R}\right]^{\frac{1}{2}} \qquad \ldots (3.2)$$

where R is the current radius of the torus and R_0 its radius at t = 0. So long as all the ring vortices are coaxial the mutually-induced velocities will not distort the rings from a circular shape, but only alter the ring diameters and move the vortex rings. Since the velocity field of a toroidal vortex far from that vortex tends to the velocity field of the equivalent line vortex ring, Davies *et al* used the ring vortex velocity field when computing the mutual interactions and the Equation 3.1 when computing the self-induced velocity. In fact, Davies and Hardin noted that the stream function for a line vortex ring involves two complete elliptic integrals and, rather than evaluate these, approximated the ring vortex as a 16-sided equilateral polygonal vortex and evaluated the velocity field by an appropriate evaluation of Equation 1.8. Their model represented the jet from a circular orifice and was assumed to remain axisymmetric, so ensuring that all the ring vortices remained coaxial. The flow started impulsively from rest, and at each time step a new vortex ring was introduced at a point near the jet orifice with a strength determined from $\dot{\Gamma} = \frac{1}{2}U_0^2$, as noted before, but U_0 here is the jet velocity. At subsequent time steps the velocity of each vortex ring was computed as the sum of its self-induced velocity and the mutually-induced velocities of all the rings. The velocity at points of the jet orifice would deviate from U_0 due to the vortex-induced velocities there, so the orifice was represented by a set of annular fluid sources and the strengths of these necessary to keep a uniform velocity U_0 over the orifice computed at each step and the contribution of these to

the vortex ring velocities added to the self- and mutually-induced velocities. In Davies and Hardin the resulting form of mixing layer development is compared with some Schlieren photographs of jet initial development, taken using a shock tube.

Leonard (1975, 1976) has developed a fully three-dimensional application of the discrete vortex method. In Leonard (1975) the method is first described. Closed vortex filaments of arbitrary shape and cross-section are represented by polygonal vortex filaments with circular cross-sections. The circulation of each straight element of a particular filament is the same though their cross-sections may differ. The cross-sections change through viscous diffusion and stretching or compression of the elements in the same way as Davies and Hardin described. Also, as in Davies and Hardin, the cross-section of a filament element is only used in computing the velocity induced on it by its neighbouring elements (which would otherwise be zero) and the velocity interactions on non-neighbouring elements are computed by assuming them to be ideal line vortex elements and applying Equation 1.8 appropriately. In fact, Leonard characterised the configuration at any time by recording the positions of the nodes or segment ends of each polygonal filament and the radii of the filaments. The velocities of these nodes were computed as the sum of contributions from all non-adjacent filaments considered as ideal line vortices and a contribution from the two adjacent elements. This latter contribution was computed by fitting a circular arc through the node and its two neighbours and applying an approximation to the self-induced velocity of the circular arc segment so formed, derived from work by Widnall, Bliss and Salay (1971) and Moore and Saffman (1972). The node positions were advanced by one time step and the vortex element stretching or compression computed. Using these, the core radii were updated and the process then repeated. In the 1975 work Leonard considered only flows with no solid boundaries. Results of simulations of oscillations of perturbed toroidal vortex rings, and of a pair of perturbed contra-rotating line vortices as is found in the wake of aircraft, were presented.

In the later paper, Leonard developed the model to include the simulation of a solid boundary within the flow field. Thus the problem of the unsteady vortex wake behind an arbitrary three-dimensional bluff body could be tackled. Leonard, in fact, developed the method for the flow behind a sphere. In order to satisfy the boundary conditions of no normal velocity at the sphere surface, Leonard used image vortices inside the sphere. He stated, however, that for general three-dimensional bodies it might be more convenient to solve the problem of finding the contribution to the vortex velocities made by the presence of the body directly. In fact, it seems to the author that a surface source/sink method could conveniently be used here - a point to which we shall return later. Of course, the flow past a sphere has a separating boundary layer giving rise to a separated shear layer as a circular cylinder does. Leonard modelled the production of vortices in the sphere wake by using $\dot{\Gamma} = \frac{1}{2}U_s^2$ as many authors of two-dimensional models have. He constrained the separation to occur at a fixed location on the sphere surface, so no 'feedback' effect of wake to separation location could occur, though feedback of wake conditions to $\dot{\Gamma}$ can, of course, occur. Computations were made of the impulsively started flow past a sphere with new ring vortices being fed into the wake at each time step and their motion computed as outlined above. The procedure was much the same as for a two-dimensional model with the difference being one of complexity of program organisation and length of computation time, rather than of fundamental principle. Good correlation was obtained between some flow characteristics of the model and some experimental observations.

4. THE APPLICATION OF THE METHOD TO THE PROBLEM OF THE TRAILING VORTEX SHEET OF AN AIRCRAFT WING

A field in which the discrete vortex method has made a considerable contribution is the study of the rolling up of the vortex sheet shed by a lifting wing of finite span into the trailing vortex pair. The variation of the loading across the wingspan results in a vortex sheet being shed behind the wing, whose vorticity axis is parallel to the aircraft's direction of motion and having finite width. The initially flat sheet rolls up from the edges (wingtips) inwards as it is convected downstream of the wing. Westwater (1935) proposed that the spatial development of the rolling up process might usefully be approximated by the time development of a two-dimensional sheet of finite width. He replaced the continuous sheet trailing from a wing with elliptical load distribution by discrete vortices, and computed the time development of the configuration by use of the complex potential. This study, of course, assumed that the sheet extended to infinity up and downstream of the wing and the effect of the wing itself is ignored, i.e. no attempt is made to incorporate the effect of the solid body in the flow. This assumption will be sufficiently valid if the spatial development of the sheet is slow enough for a quasi-two-dimensional situation to hold at any downstream location. Westwater's work showed the trailing sheet rolling up into two equal, opposite-signed vortex concentrations, starting from the wingtips and moving inwards in a similar form to the spiral predicted by the analysis of Kaden (1931).

Following Birkhoff and Fisher's discoveries about Rosenhead's work, Takami (1964) and Moore (1971) both repeated Westwater's work. Moore found that, using very accurate time integration procedures and two and four times the number of vortices to represent the sheet, the paths of vortices near the edges of the sheet were extremely contorted. This motion is convincingly shown to be due to the propensity of close line vortices to rotate about each other. In the body of a vortex sheet representation, close vortices on either side of any given vortex will approximately balance out the rotating effect on that vortex, but at the edge of the trailing vortex sheet the balancing is not present. Moore showed that the effect of the rapid mutual orbiting soon spread inwards along the sheet and vitiated the entire computation.

Two authors implemented *ad hoc* cures for this problem. Chorin and Bernard (1973) repeated Westwater's work using vortices whose stream function changed abruptly a small distance, σ, from the vortex, as given in Equation 2.6. The effect of this is to prevent the high mutually-induced velocities of very close vortex pairs and so reduce their propensity to circle one another. Computations performed using this device showed that the form of rolling up at the tips matched the Kaden spiral very well. Clements and Maull (1973) used Westwater's method to investigate the effect of different wing loading distributions on the rolling up process. They also found the high mutually-induced velocities near the tips and eliminated them by imposing a bound on the velocities. If this bound was exceeded, the two offending vortices were amalgamated into one vortex at the pair's centre of vorticity, thus effectively increasing the separation of the vortices in the region and reducing the maximum mutually-induced velocities. This device, whilst obviously less desirable than that proposed by Chorin and Bernard, was successful for their purpose.

Fink and Soh (1974) presented a new refinement of the discrete vortex method which they illustrated in a number of calculations including the trailing vortex sheet problem. They pointed out that the discrete vortex method is essentially a mechanism for dividing a continuous vortex sheet into short segments, each of which is then assumed to be represented by a discrete vortex equal in strength to the segment, located at the centre of vorticity of the segment. A vortex has no self-induced velocity, but the short segment of sheet represented by that vortex would induce a velocity on itself. The velocity can be represented by an integral with a singular integrand whose Cauchy principal value is

$$\frac{j\kappa_i}{2\pi} \frac{1}{z_{i+\frac{1}{2}} - z_{i-\frac{1}{2}}} \ln \left| \frac{z_i - z_{i+\frac{1}{2}}}{z_i - z_{i-\frac{1}{2}}} \right|$$

(where $z_{i+\frac{1}{2}}$ and $z_{i-\frac{1}{2}}$ are the ends of the segment and z_i is the position of the vortex of strength κ_i representing the segment) provided the segment's length is small enough for the sheet's radius of curvature to be large with respect to that length and the vorticity distribution to be virtually constant along it. This self-induced velocity will be zero if $z_i = \frac{1}{2}(z_{i+\frac{1}{2}} + z_{i-\frac{1}{2}})$, i.e. is the midpoint of the segment. This led Fink and Soh to propose that optimum results would be obtained if the vortices representing a sheet are equidistant from one another. They achieve this by rediscretising the sheet after each time step. Thus, an initially equispaced array of vortices was advanced by one time step giving a new set of non-equidistant positions. The position of the vortex sheet and its strength as a function of position were then established by interpolation from the vortex positions. A new discrete vortex representation of this sheet was then found, using equidistant vortices whose strength was varied to give the desired sheet strength at any position. The process was then repeated. Westwater and the other authors mentioned all use equistrength vortices of unequal spacing to represent the vorticity distribution in the trailing vortex sheet. The application of Fink and Soh's method to this problem led to the small spacing of the vortices near the tip being eliminated and, as might be expected, their calculations did not show the unnatural orbiting of the vortices near the edge of the sheet. Their method does, of course, lead to a greatly increased complexity of the calculation and must give rise to increased computing time, but no representative figures are mentioned.

Moore (1974) presented a computation in which the tightly-rolled portion of the vortex sheet near the tip was represented by a single vortex. He reasoned that the cause of the erratic motion observed by Takami and himself earlier was the inadequacy of a small number of vortices to effectively model the dynamics of a turn of the spiral part of the sheet. He therefore arranged that the tightly-rolled part of the sheet should be represented by a single vortex. As the sheet rolled up and the radius of curvature of the line through the tip-most vortices decreased, those vortices were amalgamated with the vortex representing the spiral. Thus the discrete vortices were not required to model the most tightly wound part of the sheet at all. Moore found, in extensive tests, that the chaotic motion was eliminated by this device and the exterior part of the sheet was accurately modelled.

Butter and Hancock (1971) presented an essentially three-dimensional computation which took into account the effects of the bound vorticity in the wing. The trailing sheet was represented by a number of vortices, each composed of straight segments between fixed planes downstream of the wing. The sheet was initially assumed to be flat, and the final shape - in which the vortex segments were everywhere approximately parallel to the local streamlines of the flow - was computed by an iterative procedure. The velocity at the centre of each segment of each trailing vortex filament was computed by an appropriate evaluation of Equation 1.8, and the segments sequentially aligned with the local flow velocity at their mid-points. The process was halted when a downstream station was reached at which the vortex filaments had small lateral displacement between one station and the next. A second iteration of the procedure was performed to obtain yet more accurate matching of segments and streamlines. An advantage of this procedure is its ability to simulate accurately the rolling up behind a swept wing. Also, unlike the two-dimensional calculations, the vortex sheet is not represented as extending to infinity in the upstream direction.

5. SOME FURTHER USES OF THE METHOD

The discrete vortex method is increasingly being used as a tool for studying many fluid flow related phenomena. The original use made of the method by Rosenhead, described in Section 2, has led logically to the work of Acton which is part of the body of work aimed at a better understanding of the mechanism of noise generation in mixing layers at the boundary of jets. Also aimed at such an understanding is the development of Davies and Hardin's work by Davies, Hardin, Edwards and Mason. In this latter paper the computed discrete ring vortex formation in the mixing layer is considered as a source for the acoustic field far from the jet. The results so obtained are encouraging as a simulation of jet noise production. Hardin and Mason (1976) have subsequently presented a model of the noise generation by a rectangular well in an infinite plane. Using a Shwartz-Christoffel transformation derived by the author, they constructed a two-dimensional model in which a flow parallel to a plane wall caused separation at the upstream corner of a rectangular cavity, the separated shear layer being simulated by discrete vortices. The model was started from rest and computed until a statistically stationary state had been achieved. The far field noise of this state was then derived. The importance of the model is as a representation of one type of airframe noise generator.

Chorin (1973) presented a method for the study of slightly viscous flow. He suggested that an initial vorticity distribution in a fluid could be modelled by a distribution of discrete vortices. These vortices would subsequently move with velocities derived from the mutual interaction of the vortices, together with any underlying inviscid irrotational flow field and at each time step a further perturbation would be applied to each vortex position to simulate the small viscous diffusion. This further perturbation was a random variable with Gaussian distribution of zero mean and variance $2\delta t/R$ where δt was the time step used and R the Reynolds number. This random perturbation, computed using a random number generating algorithm, provided an appropriate spreading of the vorticity in the flow as would be caused by small viscosity. The vortices, or 'vortex blobs' as Chorin called them, had the same stream function as was used by Chorin and Bernard (1973). Chorin applied the method to the wake of a circular cylinder in slightly viscous flow. The boundary condition on the cylinder was satisfied by computing a suitable source distribution over the surface to negate the normal velocities induced across the surface by the vortex blobs. New vortices were generated at the cylinder surface at each time step, their strengths being determined by the necessity of making the tangential velocity at the surface zero. Old vortices that, due to the random component of motion, crossed the boundary, were removed from the flow. Chorin stated that a three-dimensional version of the method was under development.

In Clements (1973b) and Clements and Maull (1975) a series of extensions of the model described in Clements (1973a) are developed. Amongst these are models of the flow behind a blunt-based body with low velocity base bleed, which exhibited the same effects as found by Bearman (1967) and of the same body when subjected to cross-stream oscillations, which again correlated well with experimental results. A model of the flow behind a blunt-based section with a base cavity did not correlate with experimental data. It was suggested that a secondary separation within the cavity might occur in the real flow and since the model did not consider this possibility, this could explain the poor agreement. This comment highlights one of the potential failings of discrete vortex models - the user must identify *all* the separation points and adequately model the vortex production at each. Neglect of secondary separation can vitiate the whole model, so a certain amount of inspired foresight could be necessary to achieve a satisfactory model in some circumstances! A model of the flow down a step in a plane wall showed good agreement with experiment only

when a large proportion of the vorticity was subsequently removed as it came near to the wall downstream of the step. Again, a possible explanation was advanced in that there is some experimental evidence for a three-dimensional mechanism whereby vorticity is expelled from the separation bubble into the downstream flow. Clements and Maull (1975) make a telling comment on discrete vortex methods: " ... the fundamental assumptions of the (two-dimensional) discrete vortex method - two-dimensional, inviscid flow with vorticity confined to small and well-defined regions - are quite severe, and careful examination of each flow situation for which a model is made is necessary to ensure that such assumptions are reasonable. Conversely, this weakness can be a strength in that, if a model is constructed with these assumptions and, whilst being credible and consistent within itself, it fails to predict experimental results, this points to the importance of the neglected effects in determining, to some extent, the pattern of the flow. In this way, the failure of a model can sometimes be as illuminating as its success!" Clements (1973b) also contains a description of a model of the flow from a slit jet and behind a blunt-based body fitted with a splitter plate. The latter model correlated extremely badly with experimental results. Again, this failure may be associated with an imperfect understanding of the mechanics of re-attachment of separated shear layers that approach a boundary closely. The slit jet model performed well, and subsequent development has included the simulation of markers in the jet interior fluid. Turbulent dispersion of the markers was simulated by a method similar in conception to Chorin's viscous diffusion simulation. This study was aimed at predicting the entrainment of effluents into the ring vortex formed at a chimney orifice.

Fink and Soh (1971) applied the method to the simulation of the vortex formation near a ship's bilge keel undergoing heaving motion. Their computation used a Kutta condition to determine the strength of new vortices introduced at a fixed point near the separation point. Following their development of the re-discretisation method, Fink and Soh (1974) describe applications of the method to the single vortex sheet problem of Rosenhead, to vortex formation at the tip of a semi-infinite plate moving normally to its plane, to vortex shedding behind a finite plate normal to the flow and to vortex shedding from slender lifting surfaces as well as the trailing vortex calculation described in Section 4.

The work of Zaroodny and Greenberg (1973) has pointed out an interesting application of the method in water wave analysis. They presented a model of arbitrarily large amplitude, though non-breaking, shallow-water waves. The flow in such water can be represented as that due to a sheet vortex on the water surface and another on the bed. The motion of a wave of initially given shape and vorticity distribution can be computed from the known relationship of these to the free surface motion and change of vorticity distributions. Zaroodny and Greenberg give integrals for the fluid velocity at any point in the fluid in terms of the vorticity distributions, but do not state how these are evaluated. It is evident, though, that the integrals can essentially be approximated by finite sums representing contribution from vorticity at points on the free surface and bed of the fluid region, or equivalently the vorticity distributions can be approximated by discrete vortices and the motion of the waves computed from the induced motion of these vortices.

Wardlaw (1975) has used the discrete vortex model of the flow past a circular cylinder to approximate the development of the vortices shed on the lee side of a cylindrical body whose axis is at an angle of attack to the oncoming flow (a manoeuvring missile body, for instance). He considers the impulsively-started flow past an initially expanding cylinder in a similar manner to the vortex shedding cylinder computations mentioned above. The effect of the expanding cylinder, which represents the effect of the tapered nose, is represented by a source term at the cylinder centre and the cylinder radius is increased appropriately in the initial stages of the computation. In computing the force coefficients on the cylinder, an attempt is made to allow for the effects of compressibility, although Wardlaw states that the method used is not strictly applicable to the flow conditions involved.

Kuwahara and Swenson (1971) presented a study of the stability of an arrangement of geostrophic vortices which was inspired by a problem in meteorology. Their problem was that of the motion of N identical vortices equally spaced around the perimeter of a circle at whose centre was another, not necessarily identical, vortex. The stream function of each vortex was of the form

$$\psi(x,y) = \frac{K}{2\pi} Y_0\{\mu((x - x_0)^2 + (y - y_0)^2)^{\frac{1}{2}}\} \qquad \ldots (5.1)$$

where Y_0 is the Bessel function of the second kind. In the limit $\mu \to 0$ this becomes the stream function of an ordinary two-dimensional line vortex. Such vortices occur in the approximation of meteorological fluid dynamics as nearly horizontal motion in the globe tangent plane. A linear stability analysis of the configuration was presented and the non-linear motion following a number of perturbations of the configuration was calculated using velocities derived from Equation 5.1. Variations of the parameter μ, essentially an

inverse length scale, of the relation of the centre vortex to the peripheral vortices and of the number of peripheral vortices were presented.

A flow computation method described by Christiansen (1970, 1973) should be mentioned in the context of discrete vortex methods, although it is essentially a hybrid of this method and the fixed Eulerian grid techniques of computation. Christiansen started from the standard transformation of the equations of incompressible inviscid flow

$$\left.\begin{aligned} \frac{\partial \underline{u}}{\partial t} + \underline{u}.\nabla\underline{u} + \frac{1}{\rho}\nabla p = \underline{0} \\ \nabla.\underline{u} = 0 \end{aligned}\right\} \qquad \ldots (5.2)$$

in which, for two-dimensional flow, one can introduce a stream function ψ such that $\underline{u} = \nabla \times (0,0,\psi)$. The equations 5.2 can then be written

$$\left.\begin{aligned} \zeta_t + \psi_y \zeta_x - \psi_x \zeta_y = 0 \\ \zeta = -\nabla^2\psi \end{aligned}\right\} . \qquad \ldots (5.3)$$

In fact, $\nabla \times \underline{u} = (0,0,\zeta)$, so ζ is the vorticity. In Christiansen's work the vorticity distribution $\zeta(x,y)$ was represented by a distribution of a large number of identical line vortices. The equivalent vorticity at the vertices of a fixed grid was computed by taking a weighted sum of the point vortices near that grid point. The stream function was then computed at the grid points by numerically solving Equation 5.3b. From the stream function the vortex velocities were computed by taking a weighted mean of the derivatives of the stream function at the four nearest grid points. In Christiansen and Zabusky (1973) some numerical experiments were reported. Using 3200 line vortices and a 64 × 64 grid they studied the single vortex sheet problem and the evolution of a number of vortex street-like configurations. In these experiments the number of vortices handled is much larger than that used in typical discrete vortex computations. In the usual discrete vortex computations each vortex velocity is the sum of contributions from every other vortex, thus the computation of velocities of 3200 vortices at each time step by the conventional method would be an unwieldy and costly undertaking. Christiansen's use of a grid enables him to compute the velocities at the grid points relatively quickly and then interpolate the velocities of the vortices, thus reducing the cost of the computation. On the other hand, a fixed grid is introduced and one of the most attractive features of the usual method, its economy in following the flow features which are of most interest, is lost.

6. DISCUSSION

From the description of the uses made of the method, it will be evident that its use in two-dimensional flow models is well established and its extension to axisymmetric and three-dimensional flow situations is under way. In two-dimensional models its use is almost invariably associated with the use of complex potential methods for computing the mutually-induced velocities of the vortices. The availability of a complex potential for any given boundary conditions is somewhat problematical and we are by no means guaranteed its existence. The literature reveals the use of several devices for obtaining potentials in the presence of boundaries. Milne-Thomson's circle theorem made possible the models of flow past circular cylinders. The use of Shwartz-Christoffel transformations was the basis of this author's contributions to the field. Sarpkaya used another conformal transformation to create his flat plate model. All of these means, of course, satisfy the boundary conditions exactly. There remains the possibility of using an approximate solution for the underlying potential flow field and boundary conditions such as the surface source/sink method described by Hess and Smith (1967). In this method the strengths of an arrangement of line sources distributed over the solid boundaries of the flow are found by satisfying the no-flow conditions across these boundaries. The only use of such a method known to the author is that in Chorin (1973) described above. The use of this method could greatly extend the class of problems which can be modelled using discrete vortices and, further, could be extended easily to the three-dimensional flows, in which case the line sources are replaced by point sources. The generalised Shwartz-Christoffel transformation of Soh (1971) also promises help here, though I have not yet been able to obtain a copy of this work. The problem of finding a complex potential is one that is susceptible to solution given persistence and ingenuity in the user. For axisymmetric and three-dimensional computations the mutual velocities are generally evaluated from forms of the integral in Equation 1.8. The general induction formula for the velocity induced by a segment of vortex line of circulation κ lying along $\underline{\ell}$, centre $\underline{x}'$

$$\underline{u}(\underline{x}) = -\frac{\kappa}{4\pi}\frac{(\underline{x} - \underline{x}') \times d\underline{\ell}'}{|\underline{x} - \underline{x}'|^3}$$

is known as the Biot-Savart induction law. In general it is not possible to evaluate the integral in Equation 1.8 exactly, and the approach of Davies and Hardin, and Leonard has been to approximate a curvi-

linear line vortex by a series of straight line segments and evaluate Equation 1.8 over this approximate curve.

Consideration of the stability and accuracy of the method in the computations made has been largely limited to the use of discretion in the evaluation of results and, usually, the testing of models to gauge the effects of changes in time step size and other parameters. The work of Moore on the rolling up of the trailing vortex sheet has been valuable in this respect and it has been commented that one particular source of trouble in a tightly rolled up sheet is when vortices in neighbouring rolls of the spiral are typically closer than neighbouring vortices in the same roll. Several authors have sounded *caveats* about expecting discrete vortex models to reveal very much about the fine structure of vortex flows.

An area in which problems arise is that of the generation of vorticity and the way in which the boundary layers, the separated shear layers and the discrete vortex approximations to the latter are related. Those authors who have considered models of the flow past cylinders have almost all commented on some such problems. Chaplin and Laird both used vortices near the front cylinder surface to represent the boundary layer there and both experienced difficulties in keeping the boundary layers "attached". Both authors had fixed the separation points. When Deffenbaugh and Marshall allowed the separation points to be freely determined an unrealistic result followed which they traced to the undue influence of the nearest line vortices, or equivalently to the failing of the discrete vortex method to model the flow very near a shear layer adequately. Yang and Bar-Lev (1976) have made a promising contribution to this problem in which a boundary layer expansion in powers of elapsed time, valid for small time, for the impulsive start of flow past a cylinder is combined with a two-vortex model of the wake. It is the author's opinion that special attention will have to be given to the matching of separation and wake conditions before an adequate solution can be found and that an 'inner' model of part of the flow field which will bridge the gap between boundary layer and discrete vortices could elucidate the relationship. This line is being actively pursued.

Another area requiring special attention is that of the mechanics of shear layers which, after some period in the main flow, approach flow boundaries. Authors faced with this problem have usually eliminated vortices which approach closer than some small distance to such boundaries (e.g. Sarpkaya, Clements, Hardin and Mason, and others). This procedure has served well in cases where the part of the boundary concerned is a small one, like the rear face of the shedding body, which is approached by vortices only exceptionally. However, in Clements' models of the flow down a step and of the blunt-based body with a splitter plate where reattachment is an integral feature of the flow, this mechanism is not satisfactory and further work to resolve this problem is necessary. It is notable that lack of adequate representation of the reattachment process resulted in the models more or less failing.

For the future it may be expected that the discrete vortex method will make a considerable contribution to the study of aerodynamic noise generation. The work of Davies, Hardin, Mason, Acton, Moore and Saffman have all contributed to the development of this field. Acton expressed disappointment that her work indicates that the vortex pairing process was not particularly sensitive to initial conditions, so control of the process through such conditions did not seem feasible. Nonetheless, much may be added to our understanding of the process by such models. The work of Hardin and Mason could well be extended to models of aerodynamic noise generation by other airframe non-uniformities than the rectangular cavity - a V-notch, a rectangular projection and a V-projection all seem obvious candidates.

The flat plate at incidence modelled by Sarpkaya and Belotserkovskii should lead to a model of a thin aerofoil operating in a severely stalled regime - of great interest in the prediction of the characteristics of high-performance military aircraft in violent manoeuvres. Once a better understanding of the mechanism of shear layer reattachement is established, it will be possible also to use the discrete vortex method to model the buffet loads on bodies in separated regions. The wake may either be from another upstream body, or from an upstream section of the same body. In either case, the dynamics of the separated region can be modelled by the discrete vortex method and the loading on the buffeted body calculated from the effect of this representation of the separated flow on that body.

Other uses than those outlined above exist, and will be developed in the future. The method has reached a stage of versatility and accuracy that demands its consideration as a serious tool of the aerodynamicist's trade.

REFERENCES

ABERNATHY, F.H. and KRONAUER, R.E. (1962): *The formation of vortex streets.* J. Fluid Mech., 13, 1.

ACTON, E. (1976): *The modelling of large eddies in a two-dimensional shear layer.* J. Fluid Mech., 76, 561.

BATCHELOR, G.K. (1967): *An introduction to fluid dynamics.* Cambridge University Press.

BEARMAN, P.W. (1965): *Investigation of the flow behind a two-dimensional model with a blunt trailing edge and fitted with splitter plates.* J. Fluid Mech., 21, 241.

BEARMAN, P.W. (1967): *The effect of base bleed on the flow behind a two-dimensional model with a blunt trailing edge.* Aero. Quart., 18, 207.

BEAVERS, G.S. and WILSON, T.A. (1970): *Vortex growth in jets.* J. Fluid Mech., 44, 97.

BELOTSERKOVSKII, S.M. and NISHT, M.I. (1975): *Investigation of special features of flow over a flat plate at large angles of attack.* Fluid Dynamics, 8, 772. (Translated from Russian by Consultants Bureau, New York).

BIRKHOFF, G.D. and FISHER, J. (1959): *Do vortex sheets roll up?* Rc. Circ. Mat. Palermo Ser., 2, 8, 77.

BROWN, G.L. and ROSHKO, A. (1974): *On density effects and large structures in turbulent mixing layers.* J. Fluid Mech. 64, 775.

BUTTER, D.J. and HANCOCK, G.J. (1971): *A numerical method for calculating the trailing vortex system behind a swept wing at low speed.* Aero. J. Royal Aero. Soc., 75, 564.

CHAPLIN, J.R. (1973): *Computer model of vortex shedding from a cylinder.* Proc. ASCE Hyd. Div., 99, 155.

CHORIN, A.J. (1973): *Numerical study of slightly viscous flow.* J. Fluid Mech., 57, 785.

CHORIN, A.J. and BERNARD, P.S. (1973): *Discretisation of a vortex sheet with an example of roll-up.* J. Comp. Phys., 13, 423.

CHRISTIANSEN, J.P. (1970): *Vortex - a two-dimensional hydrodynamics simulation code.* UKAEA Culham Lab. Rep., CLM-R106, HMSO.

CHRISTIANSEN, J.P. (1973): *Numerical simulation of hydromechanics by the method of point vortices.* J. Comp. Phys., 13, 363.

CHRISTIANSEN, J.P. and ZABUSKY, N.J. (1973): *Instability, coalescence and fission of finite area vortex structures.* J. Fluid Mech., 61, 219.

CLEMENTS, R.R. (1973a): *An inviscid model of two-dimensional vortex shedding.* J. Fluid Mech., 57, 321.

CLEMENTS, R.R. (1973b): *Computer models of separated flows behind two-dimensional bluff bodies.* Ph.D. Thesis, Cambridge University.

CLEMENTS, R.R. and MAULL, D.J. (1973): *The rolling up of a trailing vortex sheet.* Aero. J. Royal Aero. Soc., 77, 46.

CLEMENTS, R.R. and MAULL, D.J. (1975): *The representation of sheets of vorticity by discrete vortices.* Prog. Aerospace Sci., 16, 129.

DAVIES, P.O.A.L. and HARDIN, J.C. (1973): *Potential flow modelling of unsteady flow.* Int. Conf. on Numerical Methods in Fluid Mechanics, University of Southampton.

DAVIES, P.O.A.L., HARDIN, J.C., EDWARDS, A.V.J. and MASON, J.P. (1975): *A potential flow model for calculation of jet noise.* AIAA Paper 75-441, presented at AIAA 2nd Aero-Acoustics conference, Hampton, Va, USA.

DAVIS, D.M. (1970): *An analytical study of separated flow about a circular cylinder.* M.Sc. Thesis, Naval Postgrad. School, Monterey, Calif., USA.

DEFFENBAUGH, F.D. and MARSHALL, F.J. (1976): *Time development of the flow about an impulsively started cylinder.* AIAA J., 14, 908.

FAGE, A. and JOHANSEN, F.C. (1927): *On the flow of air behind an inclined plate of infinite span.* Proc. Royal Soc. A., 116, 170.

FINK, P.T. and SOH, W.K. (1974): *Calculation of vortex sheets in unsteady flow and applications in ship hydrodynamics.* Tenth Symp. Naval Hydrodynamics, Cambridge, Mass., USA.

GERRARD, J.H. (1967): *Numerical computation of the magnitude and frequency of the lift on a circular cylinder.* Phil. Trans. Royal Soc., 261, 137.

HAMA, F.R. and BURKE, E.R. (1960): *On the rolling up of a vortex sheet.* University of Maryland, TN No. BN-220.

HARDIN, J.C. and MASON, J.P. (1976): *A vortex model of cavity flow.* AIAA Paper 76-524, presented at AIAA 3rd Aero-Acoustics conference, Palo Alto, Calif., USA.

HESS, J.L. and SMITH, A.M.O. (1967): *Calculation of potential flow about arbitrary bodies.* Prog. Aerospace Sci., 8, 1.

KADEN, H. (1931): *Aufwicklung einer unstabilen unstetigkeits fläche.* Ing. Arch., 2, 140.

LAIRD, A.D.K. (1971): *Eddy formation behind circular cylinders.* Proc. ASCE Hyd. Div., 97, 763.

LAMB, H. (1932): *Hydrodynamics.* (6th Edition)., Dover, 1945.

LEONARD, A. (1975): *Numerical simulation of interacting, three-dimensional vortex filaments.* Lecture Notes in Physics, 35, 245, Springer-Verlag, Berlin.

LEONARD, A. (1976): *Simulation of three-dimensional separated flows with vortex filaments.* To appear in Lecture Notes in Physics.

MICHALKE, A. (1963): *On the instability and non-linear development of a disturbed shear layer.* Hermann Föttinger - Inst. fur Strömungstechnik, University of Berlin TN No.2 (in English), also Ing. Archiv., 33, 264 (in German).

MILNE-THOMSON, L.M. (1938): *Theoretical hydrodynamics.* Macmillan & Co.

MOORE, D.W. (1971): *The discrete vortex approximation of a finite vortex sheet.* Cal. Inst. Tech. Rep. AFOSR-1804-69.

MOORE, D.W. (1974): *A numerical study of the roll-up of a finite vortex sheet.* J. Fluid Mech., 63, 225.

MOORE, D.W. and SAFFMAN, P.G. (1972): *The motion of a vortex filament with axial flow.* Phil. Trans. Roy. Soc., 272, 403.

MOORE, D.W. and SAFFMAN, P.G. (1975): *The density of organised vortices in a turbulent mixing layer.* J. Fluid Mech., 69, 465.

PIERCE, D. (1961): *Photographic evidence of the formation and growth of vorticity behind plates accelerated from rest in still air.* J. Fluid Mech., 11, 460.

ROSENHEAD, L. (1931): *Formation of vortices from a surface of discontinuity.* Proc. Roy. Soc. A., 134, 170.

SARPKAYA, T. (1966): *Separated flow about lifting bodies and impulsive flow about cylinders.* AIAA J., 4, 414.

SARPKAYA, T. (1968): *An analytical study of separated flow about circular cylinders.* Trans. ASME J. Basic Engng., 90, 511.

SARPKAYA, T. (1975): *An inviscid model of two-dimensional vortex shedding for transient and asymptotically steady separated flow over an inclined plate.* J. Fluid Mech., 68, 109.

SOH, W.K. (1971): *An approximate solution for the generalised Shwartz-Christoffel transformation.* University of New South Wales, School of Mechanical Engineering, Engng. Rep. Nav. Arch., 71/3.

SOH, W.K. and FINK, P.T. (1971): *On potential flow modelling of the action of ships' bilge keels.* 4th Aust. Conf. Hyd. Fluid. Mech., Monash University.

TAKAMI, H. (1964): *Numerical experiment with discrete vortex approximation, with reference to the rolling up of a vortex sheet.* Dept. of Aero. and Astronaut., Stanford University Rep. SUDAER 202.

WARDLAW, A.B. (1975): *Multivortex model of asymmetric shedding on slender bodies at high angle of attack.* AIAA Paper 75-123.

WESTWATER, F.L. (1935): *The rolling up of a surface of discontinuity behind an aerofoil of finite span.* ARC R & M 1692.

WIDNALL, S., BLISS, D. and ZALAY, A. (1971): *Theoretical and experimental study of the stability of a vortex pair, in aircraft wake turbulence and its detection.* Ed. Olsen, J.H., Goldburg, A. and Rogers, M. Plenum Press, New York.

WINANT, C.D. and BROWAND, F.K. (1974): *Vortex pairing: the mechanism of turbulent mixing layer growth at moderate Reynolds number.* J. Fluid Mech., 63, 237.

YANG, H.T. and BAR-LEV, M. (1976): *Potential flow model for an impulsively started circular cylinder.* Trans. ASME Ser. E., 43, 213.

ZAROODNY, S.J. and GREENBERG, M.D. (1973): *On a vortex sheet approach to the numerical calculation of water waves.* J. Comp. Phys., 11, 440.

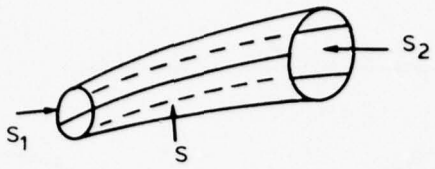

FIG. 1·1. A vortex tube. S is a surface composed of vortex lines, S_1 and S_2, the ends of a length of tube.

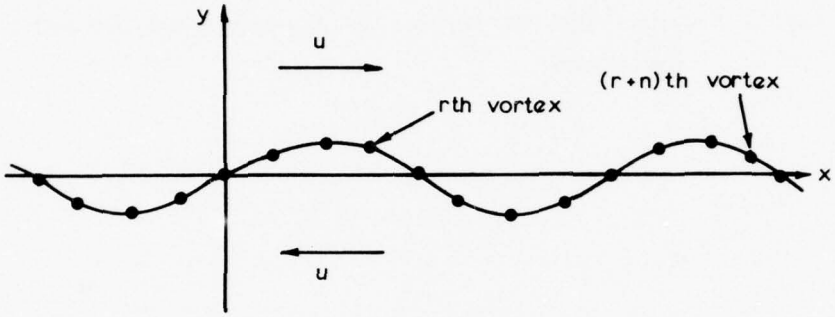

FIG. 2·1. Initial state of vortex arrays in Rosenhead's calculation.

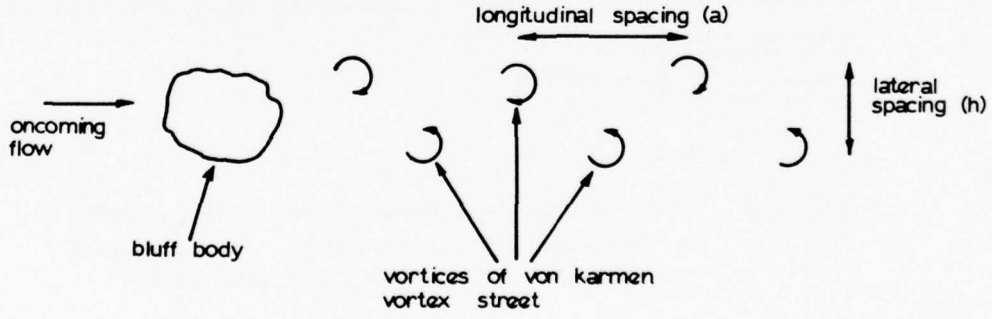

FIG. 2·2. General arrangement of a bluff body and its vortex wake in a steady flow.

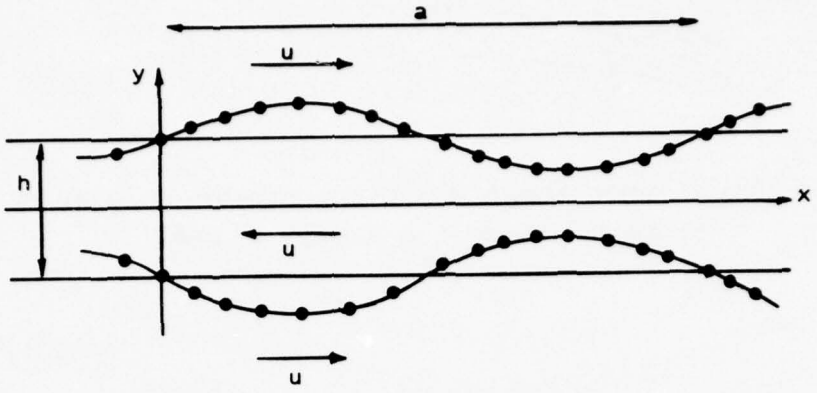

FIG. 2.3. Initial state of vortices in Abernathy and Kronauer's computation

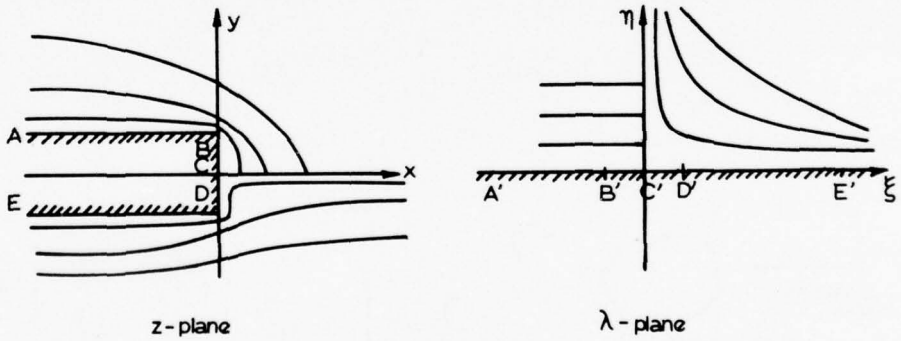

FIG. 2.4. Effect of conformal transformation mapping exterior of blunt based body to half plane. Two equivalent pairs of flows in the two planes are shown.

SOME FINITE ELEMENT METHODS IN FLUID FLOW

R. TEMAM
Faculté des Sciences Mathématiques
Université de Paris, France

Introduction.

We describe in this paper some finite element methods which has been recently introduceed for the computation of viscous and inviscid incompressible flows. The reader is assumed to be somehow familiar with the general theory of finite element methods and is referred to the basic references on the subject for the fundamental aspects of the theory.

Section 1 is devoted to the description of some finite element methods of the displacement type which apply to viscous flows, with emphasize on a linear non conforming finite element. We start by recalling the principle of the weak (or variational) formulation for the Stokes and Navier Stokes equations, and their Galerkin-finite element discretization, and then we describe some appropriate finite elements which approximate the space of divergence free vector functions.

In the case of fluid flow problems, all the numerical difficulties are not automatically overcomed by introducing a finite element discretization, and in some cases some further procedures may be desirable. Precisely Section 2 is devoted to numerical procedures which are related to the effective treatment of the constraint $\operatorname{div} u = 0$, in relation with the solution of the discrete problems arising in Section 1. At this occasion we consider a penalty method, an extrapolation algorithm, some iteration algorithms based on optimization procedures, and the augmented lagrangian method which combines the different features. Combining the technics introduceed in the first two Sections, some problems corresponding to moderate Reynolds numbers has been treated in references which are indicated in the text.

In Section 3 we introduce an interesting finite element applying to the Euler equations, which somehow, takes into account the hyperbolic character of the equations, and allows tangential discontinuities.

This paper of expository nature relies on several references which are recalled in the text. Also it relies on, and it is a complement to a recent book on the theory and numerical analysis of Navier Stokes Equations (R.T. [13]).

Plan

1. Discretization by the Finite Element Method

1.1. Weak (or Variational) Formulation of the Stokes and Navier Stokes Equations.

Let Ω be an open bounded domain in the plane R^2 and let us denote by Γ its boundary. Steady incompressible flows in Ω are governed by the Navier Stokes equations which we write in the non-dimensional form

$$(1.1) \qquad -\frac{1}{Re}\Delta u + (u.\nabla)u + \nabla p = f \quad \text{in} \quad \Omega ,$$

$$\nabla u = 0 \quad \text{in} \quad \Omega \,, \tag{1.2}$$

$$u = g \quad \text{on} \quad \Gamma \tag{1.3}$$

where $u = \{u_1, u_2\}$ is the velocity vector and p is the pressure.

For the sake of simplicity we will sometime assume that $g = 0$ (which is never an essential simplification) or we will consider as a model the Stokes equations obtained by droping the nonlinear term $(u.\nabla)$ in (1.1).

In order to get the weak formulation of this problem, we consider a vector test function v which vanishes on Γ and is divergence free ; we multiply (1.1) by v , integrate over Ω , integrate by part using Green's formula and we obtain

$$-\frac{1}{Re}\int_\Omega \Delta u.v \, dx = -\frac{1}{Re}\sum_{i=1}^{2}\int_\Gamma \frac{\partial u_i}{\partial \nu} v_i \, d\ell + \frac{1}{Re}\int_\Omega (\nabla u_1.\nabla v_1 + \nabla u_2.\nabla v_2)\, dx \,,$$

$$\int_\Omega \nabla p.v \, dx = \int_\Gamma pv.\nu \, d\ell - \int_\Omega p(\nabla v)\, dx = 0$$

$(dx = dx_1\, dx_2)$ so that

$$\frac{1}{Re}\, a(u,v) + b(u,u,v) = (f,v) \tag{1.4}$$

where

$$a(u,v) = \int_\Omega (\nabla u_1.\nabla v_1 + \nabla u_2.\nabla v_2)\, dx \,, \tag{1.5}$$

$$b(u,v,w) = \int_\Omega [(u.\nabla)v]w \, dx \,, \tag{1.6}$$

$$(f,v) = \int_\Omega fv \, dx \,. \tag{1.7}$$

The relation (1.4) will hold for each v such that

$$\nabla.v = 0 \quad \text{in} \quad \Omega \,, \quad v = 0 \quad \text{on} \quad \Gamma \,. \tag{1.8}$$

Conversely it can be proved that if $\nabla u = 0$, $u = g$ on Γ and (1.4) holds for all such v's , then there exists p such that (1.1) is satisfied. The relation (1.4) which characterizes u , represents merely the virtual work principle, v standing for some arbitrary increment δu of u .

The problem of finding u which satisfies (1.2)-(1.3) and (1.4) for each v of type (1.8) is called the weak (or variational) formulation of problem (1.1)-(1.3).

Remark 1.1. The weak formulation of the equations only involves u : then the pressure p will be found a posteriori, once the function u , solution of (1.4), is known.

Remark 1.2. In the nonlinear case, the relation (1.4) does not correspond to any minimization or any variational property of the function u . The terminology "variational formulation" is however admitted by analogy with similar situations in elasticity or the calculus of variations.

Also, in the linear case (i.e. when $(u.\nabla)u$ in (1.1) and $b(u,u,v)$ in (1.4) are deleted), the relation (1.4) characterizes u as the minimizing function of the expression

(1.9) $$E(w) = \frac{1}{2Re}\, a(w,w) - (f,w)$$

among all the functions w which satisfy (1.2)-(1.3). This property will be useful.

1.2. Galerkin and Finite Element Methods.

Let us denote by $\mathbf{V}(g)$ the space of vector functions u which satify (1.2)-(1.3).

A Galerkin approximation of Problem (1.4) consists in choosing a subspace $\mathbf{V}_h(g)$ of finite dimension m , and looking for u_h in $\mathbf{V}_h(g)$ which satisfies (1.4) for each $v \in \mathbf{V}_h(g)$. The problem then reduces to a set of quadratic equations for the component of u_h in a basis of $\mathbf{V}_h(g)$.

The conforming finite element methods consist in particular choices of the subspaces $\mathbf{V}_h(g)$, for which these equations are simplified (sparse matrices for their linearized form). More generally in the non conforming finite element methods, we introduce a similar problem with a finite dimensional space $\mathbf{V}_h(g)$ which is not included in $\mathbf{V}(g)$ but only "close", at the limit, to such a space.

The domain Ω is assumed to be covered by a family $\mathcal{T}_h$ of triangles K ; the following conditions are required :

(1.10) $$\Omega_h = \bigcup_{K \in \mathcal{T}_h} K \subset \Omega .$$

(1.11) If K and $K' \in \mathcal{T}_h$ then either $K = K'$, or $K \cap K'$ is empty or $K \cap K'$ is exactly a vertice or a complete edge of K and K' .

We will use the following notations

$$\rho_h = \sup_{K \in \mathcal{T}_h} \rho(K) , \qquad \rho'_h = \inf_{K \in \mathcal{T}_h} \rho'(K)$$

$$\theta_h = \inf_{K \in \mathcal{T}_h} \theta(K)$$

where $\rho(K)$ is the diameter of K , $\rho'(K)$ the diameter of the greatest ball included in K and $\theta(K)$ is the smallest angle in the triangle K .

As usual we will consider mesh refinments corresponding to $\rho_h \to 0$ with

$$\theta_h \geq \theta_0 > 0 .$$

1.3. Linear Non conforming Elements.

For simplicity we set $g = 0$.

We introduce the set $\mathbf{W}_h(0)$ of functions v_h of the following type :

- v_h is linear on each triangle ;
- the nodal values of v_h are the values of v_h at the mid-edges of the triangles $K \in \mathcal{T}_h$;
- $v_h(M) = 0$ at the boundary nodes (i.e. the boundary mid-sides) and $v_h(M)$ = an arbitrary vector, for each interior node (= interior mid-side).

Note that v_h is generally discontinuous along each side.

In order to take into account the constraint $\nabla.v = 0$, we also introduce the following subspace $\mathbf{V}_h(0)$ of $\mathbf{W}_h(0)$: $v_h \in \mathbf{V}_h(0)$ if $v_h \in \mathbf{W}_h(0)$ and $\nabla.v_h$ (which is piecewise constant) $= 0$ on each triangle.

The approximate version of (1.4) (with $g = 0$) is : to find $u_h \in \mathbf{V}_h(0)$ such that

$$\frac{1}{Re}\, a_h(u_h,v_h) + b_h(u_h,u_h,v_h) = (f,v_h)\ ,\ \forall\, v_h \in \mathbf{V}_h(0)\ , \tag{1.12}$$

where

$$a_h(u_h,v_h) = \sum_K \int_K (\nabla u_{1h}\ \nabla v_{1h} + \nabla u_{2h}\ \nabla v_{2h})\ dx$$

$$b_h(u_h,v_h,w_h) = \sum_K \int_K [(u_h.\nabla)v_h].w_h\ dx\ .$$

The problem (1.12) is not easy to solve because of the constraints $\nabla.u_h = \nabla.v_h = 0$ on each K. We will describe in Section 2 appropriate algorithms for the solution of these discrete equations.

Remark 1.3. i) These elements had been introduceed and studied by Crouzeix-Raviart [2]. It is shown in [14] that in the linear case the L^2-norm of the error between u and u_h is of the order of ρ_h^2 for the functions themselves and of the order of ρ_h for their derivatives.

ii) A basis of $\mathbf{V}_h(0)$ may be useful for the solution of the Stokes problem, or in the non-linear case for the solution of similar problems arising during an iterative procedure. This basis was explicited by Crouzeix and used by Thomasset (cf. [14]).

iii) These non conforming linear elements are the simplest elements which take into account the constraint $\nabla.u = 0$.

One can think of using simpler elements : the conforming linear elements, i.e. elements which are continuous, linear on each triangle (the nodal values are the values at the vertices), and which satisfy $\nabla.v_h$ (which is constant) $= 0$ on each K. Unfortunately it was found by M. Fortin [4] that this impose too many linear constraints so that the space $\mathbf{V}_h(0)$ can be reduceed to $\{0\}$ (this is already the case for a rectangular domain with the triangulation shown in figure 1). To overcome this difficulty, a weaker form of the condition div $v_h = 0$ has been proposed : average of div $v_h = 0$, average taken on all the triangles around one vertice.

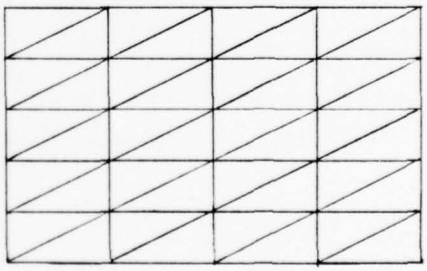

Figure 1

iv) Let us indicate an estimation of the dimension of the space $\mathbf{V}_h(0)$, when the number of triangles is sufficiently large.

Let T, E, Y denote the total number of triangles, edges and vertices in the triangulation. Then $T - E + Y$ is a constant depending only on Ω ($= 1$ if Ω is simply connected). If the number of triangles is sufficently large so that the number of boundary triangles is negligible, then $E \approx \frac{3T}{2}$ and $Y \approx \frac{T}{2}$. For linear non conforming elements, the dimension of $\mathbf{V}_h$ is the number of nodal values less the number of independant linear constraints : $\dim \mathbf{V}_h(0) \approx 2\,E - T \approx 2T \approx 4Y$.

1.4. Other Finite Elements.

Let us mention some other elements which has been proposed.

The quadratic elements has been proposed by M. Fortin (cf. [4], [13]). The functions $v_h \in \mathbf{V}_h(0)$

are continuous and reduce one each triangle to a polynomial of degree 2 ; the nodal values are the values of v_h at the vertices and the mid edges (the nodal values are 0 on the boundary nodes). Furthermore div $v_h = 0$ on each triangle.

In the linear case the error between a solution u of (1.4) and u_h of (1.12), is not optimal : the L^2 norm of the error of the derivatives is ρ_h and the L^2 norm of the functions themselves is ρ_h^2 .

Crouzeix and Raviart [2] have proposed to add on each triangle a bulb function, which is a polynomial of degree 3 vanishing identically on the boundary of K ; in the linear case the error becomes optimal : ρ_h^2 for the L^2 norm of the error between the derivatives, ρ_h^3 for the L^2 norm error for the functions.

Finally M. Bercovier introduces in [1] a quadrangular finite element. The sets $K \in \mathcal{T}_h$, $K \subset \Omega$, are quadrangles and we assume for simplicity that they are rectangles. On each rectangle v_h is a polynomial of degree ≤ 2 with respect to each variable x_1, x_2, and the nodal values are the $2 \times 8 = 16$ values of v_h at the vertices and mid-edges. The condition on the divergence is that $\text{div}_h\, v_h = 0$ on each rectangle where

$$\int_K \text{div}_h\, v_h\, r\, dx = \int_K \text{div}\, v_h\, r\, dx ,$$

for each rectangle K and each polynomial function $r \in Q_1$ (polynomes of degree ≤ 1 with respect to each variable). It is shown (cf. [1]) that $\text{div}_h\, v_h$ is defined by its value at the 4 points α_i , $1 \leq i \leq 4$ of Gauss integration on K and at these points we have precisely

$$\text{div}_h\, v_h(\alpha_i) = \text{div}\, v_h(\alpha_i) .$$

The conditions imposed on the v_h are then

$$\text{div}\, v_h(\alpha_i) = 0 , \quad i = 1,\ldots,4 .$$

Also, when non divergence free vector functions have to be considered, we note that

$$\int_K (\text{div}_h\, u)^2\, dx = \sum_{i=1}^{4} \omega_i\, (\text{div}\, u(\alpha_i))^2$$

which means that the integral in the left hand side is exactly computed by a Gauss integration formula.

The L^2 norm error between the derivatives of u and u_h is of the order of ρ_h^2 (cf. [1]).

1.5. Approximation of the pressure.

To make our notations systematic, we will denote by $\mathbf{W}_h(g)$ the spaces of finite elements previously introduceed (without any condition on div v_h) and by $\mathbf{V}_h(g)$ the corresponding space of functions satisfying in some sense div $v_h = 0$.

The approximate pressure appears as a Lagrange multiplier for the constraints "div $v_h = 0$" . By applying a Lagrange multiplier argument (cf. [13]) we find a function p_h belonging to some appropriate space X_h , and some kind of approximation $\text{div}_h\, v_h$ of div v_h , such that (compare to (1.12))

$$\frac{1}{Re}\, a(u_h,v_h) + b_h(u_h,u_h,v_h) - (p_h,\text{div}_h\, v_h) = (f,v_h) , \quad \forall\, v_h \in \mathbf{W}_h(0) . \tag{1.13}$$

For the linear non conforming elements, X_h is made of functions which are constant on each triangle K and $\text{div}_h\, v_h = \text{div}\, v_h$ on each K (= constant).

1.6. Evolution problems.

We may also consider the evolution Navier Stokes equations

$$\frac{\partial u}{\partial t} - \frac{1}{Re}\,\Delta u + (u.\nabla)u + \nabla p = f \quad \text{in} \quad \Omega \times (0,T)\ , \tag{1.14}$$

$$\nabla u = 0 \quad \text{in} \quad \Omega \times (0,T)\ , \tag{1.15}$$

$$u = g \quad \text{on} \quad \Gamma \times (0,T)\ , \tag{1.16}$$

$$u(x,0) = u_0(x) \quad \text{in} \quad \Omega\ . \tag{1.17}$$

We consider a semi-discretization in time of the problem ; (for instance a Cranck-Nickolson or a fully implicit or a multistep scheme). At each step we obtain a problem similar to (1.1)-(1.4) and the same procedure is applicable.

2. Numerical Algorithms

2.1. The artificial evolution problems.

It is classical to write that the solutions $u,p,$ of (1.1)-(1.3) are the limit as $t \longrightarrow \infty$ of the solutions of the evolution Navier Stokes equations. Actually $u,p,$ can be also considered as the limit as $t \longrightarrow \infty$ of many other evolution systems which are more convenient for approximation than the real system (1.14)-(1.17).

For instance we may consider the artificial equations

$$\left[\begin{array}{l} -\frac{1}{Re}\,\Delta u(x,t) + (u(x,t).\nabla)\,u(x,t) + \nabla p(x,t) = f(x,t) \\ \frac{\partial p}{\partial t}\,(x,t) + \nabla u(x,t) = 0 \\ u = 0 \quad \text{on} \quad \Gamma \end{array}\right. \tag{2.1}$$

or

$$\left[\begin{array}{l} -\frac{\partial \Delta u}{\partial t} - \frac{1}{Re}\,\Delta u + (u.\nabla)u + \nabla p = f \\ \frac{\partial p}{\partial t} + \nabla u = 0 \\ u = 0 \quad \text{on} \quad \Gamma\ . \end{array}\right. \tag{2.2}$$

In each case it is clear that $u(x,t)$ will not describe accurately the flow during the transient period but only at the limit $t \longrightarrow \infty$. The above equations are easier to solve than the real evolution Navier-Stokes equations and, as far as stationary problems are considered, the procedure is legitimate.

Now we can take the discrete form of one of the previous equations either at the level of the continuous problem (1.4) or directly at the level of the finite dimensional problem (1.12)-(1.13). For instance we get

$$\left[\begin{array}{l} u_h^{m+1} \in W_h(0) \quad \text{satisfies} \\ \frac{1}{Re}\,a_h(u_h^{m+1},v_h) + b_h(u_h^{m+1},u_h^{m+1},v_h) - (p_h^m,\mathrm{div}_h\, v_h) = (f,v_h) \quad \forall\, v_h \in W_h(0) \\ p_h^{m+1} \quad \text{satisfies} \\ \quad p_h^{m+1} - p_h^m + \rho\ \mathrm{div}\ u_h^{m+1} = 0 \end{array}\right. \tag{2.3}$$

(Uzawa algorithm) or for (2.2)

$$
\left[\begin{array}{l}
u_h^{m+1} \in W_h(0) \ \text{ satisfies} \\
a_h(u_h^{m+1} - u_h^m, v_h) + \rho\,\nu\, a_h(u_h^m, v_h) + \rho\, b_h(u_h^m, u_h^{m+1}, v_h) - \rho(p_h^m, \operatorname{div}_h v_h) = \rho(f, v_h) \\
\forall\ v_h \in W_h(0) \\
p_h^{m+1} \ \text{ satisfies} \\
\alpha(p_h^{m+1} - p_h^m) + \rho \operatorname{div} u_h^{m+1} = 0
\end{array}\right. \tag{2.4}
$$

(Arrow-Hurwicz algorithm).

The parameter ρ in (2.3), the parameters ρ and ρ/α in (2.4) play the role of a discretization parameter (discretization in time).

When the solution of (1.1)-(1.3) is unique, these algorithms converge under appropriate conditions on ρ and α (cf. [13]).

2.2. The penalty method and Application.

Using the concept of penalization in the calculus of variation, we can consider $\nabla u = 0$ as a constraint and introduce the following equations :

$$
-\frac{1}{Re}\Delta u + (u.\nabla)u - \frac{1}{\varepsilon}\nabla(\nabla u) = f \ \text{ in } \ \Omega \tag{2.5}
$$

$$
u_\varepsilon = 0 \ \text{ on } \ \Gamma\ , \tag{2.6}
$$

where $\varepsilon > 0$ is a small parameter.

It is shown that, for $\varepsilon \to 0$, the solution u_ε of (2.5)-(2.6) converges to the solution u of (1.1)-(1.3) ; cf. [13]. An error estimate and a full asymptotic expansion is given in M.C. Pelissier [10] ; cf. also M. Bercovier [1] and R.S. Falk [3].

Let us mention some other application.

Extrapolation procedure.

Using the principle of the penalty method, R.S. Falk proposes in [3] an extrapolation procedure which is obtained as follows (the linear and discrete version of (2.5)-(2.6) is considered $u_{h\varepsilon} \in W_h(0)$) :

We set $\varepsilon = \gamma^{-1} \rho_h^\sigma$, $\gamma > 0$, $\sigma \geqslant 0$ and the solution of the linear discrete form of (2.5)-(2.6) is denoted $u_h(\gamma)$. Then some distinct parameters $\gamma_0, \ldots, \gamma_k$, are considered and the parameters a_k which satisfy

$$
\sum_{i=0}^{k} a_i = 0\ , \quad \sum_{i=0}^{k} a_i\, \gamma_i^{-j} = 0\ , \quad 1 \leqslant j \leqslant k\ .
$$

Then the extrapolation is defined by

$$
u_h^{(k)}(\gamma) = \sum_{i=0}^{k} a_i\, u_h(\gamma_i)\ .
$$

If $\gamma_i = 2^i \gamma$, then

$$
u_h^k(\gamma) = \frac{2^k\, u_h^{(k-1)}(2\gamma) - u_h^{(k-1)}(\gamma)}{2^k - 1}\ .
$$

Augmented Lagrangian Method.

(cf. M. Fortin [5], [7], R.T. Rockafellar [11], F. Thomasset - R. Temam [14]).

Combining the idea of penalty and the algorithms considered in Section 2.1, we are led (cf. the above references) to consider the following algorithm which appears as very efficient (compare to (2.3) and (2.5)) :

$$
\left[\begin{array}{l}
u_h^{m+1} \in \mathbf{W}_h(0) \quad \text{satisfies} \\
\\
\dfrac{1}{Re}\, a_h(u_h^{m+1}, v_h) + b_h(u_h^{m+1}, u_h^{m+1}, v_h) + \dfrac{1}{\varepsilon}\,(\mathrm{div}_h\, u_h^{m+1}, \mathrm{div}_h\, v_h) - (p_h, \mathrm{div}_h\, v_h) = (f, v_h) \\
\qquad\qquad\qquad\qquad\qquad\qquad\qquad\qquad\qquad\qquad \forall\, v_h \in \mathbf{W}_h(0) \\
\\
p_h^{m+1} \quad \text{satisfies} \\
\\
p_h^{m+1} - p_h^m + \rho\, \mathrm{div}_h\, u_h^{m+1} = 0 \,.
\end{array}\right. \tag{2.7}
$$

Cf, some computations made with this method in the Appendix of [13].

3. Mixed Finite Elements for the Euler Equations

We pass now to a mixed finite element for the Euler Equations proposed by Fortin in [6]. This scheme is an extension of a method of Lesaint [9] applying to linear hyperbolic systems.

We assume for simplicity that $\Omega \subset R^2$ is simply connected. Then the curl operator

$$\psi \longmapsto \left\{\frac{\partial \psi}{\partial x_2}\,,\, -\frac{\partial \psi}{\partial x_1}\right\} \,.$$

gives a one to one mapping between the space $W(0)$ of function vanishing on Γ and the space $\mathbf{H}(0)$ of free divergence vector functions on Ω, such that $u.n = 0$ on Γ, n = the unit outward normal on Γ.

If $W_h(0)$ is an internal approximation of $W(0)$ (for instance conforming finite elements of Lagrange type), then the space

$$\mathbf{H}_h(0) = \{v_h, v_h = \mathrm{curl}\ \psi_h, \psi_h \in W_h(0)\}$$

is an approximation of $\mathbf{H}(0)$ and $\mathbf{H}_h(0) \subset \mathbf{H}(0)$.

It is easily seen that if $u_h \in \mathbf{H}_h(0)$ then $u_h.n = 0$ on $\partial\Omega_h$ and at the interface of two adjacent triangles K and K', $u_h.n$ is continuous while $u_h - (u_h.n)n = u_{h\tau}$ has no reason for being continuous. The discretization will take advantage of this discontinuity of the tangential components of u_h which is allowed in this space.

It is easily seen that the weak formulation of the Euler equations, analogous to (1.4) is :

$$
\left[\begin{array}{l}
u : [0,T] \longmapsto \mathbf{H}_h(0) \quad \text{satisfies} \\
\\
\dfrac{d}{dt}(u,v) + b(u,u,v) = (f,v)\,, \quad 0 < t < T\,, \ \forall\, v \in \mathbf{H}_h(0)
\end{array}\right. \tag{3.1}
$$

(we assumed $g = 0$).

Now let $\mathcal{T}_h$ be a triangulation of Ω and let K be a triangle, $K \in \mathcal{T}_h$, with boundary ∂K. We have :

$$b(u,u,v) = \sum_{i,j=1}^{2} \int_\Omega u_i \frac{\partial u_j}{\partial x_i} v_j \, dx$$

$$= \sum_{i,j=1}^{2} \int_\Omega \frac{\partial}{\partial x_i} (u_i u_j) \, v_j \, dx$$

$$= \sum_{i,j=1}^{2} \sum_{K \in \mathcal{C}_h} \int_K \frac{\partial}{\partial x_i} (u_i u_j) \, v_j dx \, .$$

After performing an integration by part on K, we find

$$\int_K \frac{\partial}{\partial x_i} (u_i u_j) \, v_j \, dx = - \int_K (u_i u_j) \frac{\partial v_i}{\partial x_j} \, dx + \int_{\partial K} (u.n)(u.v) \, d\ell \, . \tag{3.2}$$

The idea used by Lesaint and Fortin is to distinguish on the boundary ∂K of K two parts ∂K_- and ∂K_+ where respectively $u.n < 0$ and $u.n > 0$, i.e. the flux is coming in or is going out. On two adjacent triangles this gives the situation represented on the figure

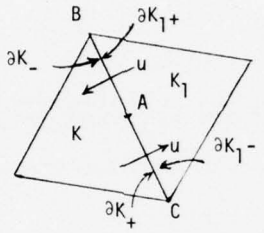

($u.n = 0$ at A, $u.n > 0$ for K_1 on AB and for K on AC).

Because of the hyperbolic character of the equations it is considered that the flow is influenced in K by the neighbouring triangles through ∂K_-. For this reason we set on $S = \partial K \cap \partial K_1$:

$$u^+(x) = \begin{cases} \text{value of } u(x) \text{ in } K \text{ if } x \in \partial K_+ \cap S \\ \\ \text{value of } u(x) \text{ in } K_1 \text{ if } x \in \partial K_- \cap S \, , \end{cases}$$

and the expression (3.2) is replaced by

$$- \int_K (u_i u_j) \frac{\partial v_i}{\partial x_j} \, dx + \int_{\partial K} (u.n)(u^+.v) \, d\ell \, .$$

This leads to the scheme

$$\frac{d}{dt} (u,v) + \sum_{i,j=1}^{2} \sum_K \{ - \int_K (u_i u_j) \frac{\partial v_i}{\partial x_j} \, dx + \int_{\partial K} (u.n)(u^+ v) \, d\Gamma \} = (f,v) \, , \quad \forall \, v \in \mathbf{H}_h(0) \, . \tag{3.3}$$

More generally, for $0 \leqslant \alpha \leqslant 1$ one can consider

$$\frac{d}{dt} (u.v) + \sum_{i,j=1}^{2} \sum_K \{ - \int_K (u_i u_j) \frac{\partial v_i}{\partial x_j} + \int_{\partial K} (u.n)((1-\alpha)u^- + \alpha u^+) \, d\ell \} = (f,v) \, . \tag{3.4}$$

For $\alpha = \frac{1}{2}$ we obtain "centered" discrete differentiations ; for $\alpha < \frac{1}{2}$ the decentered discretization is against the flow, for $\alpha > 1/\varepsilon$ the discretization is decentered in the direction of the flow.

It is shown in [6] that the scheme is dissipative for $\alpha > \frac{1}{2}$ conservative for $\alpha = \frac{1}{2}$, and of course unstable for $\alpha < \frac{1}{2}$.

Numerical experiments have been done by F. Thomasset. A version of this scheme applying to the Navier Stokes equations is given in [6], and [15].

References

[1] M. Bercovier - Thèse, Université de Rouen 1976 et Rapports de l'Université de Jerusalem.

[2] M. Crouzeix, P.A. Raviart - Conforming and nonconforming finite element methods for solving the Stationary Stokes equations.
R.A.I.R.O., R.3, 1973, p.33-76.

[3] R.S. Falk - An analysis of the penalty method and extrapolation for the stationary Stokes equations.
Advances in Computer Methods for P.D.E.'s, R. Vichnevelsky editor, Proceedings of A.I.C.A. Symposium.

[4] M. Fortin - Calcul numérique des écoulements des fluides de Bingham et des fluides newtoniens incompressibles par la méthode des éléments finis.
Thèse, Université de Paris 1972.

[5] M. Fortin - Minimization of some non differentiable Functionals by the augmented Lagrangian Method of Hestenes and Pawell.
Applied Math. and Optimization, vol.2, n°3, 1975/76, p.236-250.

[6] M. Fortin - Résolution numérique des équations de Navier-Stokes par des élêments finis de type mixte.
I.R.I.A. - L.A.B.O.R.I.A., Rapport de Recherche n°184, Août 1976.

[7] M. Fortin - Cours de 3ème cycle, Université de Paris-Sud, Orsay, 1975/76.

[8] M. Fortin, R. Glowinski - To appear.

[9] P. Lesaint - Sur la résolution des systèmes hyperboliques du premier ordre par des méthodes d'éléments finis.

[10] M.C. Pelissier - Résolution numérique de quelques problèmes raides en mécanique des milieux faiblement compressibles,
Calcolo, 12, 1975, p.275-314.

[11] R.T. Rockafellar - Augmented Lagrange multiplier functions and duality in nonconvex programming.
SIAM J. Control.

[12] R. Temam - On the Euler equations of incompressible perfect fluids.
J. Funct. Anal., vol.20, 1975, p.32-43.

[13] R. Temam - Navier Stokes equations, Theory and Numerical Analysis.
North Holland Publ. Comp., Amsterdam 1977.

[14] R. Temam, J.F. Thomasset - Numerical solution of Navier Stokes equations by a finite element Method.
Conference at Rapallo, Italy June 1976, On finite element Methods in Fluid Flows. To appear.

[15] F. Thomasset - Numerical solution of the Navier Stokes equations by Finite Element Methods.
Lecture at this Conference.

FIGURES

All the computations were made by F.Thomasset (cf [15])

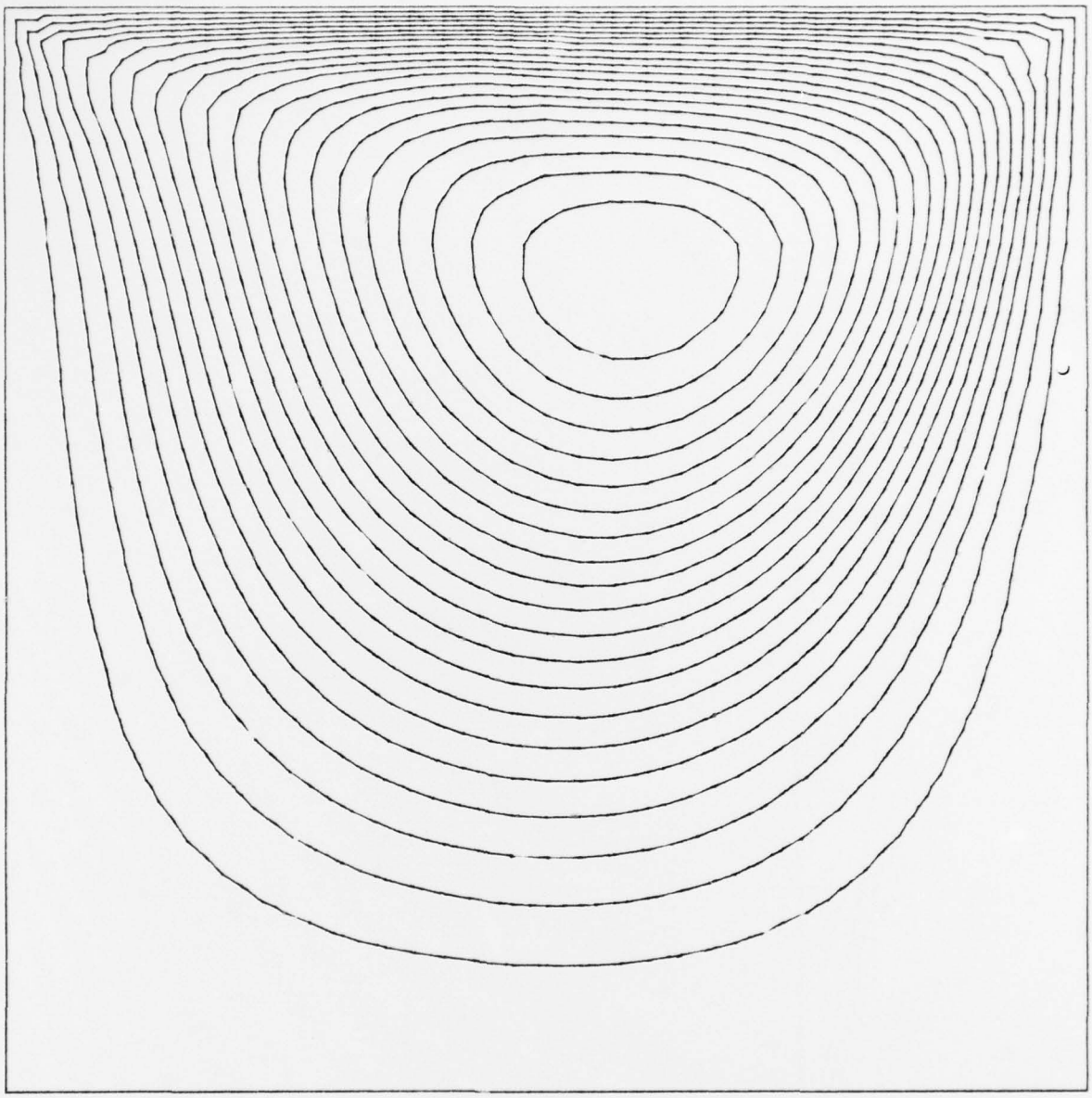

Fig.1 Streamlines for the flow in a square cavity, computed by the non conforming finite element method ($\nu = 10^{-2}$, length of the edge = 1, upper side moving with velocity 1)

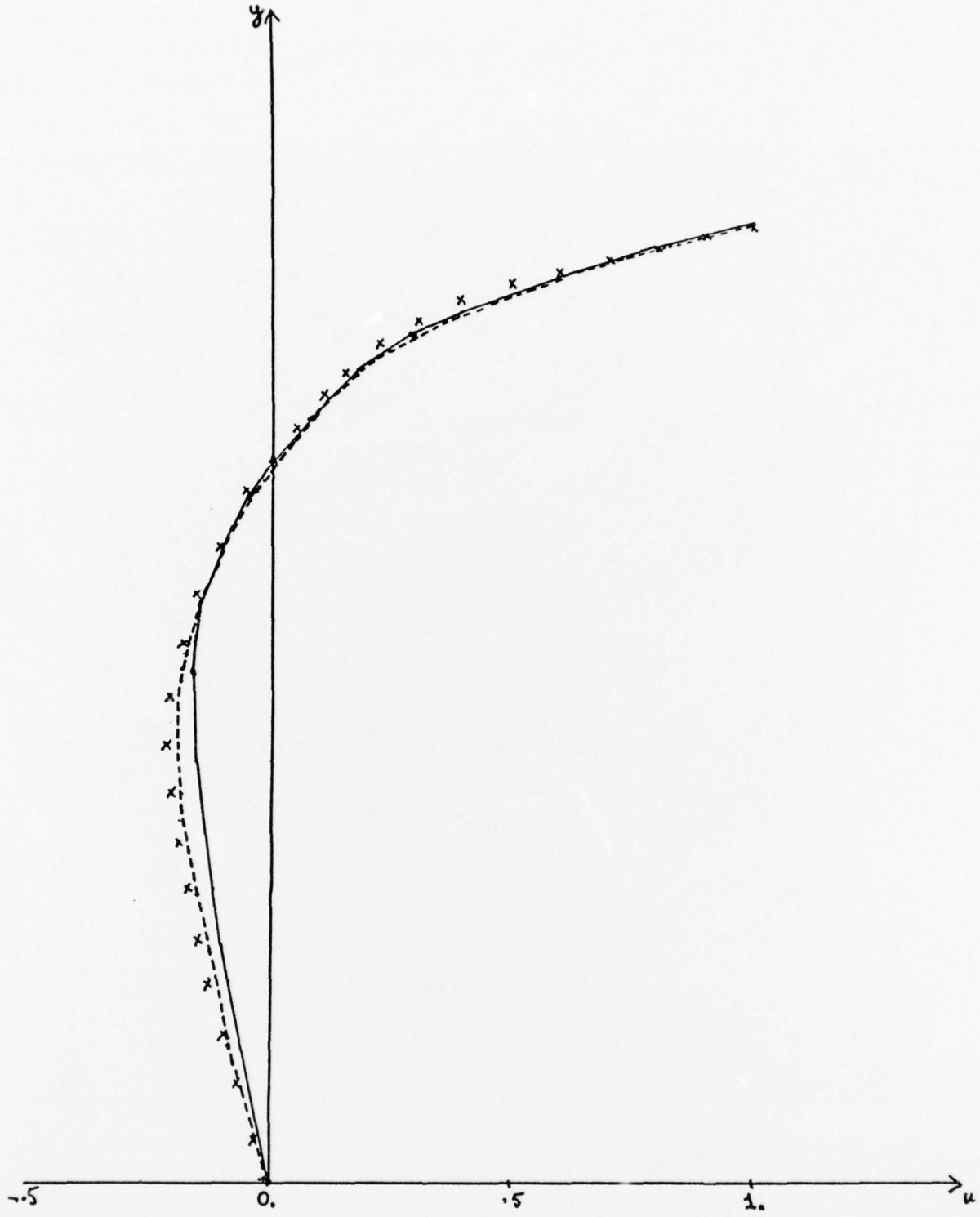

Fig.2 Flow in a square cavity (same conditions as in Figure 1): velocity u along the axis x = 0.5. Results with the non conforming finite element method, - - - - 2048 triangles, —— 512 triangles; x = results of O.R.Burggraf (J. Fluid Mech., Vol.24, Part I, pp.113-151, 1966)

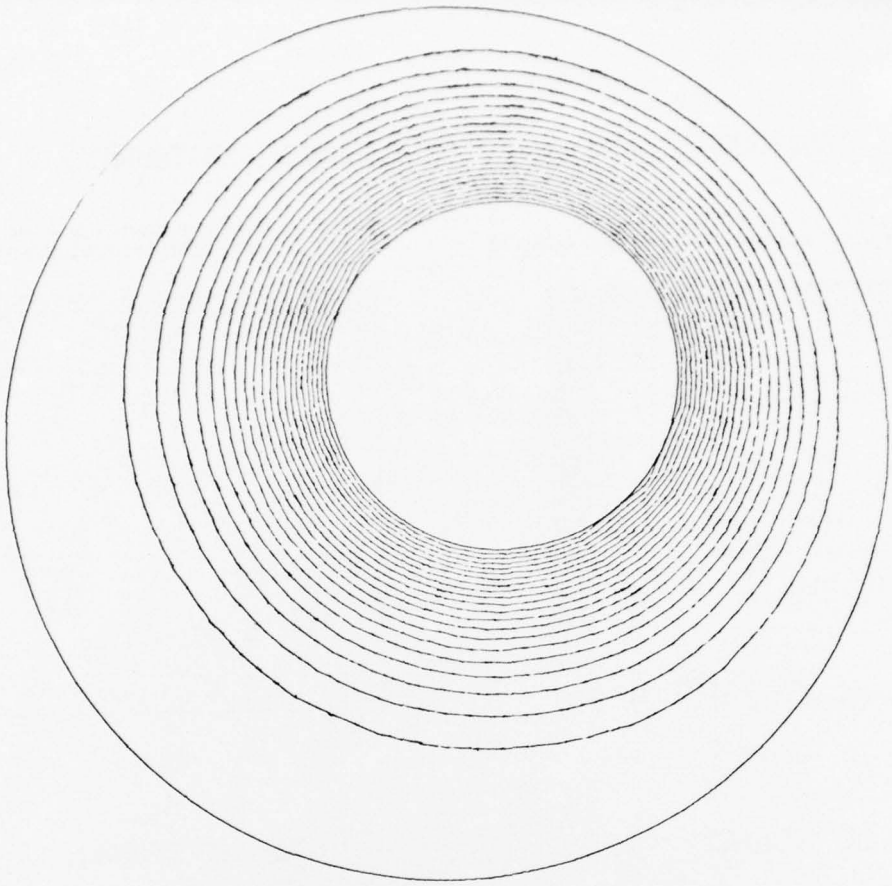

Fig.3 Streamlines for the flow between two rotating cylinders. Angular speed of interior circle = 1, outer circle at rest, $\nu = .5$, Re = 80. Non conforming finite elements

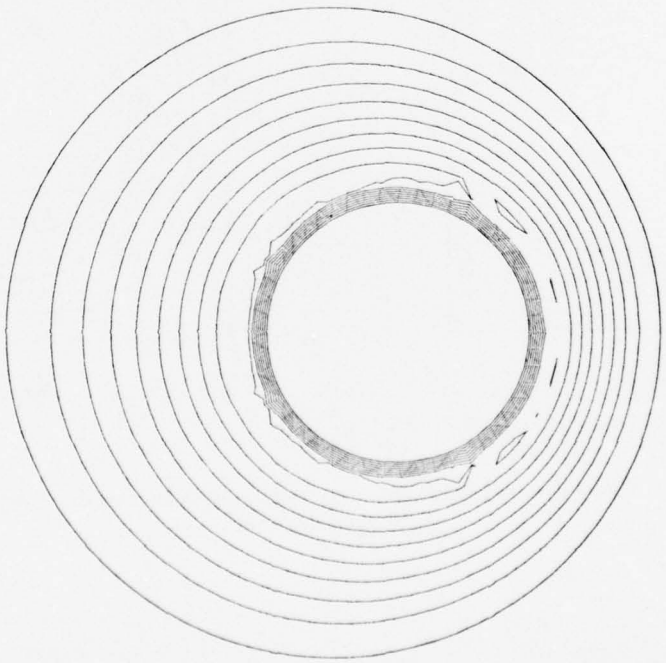

Fig.4 Flow between rotating cylinders

LIGNES ISO-TOURBILLON

TEMPS T = 0.733E02 . VISCOSITE = 0.100E-03
. MAX . DE ROT(U) =0.292E02 . MIN . DE ROT(U) =-0.688E02

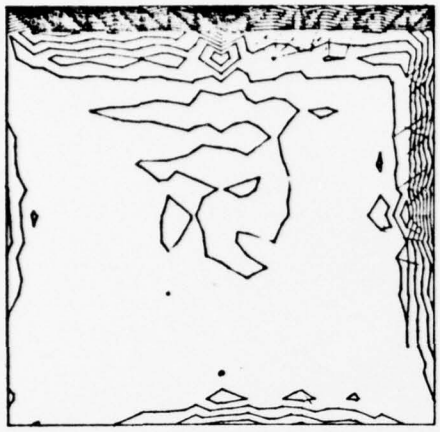

Figure 5

LIGNES ISO-TOURBILLON

TEMPS T = 0.164E02 . VISCOSITE = 0.100E-02
. MAX . DE ROT(U) =0.347E02 . MIN . DE ROT(U) =-0.569E0

Figure 6

LIGNES DE COURANT

TEMPS T = 0.733E02 . VISCOSITE = 0.100E-03
. MAX . DE PSI =0.925E-03 . MIN . DE PSI =-0.087E00

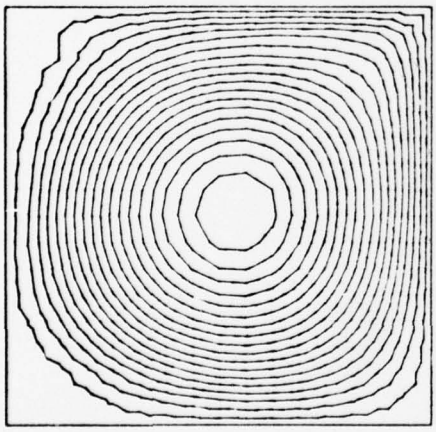

Figure 7

LIGNES DE COURANT

TEMPS T = 0.164E02 . VISCOSITE = 0.100E-02
. MAX . DE PSI =0.316E-02 . MIN . DE PSI =-0.114E00

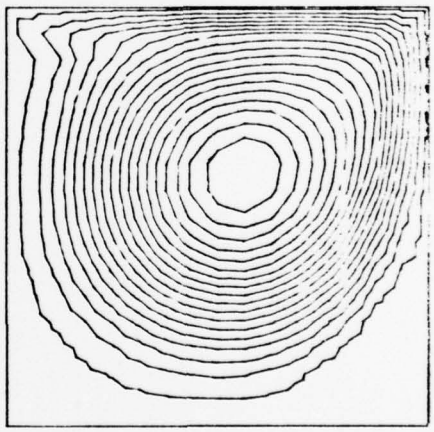

Figure 8

Figs.5, 6, 7, 8 Vortex lines and streamlines, flow in a cavity (same conditions as in Figure 1) mixed finite elements

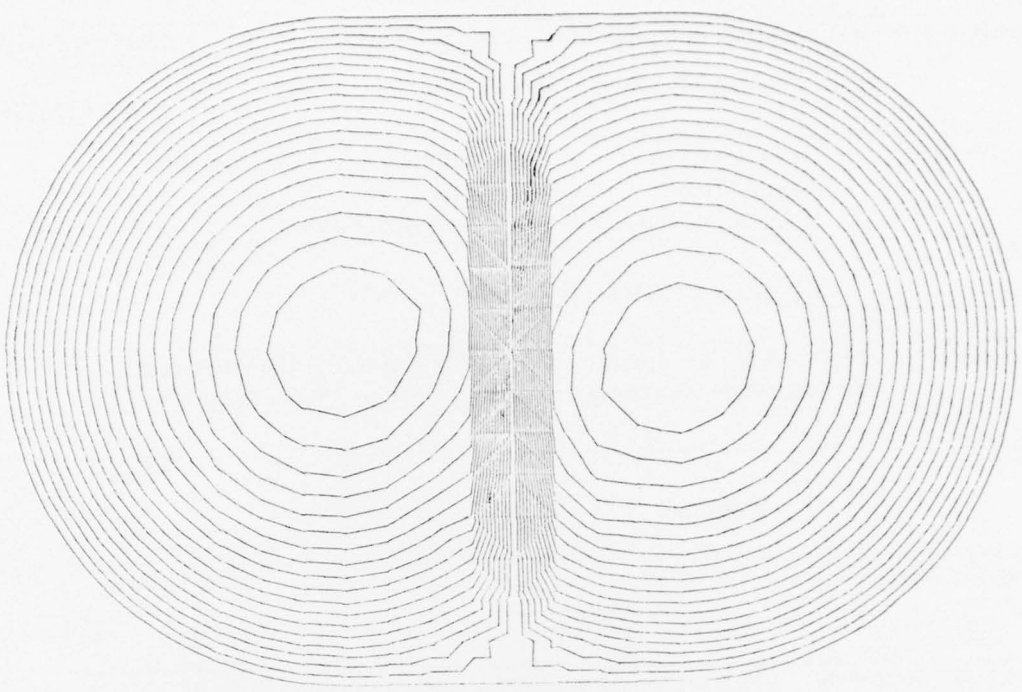

Figure 9

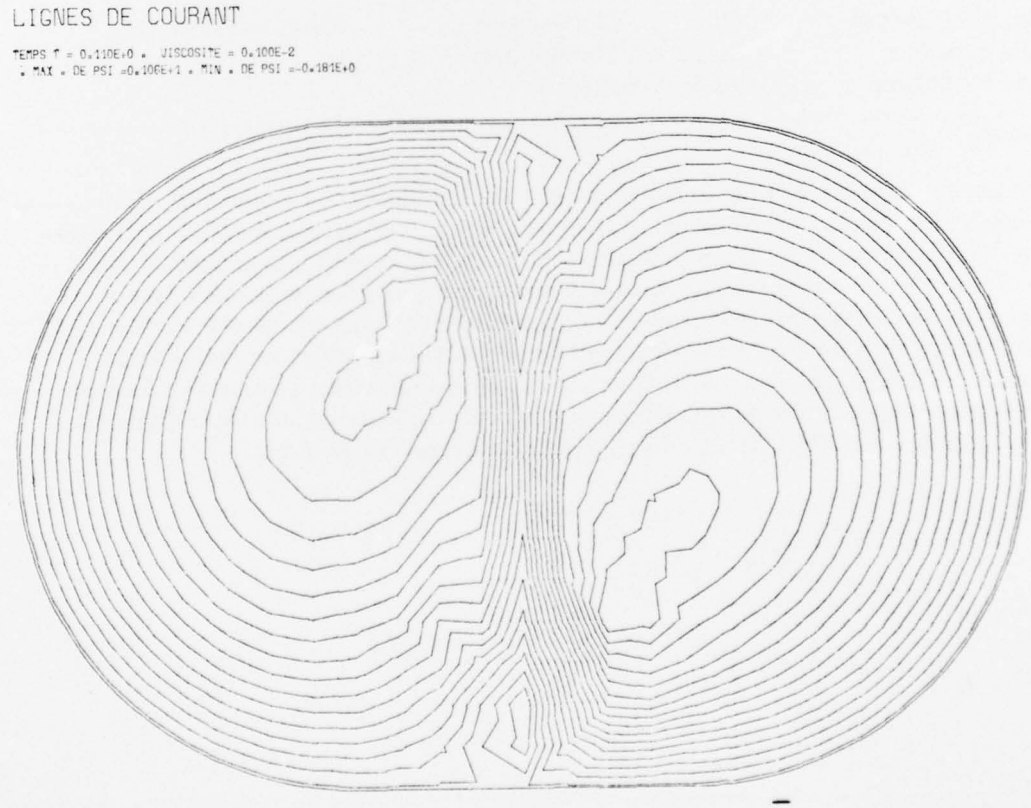

Figure 10

Figs.9 and 10 Collision of two vortices (streamlines). Mixed finite elements

REPORT DOCUMENTATION PAGE

1. Recipient's Reference	2. Originator's Reference	3. Further Reference	4. Security Classification of Document
	AGARD-LS-86	ISBN 92-835-1241-3	UNCLASSIFIED

5. Originator Advisory Group for Aerospace Research and Development
North Atlantic Treaty Organization
7 rue Ancelle, 92200 Neuilly sur Seine, France

6. Title COMPUTATIONAL FLUID DYNAMICS

7. Presented at the Von Kármán Institute on 21–23 March and at the Wright-Patterson Air Force Base, Dayton, Ohio 45433, USA on 25–27 April 1977.

8. Author(s)	9. Date
Various	April 1977
10. Author's Address	**11. Pages**
Various	174

12. Distribution Statement This document is distributed in accordance with AGARD policies and regulations, which are outlined on the Outside Back Covers of all AGARD publications.

13. Keywords/Descriptors

Numerical analysis	Finite element analysis	Turbulent flow
Fluid dynamics	Navier-Stokes equations	
Fluid mechanics	Flow distribution	

14. Abstract

This Lecture Series is devoted to recent advances in the theory and application of numerical methods to solve complex problems of fluid mechanics. Particular emphasis is given to an introduction of the Finite Element Method and the advances which have been obtained so far. Further major topics such as numerical turbulence modelling, relaxation methods in fluid dynamics, flow representation, including separated regions, by discrete vortices and recent advances in the treatment of the full Navier-Stokes equations are presented and discussed in detail. The material in this publication was assembled to support a Lecture Series under the joint sponsorship of the Von Kármán Institute and the Fluid Dynamics Panel, together with the Consultant and Exchange Program of AGARD.

AGARD Lecture Series No.86
Advisory Group for Aerospace Research and Development, NATO
COMPUTATIONAL FLUID DYNAMICS
Published April 1977
174 pages

This Lecture Series is devoted to recent advances in the theory and application of numerical methods to solve complex problems of fluid mechanics. Particular emphasis is given to an introduction of the Finite Element Method and the advances which have been obtained so far. Further major topics such as numerical turbulence modelling, relaxation methods in fluid dynamics, flow representation, including separated regions, by discrete vortices and recent advances in the

P.T.O.

AGARD-LS-86

Numerical analysis
Fluid dynamics
Fluid mechanics
Finite element analysis
Navier-Stokes equations
Flow distribution
Turbulent flow

AGARD Lecture Series No.86
Advisory Group for Aerospace Research and Development, NATO
COMPUTATIONAL FLUID DYNAMICS
Published April 1977
174 pages

This Lecture Series is devoted to recent advances in the theory and application of numerical methods to solve complex problems of fluid mechanics. Particular emphasis is given to an introduction of the Finite Element Method and the advances which have been obtained so far. Further major topics such as numerical turbulence modelling, relaxation methods in fluid dynamics, flow representation, including separated regions, by discrete vortices and recent advances in the

P.T.O.

AGARD-LS-86

Numerical analysis
Fluid dynamics
Fluid mechanics
Finite element analysis
Navier-Stokes equations
Flow distribution
Turbulent flow

AGARD Lecture Series No.86
Advisory Group for Aerospace Research and Development, NATO
COMPUTATIONAL FLUID DYNAMICS
Published April 1977
174 pages

This Lecture Series is devoted to recent advances in the theory and application of numerical methods to solve complex problems of fluid mechanics. Particular emphasis is given to an introduction of the Finite Element Method and the advances which have been obtained so far. Further major topics such as numerical turbulence modelling, relaxation methods in fluid dynamics, flow representation, including separated regions, by discrete vortices and recent advances in the

P.T.O.

AGARD-LS-86

Numerical analysis
Fluid dynamics
Fluid mechanics
Finite element analysis
Navier-Stokes equations
Flow distribution
Turbulent flow

treatment of the full Navier-Stokes equations are presented and discussed in detail. The material in this publication was assembled to support a Lecture Series under the joint sponsorship of the Von Kármán Institute and the Fluid Dynamics Panel, together with the Consultant and Exchange Program of AGARD. Presented at the Von Kármán Institute on 21-23 March, and at Wright-Patterson Air Force Base, Dayton, Ohio 45433, USA on 25-27 April 1977.

ISBN 92-835-1241-3

treatment of the full Navier-Stokes equations are presented and discussed in detail. The material in this publication was assembled to support a Lecture Series under the joint sponsorship of the Von Kármán Institute and the Fluid Dynamics Panel, together with the Consultant and Exchange Program of AGARD. Presented at the Von Kármán Institute on 21-23 March, and at Wright-Patterson Air Force Base, Dayton, Ohio 45433, USA on 25-27 April 1977.

ISBN 92-835-1241-3

treatment of the full Navier-Stokes equations are presented and discussed in detail. The material in this publication was assembled to support a Lecture Series under the joint sponsorship of the Von Kármán Institute and the Fluid Dynamics Panel, together with the Consultant and Exchange Program of AGARD. Presented at the Von Kármán Institute on 21-23 March, and at Wright-Patterson Air Force Base, Dayton, Ohio 45433, USA on 25-27 April 1977.

ISBN 92-835-1241-3

treatment of the full Navier-Stokes equations are presented and discussed in detail. The material in this publication was assembled to support a Lecture Series under the joint sponsorship of the Von Kármán Institute and the Fluid Dynamics Panel, together with the Consultant and Exchange Program of AGARD. Presented at the Von Kármán Institute on 21-23 March, and at Wright-Patterson Air Force Base, Dayton, Ohio 45433, USA on 25-27 April 1977.

ISBN 92-835-1241-3

AGARD

NATO OTAN

7 RUE ANCELLE · 92200 NEUILLY-SUR-SEINE

FRANCE

Telephone 745.08.10 · Telex 610176

DISTRIBUTION OF UNCLASSIFIED AGARD PUBLICATIONS

AGARD does NOT hold stocks of AGARD publications at the above address for general distribution. Initial distribution of AGARD publications is made to AGARD Member Nations through the following National Distribution Centres. Further copies are sometimes available from these Centres, but if not may be purchased in Microfiche or Photocopy form from the Purchase Agencies listed below.

NATIONAL DISTRIBUTION CENTRES

BELGIUM
Coordonnateur AGARD – VSL
Etat-Major de la Force Aérienne
Caserne Prince Baudouin
Place Dailly, 1030 Bruxelles

CANADA
Defence Scientific Information Service
Department of National Defence
Ottawa, Ontario K1A OZ2

DENMARK
Danish Defence Research Board
Østerbrogades Kaserne
Copenhagen Ø

FRANCE
O.N.E.R.A. (Direction)
29 Avenue de la Division Leclerc
92 Châtillon sous Bagneux

GERMANY
Zentralstelle für Luft- und Raumfahrt-
dokumentation und -information
Postfach 860880
D-8 München 86

GREECE
Hellenic Armed Forces Command
D Branch, Athens

ICELAND
Director of Aviation
c/o Flugrad
Reykjavik

ITALY
Aeronautica Militare
Ufficio del Delegato Nazionale all'AGARD
3, Piazzale Adenauer
Roma/EUR

LUXEMBOURG
See Belgium

NETHERLANDS
Netherlands Delegation to AGARD
National Aerospace Laboratory, NLR
P.O. Box 126
Delft

NORWAY
Norwegian Defence Research Establishment
Main Library
P.O. Box 25
N-2007 Kjeller

PORTUGAL
Direccao do Servico de Material
da Forca Aerea
Rua de Escola Politecnica 42
Lisboa
Attn: AGARD National Delegate

TURKEY
Department of Research and Development (ARGE)
Ministry of National Defence, Ankara

UNITED KINGDOM
Defence Research Information Centre
Station Square House
St. Mary Cray
Orpington, Kent BR5 3RE

UNITED STATES
National Aeronautics and Space Administration (NASA),
Langley Field, Virginia 23365
Attn: Report Distribution and Storage Unit

THE UNITED STATES NATIONAL DISTRIBUTION CENTRE (NASA) DOES NOT HOLD STOCKS OF AGARD PUBLICATIONS, AND APPLICATIONS FOR COPIES SHOULD BE MADE DIRECT TO THE NATIONAL TECHNICAL INFORMATION SERVICE (NTIS) AT THE ADDRESS BELOW.

PURCHASE AGENCIES

Microfiche or Photocopy

National Technical
Information Service (NTIS)
5285 Port Royal Road
Springfield
Virginia 22151, USA

Microfiche

Space Documentation Service
European Space Agency
10, rue Mario Nikis
75015 Paris, France

Microfiche

Technology Reports
Centre (DTI)
Station Square House
St. Mary Cray
Orpington, Kent BR5 3RF
England

Requests for microfiche or photocopies of AGARD documents should include the AGARD serial number, title, author or editor, and publication date. Requests to NTIS should include the NASA accession report number. Full bibliographical references and abstracts of AGARD publications are given in the following journals:

Scientific and Technical Aerospace Reports (STAR),
published by NASA Scientific and Technical
Information Facility
Post Office Box 8757
Baltimore/Washington International Airport
Maryland 21240, USA

Government Reports Announcements (GRA),
published by the National Technical
Information Services, Springfield
Virginia 22151, USA

Printed by Technical Editing and Reproduction Ltd
Harford House, 7–9 Charlotte St, London W1P 1HD

ISBN 92-835-1241-3